AFRL-VA-WP-TR-2000-3027

CONTROL-SURFACE DEFLECTION EFFECTS ON THE INNOVATIVE CONTROL EFFECTORS (ICE 101) DESIGN

GREGORY A. ADDINGTON, PH.D.
JAMES H. MYATT, PH.D.

AFRL/VACA
AIR VEHICLES DIRECTORATE
AIR FORCE RESEARCH LABORATORY
AIR FORCE MATERIEL COMMAND
WRIGHT-PATTERSON AFB, OH 45433-7521

MARCH 2000

FINAL REPORT FOR 10/01/1998 – 09/30/1999

AIR VEHICLES DIRECTORATE
AIR FORCE RESEARCH LABORATORY
AIR FORCE MATERIEL COMMAND
WRIGHT-PATTERSON AIR FORCE BASE OH 45433-7542

Unlimited, Statement A

NOTICE

USING GOVERNMENT DRAWINGS, SPECIFICATIONS, OR OTHER DATA INCLUDED IN THIS DOCUMENT FOR ANY PURPOSE OTHER THAN GOVERNMENT PROCUREMENT DOES NOT IN ANY WAY OBLIGATE THE US GOVERNMENT. THE FACT THAT THE GOVERNMENT FORMULATED OR SUPPLIED THE DRAWINGS, SPECIFICATIONS, OR OTHER DATA DOES NOT LICENSE THE HOLDER OR ANY OTHER PERSON OR CORPORATION; OR CONVEY ANY RIGHTS OR PERMISSION TO MANUFACTURE, USE, OR SELL ANY PATENTED INVENTION THAT MAY RELATE TO THEM.

THIS REPORT IS RELEASABLE TO THE NATIONAL TECHNICAL INFORMATION SERVICE (NTIS). AT NTIS, IT WILL BE AVAILABLE TO THE GENERAL PUBLIC, INCLUDING FOREIGN NATIONS.

THIS TECHNICAL REPORT HAS BEEN REVIEWED AND IS APPROVED FOR PUBLICATION.

GREGORY A. ADDINGTON, Ph.D.
Project Engineer
Control Theory Optimization Branch

James K Hall
JAMES K. HALL, Capt, USAF
Chief, Control Theory Optimization Branch
Control Science Division

John A. Bowlus
JOHN BOWLUS, Chief
Control Science Division
Air Vehicles Directorate

Do not return copies of this report unless contractual obligations or notice on a specific document require its return.

REPORT DOCUMENTATION PAGE

Form Approved
OMB No. 0704-0188

1. AGENCY USE ONLY *(Leave blank)*

2. REPORT DATE
MARCH 2000

3. REPORT TYPE AND DATES COVERED
FINAL REPORT FOR 10/01/1998 - 09/30/1999

4. TITLE AND SUBTITLE
CONTROL-SURFACE DEFLECTION EFFECTS ON THE INNOVATIVE CONTROL EFFECTORS (ICE 101) DESIGN

5. FUNDING NUMBERS
C IN-HOUSE
PE 62201
PR 2403
TA 05
WU 9L

6. AUTHOR(S)
GREGORY A. ADDINGTON, PH.D.
JAMES H. MYATT, PH.D.

7. PERFORMING ORGANIZATION NAME(S) AND ADDRESS(ES)
AFRL/VACA
AIR VEHICLES DIRECTORATE
AIR FORCE RESEARCH LABORATORY
AIR FORCE MATERIEL COMMAND
WRIGHT-PATTERSON AFB, OH 45433-7521

8. PERFORMING ORGANIZATION REPORT NUMBER

9. SPONSORING/MONITORING AGENCY NAME(S) AND ADDRESS(ES)
AIR VEHICLES DIRECTORATE
AIR FORCE RESEARCH LABORATORY
AIR FORCE MATERIEL COMMAND
WRIGHT-PATTERSON AFB, OH 45433-7542
POC: GREGORY A. ADDINGTON, AFRL/VACA, 937-255-8490

10. SPONSORING/MONITORING AGENCY REPORT NUMBER
AFRL-VA-WP-TR-2000-3027

11. SUPPLEMENTARY NOTES

12a. DISTRIBUTION AVAILABILITY STATEMENT

APPROVED FOR PUBLIC RELEASE, DISTRIBUTION UNLIMITED.

12b. DISTRIBUTION CODE

13. ABSTRACT *(Maximum 200 words)*

A static wind tunnel test of the Innovative Controls Effectors (ICE 101) conceptual aircraft configuration was conducted in the Air Force Research Laboratory's Vertical Wind Tunnel. This entry characterized the increments to the aerodynamic loading provided by the various control surfaces while using a more finely-resolved test matrix in angle of attack and sideslip than typically seen in wind tunnel testing. The purpose for obtaining these data was to determine the effect which control surface deflection had on critical state locations in preparation for the test of a second ICE model built with remotely-actuated control surfaces. (Critical states are discrete flight mechanical states where the aerodynamic response looses its analytic dependence on one or more state variables.) These data demonstrate that the aerodynamic increments are in many cases at minimum nonlinear functions of the surface deflection angle, and strongly suggest that some critical states do shift in angle of attack and/or sideslip with changing deflection angle.

14. SUBJECT TERMS
Nonlinear aerodynamics, stability and control, wind tunnel testing, data analysis, aerodynamic modeling, high angle of attack aerodynamics.

15. NUMBER OF PAGES
199

16. PRICE CODE

17. SECURITY CLASSIFICATION OF REPORT	18. SECURITY CLASSIFICATION OF THIS PAGE	19. SECURITY CLASSIFICATION OF ABSTRACT	20. LIMITATION OF ABSTRACT
UNCLASSIFIED	UNCLASSIFIED	UNCLASSIFIED	SAR

Standard Form 298 (Rev. 2-89) (EG)
Prescribed by ANSI Std. 239.18
Designed using Perform Pro, WHS/DIOR, Oct 94

Table of Contents

List of Figures

Nomenclature

AMT .... All-Moving Tip
b .... Trailing-Edge Wing Span (ft)
c .... Mean Aerodynamic Chord (ft)
C_l .... Rolling-Moment Coefficient, l/qSb
C_m .... Pitching-Moment Coefficient, m/qSc
C_N .... Normal-Force Coefficient, N/qS
C_n .... Yawing-Moment Coefficient, n/qSb
ICE .... Innovative Control Effectors
l .... Rolling Moment (ft-lb)
LEF .... Leading-Edge Flap
m .... Pitching Moment (ft-lb)
MAT .... Multi-Axis Test Rig
N .... Normal Force (lb)
n .... Yawing moment (ft-lb)
PF .... Pitch Flap
q .... Freestream Dynamic Pressure (lb/ft^2)
S .... Wing Area (ft^2)
SPLR .... Spoiler
SSD .... Spoiler Slot Deflector
TEF .... Trailing-Edge Flap
VWT .... AFRL Vertical Wind Tunnel
α .... Wind-Axis Angle of Attack
β .... Wind-Axis Sideslip Angle

1.0 Introduction

The Innovative Control Effectors (ICE) program,[1,2] conducted cooperatively between Wright Laboratory (now a part of Air Force Research Laboratory) and Lockheed Martin Tactical Aircraft Systems, developed a conceptual fighter configuration to fill the future USAF strike fighter mission. This aircraft was designed to be an agile multi-role fighter with significant low-observability features, necessitating a tailless design capable of flying at high angles of attack. The design developed by Lockheed-Martin Tactical Aircraft Systems, designated ICE 101, is an all-flying delta-wing configuration with a 65° leading-edge sweep and sawtooth trailing edge, as shown in Figure 1. This design possesses five sets of control surfaces (see Figure 2 and References 1 and 2): conventional leading-edge flaps; pitch flaps; trailing-edge flaps (elevons); all-moving tips; and spoiler slot deflectors (the upper surface of which can be used as a spoiler alone).

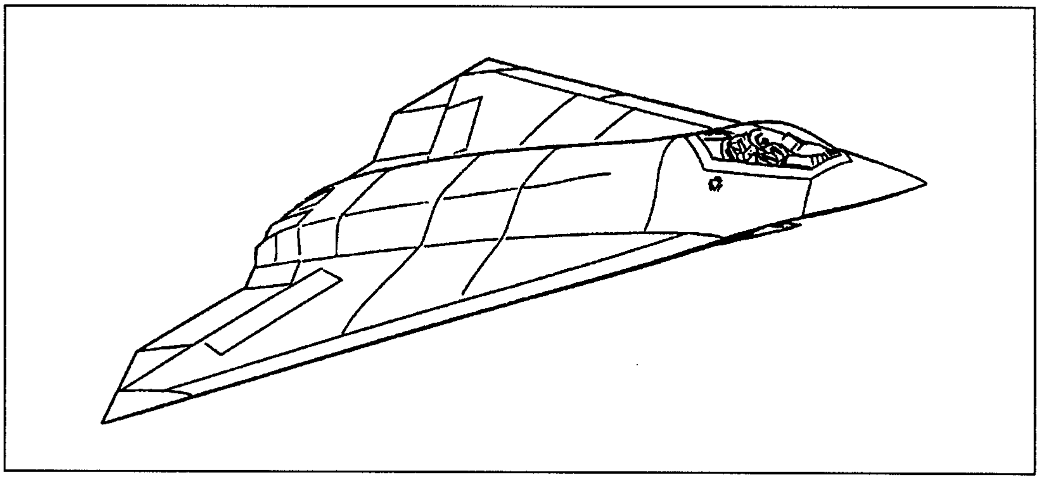

Figure 1 ICE 101 Conceptual Aircraft Design

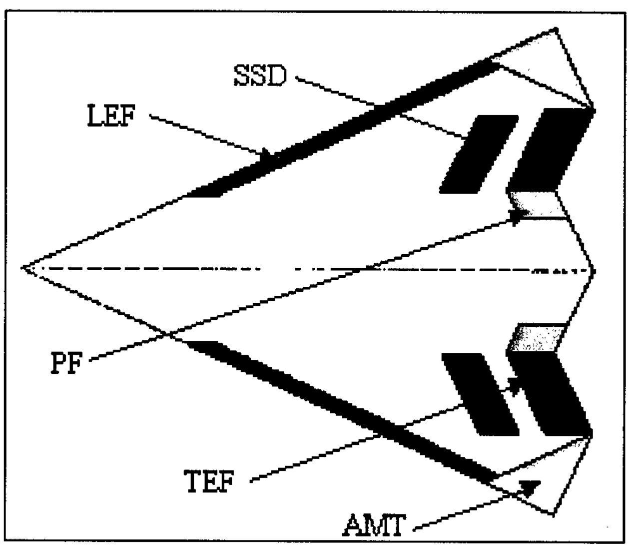

Figure 2 ICE Control Effectors Approximate Locations (Not to Scale)

Research using a more generic 65° delta wing model has demonstrated that not only is the aerodynamic response a nonlinear function of the flight mechanical state variables, but it can change discontinuously with those variables.[3,4,5,6] These discontinuities, known as critical states, have been shown empirically to be related to bifurcations in the surrounding flow field, *e.g.*, coinciding with the onset of flow separation, leading-edge vortex burst, or the appearance / disappearance of more subtle flow structures.[6] Furthermore, the crossing of a critical state during one degree of freedom motions has been shown to introduce a transient in the aerodynamic response of remarkably long duration in addition to the slower-than-convective-time-scale response which results in the presence of vortex burst or stall onset.[4,5]

Given the similarity of the planforms between the ICE 101 and the basic 65° delta wing, the likelihood that the ICE 101 model would exhibit many of the same sorts of nonlinear and even discontinuous aerodynamic response characteristics is substantial and has indeed been shown to a small extent.[7] The dependence of critical state locations on the control surface deflections is unknown; however, as these surfaces affect the pressure gradient over the model surface, an effect on critical state locations was presumed likely. Should the control surfaces affect critical state locations or their transient response characteristics, the impact on the flight control law design could be significant. Given the potential impact that these effects would have on an air vehicle's design process, a wind tunnel test investigating these effects was warranted.

The data included in this report are the results from an entry into the AFRL Vertical Wind Tunnel using the lightweight ICE 101 rotary balance model. To isolate regions in the angle of attack – sideslip domain where the aerodynamic responses changed discontinuously with both those variables and control surface deflections, a test matrix was developed to have more finely-resolved increments in these variables than typically found in wind tunnel tests. These data were then reviewed for changes in discontinuity locations in the angle of attack – sideslip plane and for conditions where the aerodynamic responses appeared to be nonlinear functions of the control surface deflection angle. The conduct of this test was as described in the following section, which is followed by a limited discussion and summary of the results. The complete data set is found in the Appendices.

Although these data are useful in and of themselves, their primary use will be in guiding test matrix formulation for the testing of a geometrically-identical model with remotely-actuated control surfaces. In this test, the transient aerodynamic responses to control surface deflections will be measured in an effort to determine the correlation to control surface deflections, including nonlinearities in both time and surface deflection angle.

2.0 Experimental Procedures

This wind tunnel test was conducted in the AFRL Vertical Wind Tunnel located at Wright-Patterson AFB, OH. This facility is a closed-loop, open test section facility with a relatively low freestream turbulence level.

This test used the static capabilities of the VWT's Multi-Axis Test Rig. This rig is a framework which minimizes interference effects while allowing displacements in angle of attack and sideslip as well as wind-axis rotary and body-axis harmonic motion. A photograph of the MAT rig with the ICE lightweight model is shown in Figure 3. The MAT rig is fully described in Reference 8.

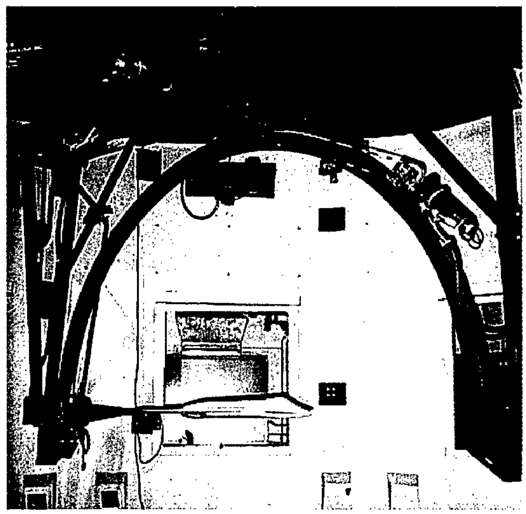

Figure 3 The ICE 101 Lightweight Model in the VWT

The lightweight ICE 101 rotary balance model was used as the test body. Constructed of fiberglass laid over a foam core and reinforced by balsa wood and plywood, this model is sufficiently light as to avoid imparting significant inertial loads during rotary or forced-oscillation testing at rates scaled to model dimensions and freestream velocity, yet is strong enough not to yield at dynamic pressures of 5 psf and stiff enough not to deform during dynamic testing. This model also has movable control surfaces held in place by rods and set screws, which (with the exception of the SSD's which were fixed at neutral or maximum deflection only) may be set at any angle between their maximum deflection angles. Deflection angles were set using templates fit to each control surface.

These experiments were conducted at a wide range of angle of attack and sideslip combinations, as detailed in Table 1. All data were acquired using a freestream dynamic pressure of 3 psf, which translates to an approximate freestream velocity of 50 fps (dependent on test section conditions) and a Reynolds number of 830,000 based on root chord. As is noted in Table 1, a portion of these data were acquired at sideslip angles of –20° to 0°, but to simplify their presentation they will be presented with the remaining data using positive sideslip angles. To convert these data, the sideslip angle, rolling moment coefficient and yawing moment coefficients were multiplied by –1, in following with anti-symmetry.

Table 1 Control Surface Deflection Angles

Control Surface	Deflection Angles (left / right)	β*
Baseline (all surfaces neutral)	n/a	-20°:2°:20°
Leading-Edge Flap	10/0	-6°:2°:20°
	30/0	-6°:2°:20°
	0/10	-6°:2°:20°
	0/30	-6°:2°:20°
	30/30	-6°:2°:20°
Pitch Flap	30/30	-6°:2°:20°
	-30/-30	-6°:2°:20°
Elevon	30/0	-6°:2°:20°
	-30/0	-6°:2°:20°
	0/30	-6°:2°:20°
	0/-30	-6°:2°:20°
	-30/30	-20°:2°:20°
All-Moving Tips	-10/0	-20°:2°:20°
	30/0	-20°:2°:20°
	60/0	-20°:2°:20°
	60/30	-20°:2°:20°
Spoiler	60/0	-20°:2°:20°
	60/60	-6°:2°:20°
Spoiler / Slot Deflector	60/0	-20°:2°:20°
	60/60	-6°:2°:20°

* - all data acquired for $\alpha = (0°:5°:45°)$

3.0 Results

The complete dataset from this wind tunnel entry may be found in the Appendices. A small subset of these data are discussed below. All of the cases presented in this section are examples of data which show a significant alteration of the nonlinear behavior and/or a change in the apparent critical state location as brought about by deflection of a control surface. However, in most of the conditions investigated the aerodynamic response was altered by a simple linear increment.

In the following discussion, the control surface deflection angles will be presented in the form *m*/*n*. In this format, *m* is the deflection of the left and *n* the right control surface. All deflections are given in degrees, with the free edge (AMT trailing edge) deflected downward being positive. Which of the control surfaces are being discussed will be listed immediately prior to the ratio or will be obvious from context as only one control surface pair was deflected at a time.

3.1 Baseline Data

Figure 4 – 8 display normal force, pitching moment, rolling moment and yawing moment data in coefficient form for the ICE 101 lightweight model with all control surfaces at their undeflected locations. In Figure 4 normal-force coefficient data is shown as a function of angle of attack for $\beta = 0°$ and $10°$. Although these data are clearly nonlinear functions of angle of attack, they exhibit no obvious signs of containing discontinuities. However, the slope of these data change sign at $\alpha \approx 35°$, which is associated with the loss of leading-edge suction on delta wing planforms. The disappearance of this structure would be a bifurcation in the flow field topology and hence would likely be a critical state.[6]

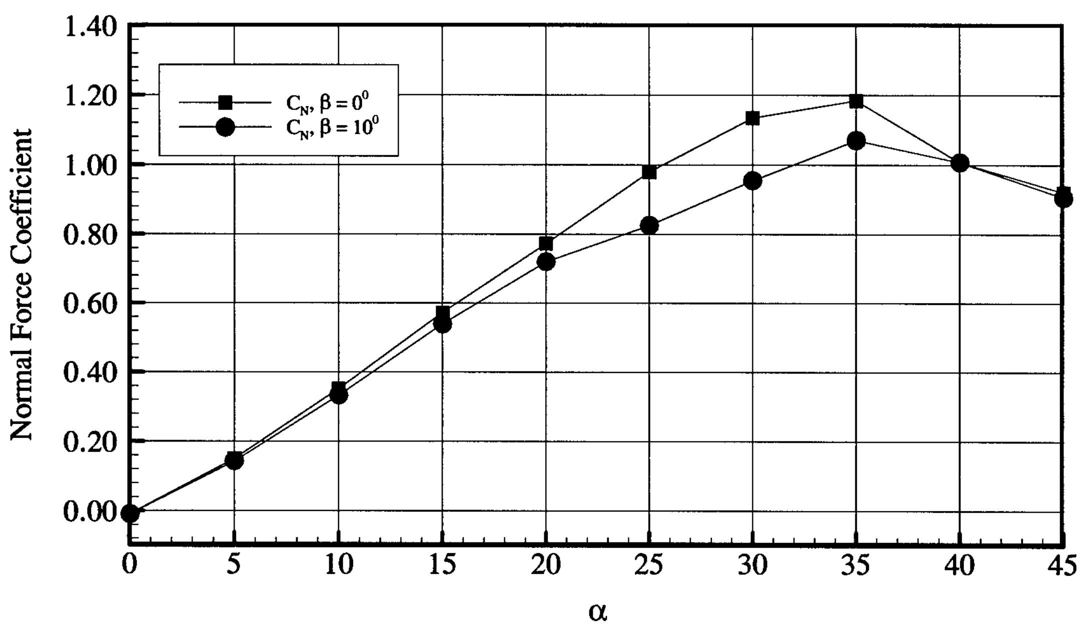

Figure 4 Normal Force Coefficient as a Function of Angle of Attack, No Control Deflections, $\beta = 0°$ and $10°$

Figures 5 and 6 present pitching-moment, rolling-moment and yawing-moment coefficient as functions of angle of attack for $\beta = 0°$ and $10°$, respectively. These data contain more clear indications of the presence of critical states. In particular, pitching-moment-coefficient data in Figure 5 changed slope at $\alpha = 10°$, $30°$ and $40°$; all three moments shown in Figure 6 exhibited similar changes in slope at several different angles of attack. Obviously, a mere change in slope does not mean a critical state was present, since continuous functions may easily fit these data. However, previous results strongly suggest that at least some of these locations were critical states, the sparseness of the data precluding a definitive statement.

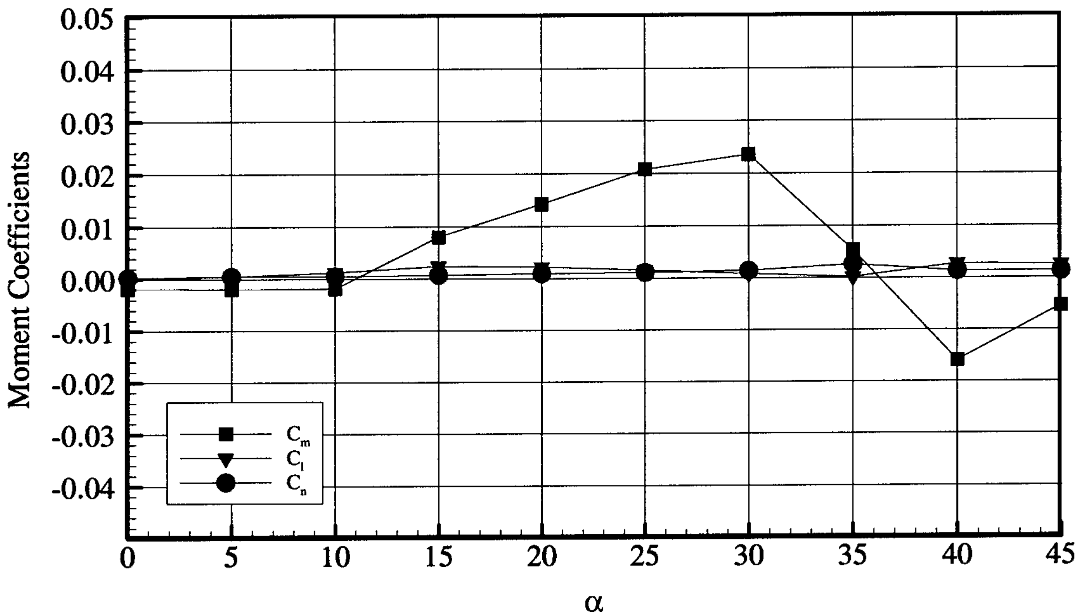

Figure 5 Pitching-Moment, Rolling-Moment and Yawing-Moment Coefficients as a Function of Angle of Attack, No Control Deflections, $\beta = 0°$

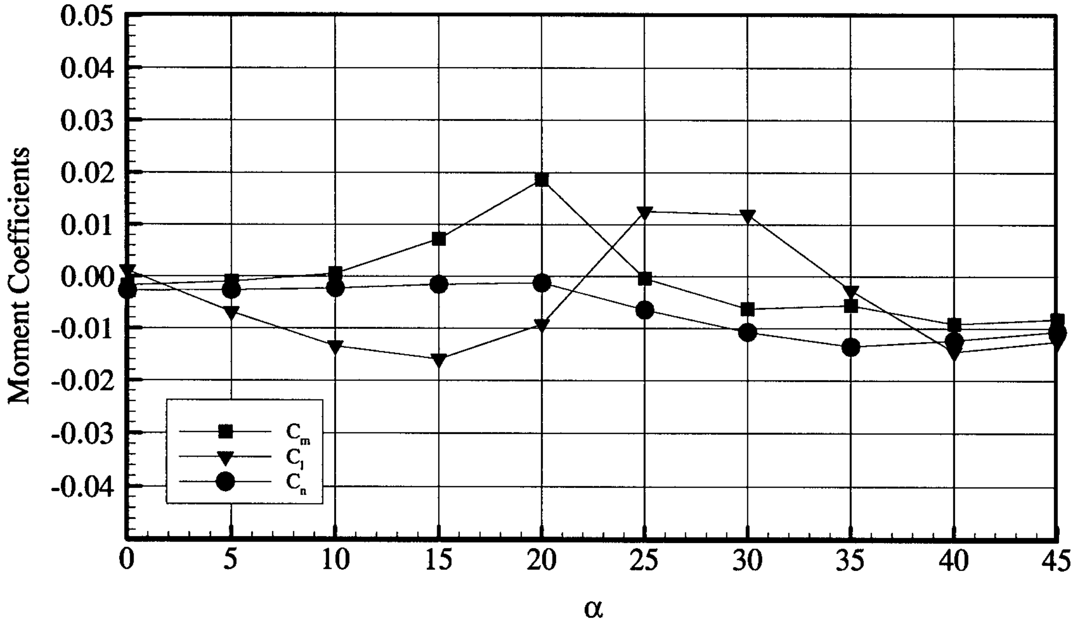

Figure 6 Pitching-Moment, Rolling-Moment and Yawing-Moment Coefficients as a Function of Angle of Attack, No Control Deflections, $\beta = 10°$

Finally, Figures 7 and 8 present the same moment coefficients but as functions of sideslip angle for $\alpha = 20°$ and 25°. The data contained in these two figures demonstrate the magnitude of change a 5° increase in angle of attack can cause in the aerodynamic loading. The largest change occurred in pitching moment, with a large change in magnitude occurring between $\beta = 8°$ and 10°. Such a large magnitude shift was observed in the 65° pure delta wing data, associated with the crossing of leading-edge vortex burst across the leeward trailing edge.[3,6] The character of the rolling moment coefficient also changed, indicating a large asymmetry in the flowfield formed between $\alpha = 20°$ and 25°. Such an asymmetry would also be consistent with asymmetric vortex burst locations. This result was significant as leading-edge-vortex burst has been found to be a significant driving force of the aerodynamic loading of delta wings and the nonlinearity of those loading with respect to both the state variables of flight mechanics and time during dynamic testing.

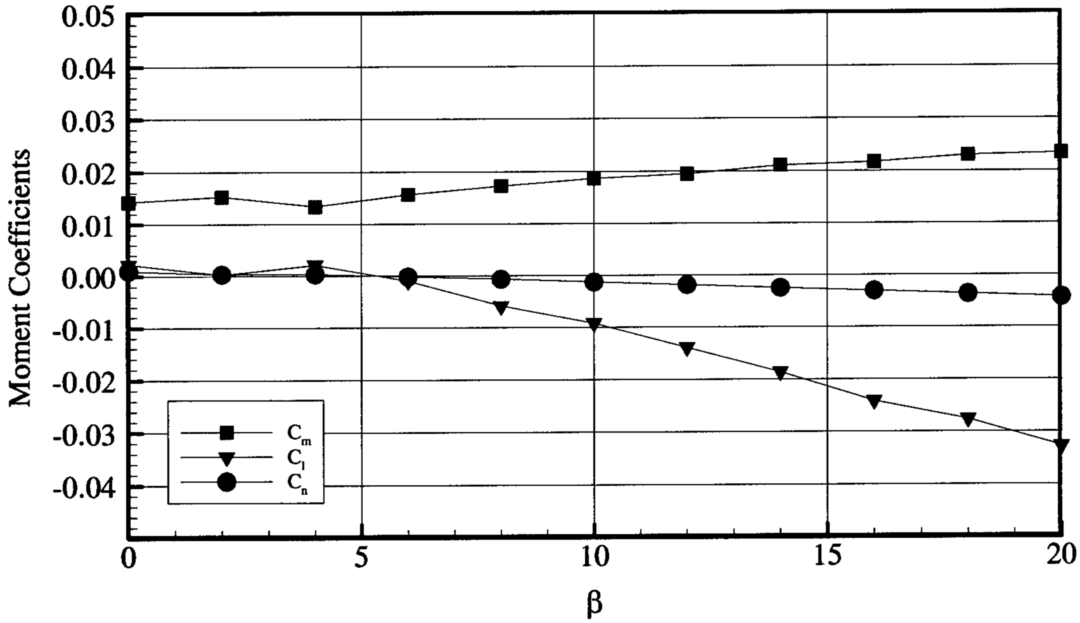

Figure 7 Pitching-Moment, Rolling-Moment and Yawing-Moment Coefficients as a Function of Sideslip Angle, No Control Deflections, $\alpha = 20°$

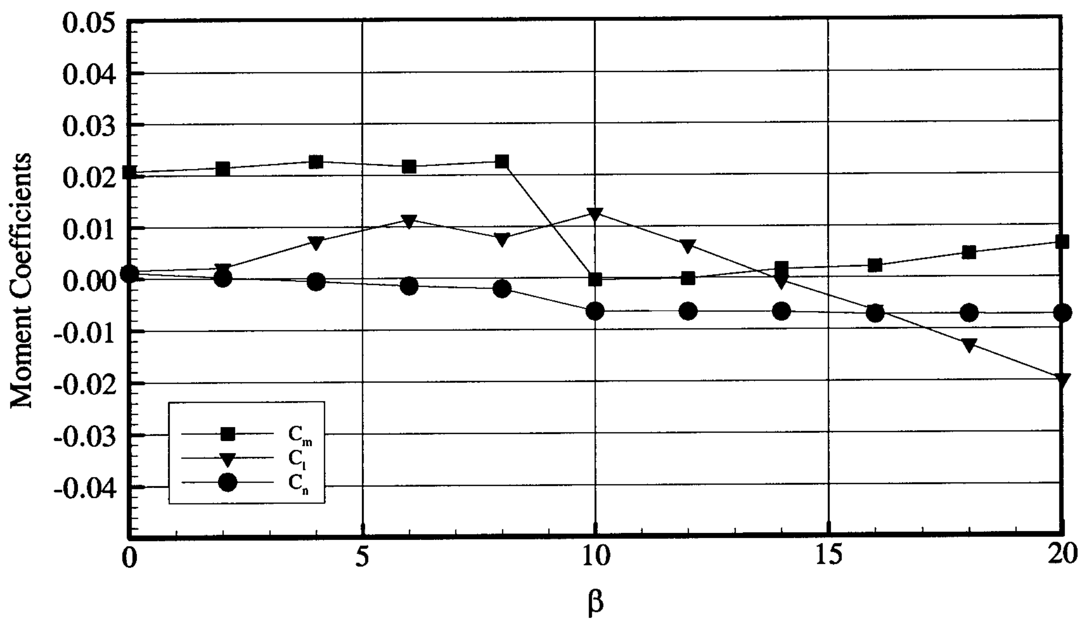

Figure 8 Pitching-Moment, Rolling-Moment and Yawing-Moment Coefficients as a Function of Sideslip Angle, No Control Deflections, $\alpha = 25°$

3.2 LEF

Data acquired with the ICE LEF's configured at different combinations of deflection angles are shown in Figures 9 – 13. These data are presented in their entirety in Appendix A as a function of angle of attack and Appendix B as a function of sideslip.

The data presented in Figure 9 demonstrate that the pitching moment as a function of sideslip at $\alpha = 25°$ with different LEF configurations followed the same trend as for the baseline configuration case except for the 0/30 deflection. These data were of the same order of magnitude and general character for $\beta \leq 8°$, where the data deviated from the overall trend. Indeed, the large change in magnitude – an apparent critical state – which was prevalent in the remaining data between $8° < \beta < 10°$ was replaced by a protracted region of apparently-continuous positive slope. The remaining data showed little variation with LEF deflection with the exception of the 0/10 deflection, indicating little control power throughout the sideslip range for the left LEF. The accompanying rolling-moment-coefficient data (Figure 10) indicate that the apparent critical state which resided at $\beta \approx 10°$ for most of the conditions tested was apparently shifted to $\beta \approx 4° - 6°$ for the 0/30 LEF setting. This shift would explain the transition to the nearly-constant negative slope at the smaller sideslip angle. Finally, yawing-moment-coefficient data (Figure 11), like the pitching-moment-coefficient data, demonstrate that the effect of the apparent critical state at $\beta \approx 10°$ was suppressed by the 0/30 LEF setting.

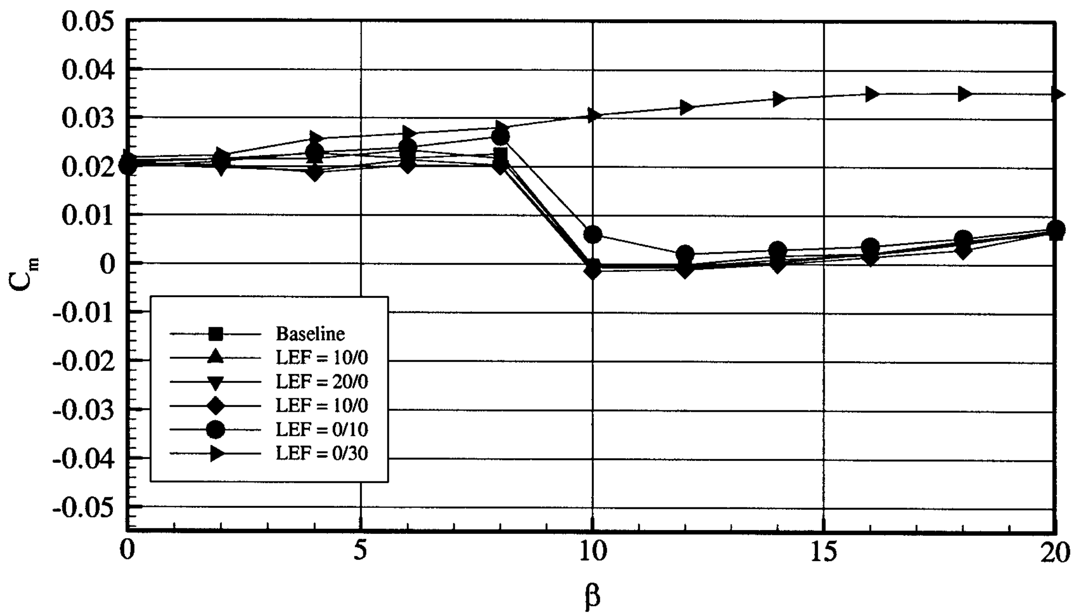

Figure 9 Pitching-Moment Coefficient Data as a Function of Sideslip Angle with LEF Deflections, $\alpha = 25°$

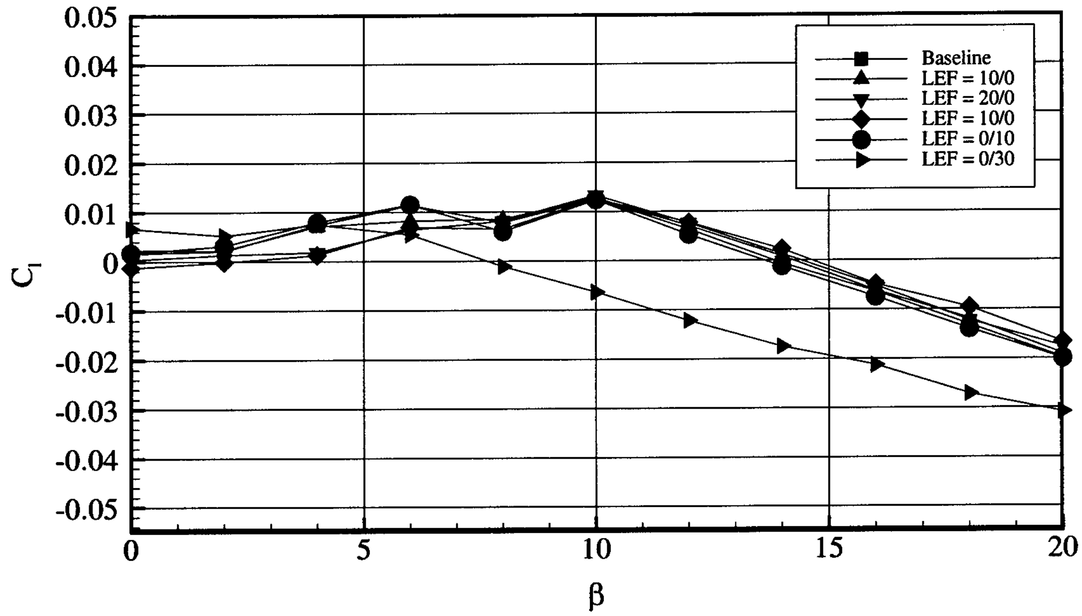

Figure 10 Rolling-Moment Coefficient Data as a Function of Sideslip Angle with LEF Deflections, $\alpha = 25°$

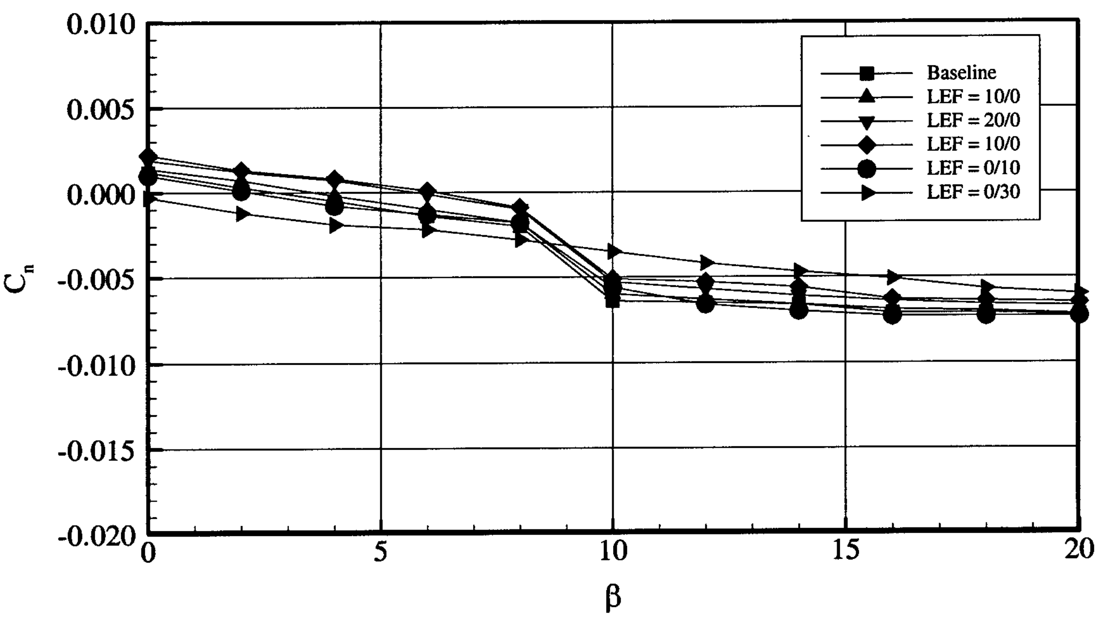

Figure 11 Yawing-Moment Coefficient Data as a Function of Sideslip Angle with LEF Deflections, $\alpha = 25°$

Figures 12 and 13 present rolling-moment and yawing-moment-coefficient data as a function of angle of attack at zero sideslip. As was the case previously, all of the data followed the same trends except for those taken with the leading edge flap configuration 0/30. These data show that between 15° < α < 30° the rolling moment coefficient deviated significantly from the remainder of the data, while yawing moment deviated in trend if not magnitude for all α > 5°.

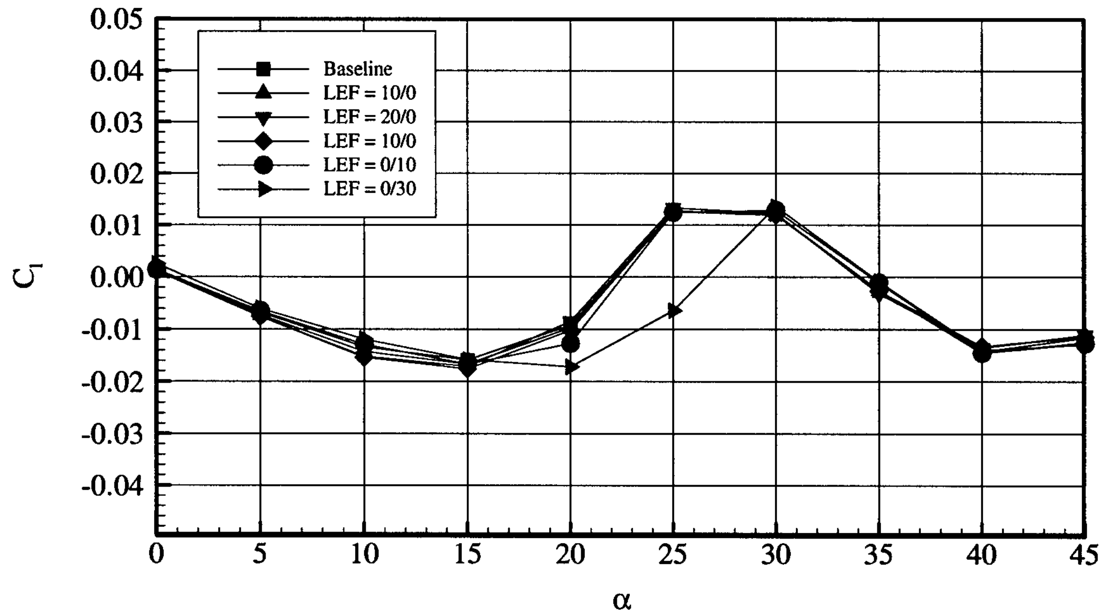

Figure 12 Rolling-Moment Coefficient as a Function of Angle of Attack with LEF Deflections, β = 10°

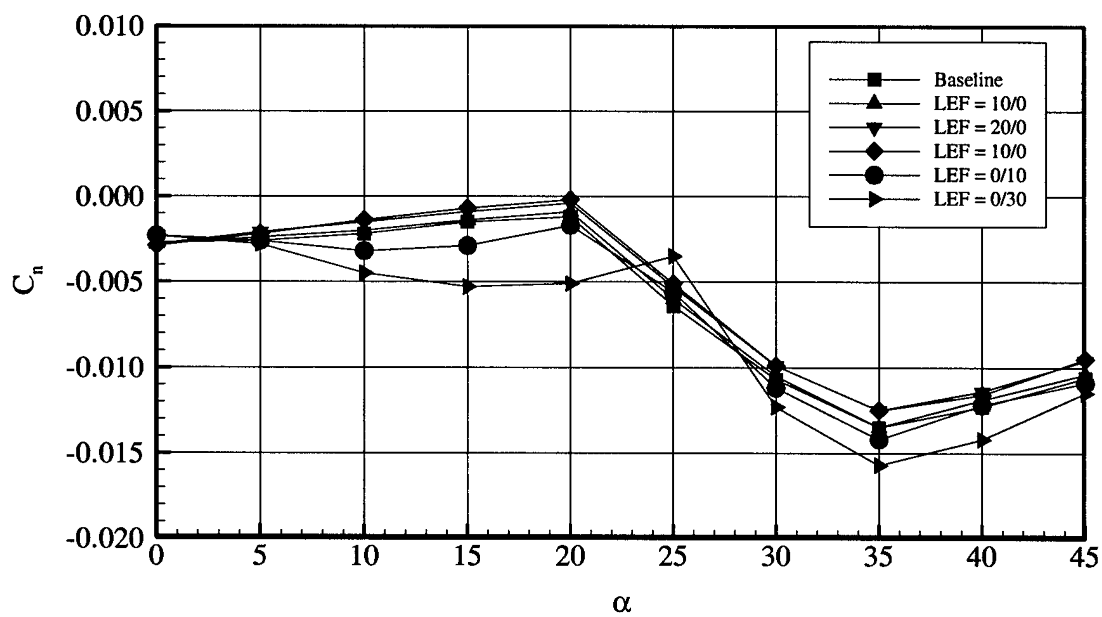

Figure 13 Yawing-Moment Coefficient as a Function of Angle of Attack with LEF Deflections, β = 10°

3.3 TEF

Data acquired with the ICE TEF's configured at different combinations of deflection angles are shown in Figures 14 – 16. These data are presented in their entirety in Appendix C as a function of angle of attack and Appendix D as a function of sideslip.

The pitching-moment-coefficient data in Figure 14 indicate that the critical state at $\beta \approx 10°$, $\alpha = 25°$, was shifted by deflections of the trailing-edge flaps. TEF deflections of 0/-30 and –30/30 appeared to shift this critical state to greater sideslip angles (between 10° and 12°), while a deflection of 30/0 appeared to shift the large decrement to a lesser sideslip angle (between 6° and 8°). Furthermore, a deflection of 0/30 caused the decrement to increase in total magnitude but lessen in apparent slope, with the total decrease in pitching moment occurring between $\beta \approx 8°$ and 12°. Whether this result indicates the suppression of the critical state, a splitting of the effect into a greater number of critical states or some other alteration of the phenomenon could not be determined without additional data.

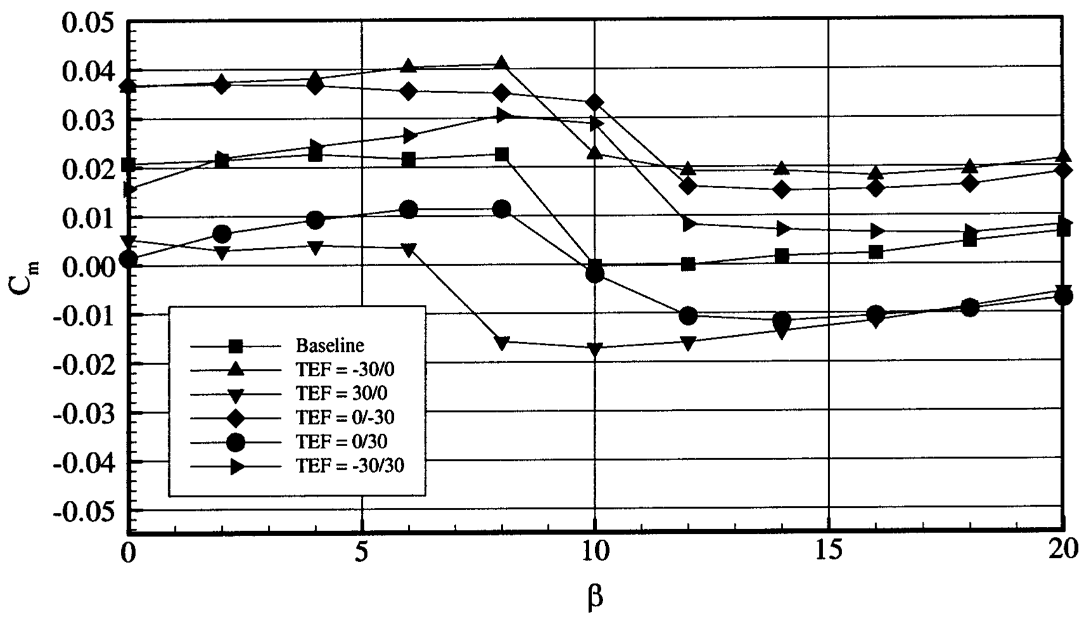

Figure 14 Pitching-Moment Coefficient as a Function of Sideslip Angle with TEF Deflections, $\alpha = 25°$

Pitching- and rolling-moment-coefficient data acquired at $\beta = 10°$ are shown as a function of sideslip in Figures 15 and 16, respectively. In these data, the TEF deflections of 0/-30 and –30/30 appear to have shifted the respective maxima from $\alpha \approx 20°$ to approaching 25°. The trends of the remaining data were comparable.

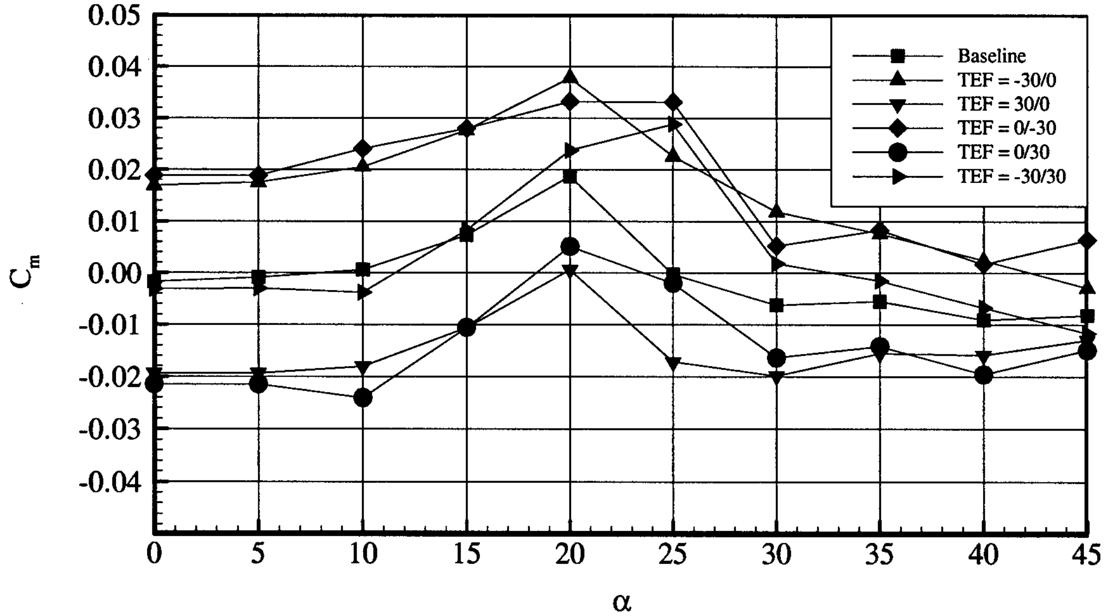

Figure 15 Pitching-Moment Coefficient as a Function of Angle of Attack with TEF Deflections, β = 10°

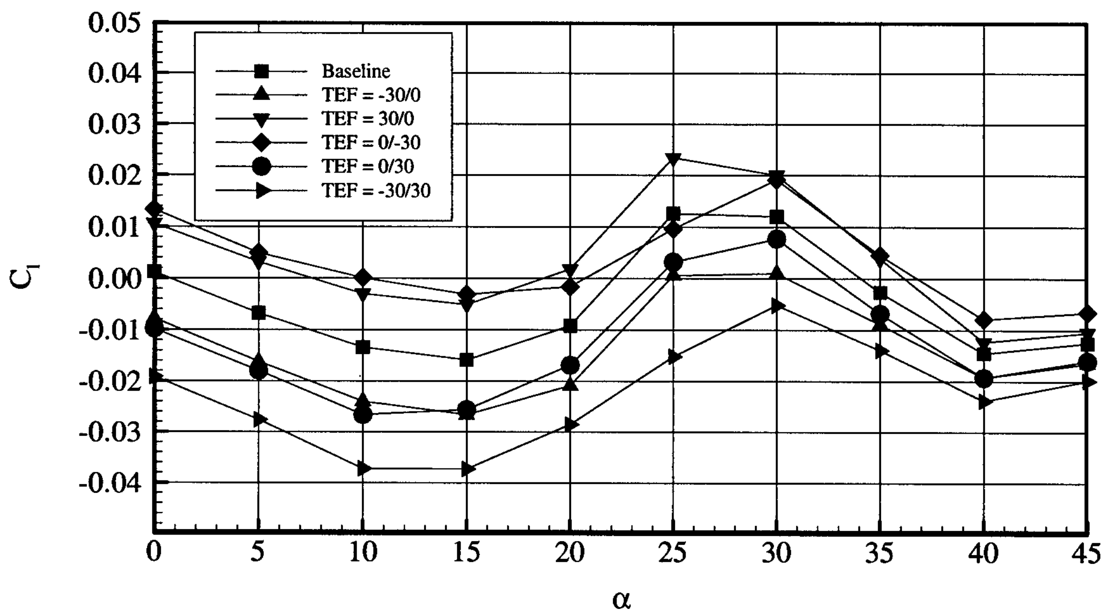

Figure 16 Rolling-Moment Coefficient as a Function of Angle of Attack with TEF Deflections, β = 10°

3.4 PF

Data acquired with the ICE PF's configured at different combinations of deflection angles are shown in Figures 17 – 19. These data are presented in their entirety in Appendix E as a function of angle of attack and Appendix F as a function of sideslip.

Pitching-moment-coefficient data acquired at $\alpha = 25°$ are shown as a function of sideslip angle in Figure 17. These data show that the large decrement in pitching-moment coefficient which occurred in the baseline data between $\beta = 8°$ and $10°$ was spread out over a much larger range of sideslip angles for a -30/-30 pitch flap setting. Whether this apparent discontinuity had been suppressed or lessened in magnitude was not immediately discernable without additional data. The 30/30 pitch flap setting, on the other hand, displaced the apparent discontinuity to between $\beta = 10°$ and $12°$.

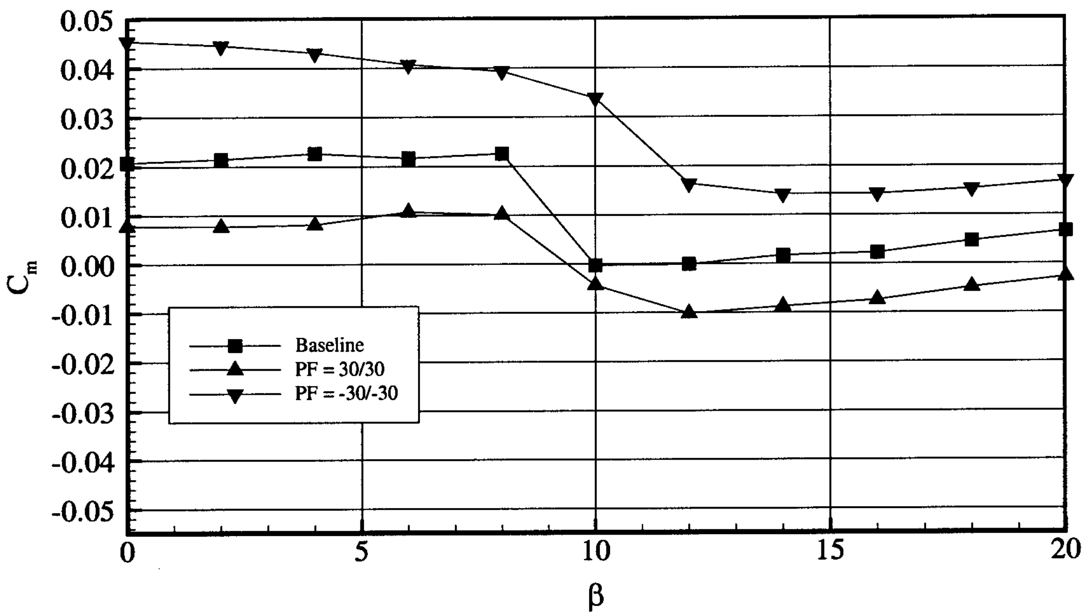

Figure 17 Pitching-Moment Coefficient as a Function of Sideslip Angle with PF Deflections, $\alpha = 25°$

Rolling-moment-coefficient data, both as functions of sideslip angle (Figure 18) and angle of attack (Figure 19) show that the -30/-30 pitch flap setting suppressed local peaks in these data. Similar to the pitching-moment-coefficient data, it was not clear whether one or more critical states had been averted, shifted, or some combination therein.

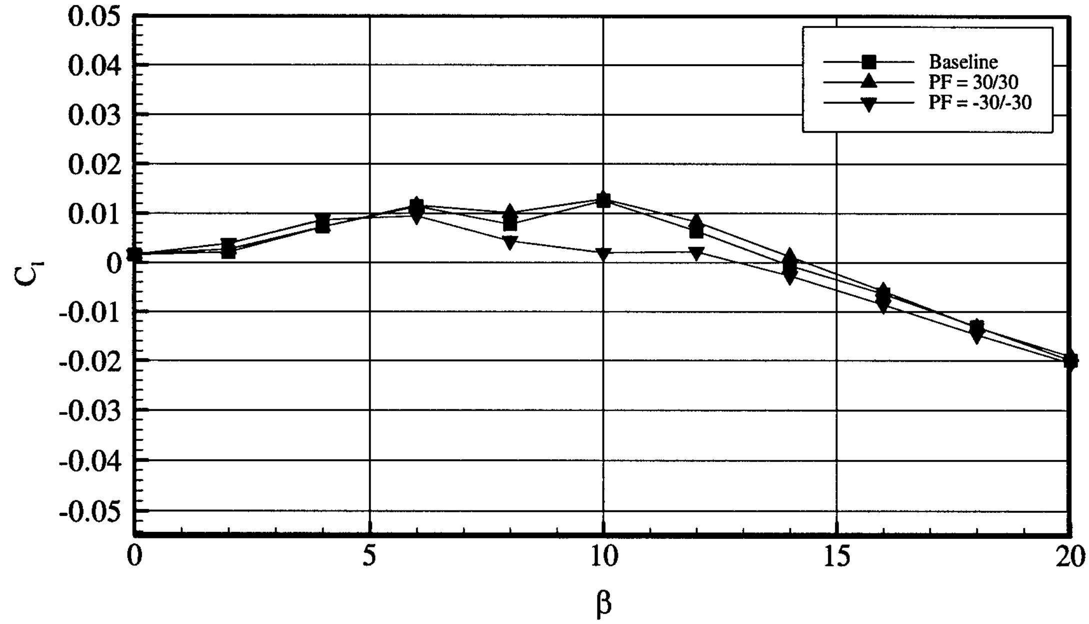

Figure 18 Rolling-Moment Coefficient as a Function of Sideslip Angle with PF Deflections, $\alpha = 25°$

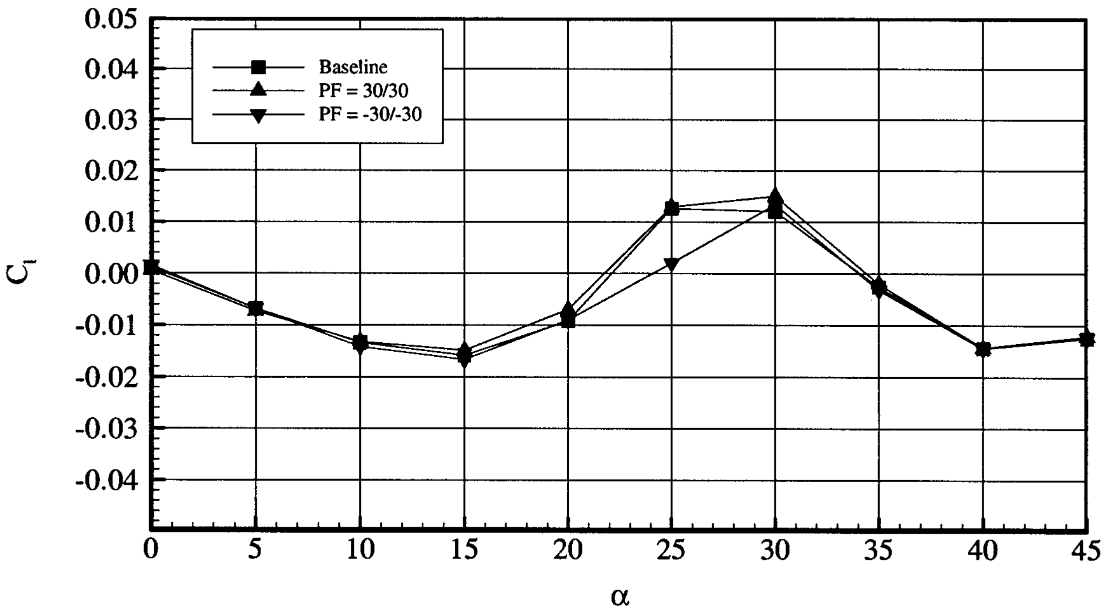

Figure 19 Rolling-Moment Coefficient as a Function of Angle of Attack with PF Deflections, $\beta = 10°$

3.5 AMT

Data acquired with the ICE AMT's configured at different combinations of deflection angles are shown in Figures 20 and 21. These data are presented in their entirety in Appendix G as a function of angle of attack and Appendix H as a function of sideslip.

Figure 20 presents one of the few cases where an effect with significant nonlinear if not discontinuous behavior could be found at low sideslip and angle of attack. In these data for a constant 6° sideslip, the pitching-moment coefficient remained relatively flat in the baseline configuration and with the all-moving tips deflected to –10/0 for $\alpha \leq 10°$, but the data had a positive slope for deflections of 30/0, 60/0 and 60/60. All deflected-AMT data beyond $\alpha = 10°$ followed the baseline data trend, perhaps indicating a transition in the nature of the pitching moment's dependence on AMT deflection.

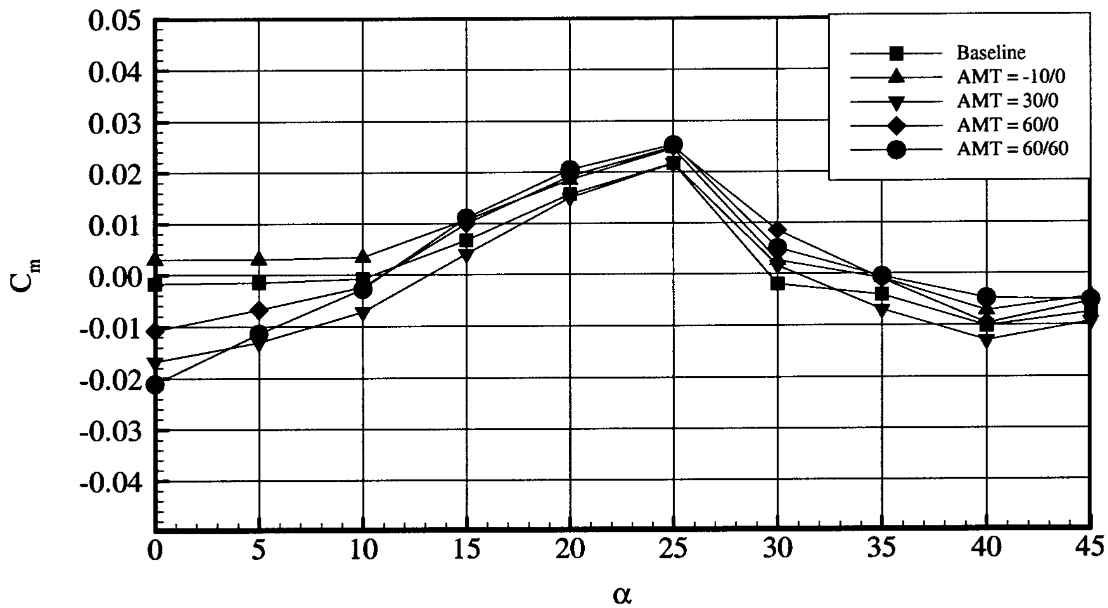

Figure 20 Pitching-Moment Coefficient as a Function of Angle of Attack with AMT Deflections, $\beta = 6°$

Figure 21 presents rolling-moment-coefficient data as a function of sideslip angle at a constant $\alpha = 25°$. These results show that AMT deflections of 60/0 and 60/60 caused a deviation in the trend of these data away from that of the baseline and other AMT deflections for $4° < \beta < 10°$. This alteration of the data trend may be indicative of a suppression of a critical state at $\beta \approx 2°$ or may be the result of a nonlinear dependence of rolling moment on AMT deflection.

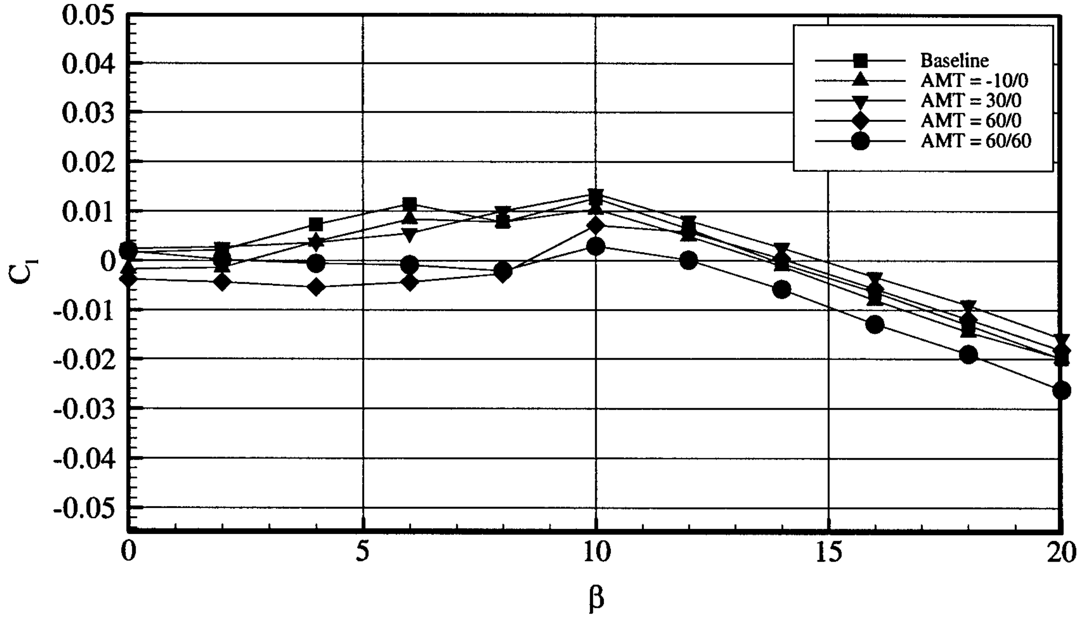

Figure 21 Rolling-Moment Coefficient as a Function of Sideslip Angle with AMT Deflections, $\alpha = 25°$

3.6 Spoiler

Data acquired with the ICE spoilers configured at different combinations of deflection angles are shown in Figures 22 – 24. These data are presented in their entirety in Appendix I as a function of angle of attack and Appendix J as a function of sideslip.

The pitching-moment-coefficient and rolling-moment-coefficient data shown in Figures 22 and 23 indicate that the deployment of the spoiler(s) tended to delay the encountering of the apparent critical states. In the pitching-moment-coefficient data, the discontinuity at $\beta \approx 8° - 10°$ and $\alpha = 25°$ (Figure 22) and the peak at $\alpha \approx 20°$ for $\beta = 10°$ were delayed by spoiler deployment, while the peak in rolling-moment coefficient between $\alpha = 25°$ and $30°$ for $\beta = 10°$ was delayed to closer to 30°.

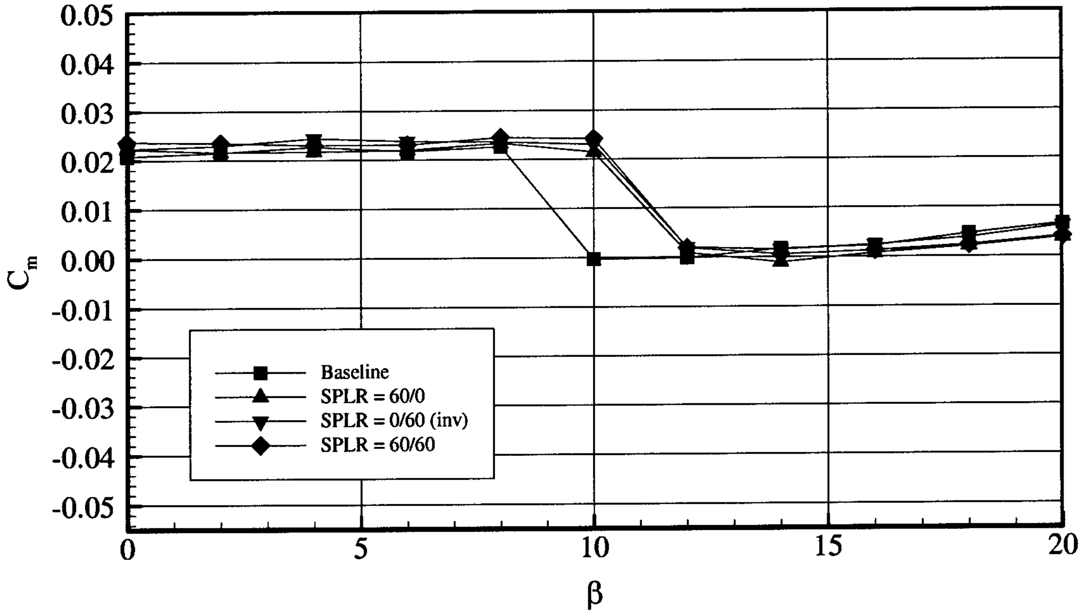

Figure 22 Pitching-Moment Coefficient as a Function of Sideslip Angle with Spoiler-Alone Deflections, $\alpha = 25°$

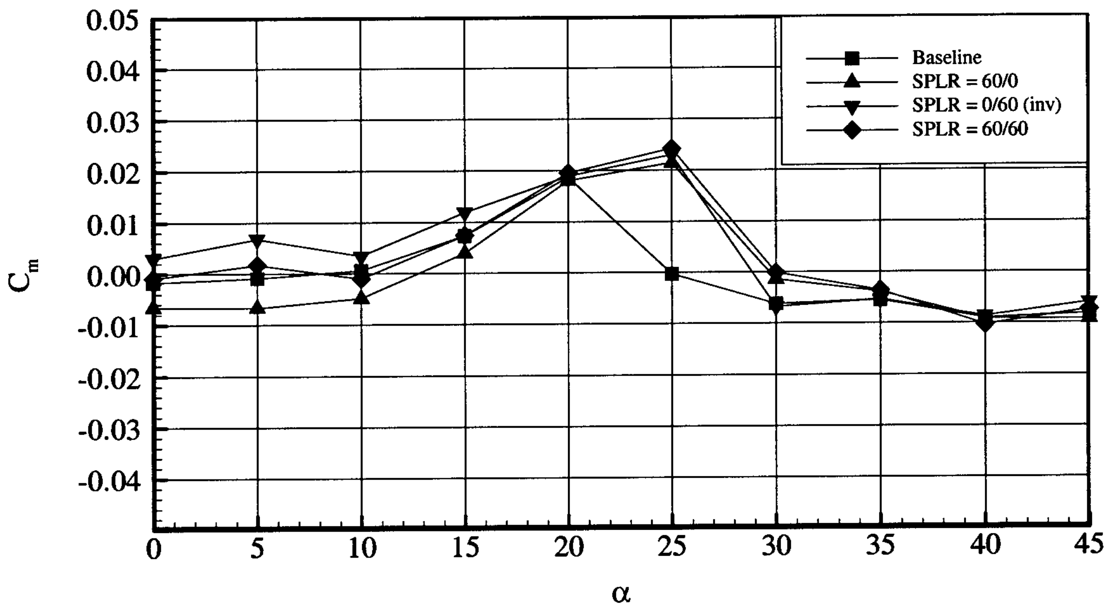

Figure 23 Pitching-Moment Coefficient as a Function of Angle of Attack with Spoiler-Alone Deflections, $\beta = 10°$

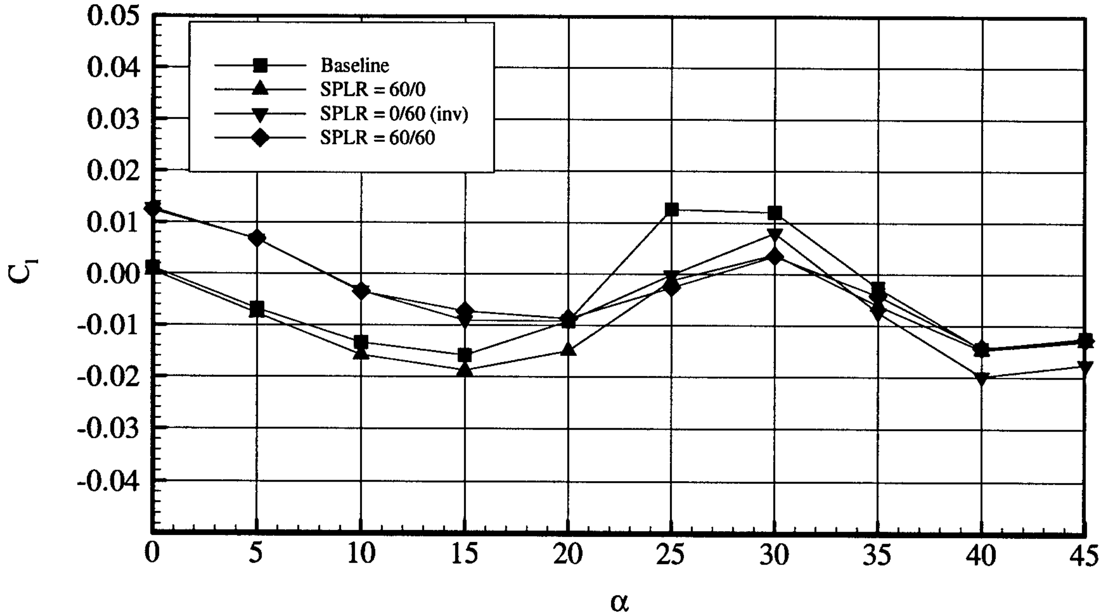

Figure 24 Rolling-Moment Coefficient as a Function of Angle of Attack with Spoiler-Alone Deflections, β = 10°

3.7 SSD

Data acquired with the ICE LEF's configured at different combinations of deflection angles are shown in Figures 25 and 26. These data are presented in their entirety in Appendix K as a function of angle of attack and Appendix L as a function of sideslip.

The pitching-moment-coefficient data shown in Figure 25 indicate that the apparent critical state present in the baseline data at $\beta = 8° - 10°$, $\alpha = 25°$, was delayed to greater sideslip angles and the magnitude of the decrement decreased with SSD deployment. Rolling-moment-coefficient-data shown in Figure 26 indicate that the local maxima found in the baseline configuration data at $\beta = 6°$ and $10°$ were suppressed.

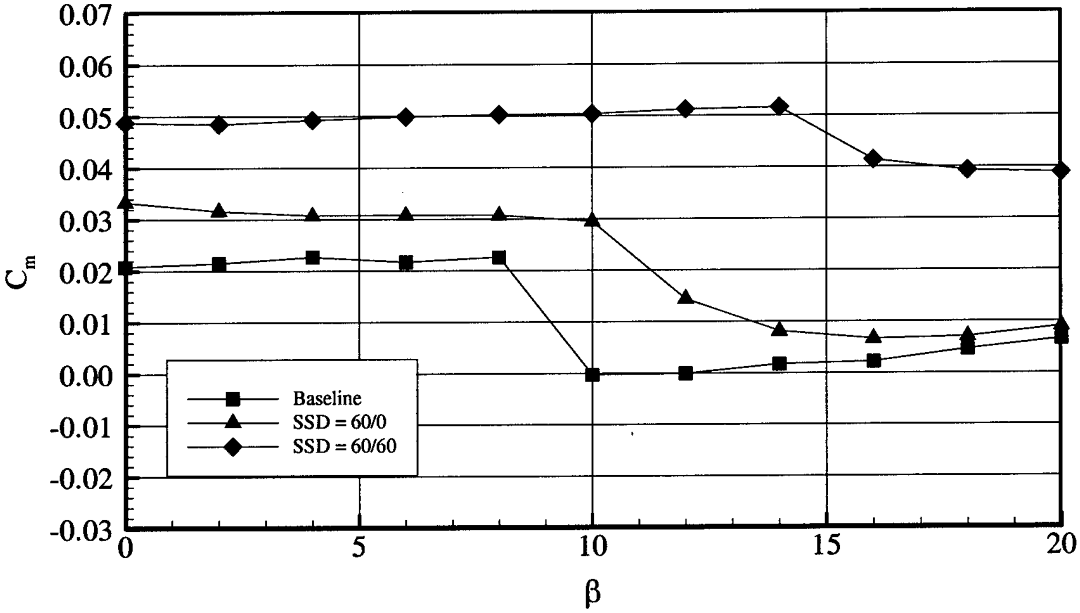

Figure 25 Pitching-Moment Coefficient as a Function of Sideslip Angle with SSD Deflections, α = 25°

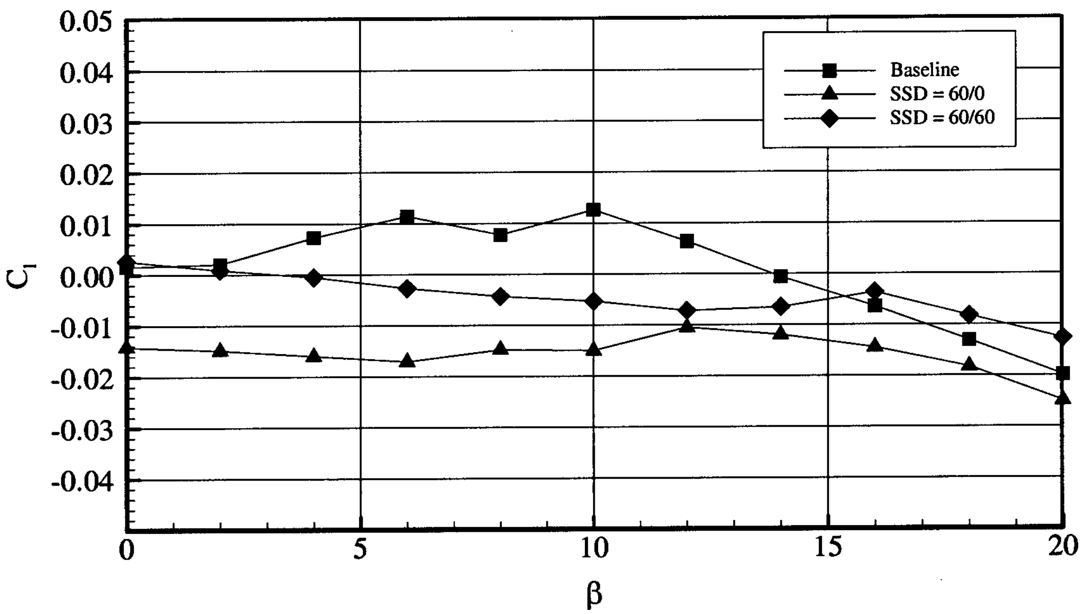

Figure 26 Rolling-Moment Coefficient as a Function of Sideslip Angle with SSD Deflections, α = 25°

4.0 Discussion

Common practice in developing aerodynamic models for the aerodynamic increments provided by control surface deflections is to utilize a derivative coefficient, for example,

$$\Delta C_l = C_{l_{\delta_{AMT}}} * \delta_{AMT}$$

where

$$C_{l_{\delta_{AMT}}} = \frac{dC_l}{d\delta_{AMT}}$$

and δ_{AMT} is the deflection of the AMTs.[9] Proper calculation of the stability derivative, from the linearization from which the stability derivative approach is derived, is to make $C_{l_{\delta_{AMT}}}$ a function of the control surface deflection angle and the remainder of the vehicle state, *i.e.*, α, β, Mach number, *etc.*. Unfortunately, it is not uncommon to simplify these relationships to the greatest extents possible if not forgo the process entirely, and make these coefficients constants with respect to some or all of the state variables. Such a simplification obviously reduces greatly the size of the database required for defining the vehicle's aerodynamic characteristics, and therefore the cost of developing this database.

From the review of the data presented in this report, the hazards in simplifying the aerodynamic model for control surface deflection effects are readily apparent. In these data a number of examples of nonlinear behavior are seen, indicating that at a minimum the control-surface-induced increment was a nonlinear function of the surface deflection magnitude. Furthermore, some instances of apparent discontinuities in the total response was seen to be added, deleted, or shifted with respect to angle of attack and/or sideslip. Obviously, the common practice of simplifying and minimizing the aerodynamic database for control surface deflection effects would cause these important effects to be overlooked, potentially adding significant costs from the need to redesign the flight control law – or possibly the vehicle itself – to correct for these omissions.

Without detailed flow visualization or flow survey data, determining the exact cause for the observed nonlinear and discontinuous behavior of these data is not possible; however, from previous experience a reasonable hypothesis may be generated. As is shown in Figure 27, the ICE 101 model's delta-wing planform generates a strong helical vortex along the leading edge (the leading-edge vortex, or LEV). Based on experience with a generic 65° delta wing,[3] flow field topology bifurcations, such as LEV burst and the formation and bursting of secondary vortex structures, may be anticipated to occur in the ICE 101-generated flow field. These phenomena and other such flow field bifurcations have been shown empirically to be associated with many critical states.[6] Given that deflections of the control surfaces modify the local geometry of the body – and hence the local pressure profiles – the flow field topology can be anticipated to be functions of these deflections as it is a function of the angles of attack and sideslip (and the remainder of the state variables). This modification of the boundary conditions thus alters the dynamical system which defines the occurrence of topological bifurcations, and hence the occurrence of critical states.

Regardless of their exact cause, the manipulation of these nonlinear effects and apparent discontinuities has one important implication: the effects of critical states may be manipulated

through the geometric alteration of the vehicle body. Although this result may be inferred from the copious studies of such phenomena as the effect of blowing on LEV burst point location, these results are direct evidence of the influence control surfaces have on aerodynamic nonlinearity. Further study of this causal relationship ought to lead to more elegant means of controlling these aerodynamic effects, either through tailoring of the control surface deflection schedule or possibly through micro-scale flow control and active wing shaping technology.

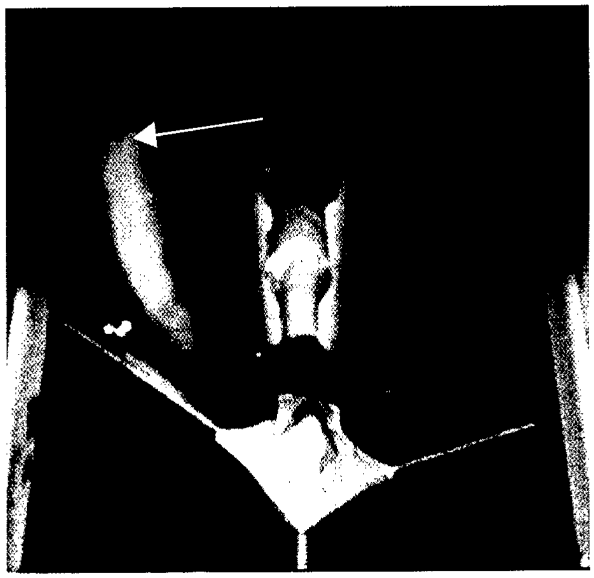

Figure 27 The ICE 101 Model in the SARL Wind Tunnel, Showing the LEV Structure
(Note the presence of LEV burst aft of the trailing edge (arrow).)

5.0 Summary

The data detailed in this report demonstrate the effect which control-surface deflection can have on the nonlinear aerodynamic forces and moments generated by the ICE 101's delta wing planform. Most significantly, a number of instances were found where possible discontinuities found in the baseline-configuration were moved in angle of attack or sideslip angle, or the effect was suppressed through deflection of a control surface. The majority of these instances were isolated to flight conditions centered on $\alpha = 25°$ and / or $\beta = 10°$, leading to the hypothesis that these results may be related to the presence of LEV burst over the planform. However, in the absence of flow field measurements and flow visualization, this hypothesis cannot be tested. In many other instances, few of which were discussed in the body of this report, the aerodynamic force and increments appeared to be nonlinear functions of angle of attack and sideslip angle.

These results are significant from the perspective of flight control since such aerodynamic characteristics are seldom provided for in flight control systems. They also suggest that such nonlinear effects may be manipulated using flow control devises at least on the macroscopic scale.

6.0 References

[1]Dorsett, K.M., and D.R. Mehl, "Innovative Control Effectors (ICE)," WL-TR-96-3043, Wright Laboratories, Wright-Patterson AFB, OH, January 1996.

[2]Dorsett, K.M., S.P. Fears and H.P. Houlden, "Innovative Control Effectors (ICE) Phase II," WL-TR-97-3059, Wright Laboratories, Wright-Patterson AFB, OH, July 1997.

[3]Jenkins, J.E., and E.S. Hanff, "Highlights of the IAR/WL Delta Wing Program," presented at Workshop III – Delta Wings: Unsteady Aerodynamics and Modeling, AIAA Atmospheric Flight Mechanics Conference, 8 August 1995.

[4]Jenkins, J.E., "Nonlinear Aerodynamic Characteristics of a 65 Degree Delta Wing in Rolling Motion: Implications to Testing and Flight Mechanics," AIAA Paper 97-0742, January 1997.

[5]Myatt, J.H., "A Nonlinear Indicial Response Model for the Rolling 65-Degree Delta Wing," AIAA Paper 96-3406, July 1997.

[6]Addington, G.A., The Role of Flow Structure in Determining the Aerodynamic Response of a Delta Wing, University of Notre Dame Ph.D. Dissertation, 1998.

[7]Gilliard, W., "Innovative Control Effectors (Configuration 101) Dynamic Wind Tunnel Test Report: Rotary Balance and Forced Oscillation Tests," AFRL-VA-WP-TR-1998-3043, July 1998.

[8]Hultberg, R. S., "Multi-Axis Test Rig for the AFRL Vertical Wind Tunnel," AFRL-VA-WP-TR-1998-3036, Air Force Research Laboratory, Wright-Patterson AFB, OH, May 1998.

[9]Nelson, Robert C., Flight Stability and Automatic Control, 2nd ed., McGraw-Hill, 1998.

Appendix A Leading-Edge-Flap-Deflection Data as a Function of Angle of Attack

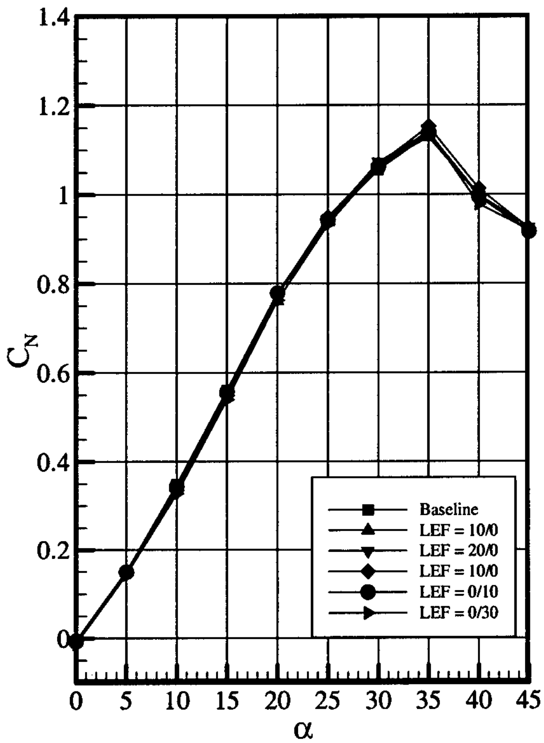

Figure A1a Normal Force Coefficient as a Function of α, β = -6°

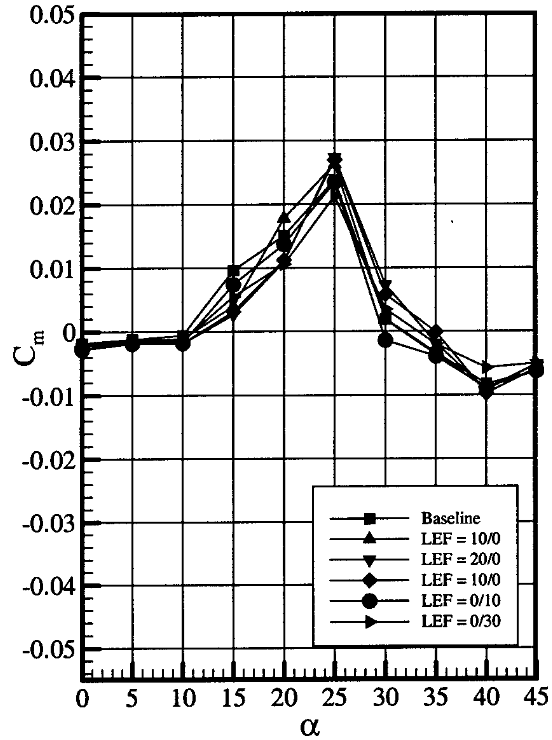

Figure A1b Pitching Moment Coefficient as a Function of α, β = -6°

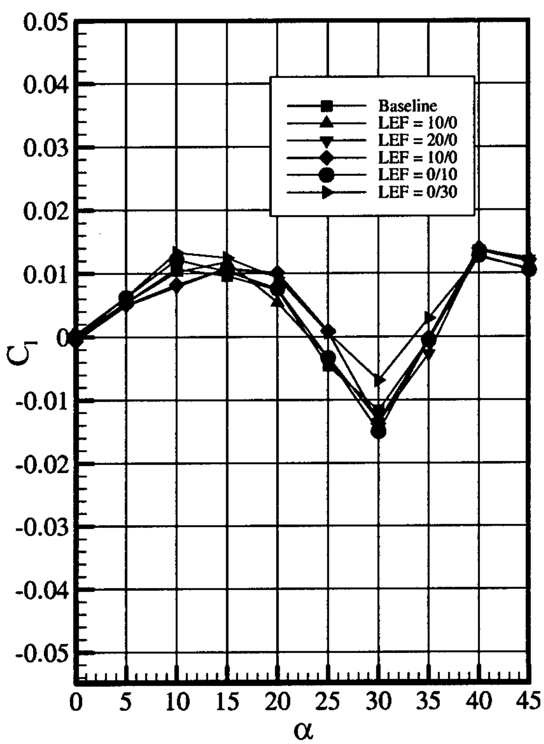

Figure A1c Rolling Moment Coefficient as a Function of α, β = -6°

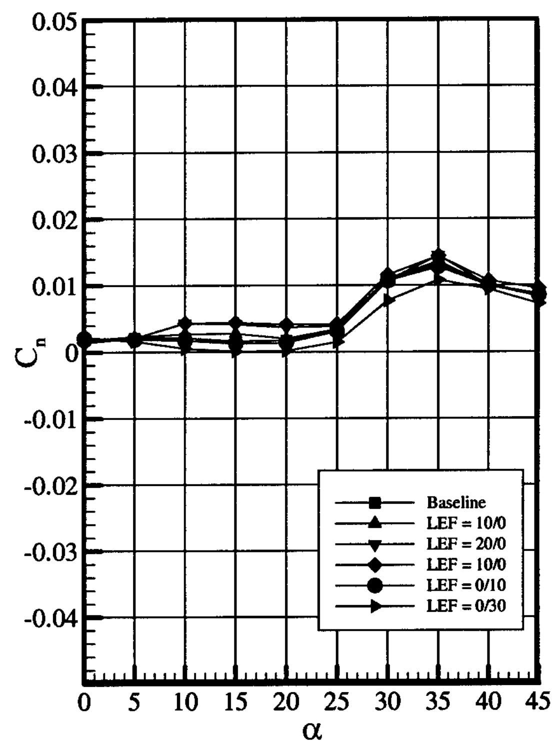

Figure A1d Yawing Moment Coefficient as a Function of α, β = -6°

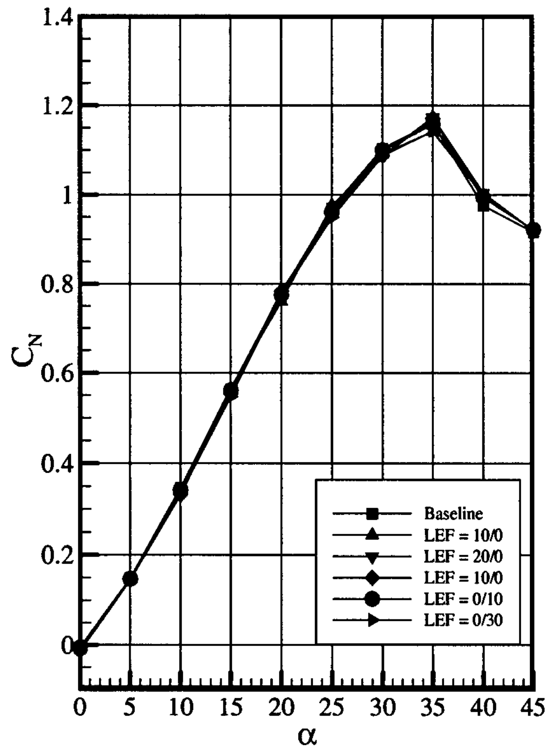

Figure A2a Normal Force Coefficient as a Function of α, β = -4°

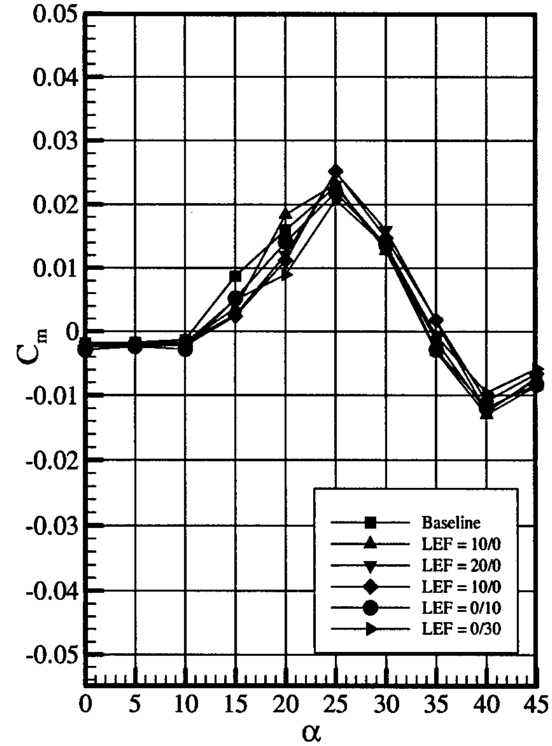

Figure A2b Pitching Moment Coefficient as a Function of α, β = -4°

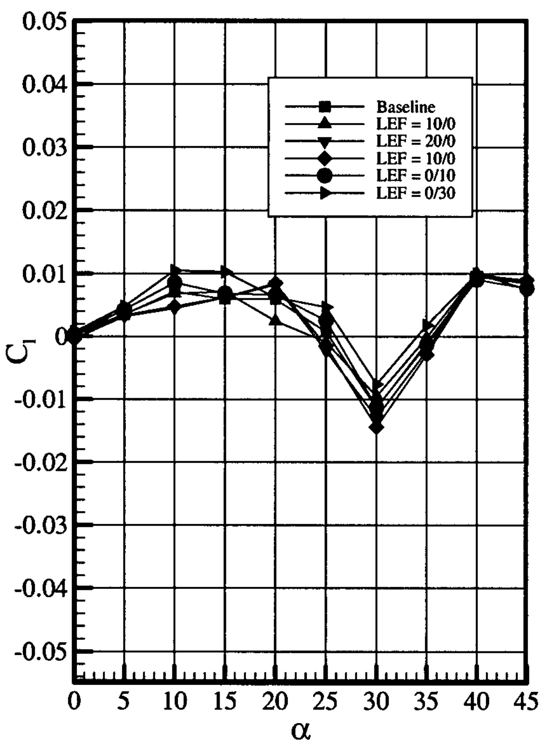

Figure A2c Rolling Moment Coefficient as a Function of α, β = -4°

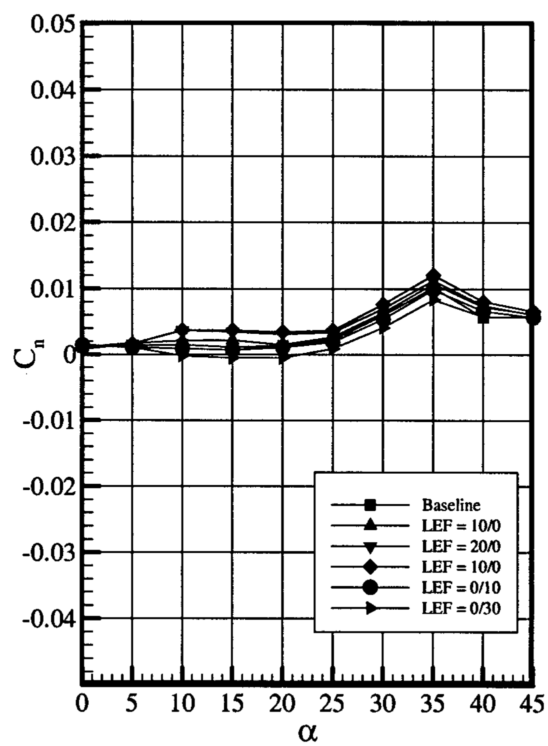

Figure A2d Yawing Moment Coefficient as a Function of α, β = -4°

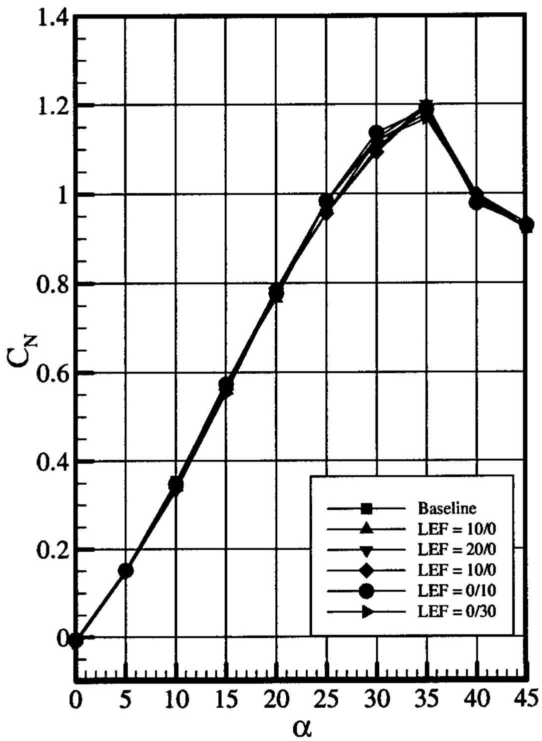

Figure A3a Normal Force Coefficient as a Function of α, $\beta = -2^{\circ}$

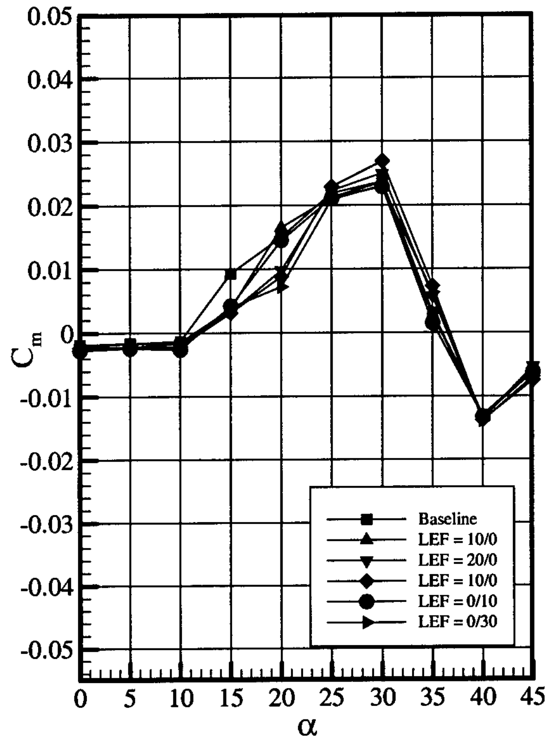

Figure A3b Pitching Moment Coefficient as a Function of α, $\beta = -2^{\circ}$

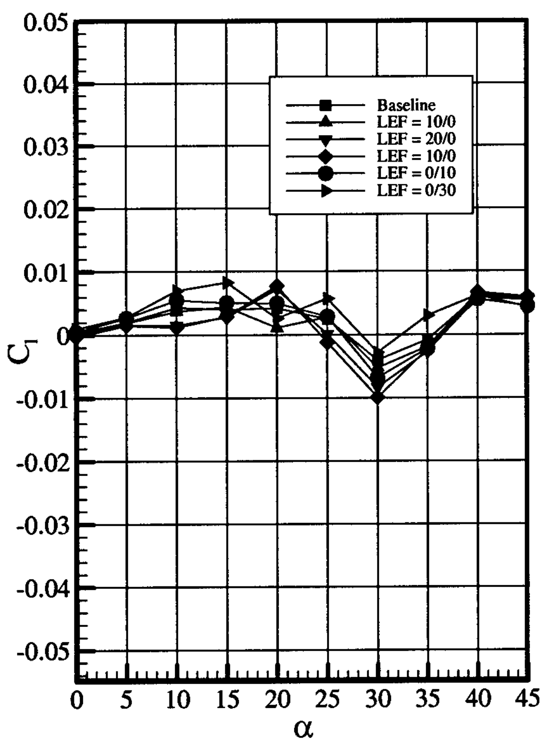

Figure A3c Rolling Moment Coefficient as a Function of α, $\beta = -2^{\circ}$

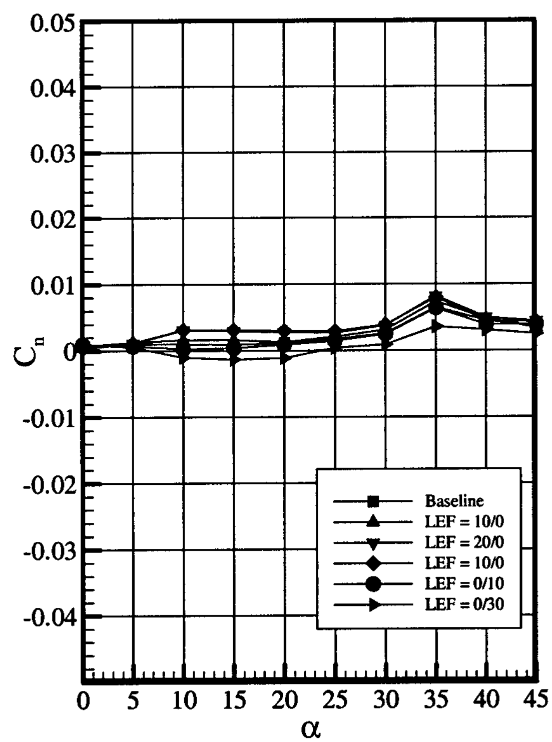

Figure A3d Yawing Moment Coefficient as a Function of α, $\beta = -2^{\circ}$

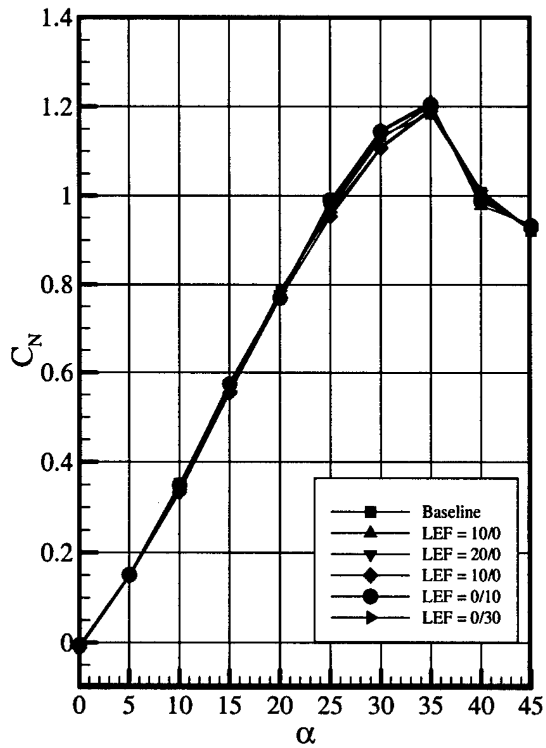

Figure A4a Normal Force Coefficient as a Function of α, β = 0°

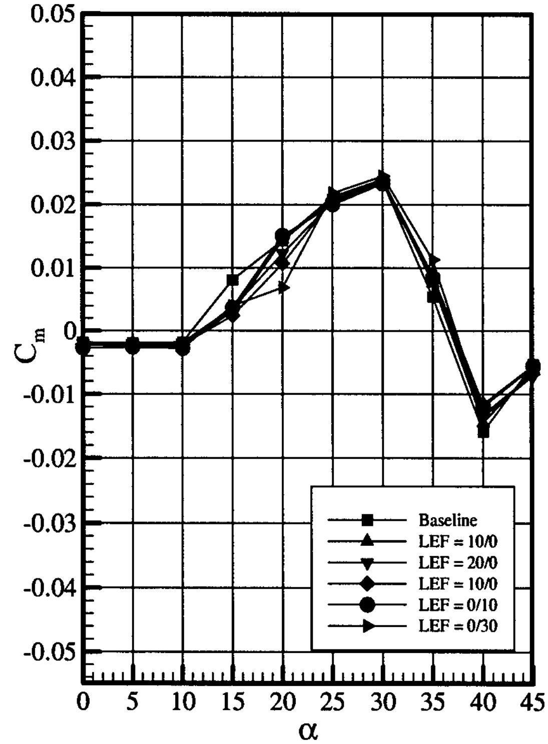

Figure A4b Pitching Moment Coefficient as a Function of α, β = 0°

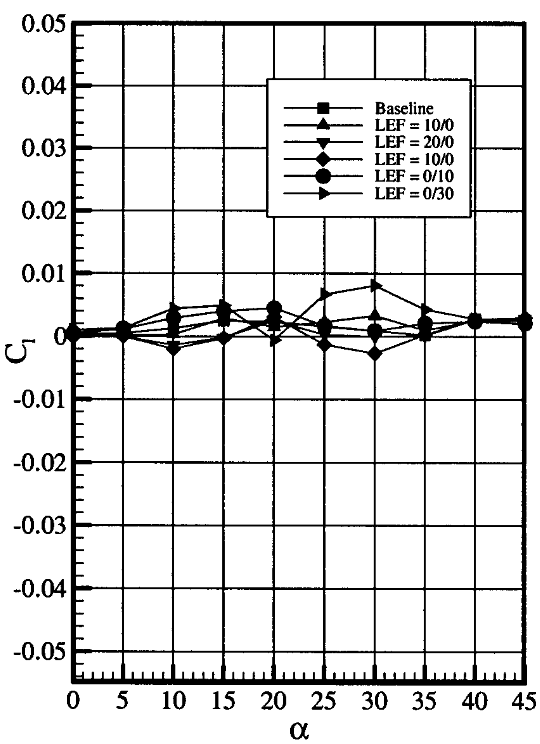

Figure A4c Rolling Moment Coefficient as a Function of α, β = 0°

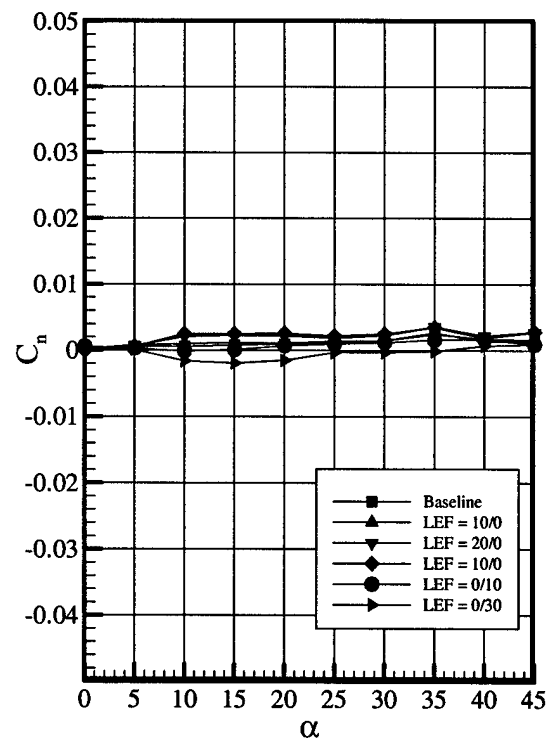

Figure A4d Yawing Moment Coefficient as a Function of α, β = 0°

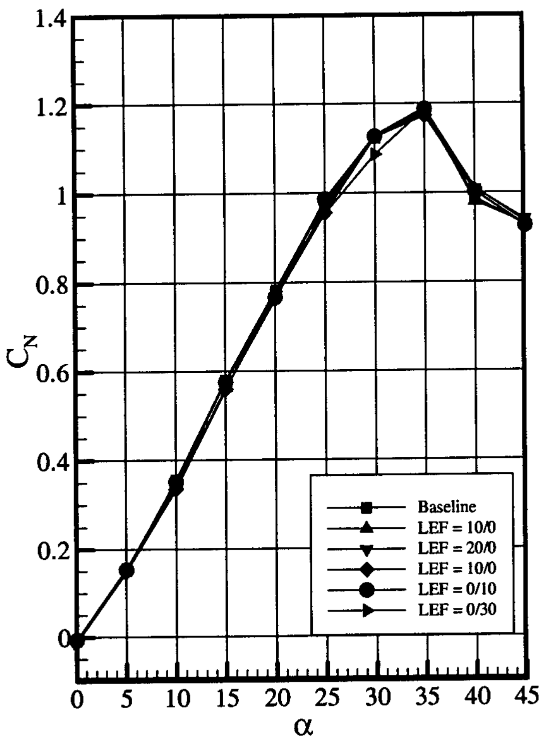

Figure A5a Normal Force Coefficient
as a Function of α, β = 2°

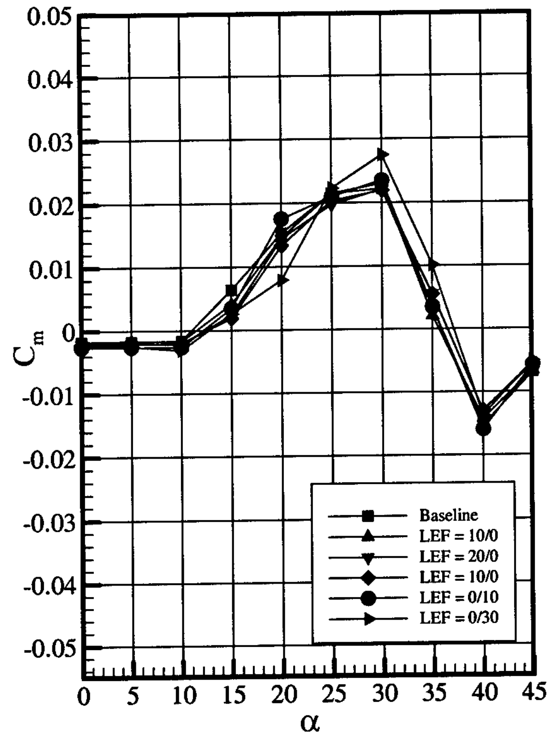

Figure A5b Pitching Moment Coefficient
as a Function of α, β = 2°

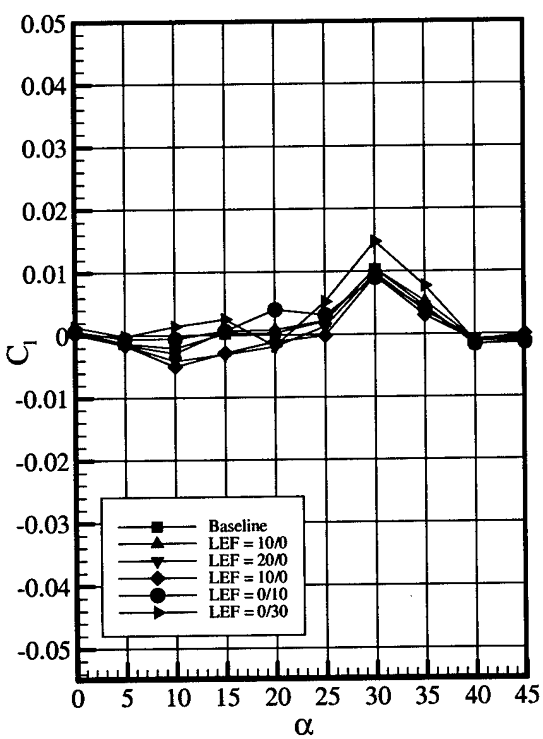

Figure A5c Rolling Moment Coefficient
as a Function of α, β = 2°

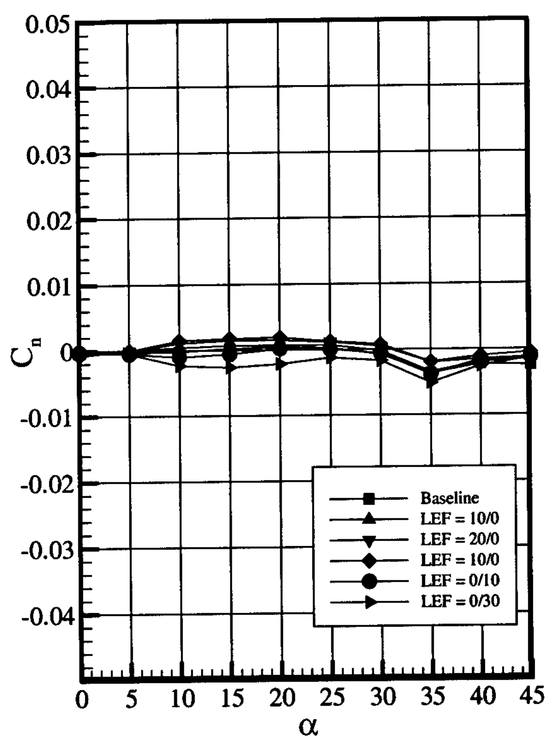

Figure A5d Yawing Moment Coefficient
as a Function of α, β = 2°

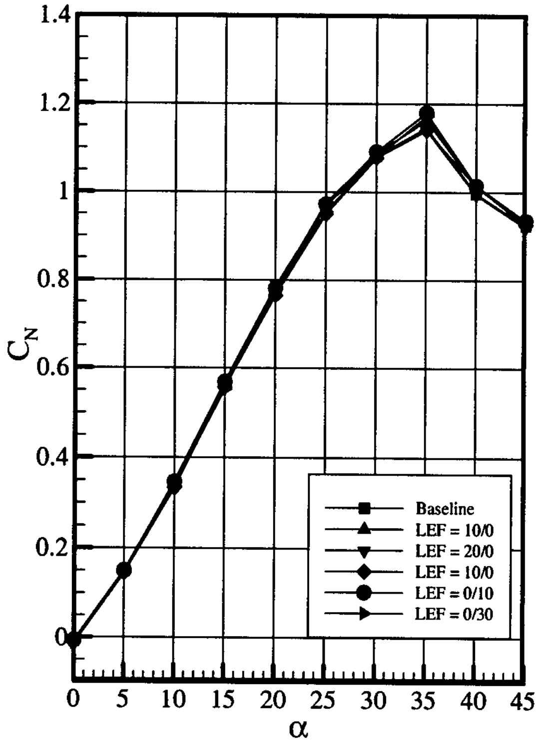

Figure A6a Normal Force Coefficient
as a Function of α, $\beta = 4^{\circ}$

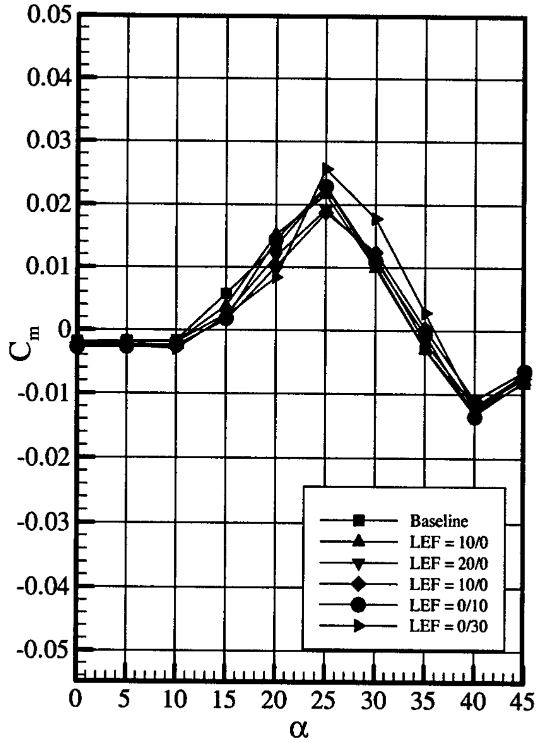

Figure A6b Pitching Moment Coefficient
as a Function of α, $\beta = 4^{\circ}$

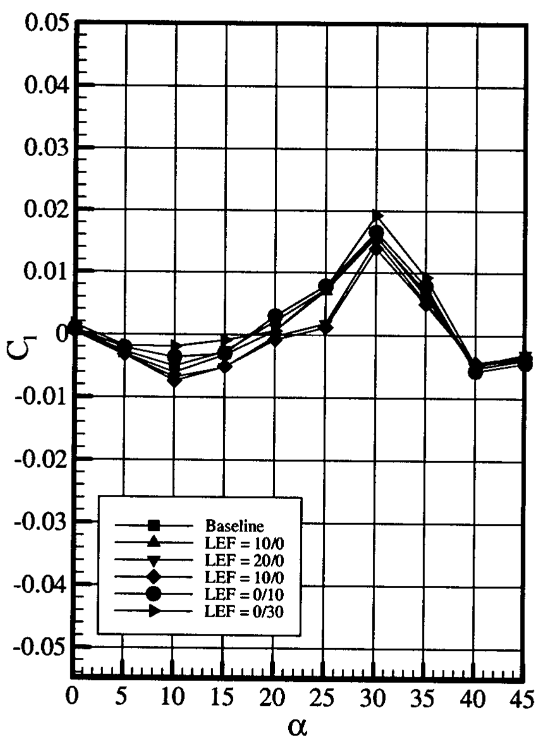

Figure A6c Rolling Moment Coefficient
as a Function of α, $\beta = 4^{\circ}$

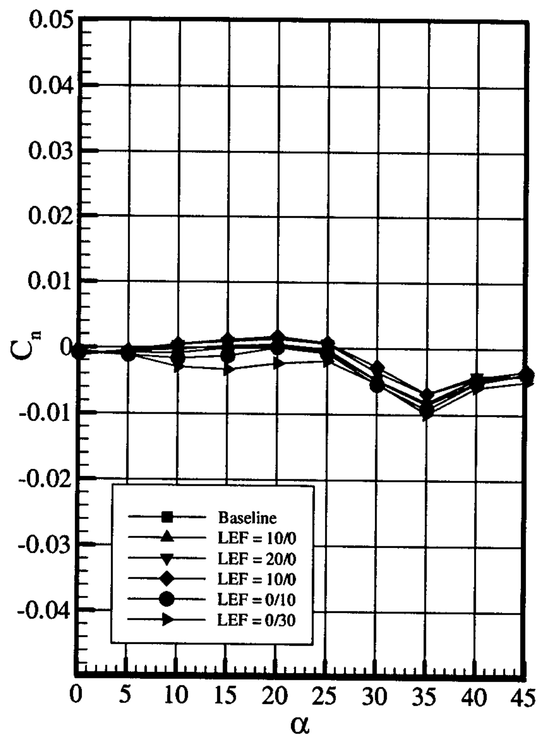

Figure A6d Yawing Moment Coefficient
as a Function of α, $\beta = 4^{\circ}$

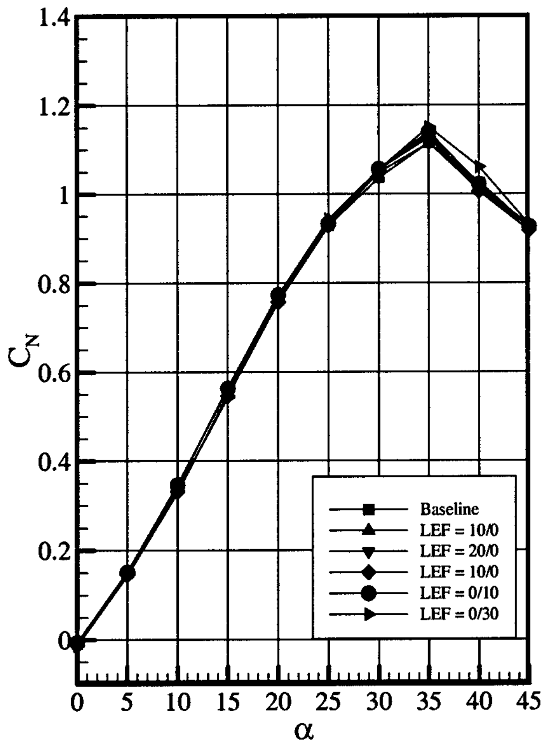

Figure A7a Normal Force Coefficient as a Function of α, β = 6°

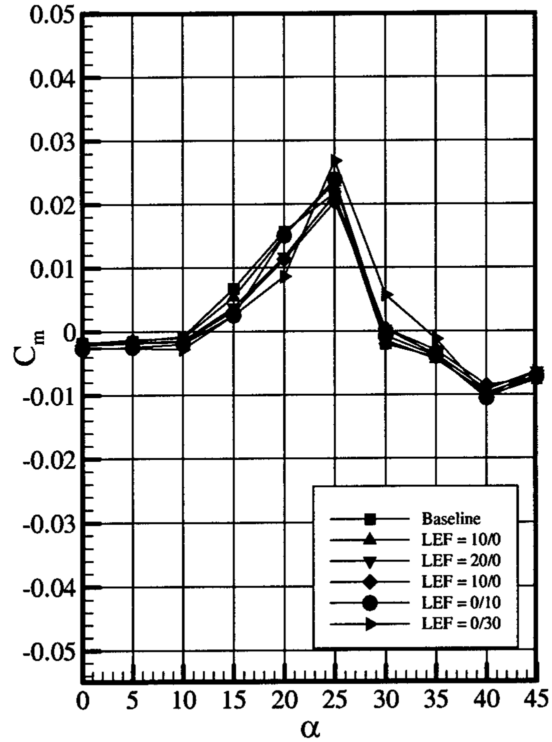

Figure A7b Pitching Moment Coefficient as a Function of α, β = 6°

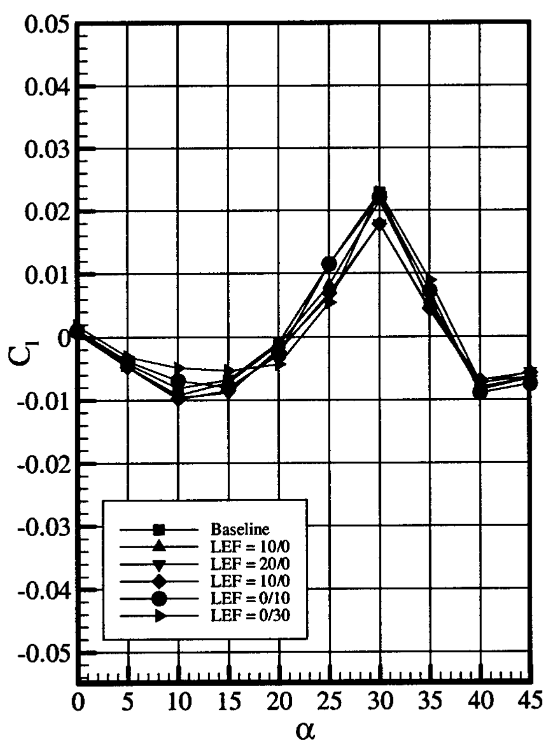

Figure A7c Rolling Moment Coefficient as a Function of α, β = 6°

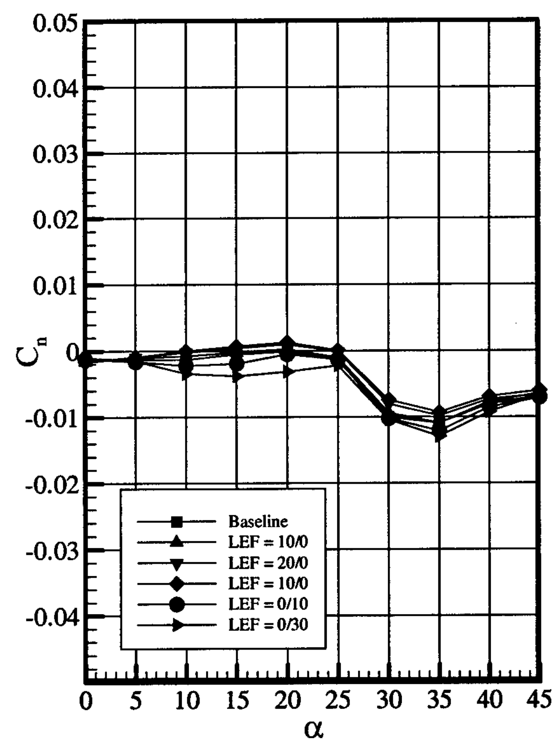

Figure A7d Yawing Moment Coefficient as a Function of α, β = 6°

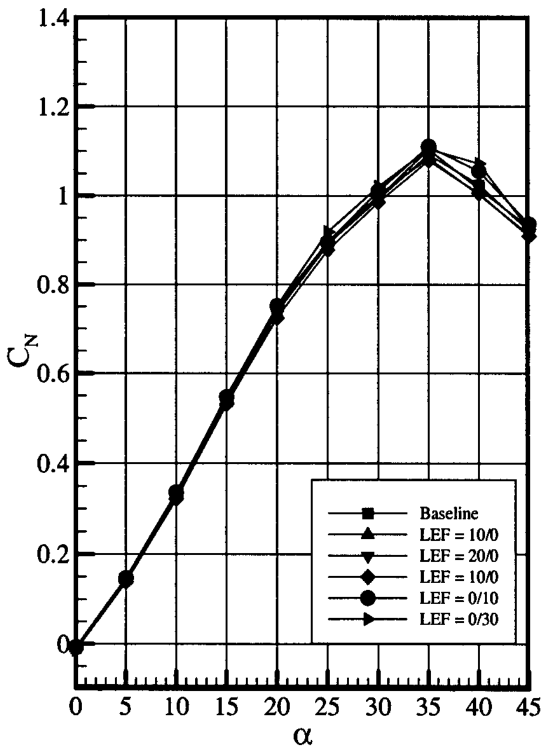

Figure A8a Normal Force Coefficient as a Function of α, $\beta = 8^\circ$

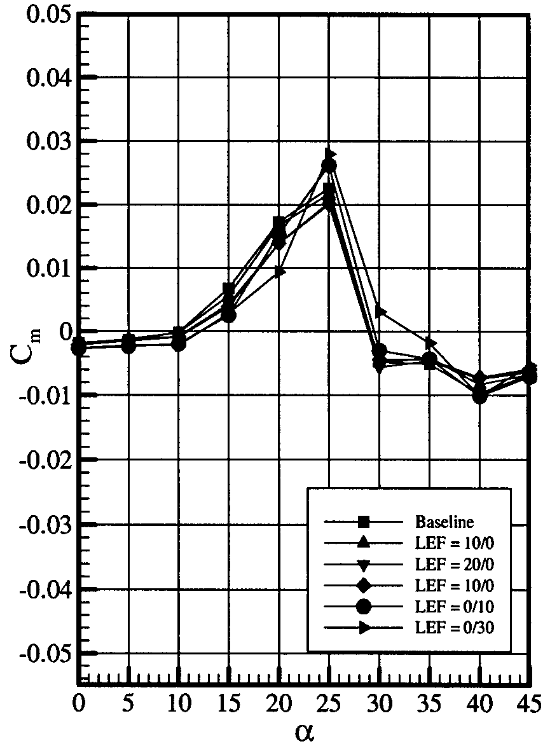

Figure A8b Pitching Moment Coefficient as a Function of α, $\beta = 8^\circ$

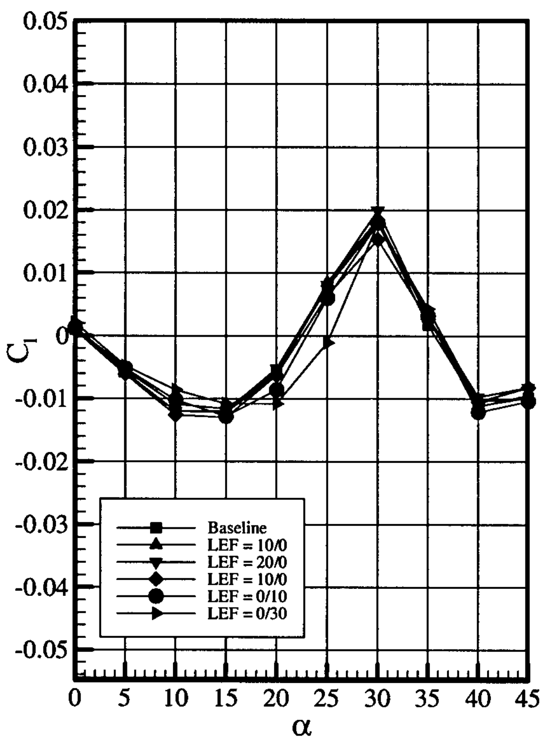

Figure A8c Rolling Moment Coefficient as a Function of α, $\beta = 8^\circ$

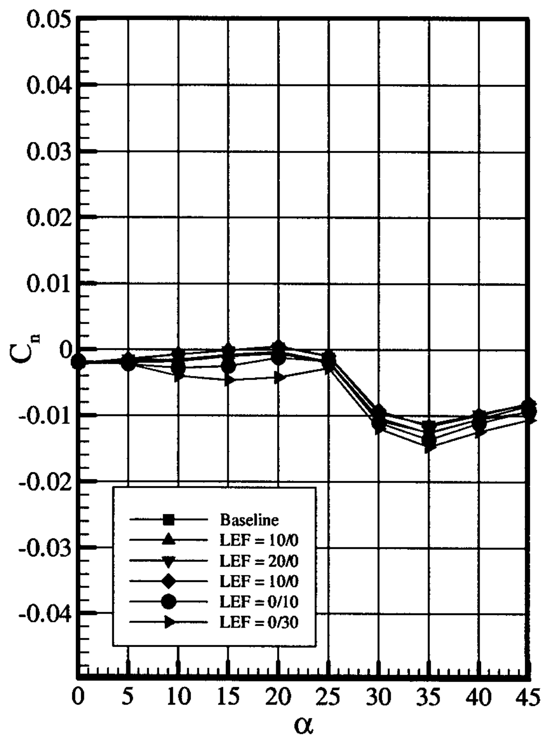

Figure A8d Yawing Moment Coefficient as a Function of α, $\beta = 8^\circ$

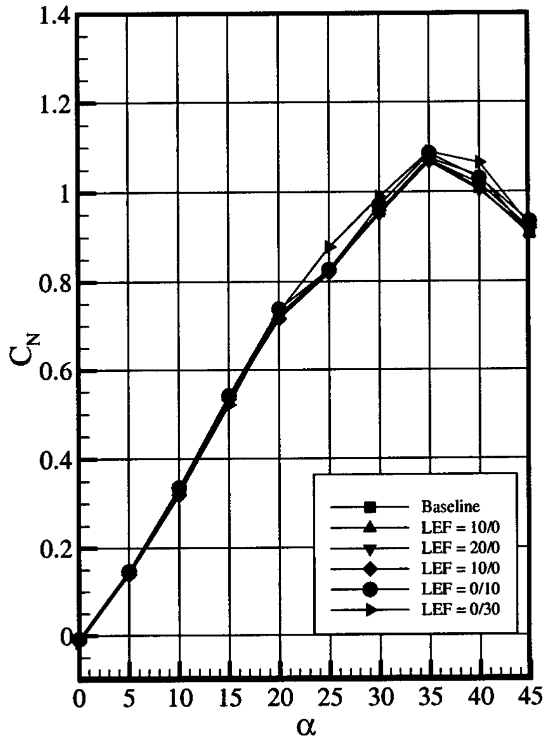

Figure A9a Normal Force Coefficient as a Function of α, $\beta = 10^{\circ}$

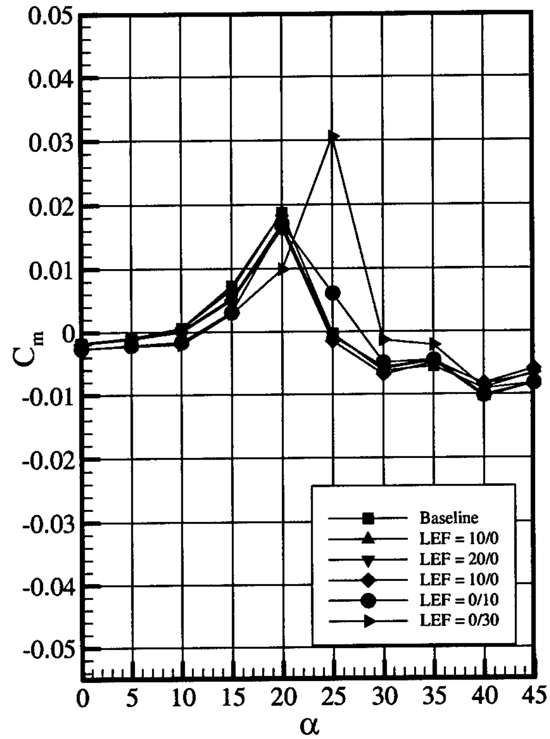

Figure A9b Pitching Moment Coefficient as a Function of α, $\beta = 10^{\circ}$

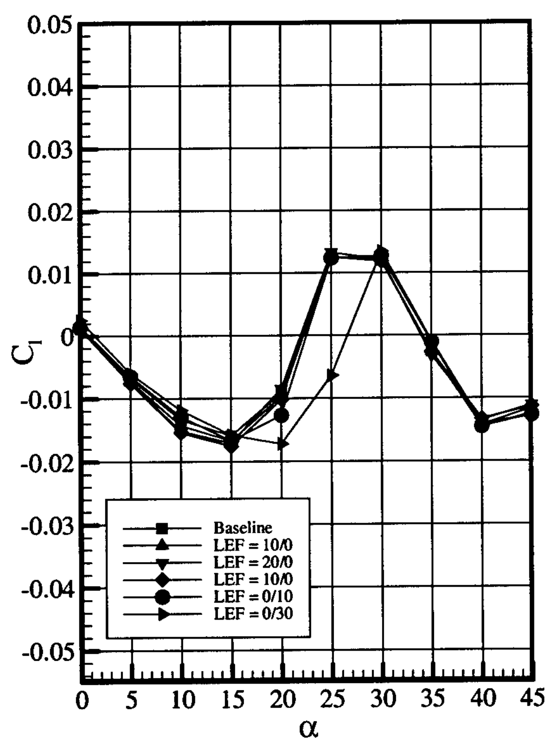

Figure A9c Rolling Moment Coefficient as a Function of α, $\beta = 10^{\circ}$

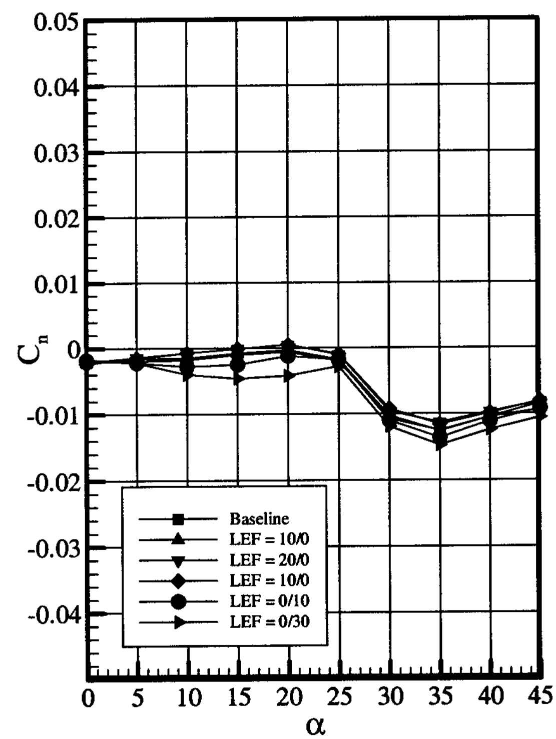

Figure A9d Yawing Moment Coefficient as a Function of α, $\beta = 10^{\circ}$

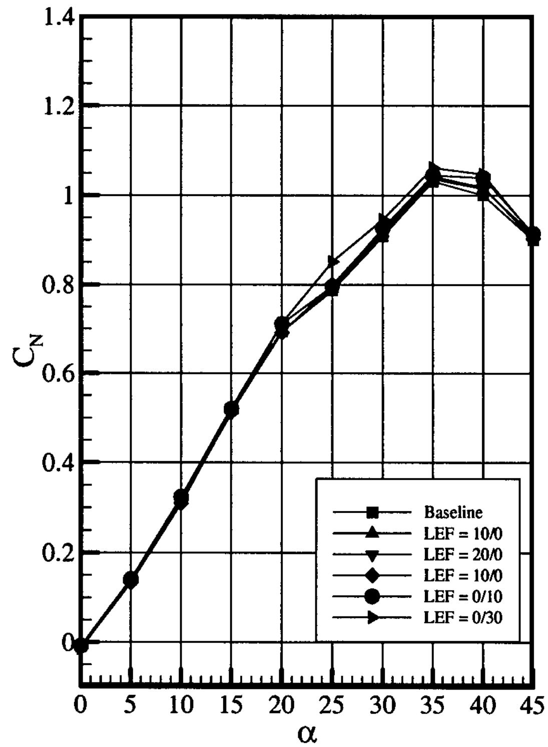

Figure A10a Normal Force Coefficient as a Function of α, β = 12°

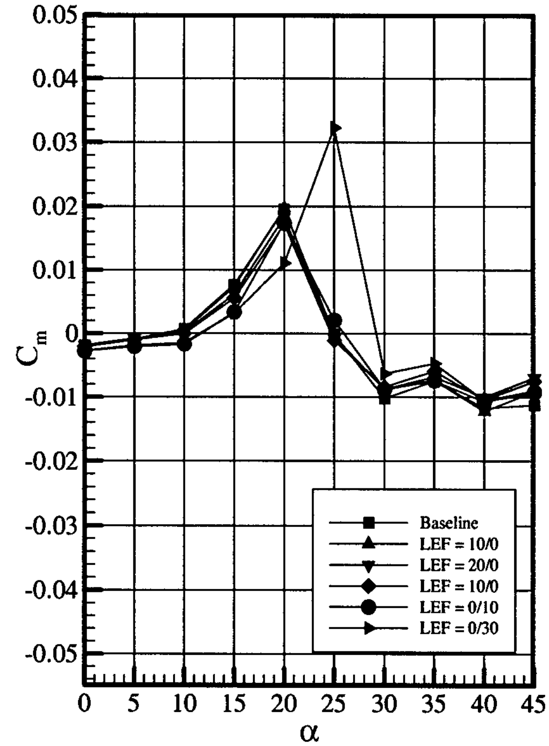

Figure A10b Pitching Moment Coefficient as a Function of α, β = 12°

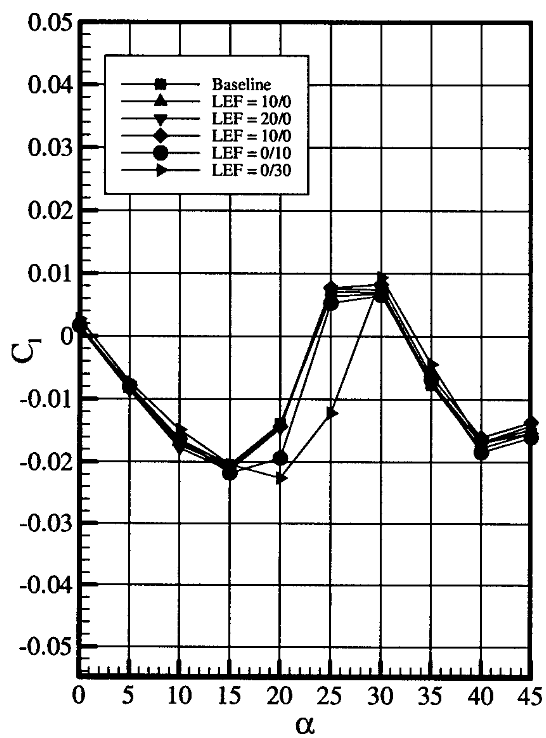

Figure A10c Rolling Moment Coefficient as a Function of α, β = 12°

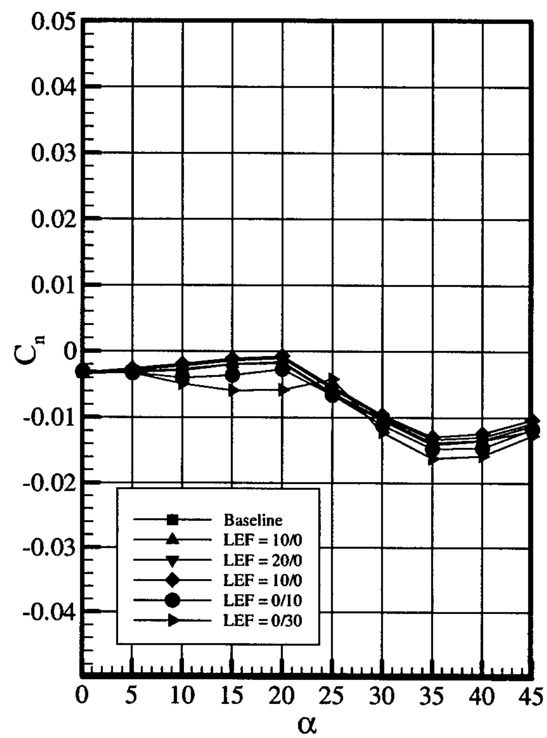

Figure A10d Yawing Moment Coefficient as a Function of α, β = 12°

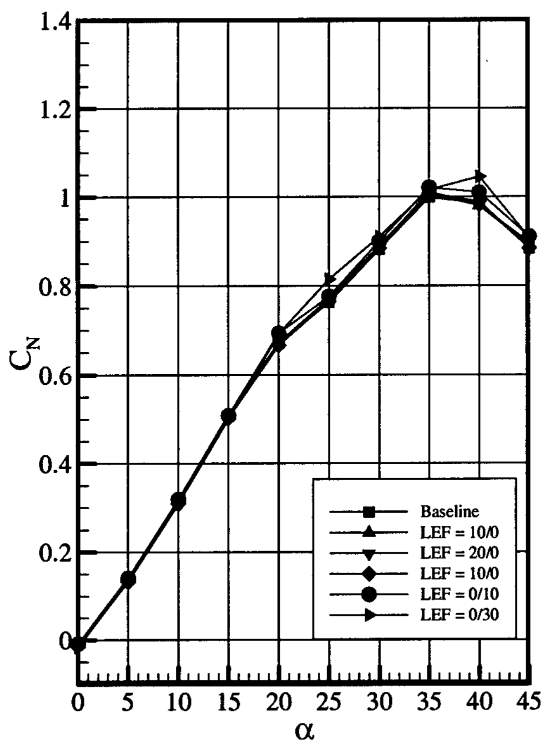

Figure A11a Normal Force Coefficient as a Function of α, β = 14°

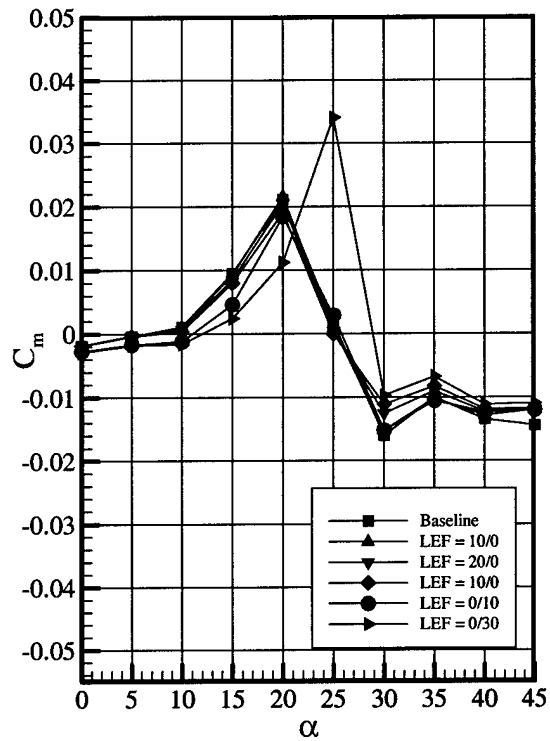

Figure A11b Pitching Moment Coefficient as a Function of α, β = 14°

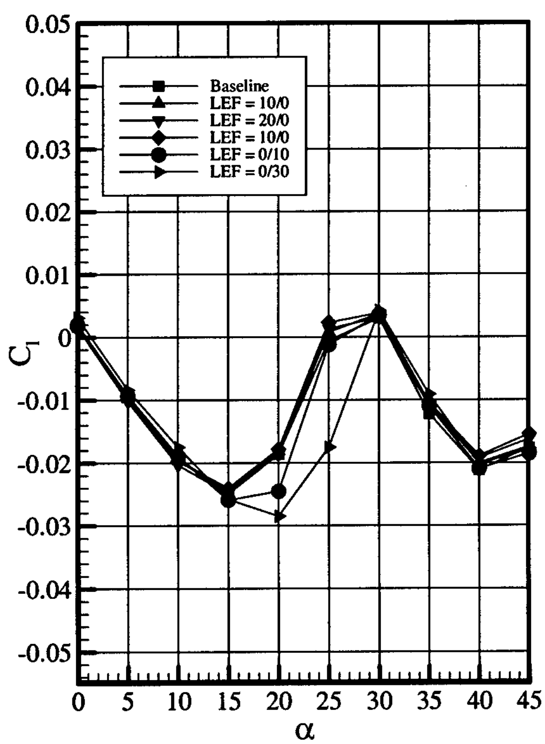

Figure A11c Rolling Moment Coefficient as a Function of α, β = 14°

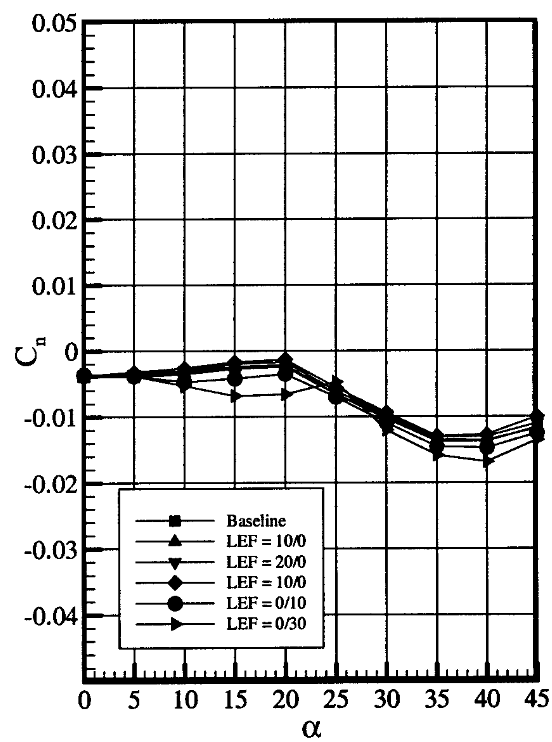

Figure A11d Yawing Moment Coefficient as a Function of α, β = 14°

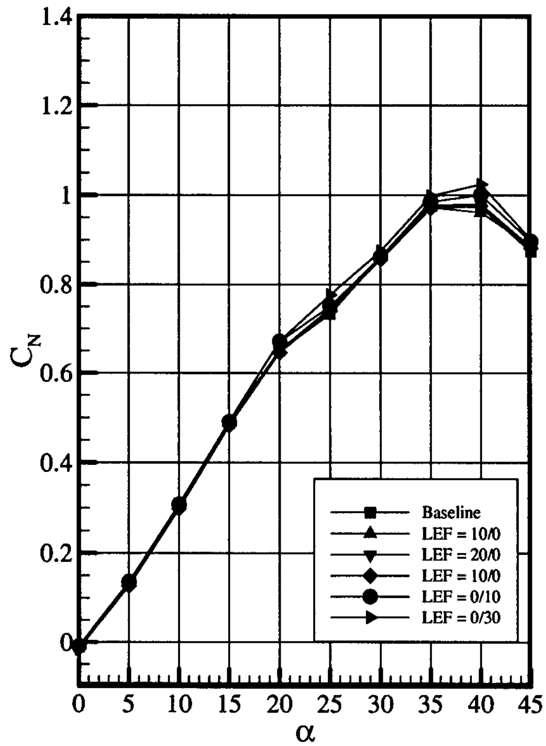

Figure A12a Normal Force Coefficient
as a Function of α, $\beta = 16^{\circ}$

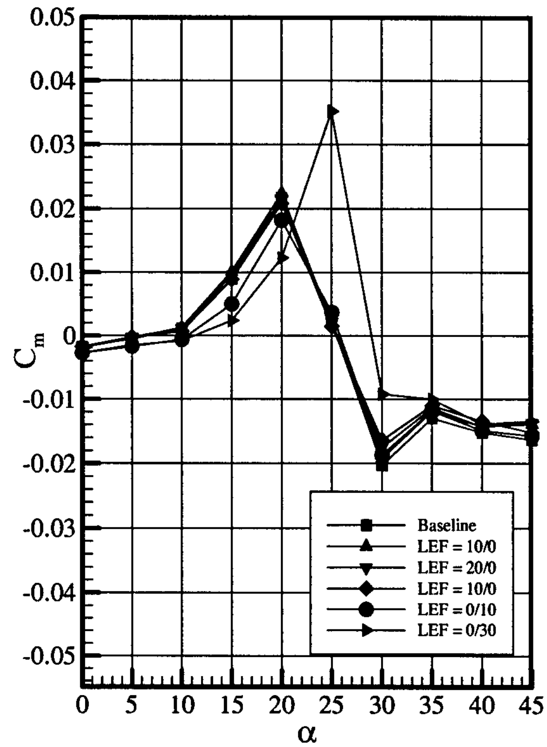

Figure A12b Pitching Moment Coefficient
as a Function of α, $\beta = 16^{\circ}$

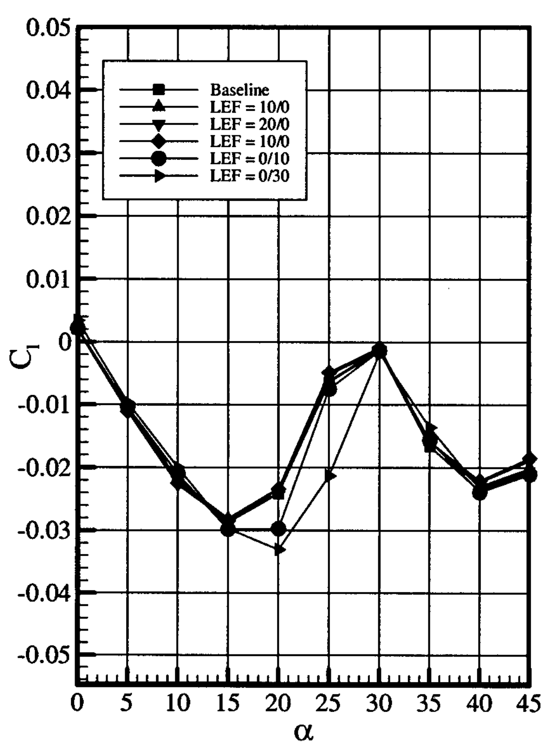

Figure A12c Rolling Moment Coefficient
as a Function of α, $\beta = 16^{\circ}$

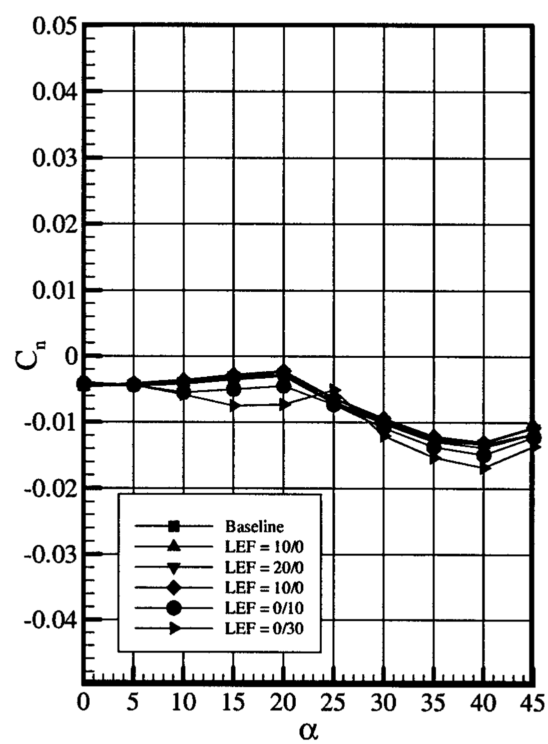

Figure A12d Yawing Moment Coefficient
as a Function of α, $\beta = 16^{\circ}$

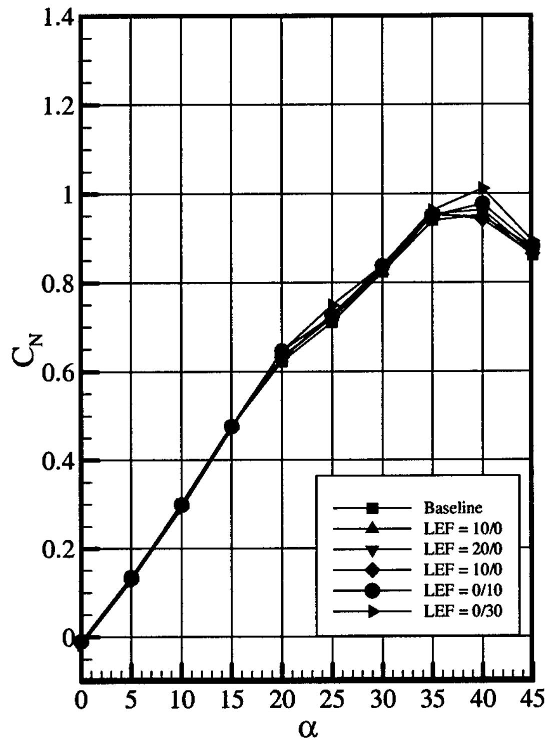

Figure A13a Normal Force Coefficient as a Function of α, β = 18°

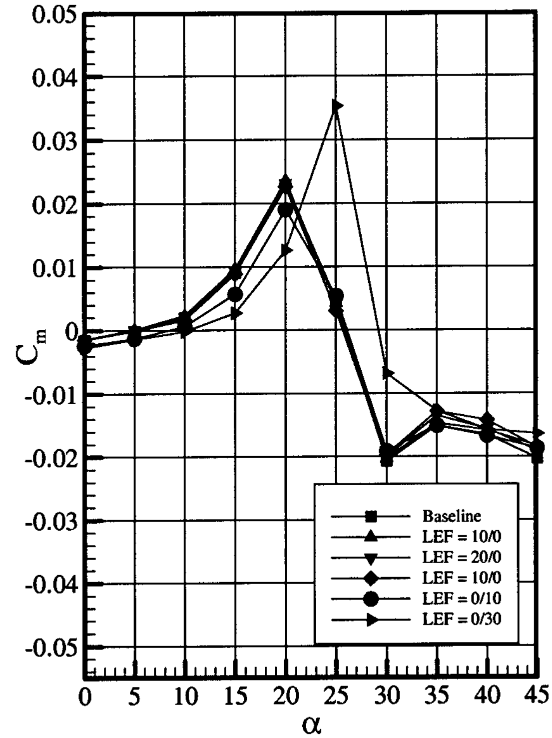

Figure A13b Pitching Moment Coefficient as a Function of α, β = 18°

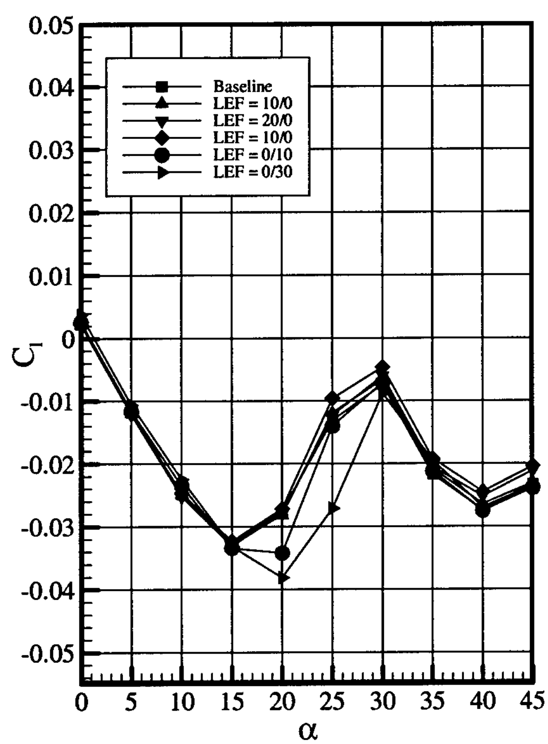

Figure A13c Rolling Moment Coefficient as a Function of α, β = 18°

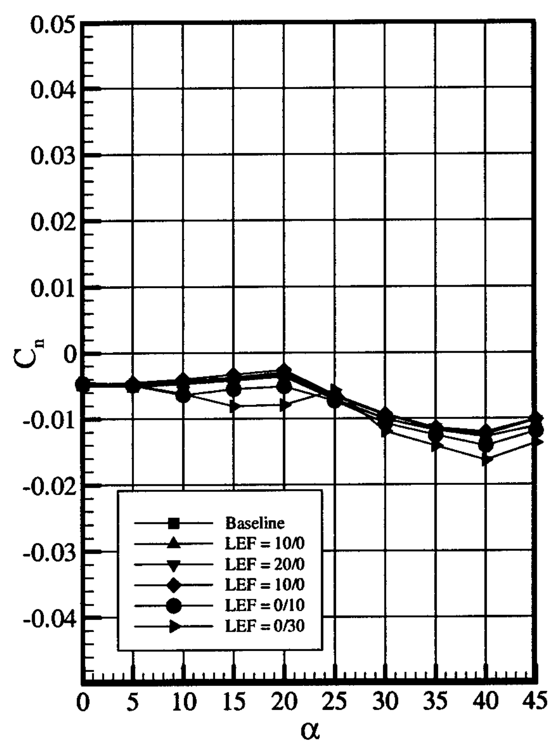

Figure A13d Yawing Moment Coefficient as a Function of α, β = 18°

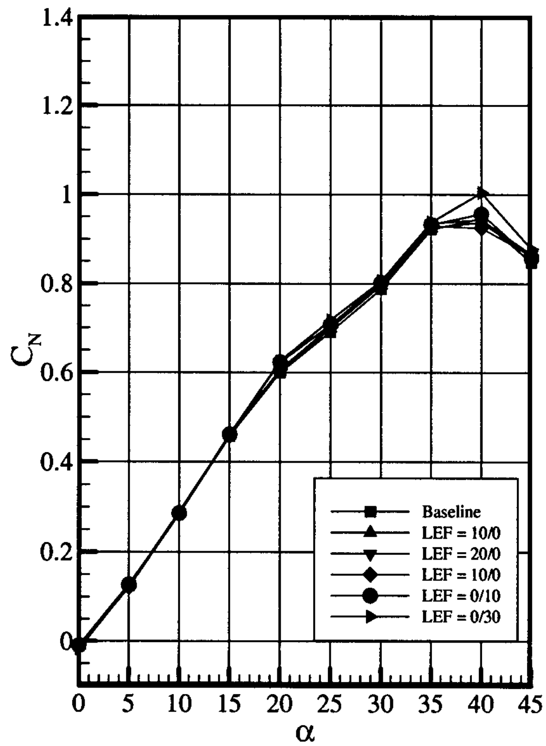

Figure A14a Normal Force Coefficient as a Function of α, β = 20°

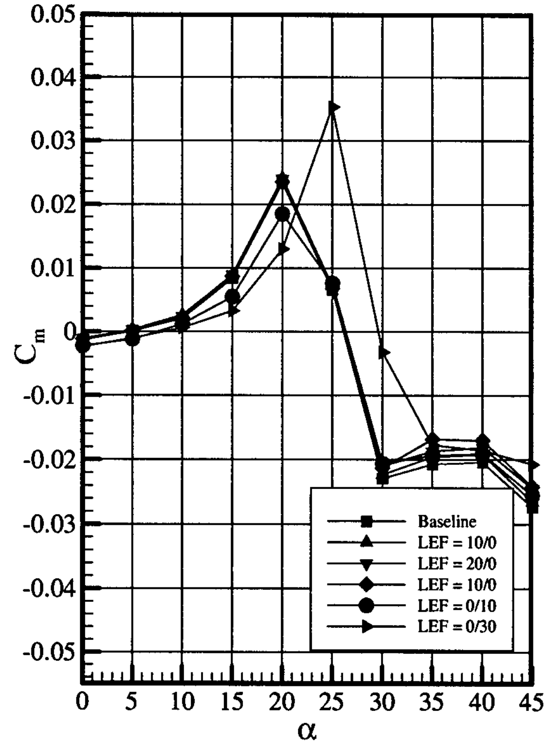

Figure A14b Pitching Moment Coefficient as a Function of α, β = 20°

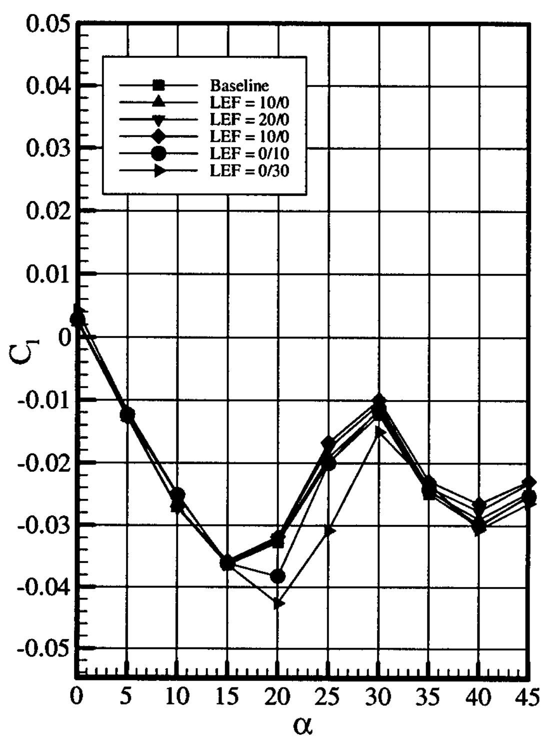

Figure A14c Rolling Moment Coefficient as a Function of α, β = 20°

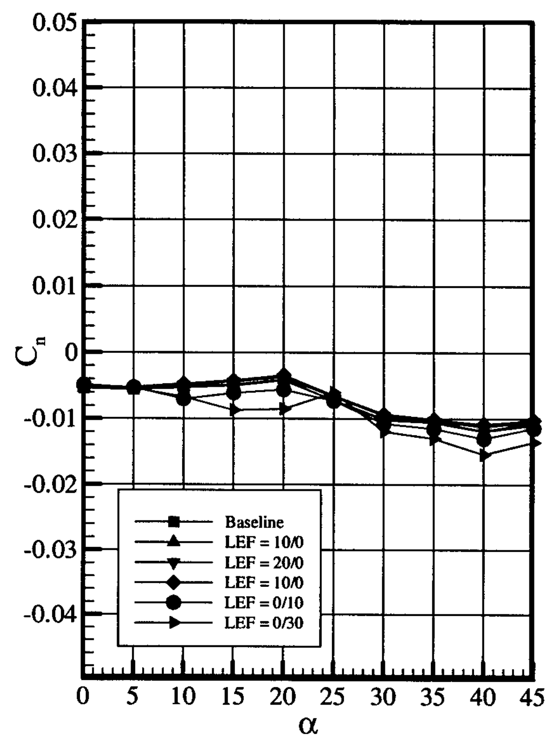

Figure A14d Yawing Moment Coefficient as a Function of α, β = 20°

Appendix B Leading-Edge-Flap-Deflection Data as a Function of Sideslip Angle

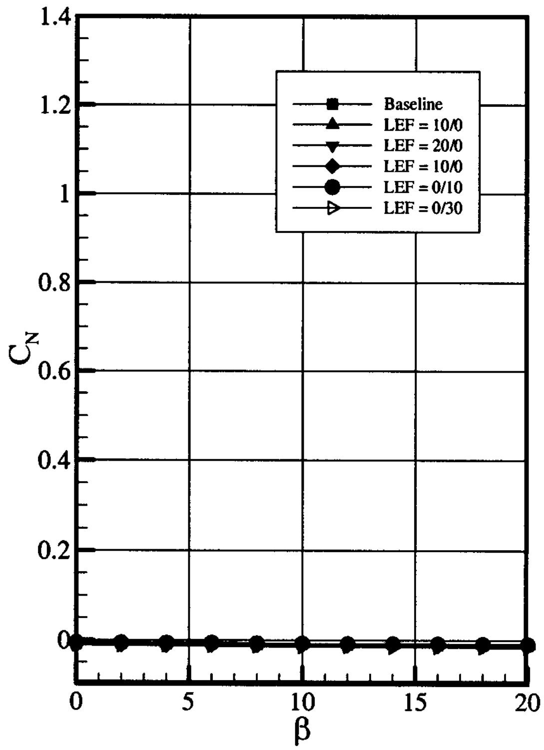

Figure B1a Normal Force Coefficient as a Function of β, $\alpha = 0^\circ$

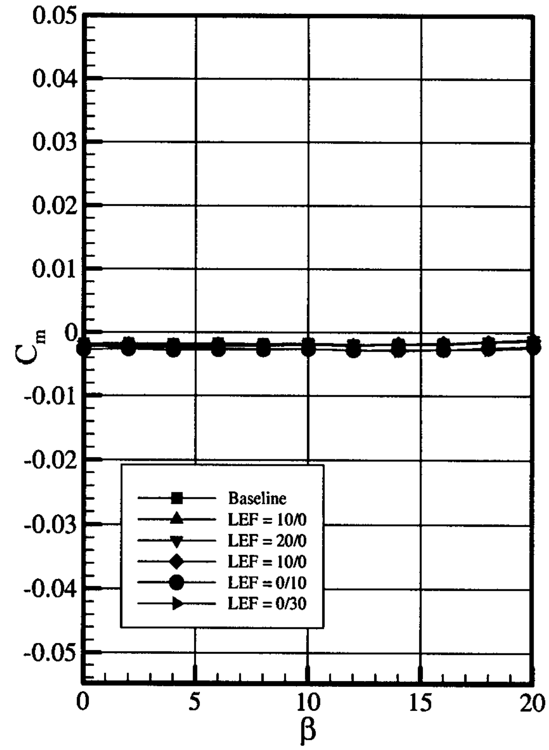

Figure B1b Pitching Moment Coefficient as a Function of β, $\alpha = 0^\circ$

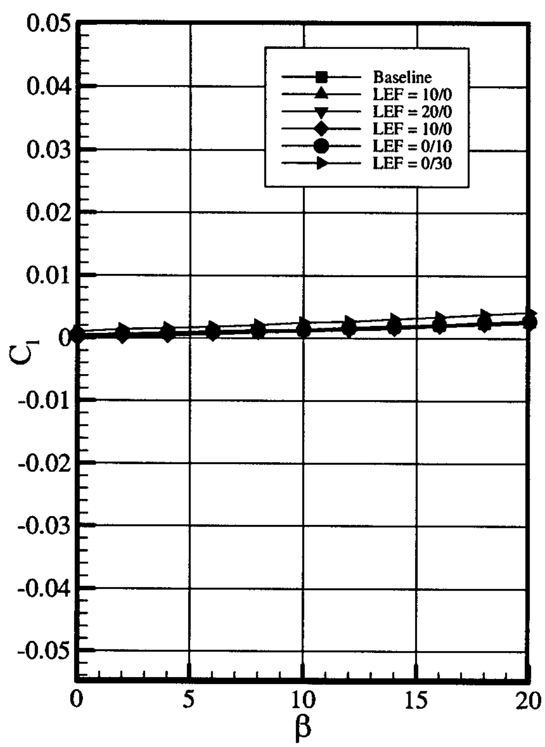

Figure B1c Rolling Moment Coefficient as a Function of β, $\alpha = 0^\circ$

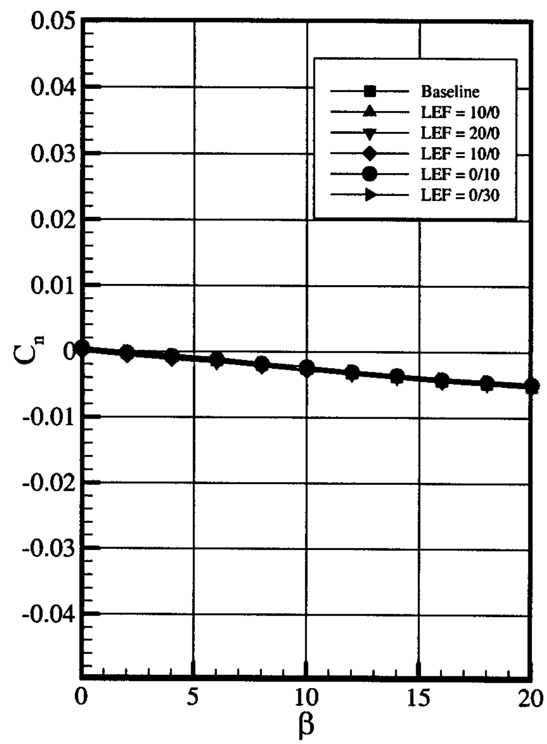

Figure B1d Yawing Moment Coefficient as a Function of β, $\alpha = 0^\circ$

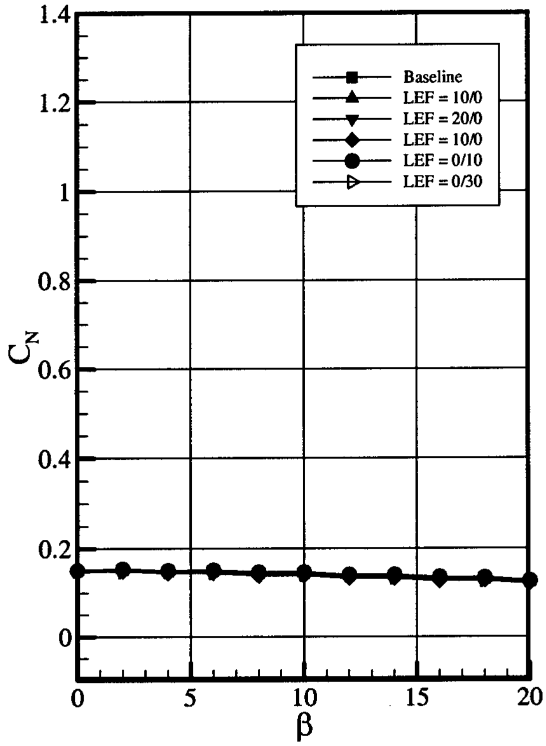

Figure B2a Normal Force Coefficient as a Function of β, α = 5°

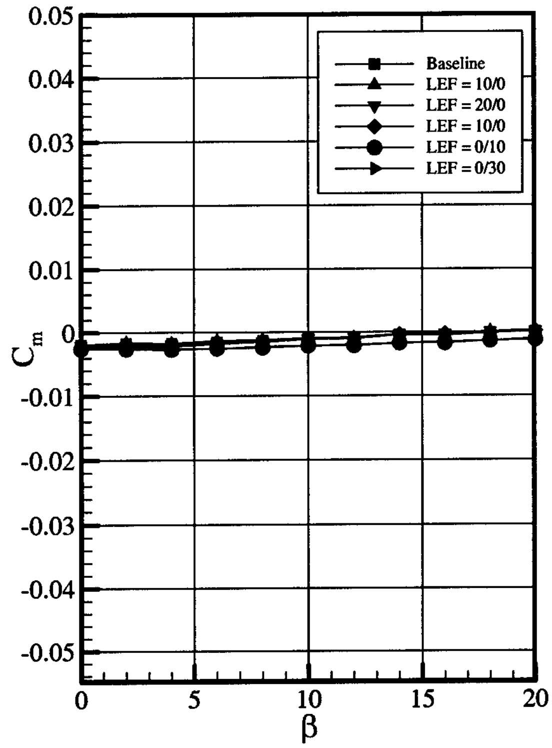

Figure B2b Pitching Moment Coefficient as a Function of β, α = 5°

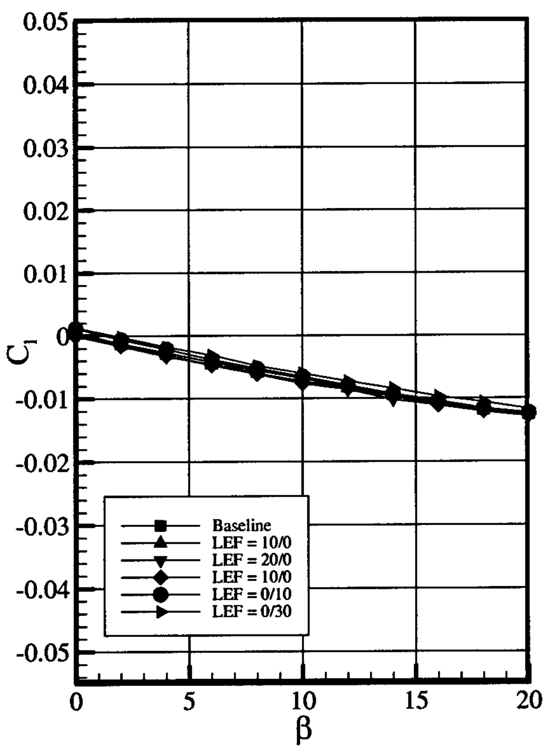

Figure B2c Rolling Moment Coefficient as a Function of β, α = 5°

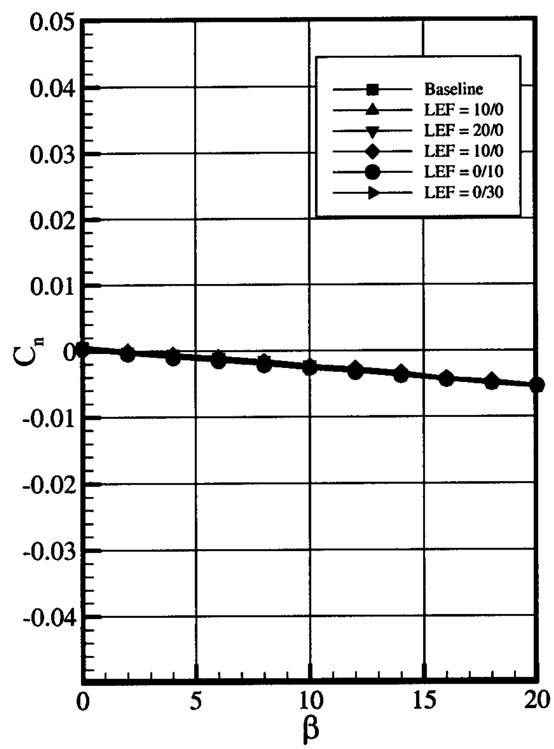

Figure B2d Yawing Moment Coefficient as a Function of β, α = 5°

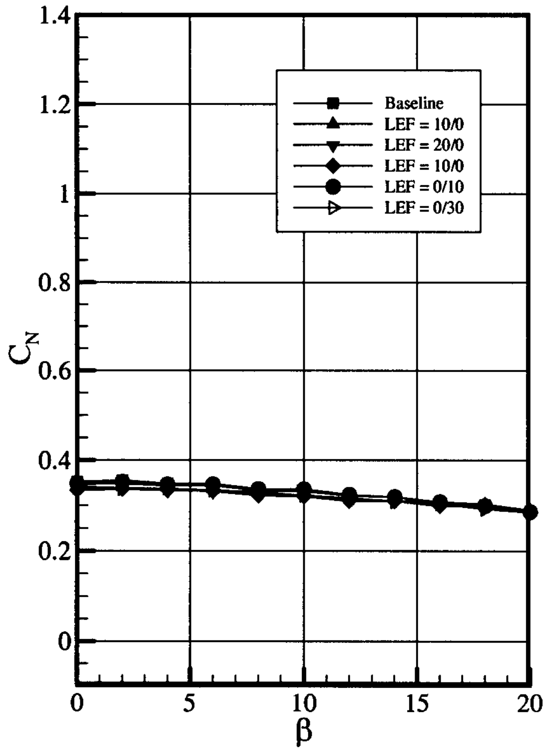

Figure B3a Normal Force Coefficient as a Function of β, α = 10°

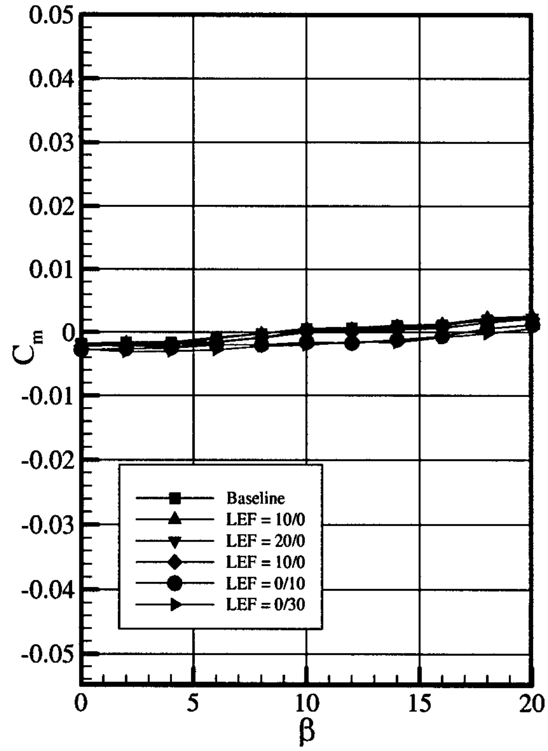

Figure B3b Pitching Moment Coefficient as a Function of β, α = 10°

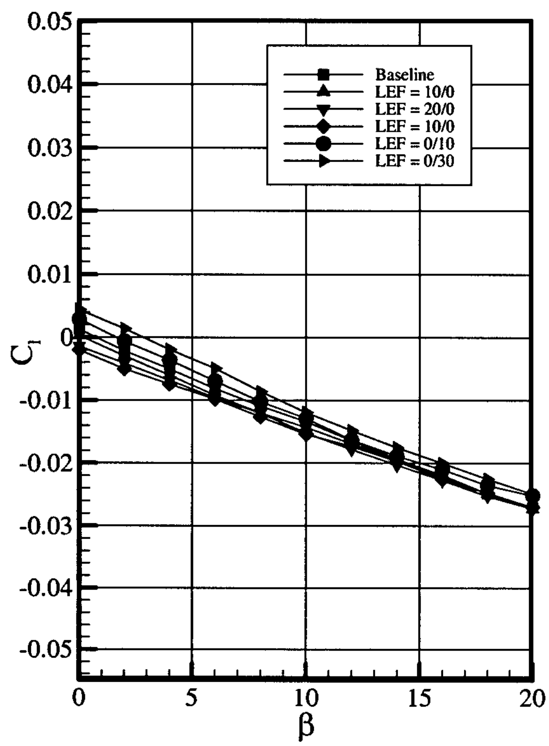

Figure B3c Rolling Moment Coefficient as a Function of β, α = 10°

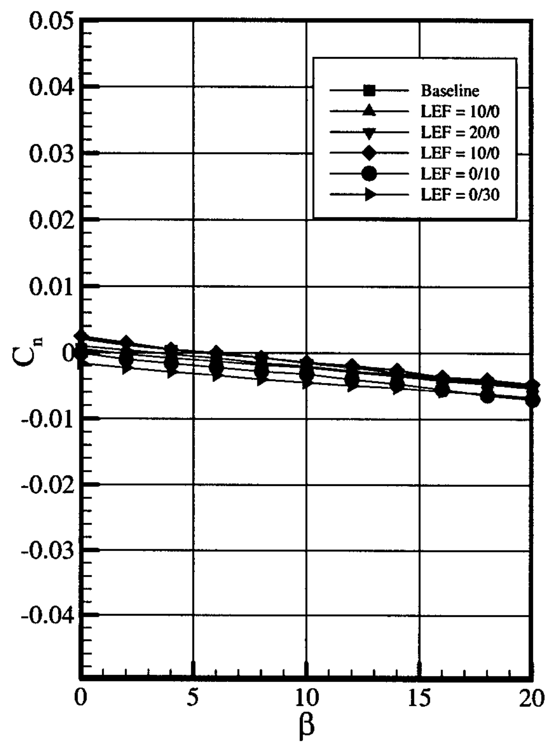

Figure B3d Yawing Moment Coefficient as a Function of β, α = 10°

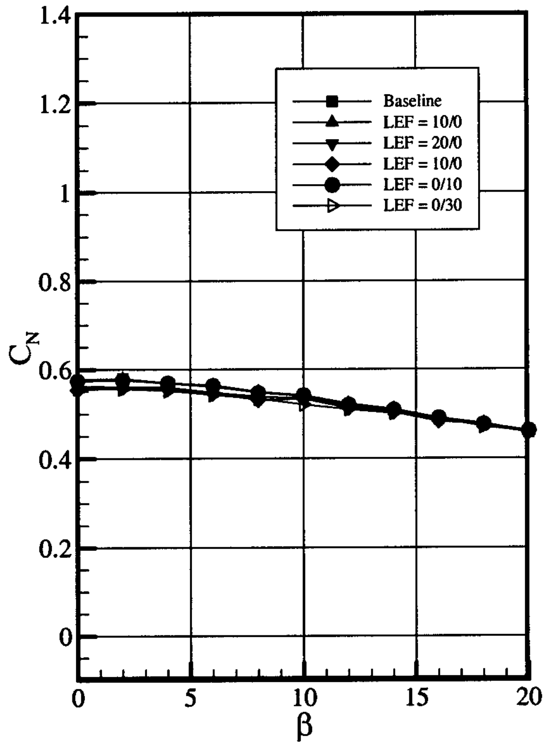

Figure B4a Normal Force Coefficient
as a Function of β, $\alpha = 15^{\circ}$

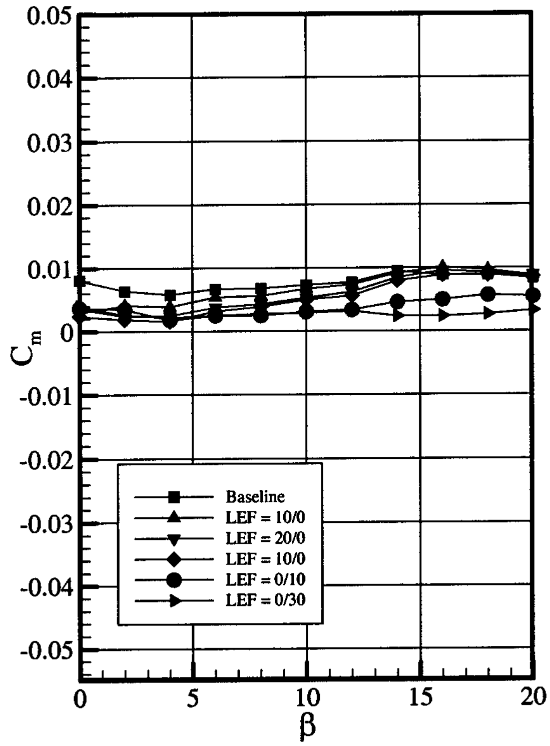

Figure B4b Pitching Moment Coefficient
as a Function of β, $\alpha = 15^{\circ}$

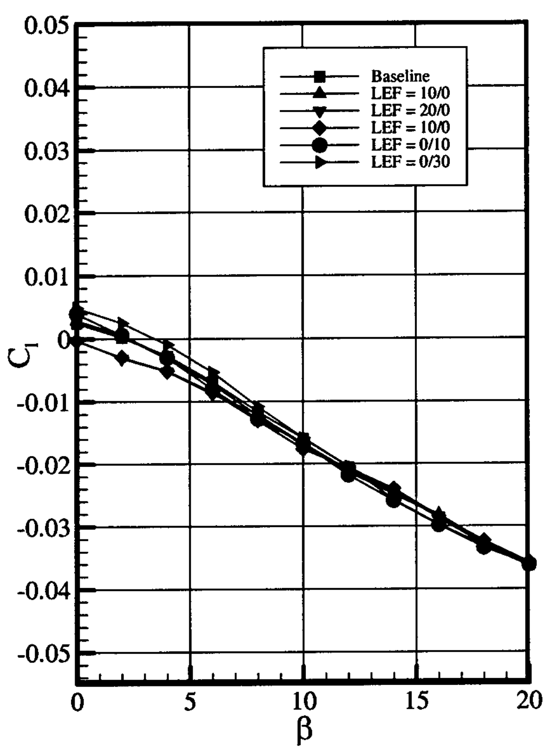

Figure B4c Rolling Moment Coefficient
as a Function of β, $\alpha = 15^{\circ}$

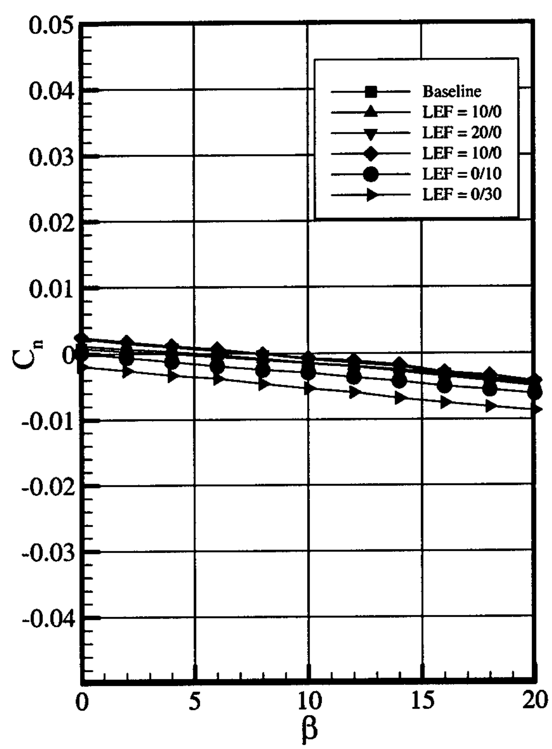

Figure B4d Yawing Moment Coefficient
as a Function of β, $\alpha = 15^{\circ}$

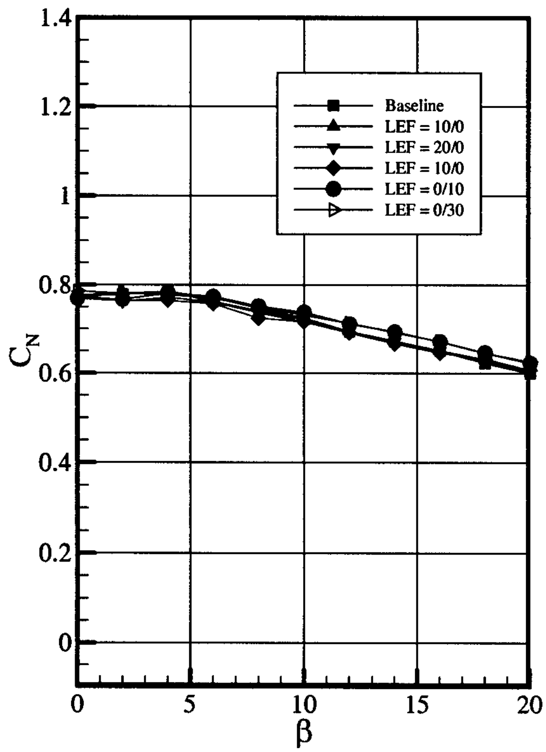

Figure B5a Normal Force Coefficient
as a Function of β, α = 20°

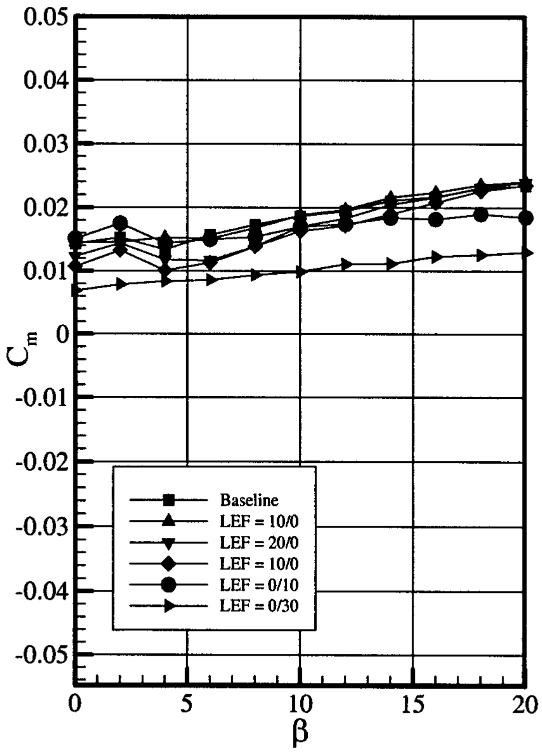

Figure B5b Pitching Moment Coefficient
as a Function of β, α = 20°

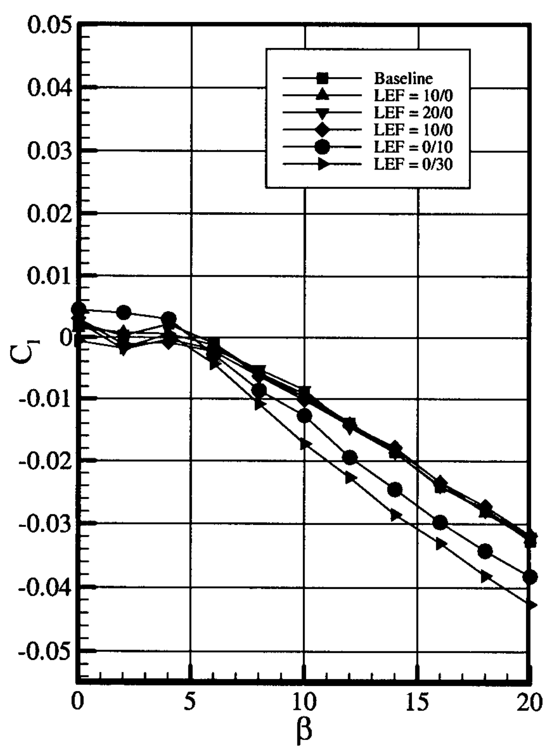

Figure B5c Rolling Moment Coefficient
as a Function of β, α = 20°

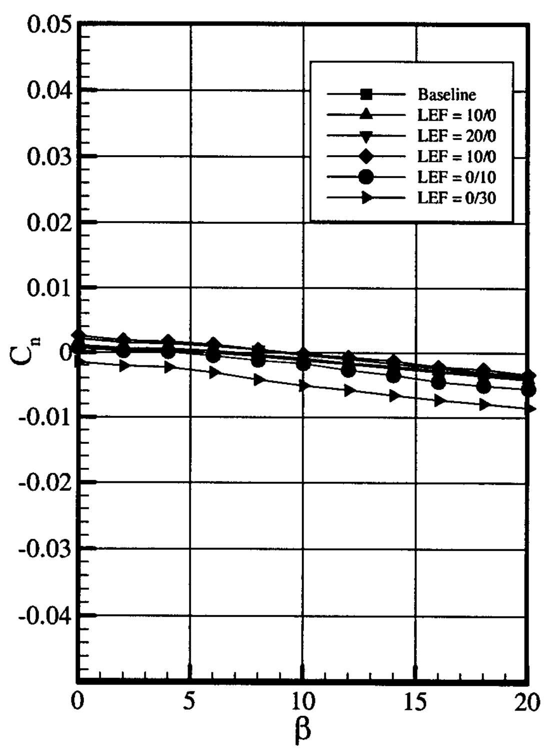

Figure B5d Yawing Moment Coefficient
as a Function of β, α = 20°

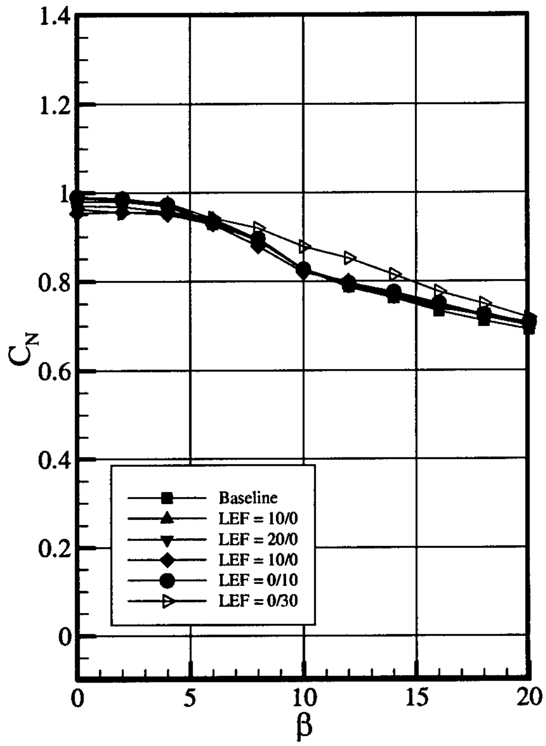

Figure B6a Normal Force Coefficient as a Function of β, α = 25°

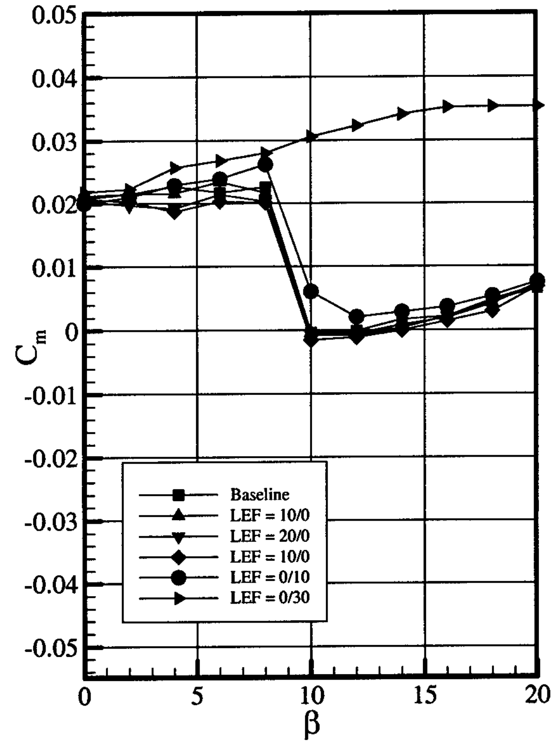

Figure B6b Pitching Moment Coefficient as a Function of β, α = 25°

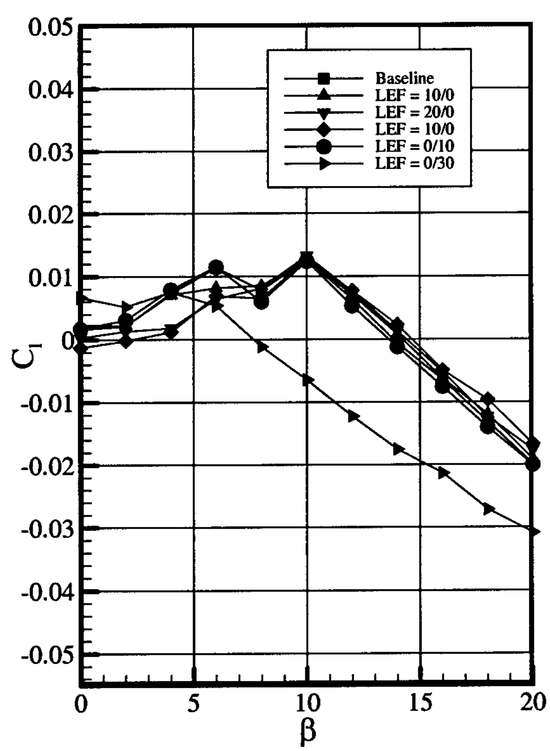

Figure B6c Rolling Moment Coefficient as a Function of β, α = 25°

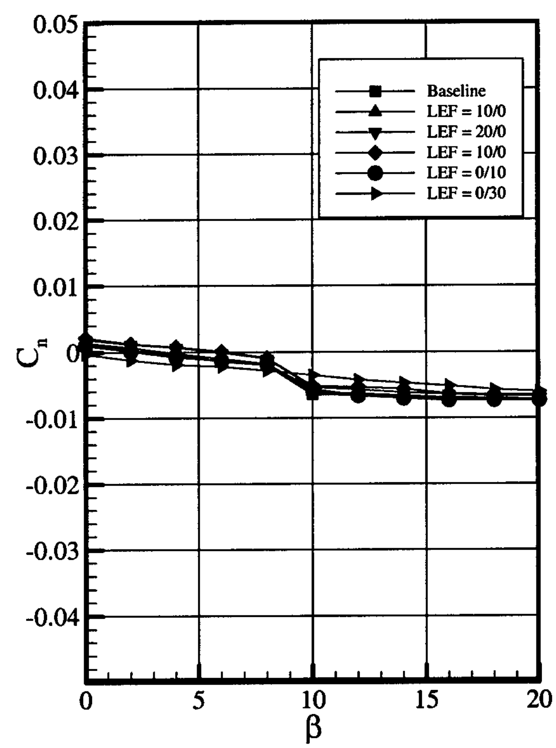

Figure B6d Yawing Moment Coefficient as a Function of β, α = 25°

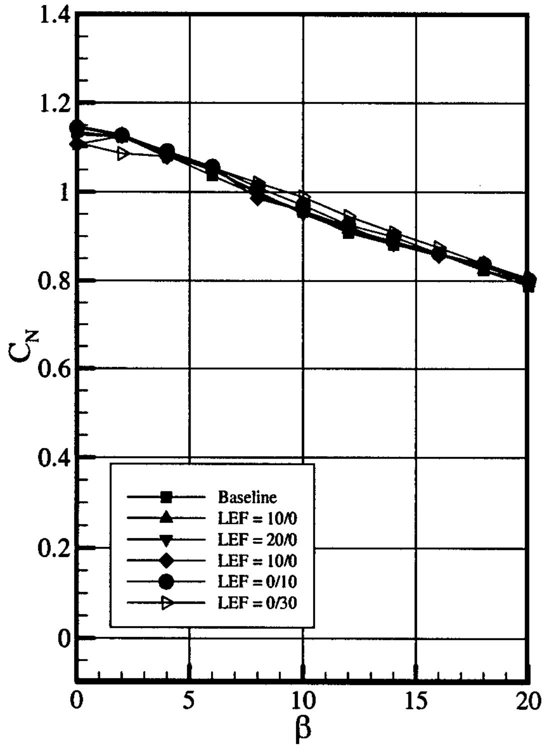

Figure B7a Normal Force Coefficient as a Function of β, α = 30°

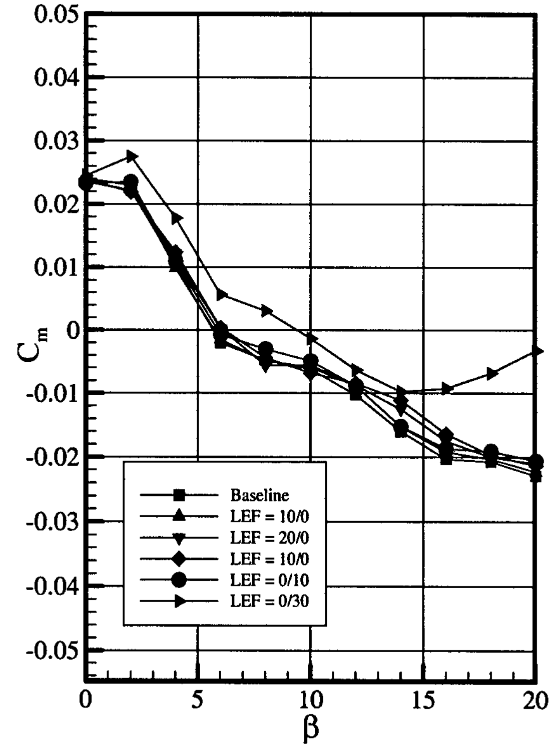

Figure B7b Pitching Moment Coefficient as a Function of β, α = 30°

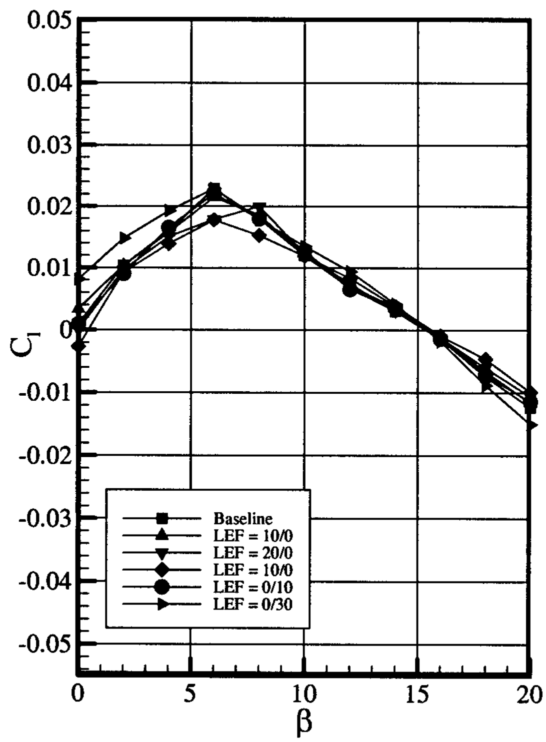

Figure B7c Rolling Moment Coefficient as a Function of β, α = 30°

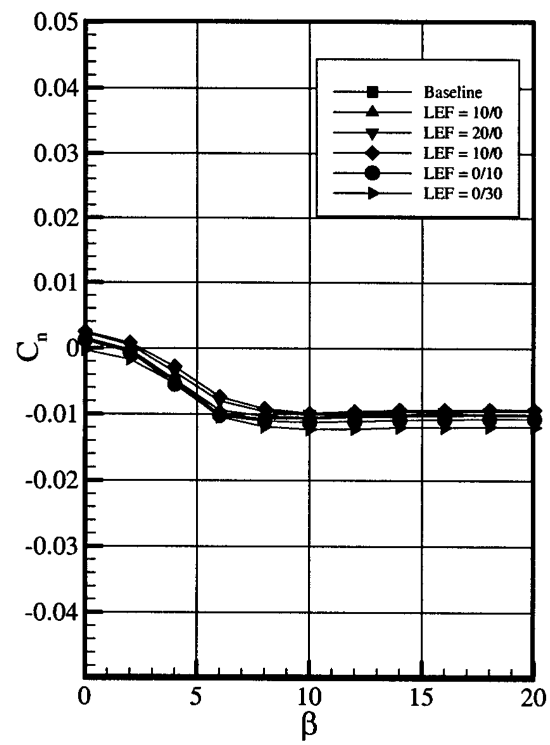

Figure B7d Yawing Moment Coefficient as a Function of β, α = 30°

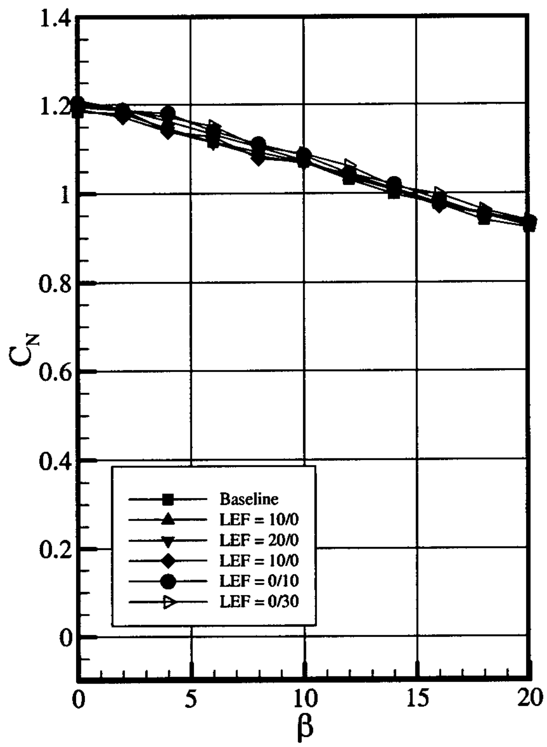

Figure B8a Normal Force Coefficient as a Function of β, α = 35°

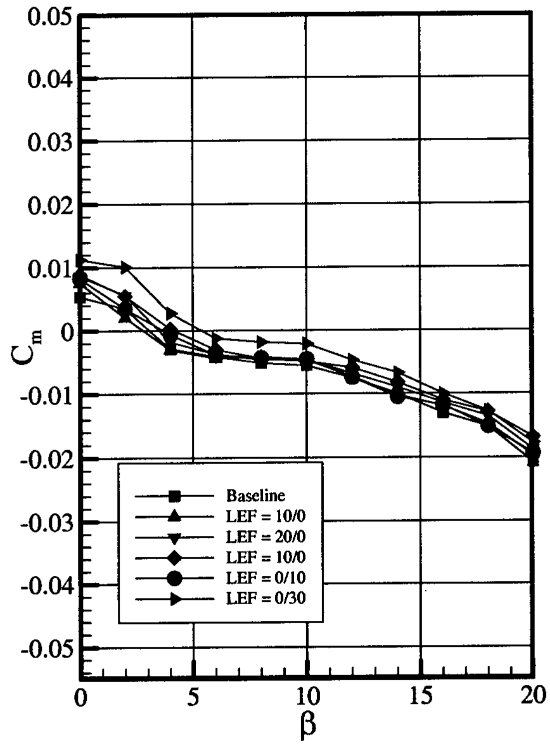

Figure B8b Pitching Moment Coefficient as a Function of β, α = 35°

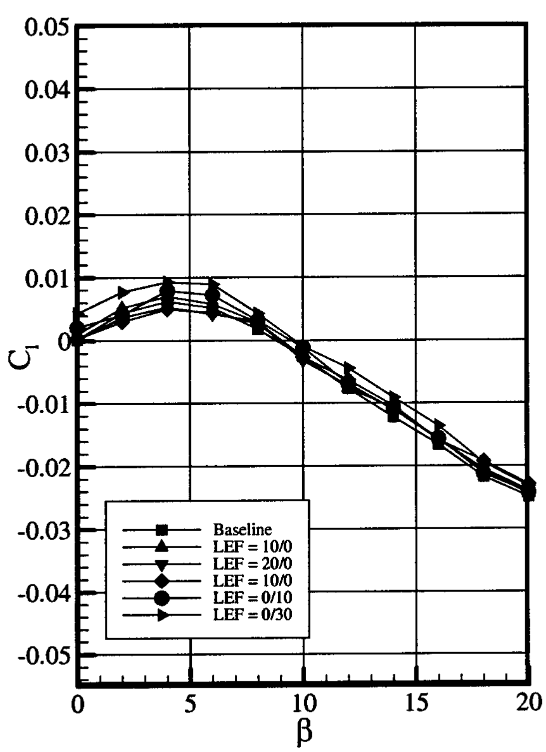

Figure B8c Rolling Moment Coefficient as a Function of β, α = 35°

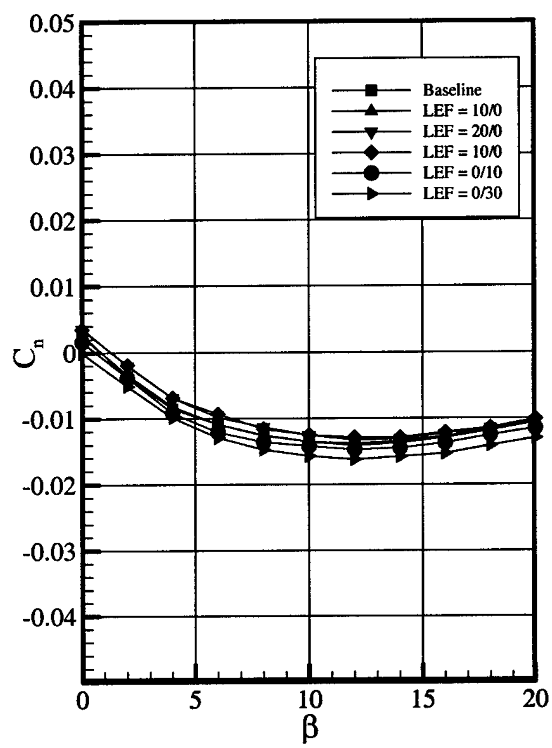

Figure B8d Yawing Moment Coefficient as a Function of β, α = 35°

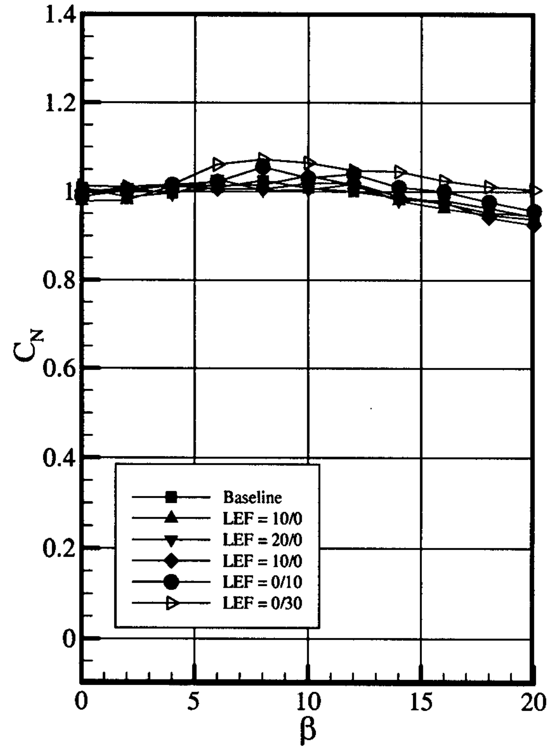

Figure B9a Normal Force Coefficient as a Function of β, α = 40°

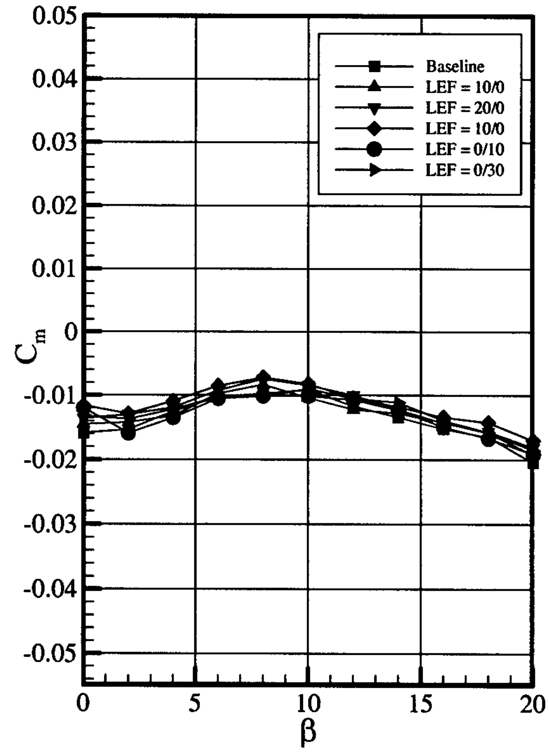

Figure B9b Pitching Moment Coefficient as a Function of β, α = 40°

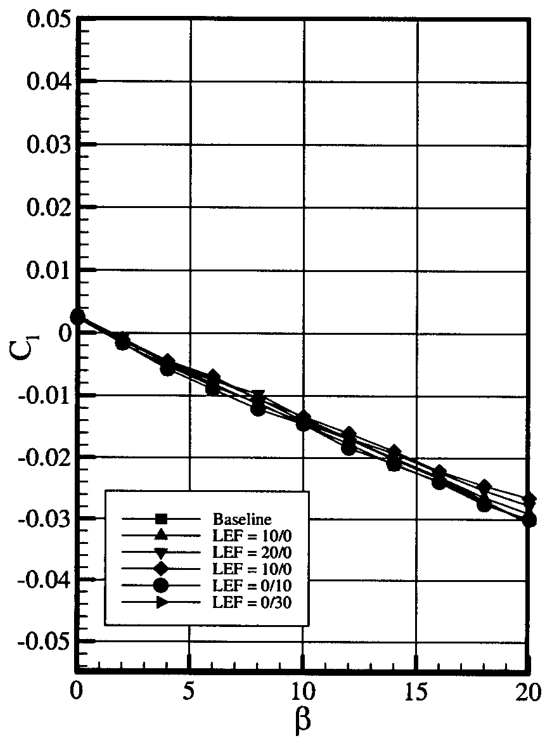

Figure B9c Rolling Moment Coefficient as a Function of β, α = 40°

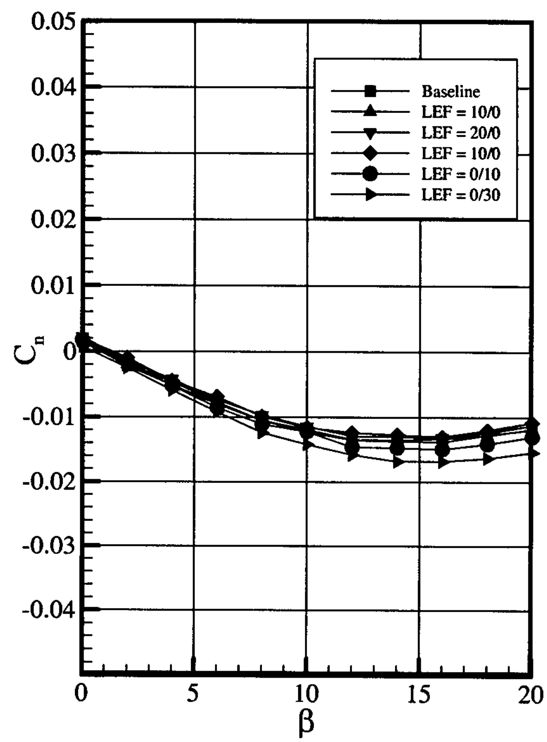

Figure B9d Yawing Moment Coefficient as a Function of β, α = 40°

Appendix C Trailing-Edge-Flap-Deflection Data as a Function of Angle of Attack

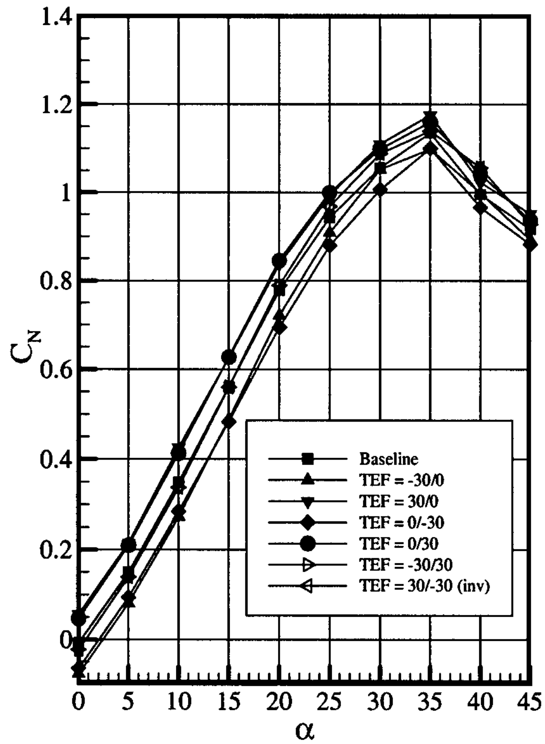

Figure C1a Normal Force Coefficient
as a Function of α, β = -6°

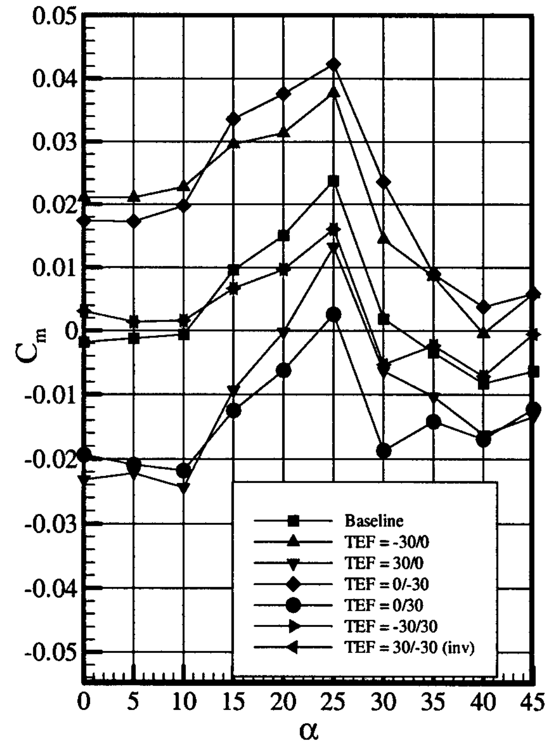

Figure C1b Pitching Moment Coefficient
as a Function of α, β = -6°

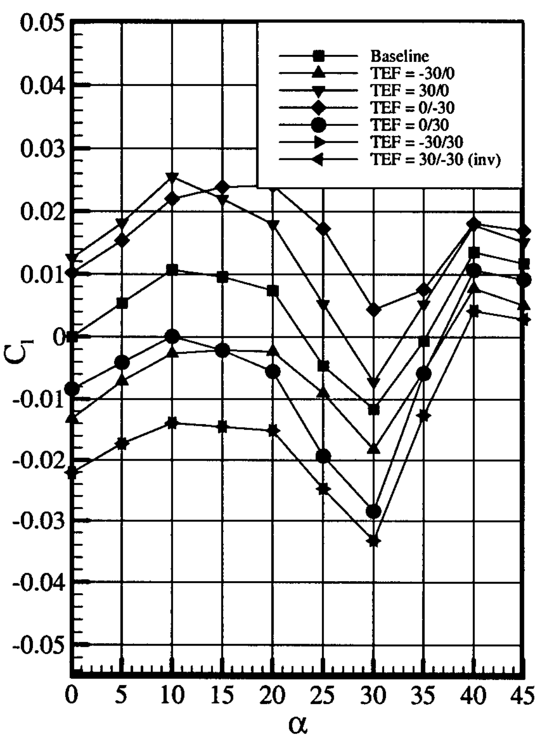

Figure C1c Rolling Moment Coefficient
as a Function of α, β = -6°

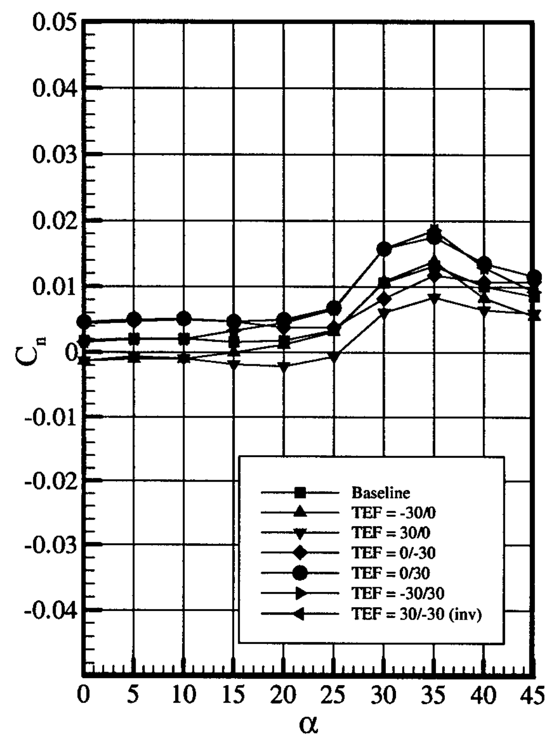

Figure C1d Yawing Moment Coefficient
as a Function of α, β = -6°

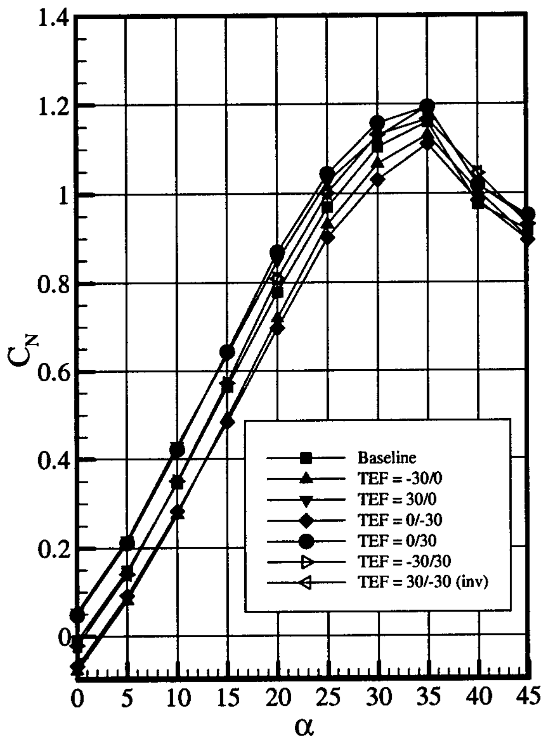

Figure C2a Normal Force Coefficient as a Function of α, $\beta = -4^{\circ}$

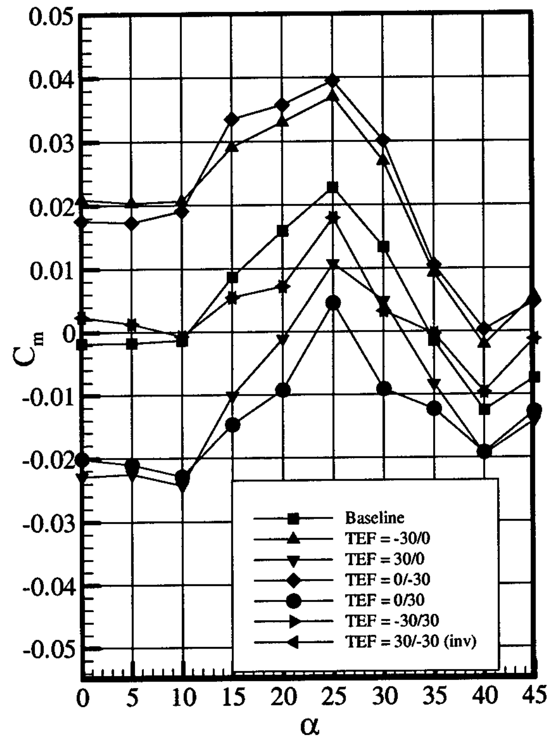

Figure C2b Pitching Moment Coefficient as a Function of α, $\beta = -4^{\circ}$

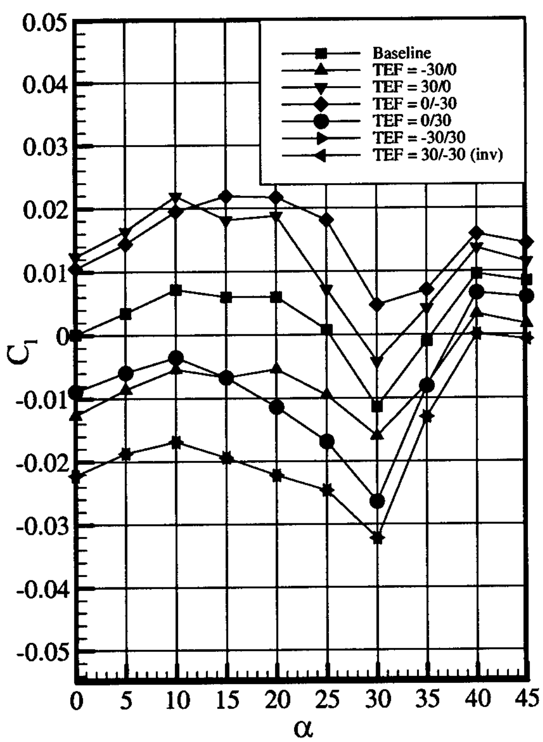

Figure C2c Rolling Moment Coefficient as a Function of α, $\beta = -4^{\circ}$

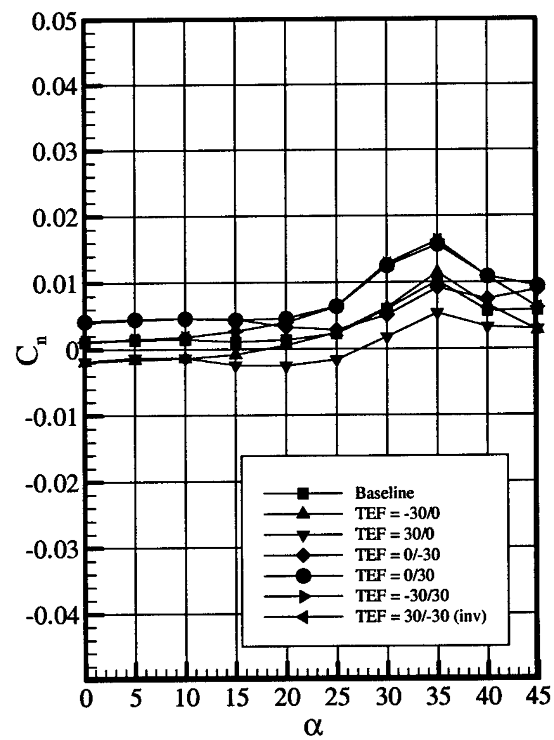

Figure C2d Yawing Moment Coefficient as a Function of α, $\beta = -4^{\circ}$

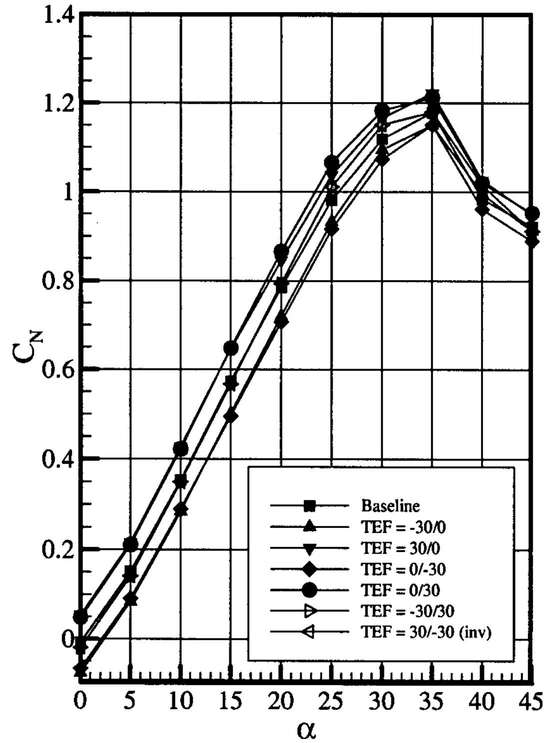

Figure C3a Normal Force Coefficient as a Function of α, β = -2°

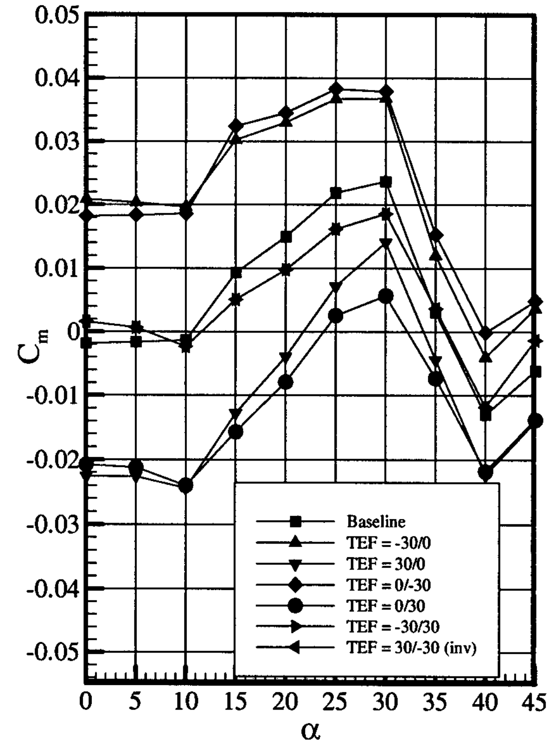

Figure C3b Pitching Moment Coefficient as a Function of α, β = -2°

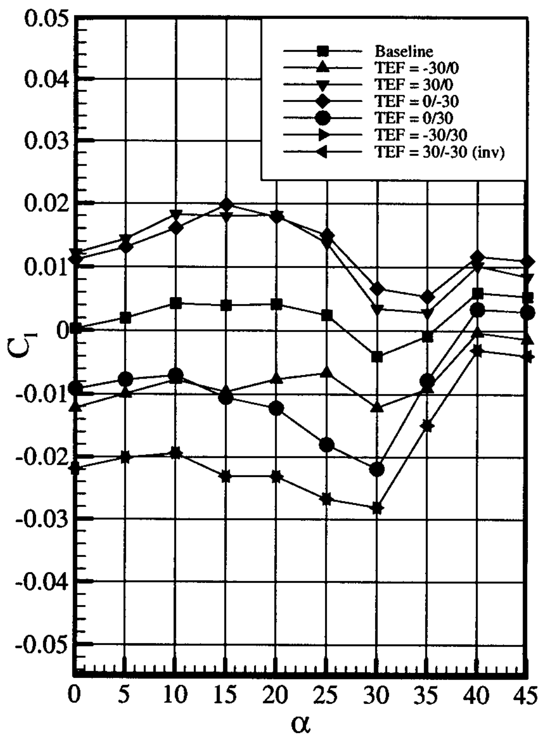

Figure C3c Rolling Moment Coefficient as a Function of α, β = -2°

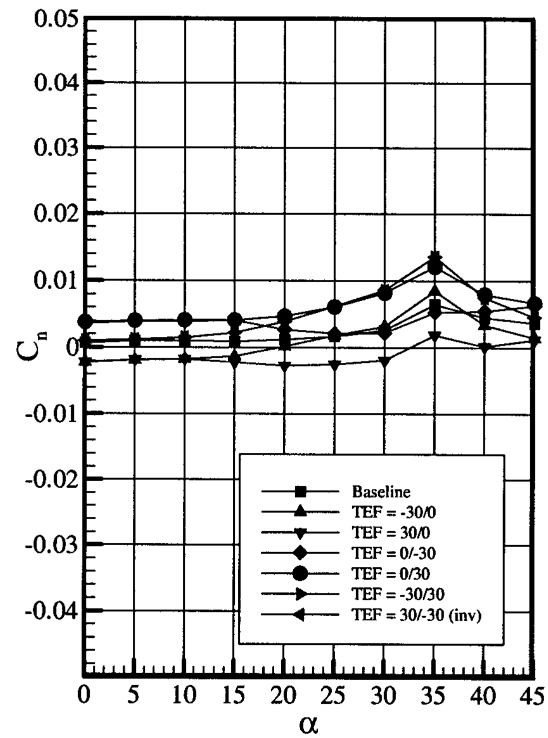

Figure C3d Yawing Moment Coefficient as a Function of α, β = -2°

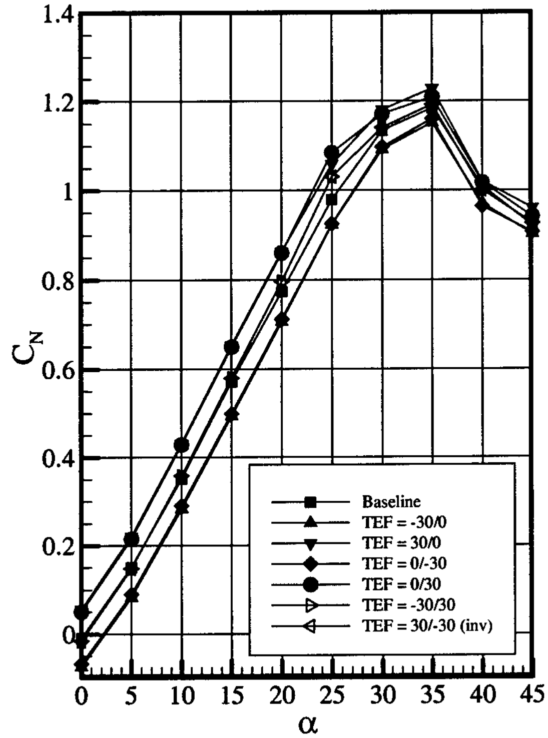

Figure C4a Normal Force Coefficient
as a Function of α, $\beta = 0^{\circ}$

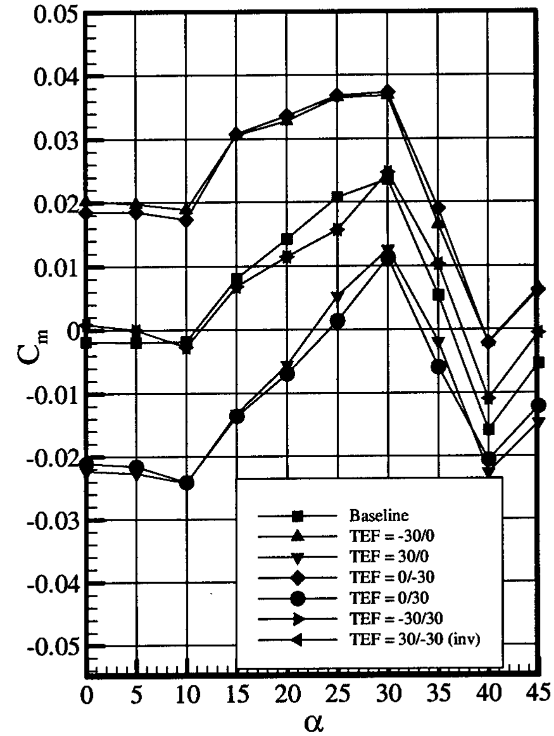

Figure C4b Pitching Moment Coefficient
as a Function of α, $\beta = 0^{\circ}$

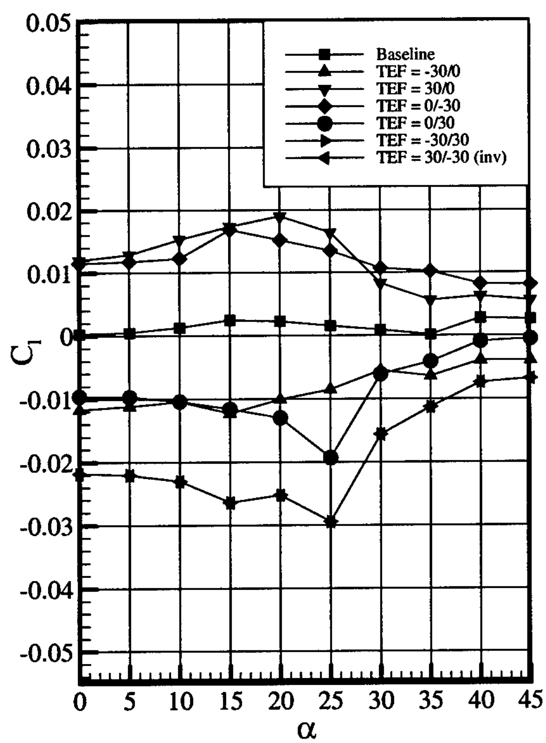

Figure C4c Rolling Moment Coefficient
as a Function of α, $\beta = 0^{\circ}$

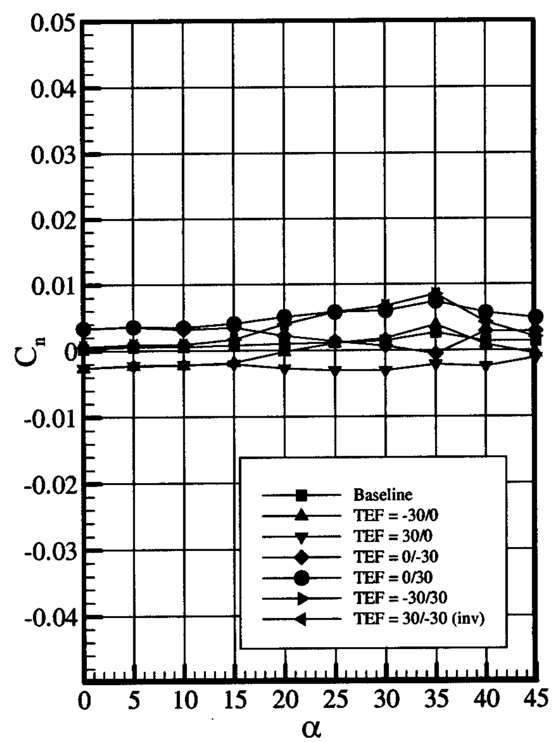

Figure C4d Yawing Moment Coefficient
as a Function of α, $\beta = 0^{\circ}$

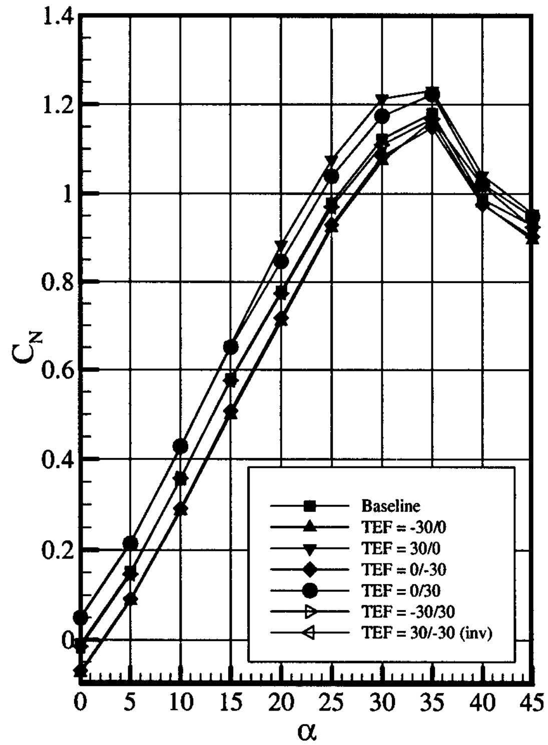

Figure C5a Normal Force Coefficient as a Function of α, β = 2°

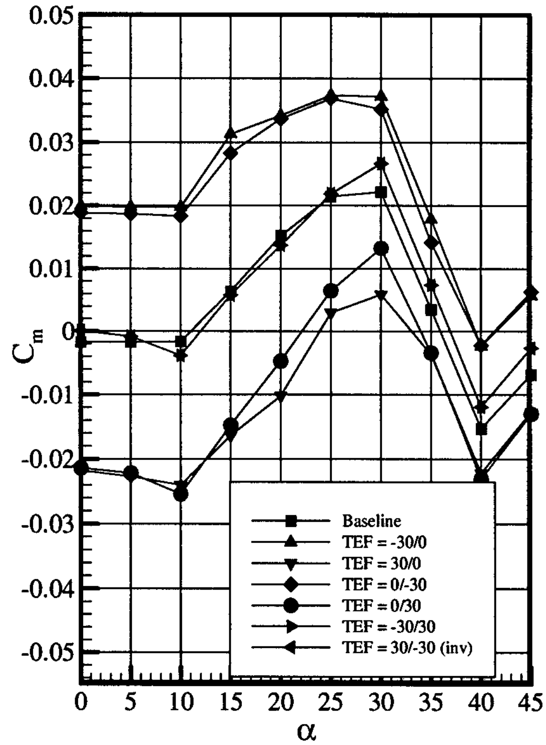

Figure C5b Pitching Moment Coefficient as a Function of α, β = 2°

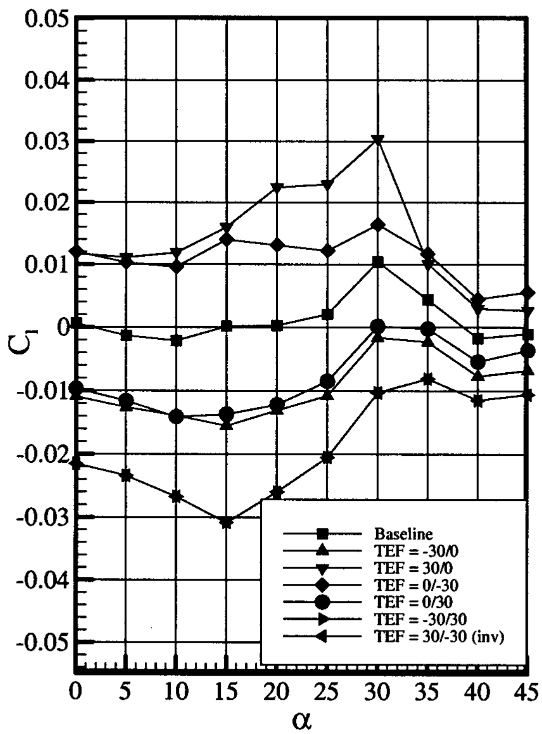

Figure C5c Rolling Moment Coefficient as a Function of α, β = 2°

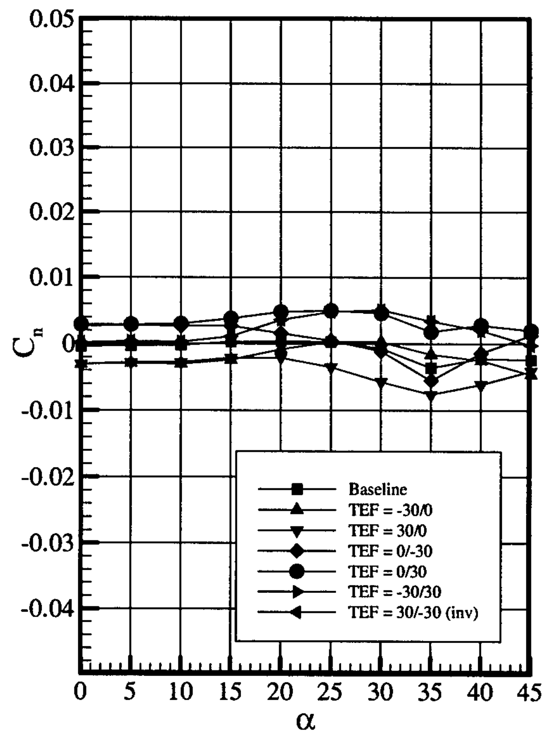

Figure C5d Yawing Moment Coefficient as a Function of α, β = 2°

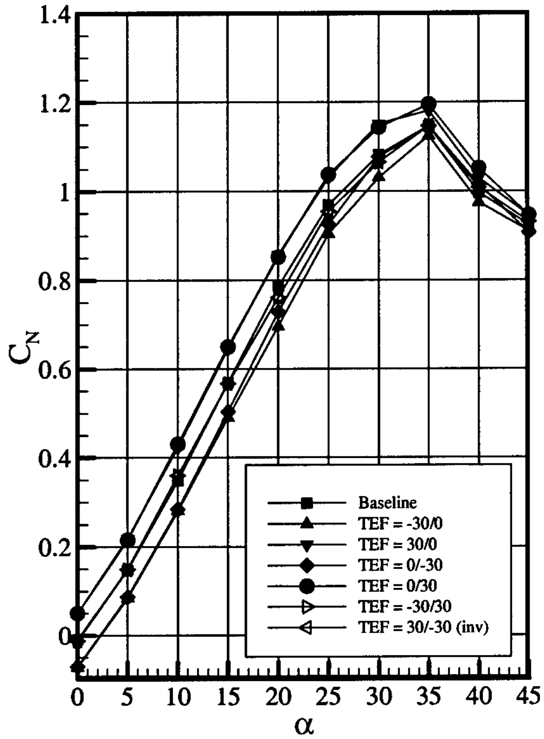

Figure C6a Normal Force Coefficient as a Function of α, β = 4°

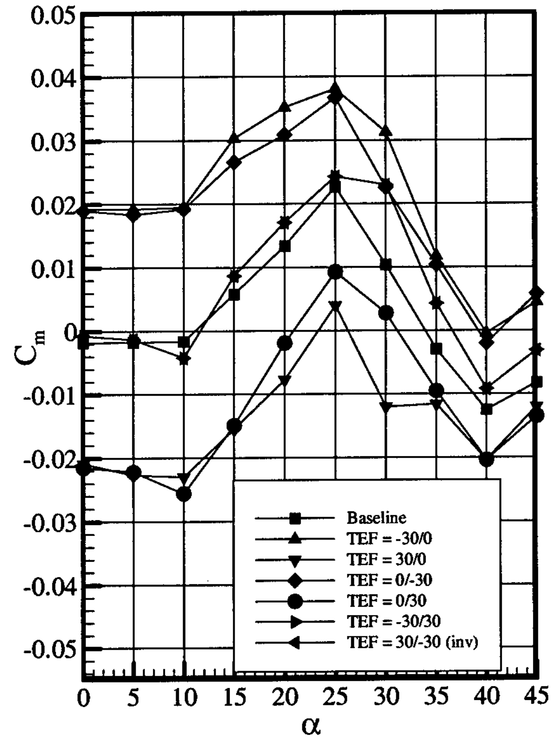

Figure C6b Pitching Moment Coefficient as a Function of α, β = 4°

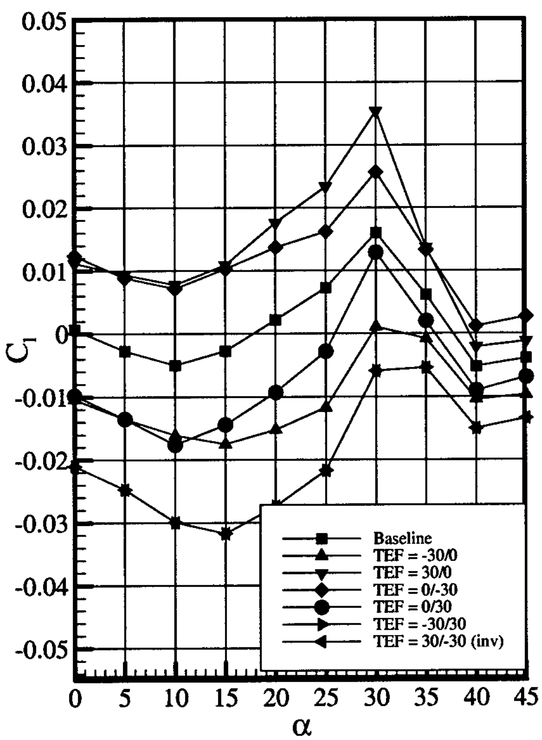

Figure C6c Rolling Moment Coefficient as a Function of α, β = 4°

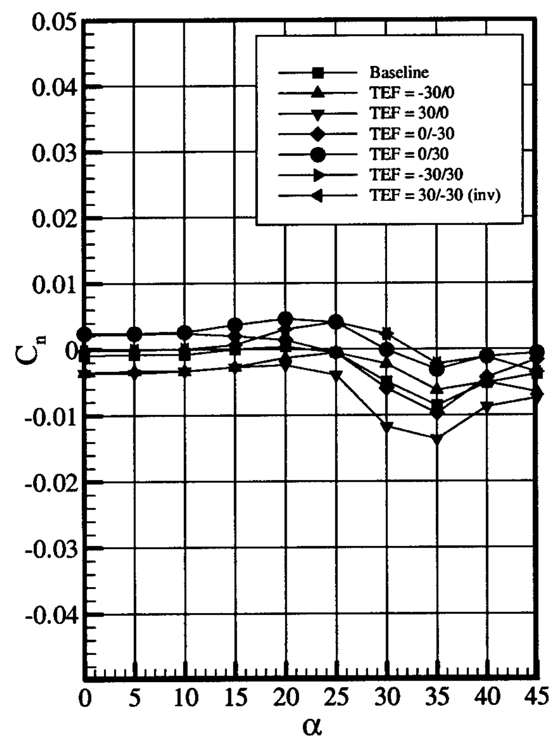

Figure C6d Yawing Moment Coefficient as a Function of α, β = 4°

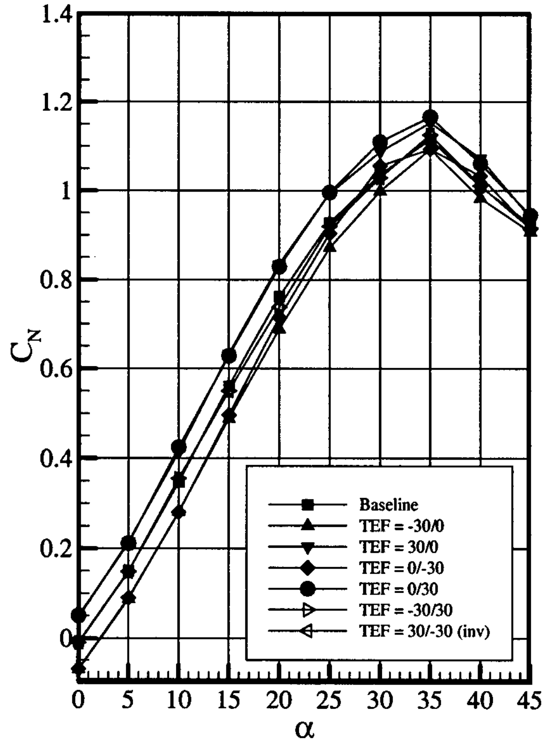

Figure C7a Normal Force Coefficient as a Function of α, $\beta = 6^{\circ}$

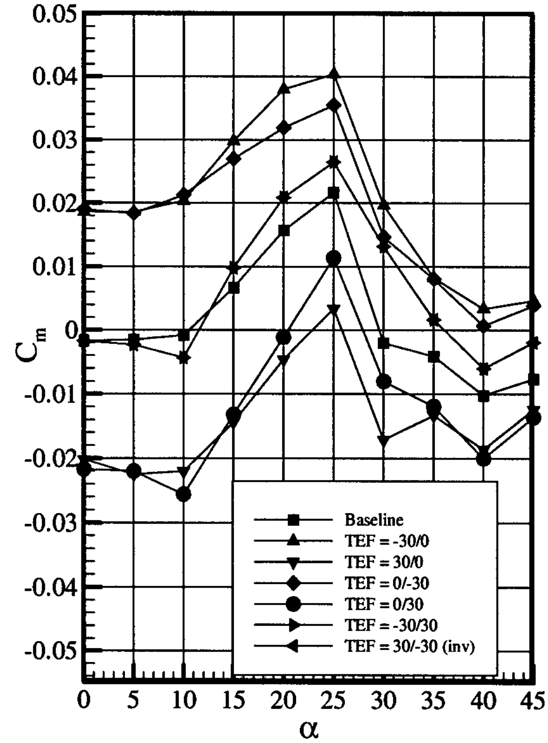

Figure C7b Pitching Moment Coefficient as a Function of α, $\beta = 6^{\circ}$

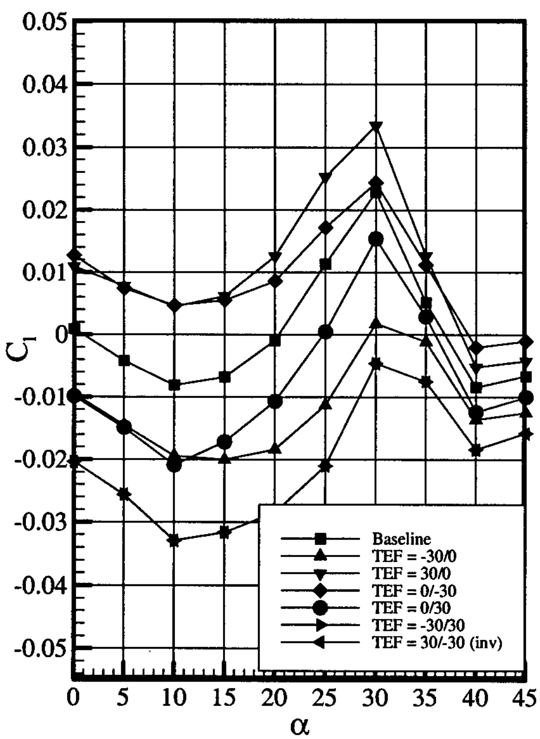

Figure C7c Rolling Moment Coefficient as a Function of α, $\beta = 6^{\circ}$

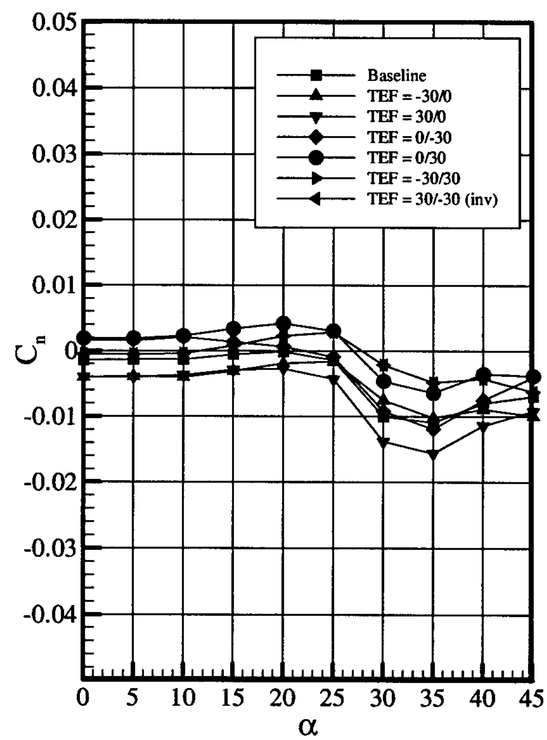

Figure C7d Yawing Moment Coefficient as a Function of α, $\beta = 6^{\circ}$

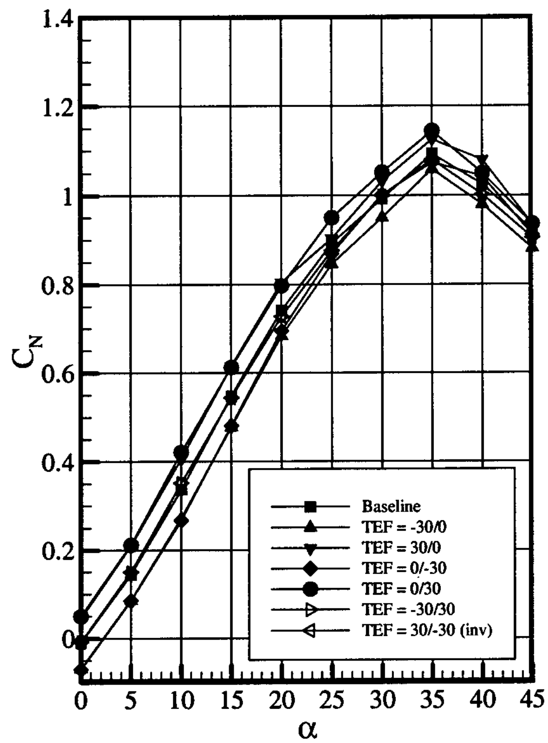

Figure C8a Normal Force Coefficient as a Function of α, β = 8°

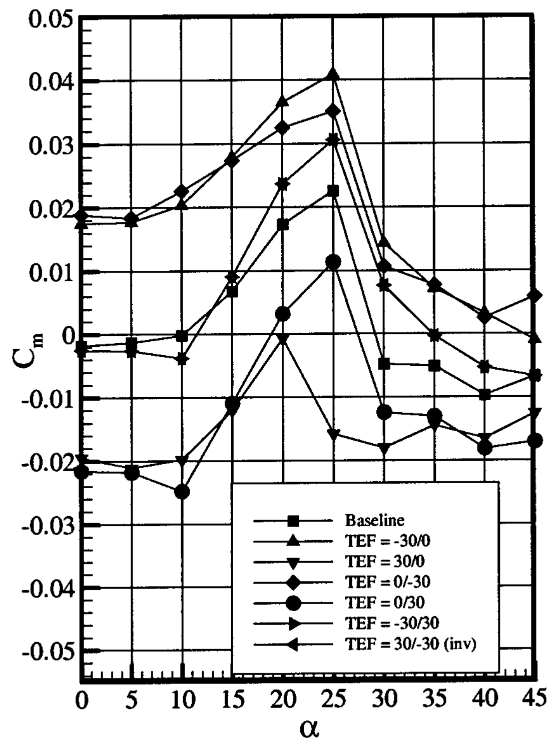

Figure C8b Pitching Moment Coefficient as a Function of α, β = 8°

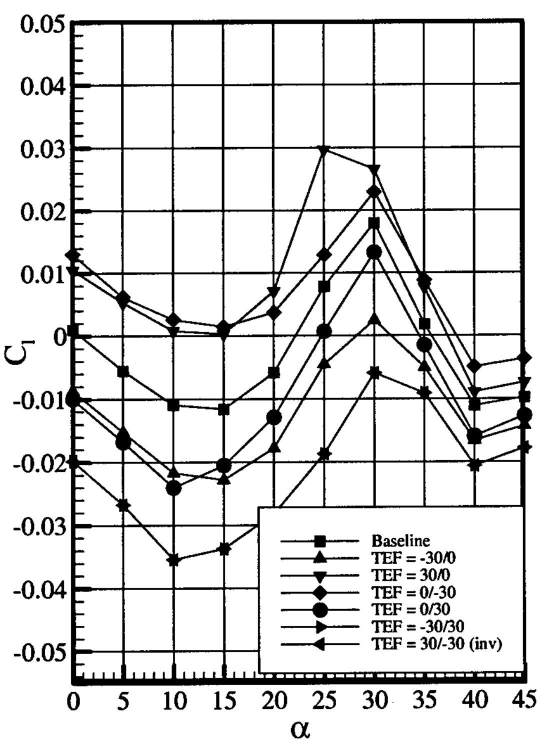

Figure C8c Rolling Moment Coefficient as a Function of α, β = 8°

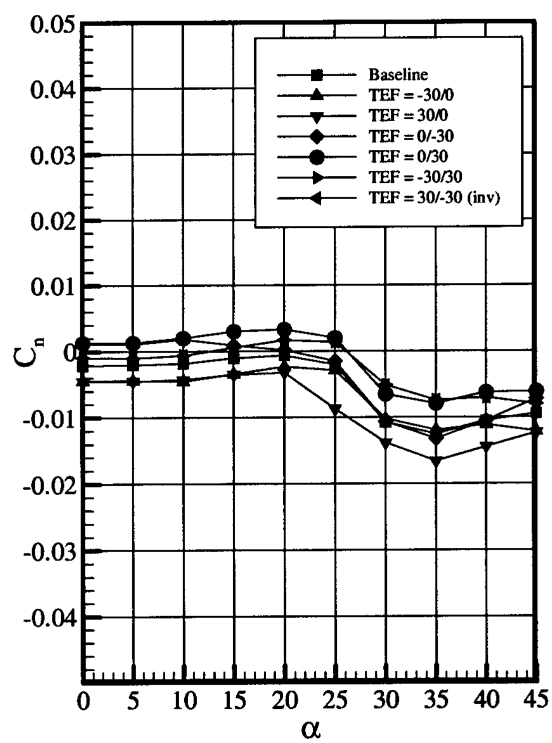

Figure C8d Yawing Moment Coefficient as a Function of α, β = 8°

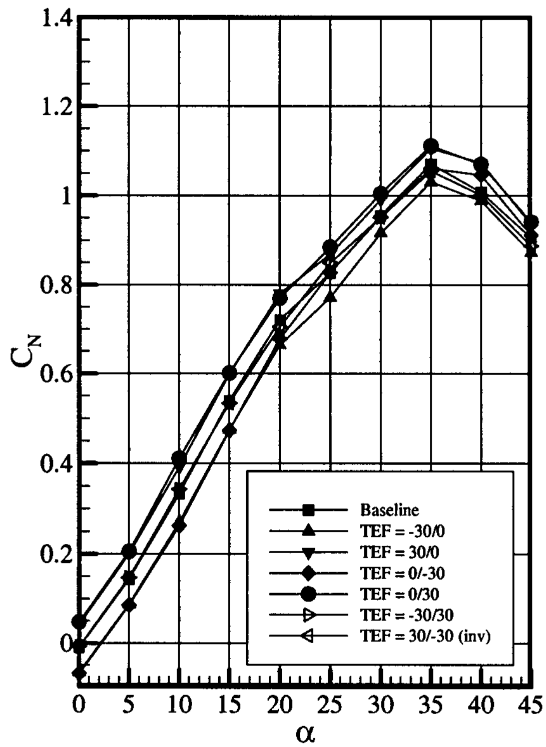

Figure C9a Normal Force Coefficient
as a Function of α, β = 10°

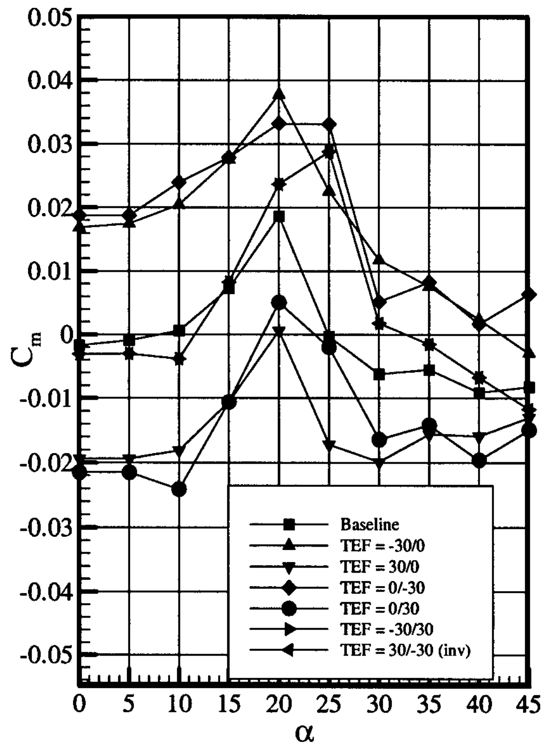

Figure C9b Pitching Moment Coefficient
as a Function of α, β = 10°

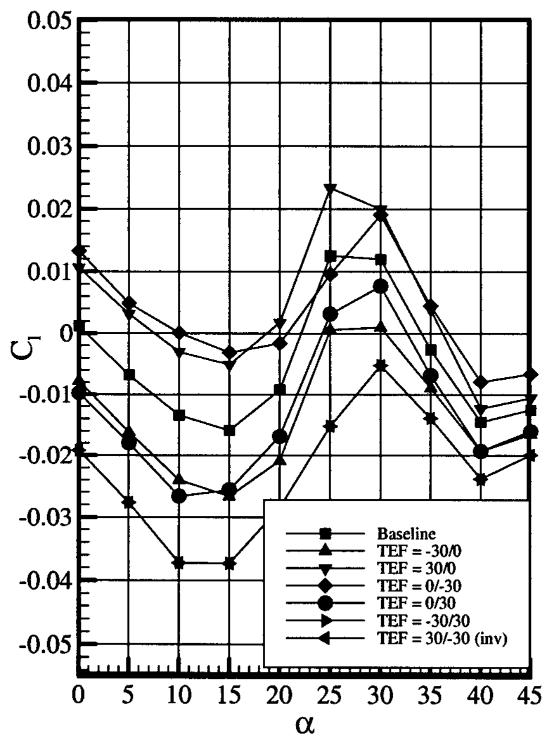

Figure C9c Rolling Moment Coefficient
as a Function of α, β = 10°

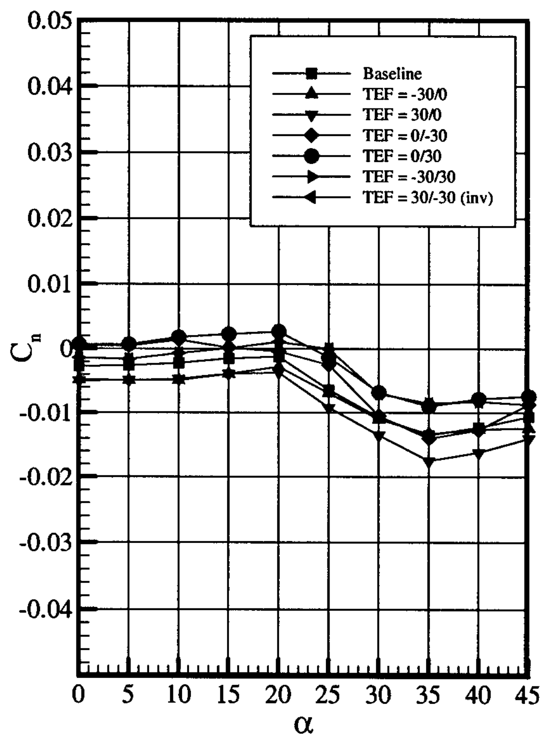

Figure C9d Yawing Moment Coefficient
as a Function of α, β = 10°

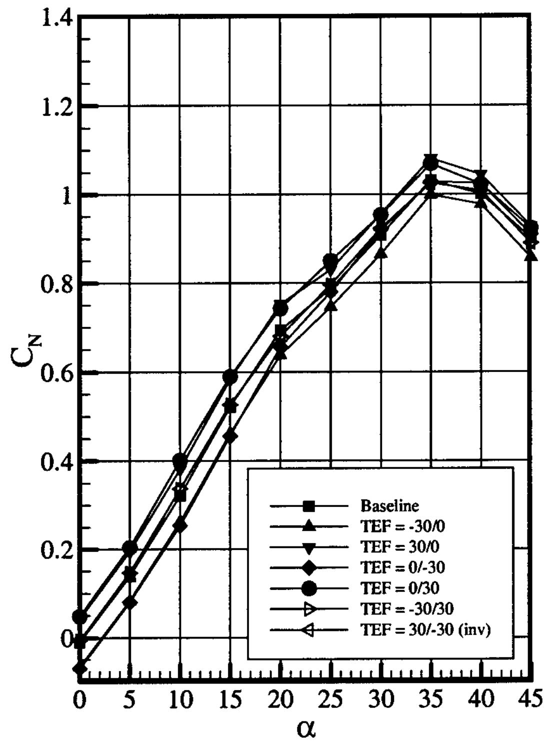

Figure C10a Normal Force Coefficient as a Function of α, β = 12°

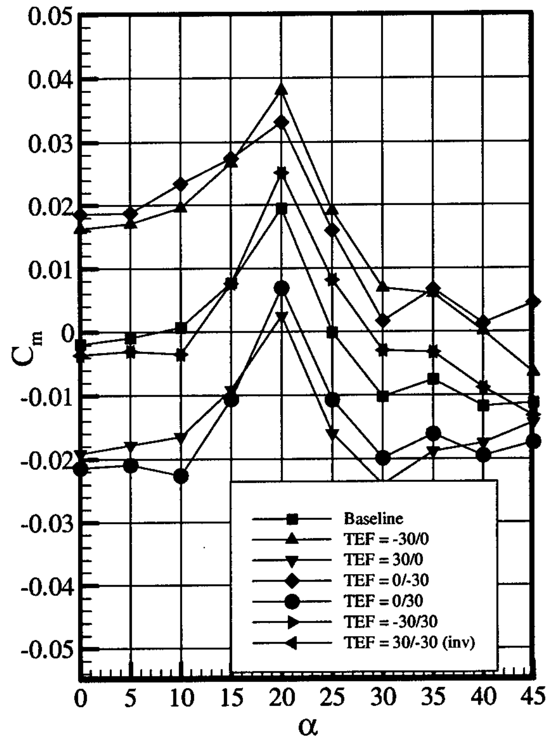

Figure C10b Pitching Moment Coefficient as a Function of α, β = 12°

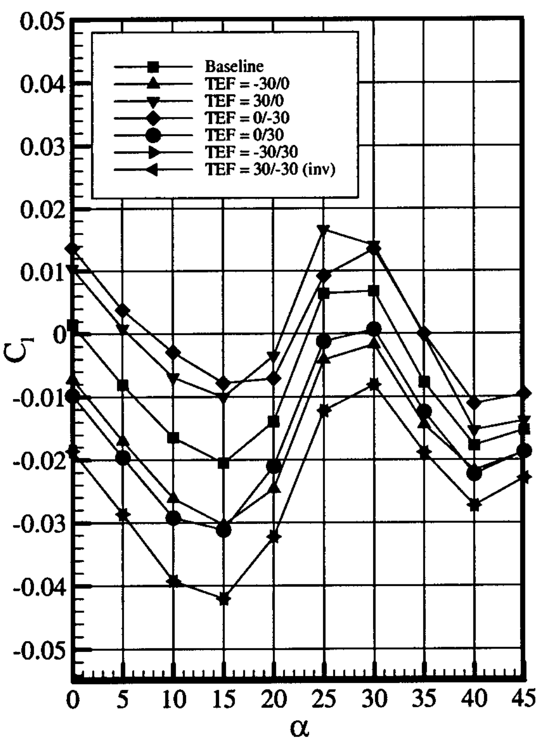

Figure C10c Rolling Moment Coefficient as a Function of α, β = 12°

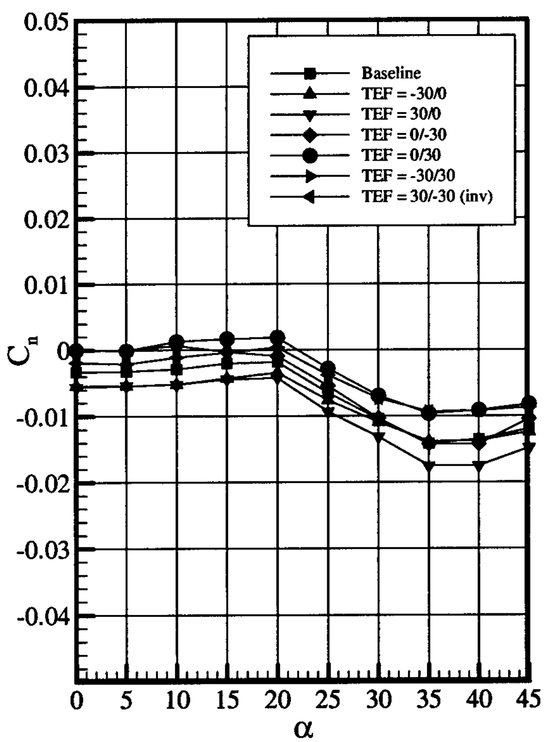

Figure C10d Yawing Moment Coefficient as a Function of α, β = 12°

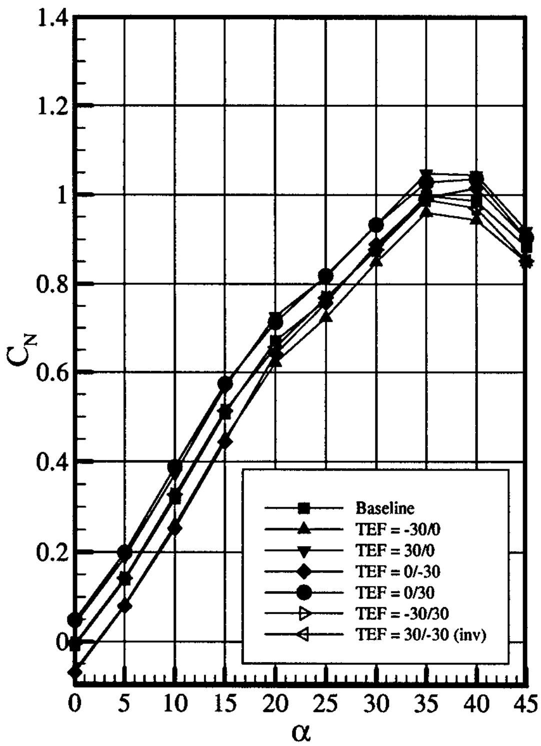

Figure C11a Normal Force Coefficient as a Function of α, $\beta = 14^{\circ}$

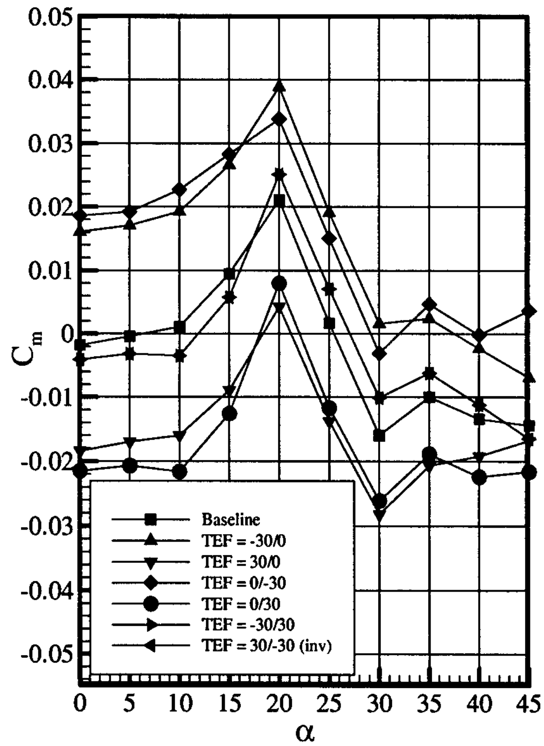

Figure C11b Pitching Moment Coefficient as a Function of α, $\beta = 14^{\circ}$

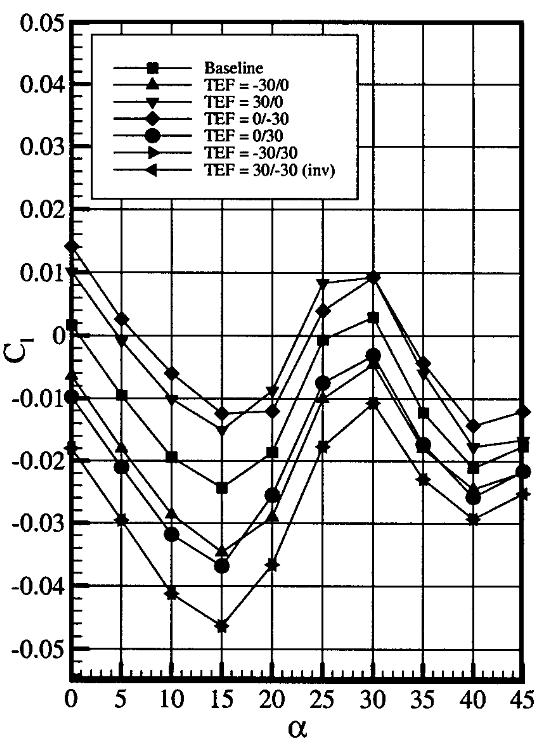

Figure C11c Rolling Moment Coefficient as a Function of α, $\beta = 14^{\circ}$

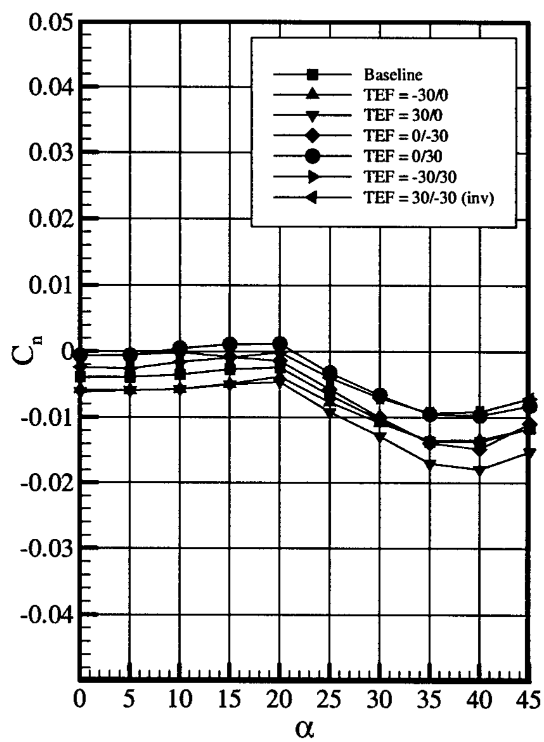

Figure C11d Yawing Moment Coefficient as a Function of α, $\beta = 14^{\circ}$

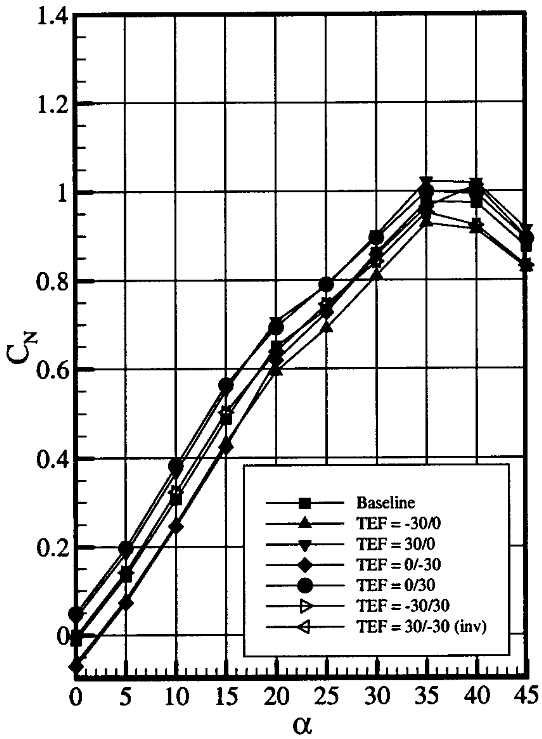

Figure C12a Normal Force Coefficient as a Function of α, β = 16°

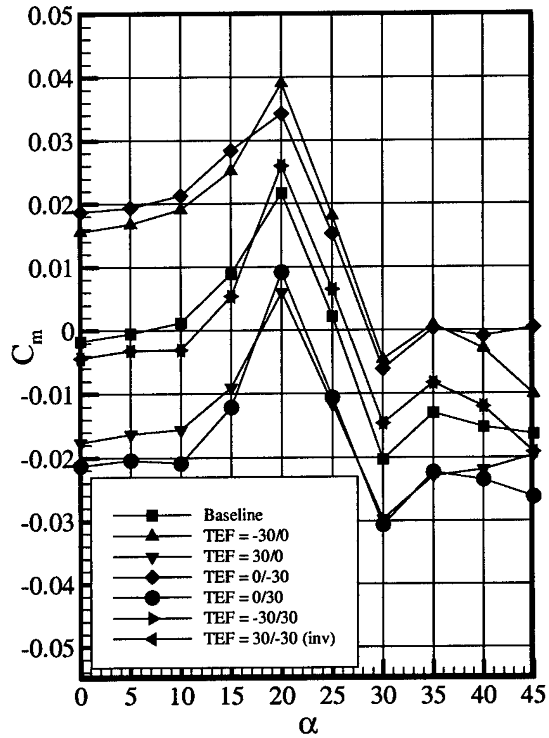

Figure C12b Pitching Moment Coefficient as a Function of α, β = 16°

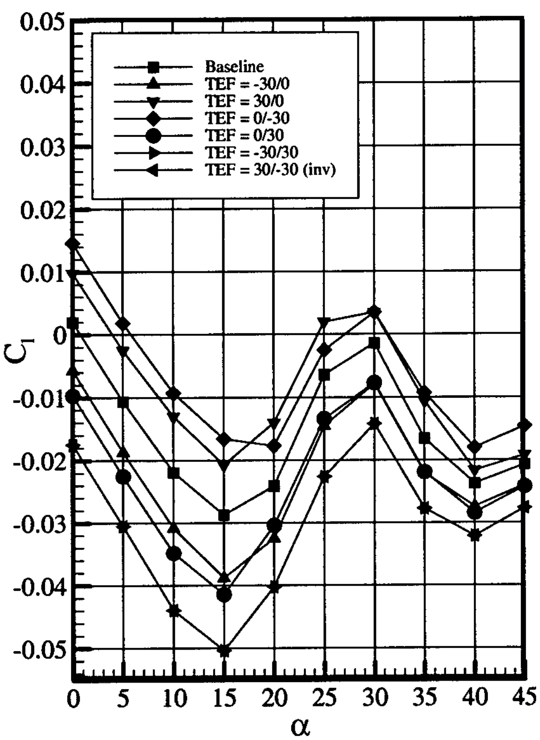

Figure C12c Rolling Moment Coefficient as a Function of α, β = 16°

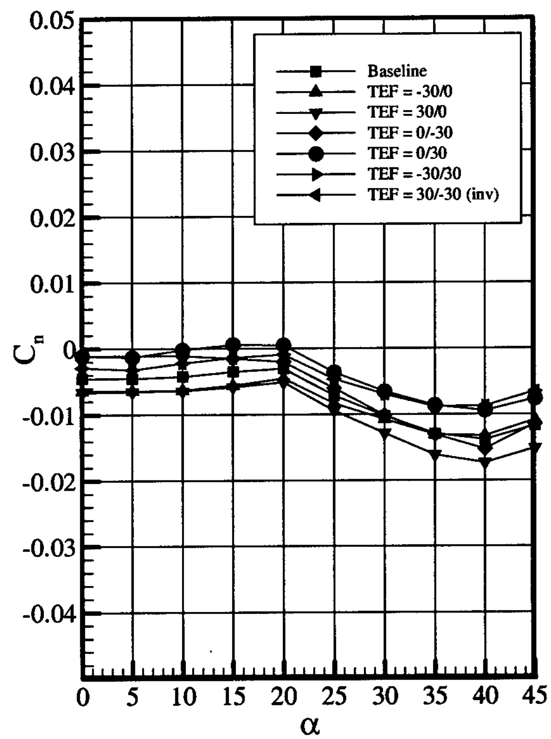

Figure C12d Yawing Moment Coefficient as a Function of α, β = 16°

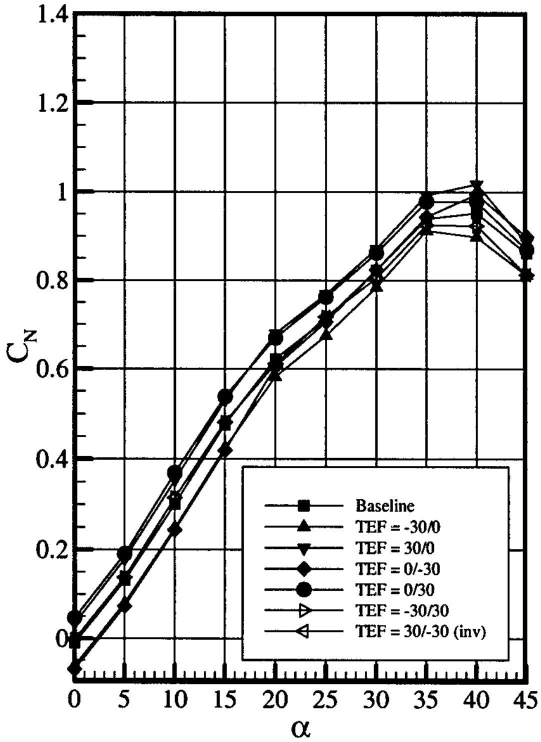

Figure C13a Normal Force Coefficient as a Function of α, β = 18°

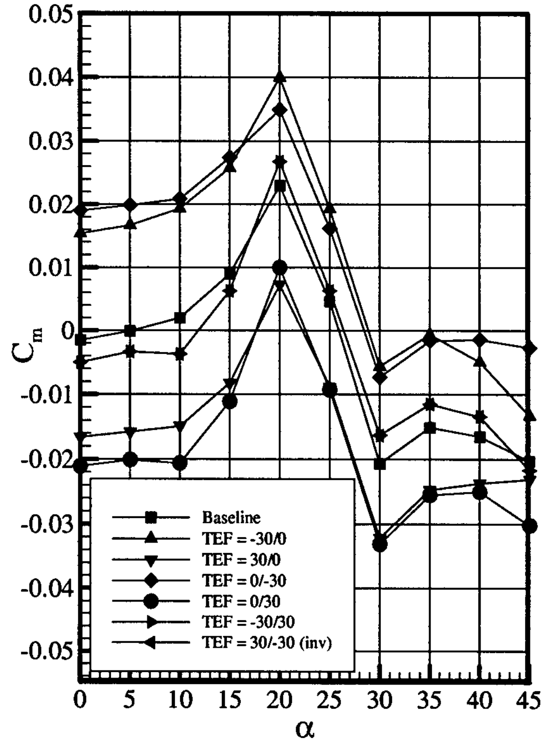

Figure C13b Pitching Moment Coefficient as a Function of α, β = 18°

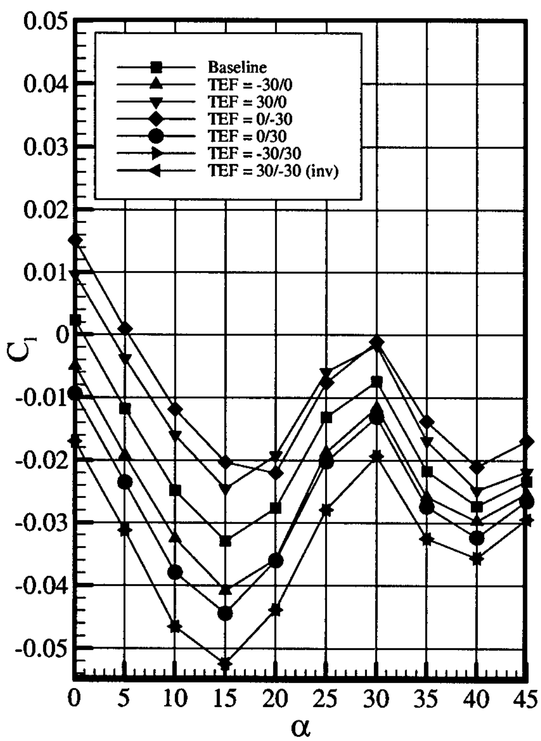

Figure C13c Rolling Moment Coefficient as a Function of α, β = 18°

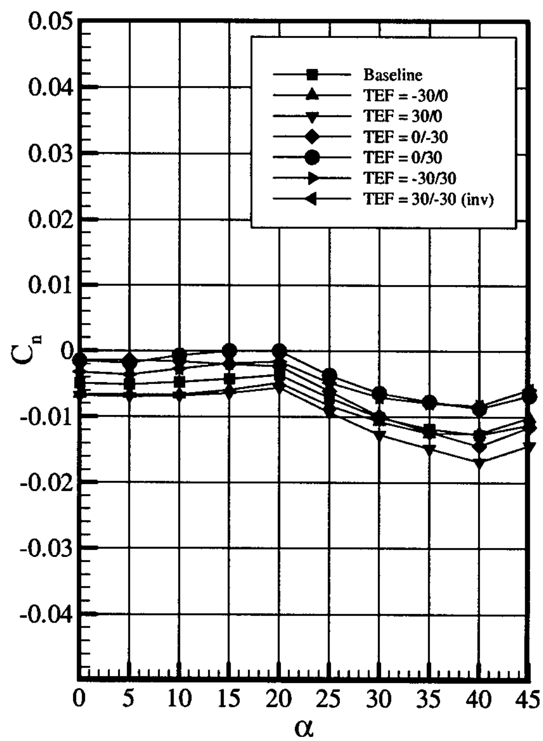

Figure C13d Yawing Moment Coefficient as a Function of α, β = 18°

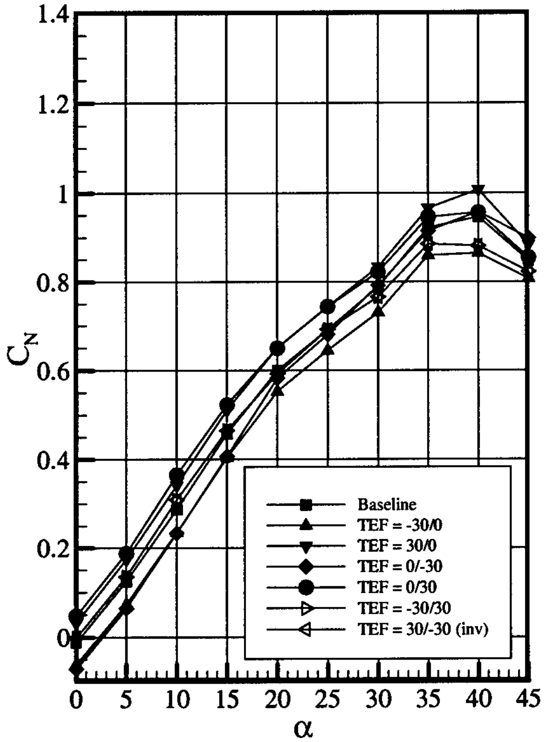

Figure C14a Normal Force Coefficient as a Function of α, β = 20°

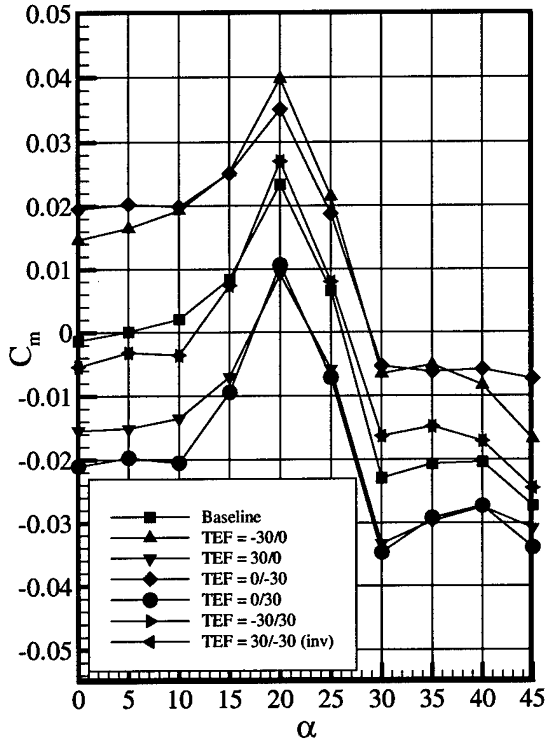

Figure C14b Pitching Moment Coefficient as a Function of α, β = 20°

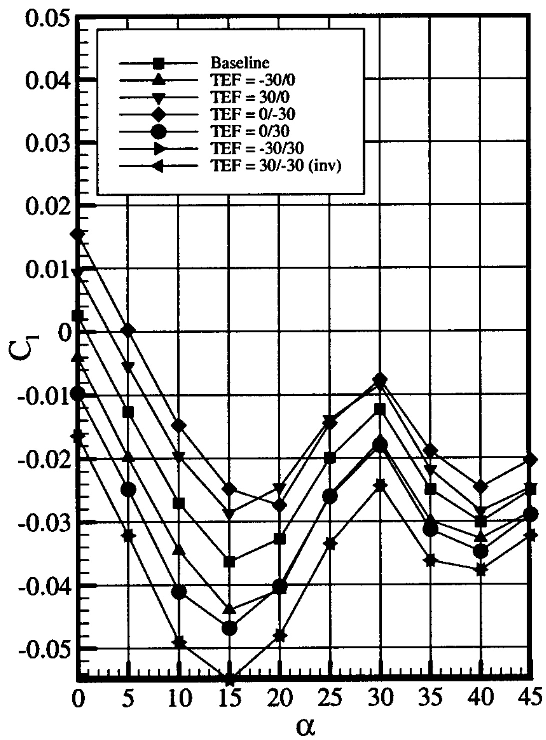

Figure C14c Rolling Moment Coefficient as a Function of α, β = 20°

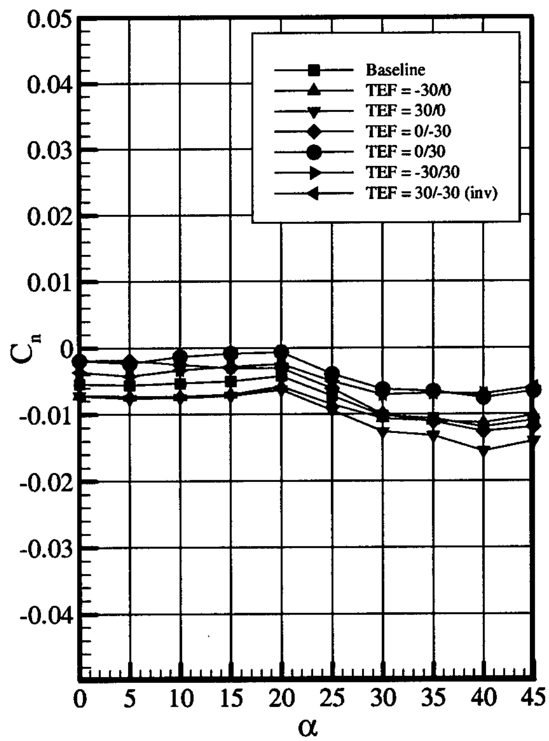

Figure C14d Yawing Moment Coefficient as a Function of α, β = 20°

Appendix D Trailing-Edge-Flap-Deflection Data as a Function of Sideslip Angle

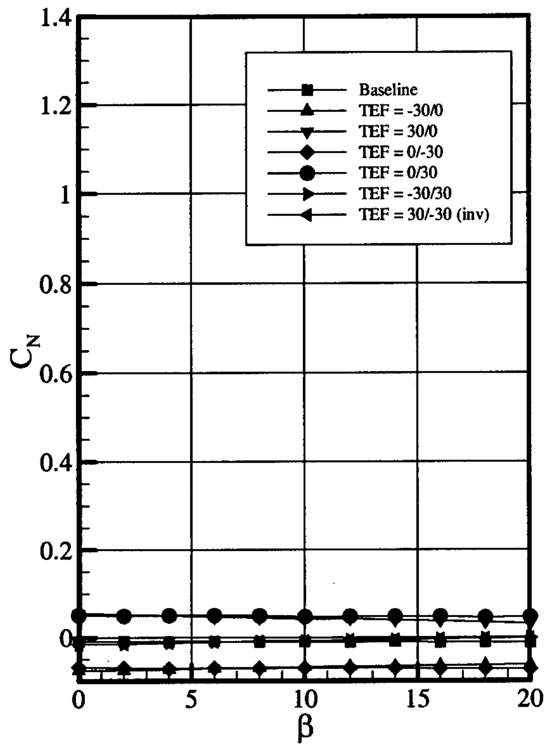

Figure D1a Normal Force Coefficient as a Function of β, α = 0°

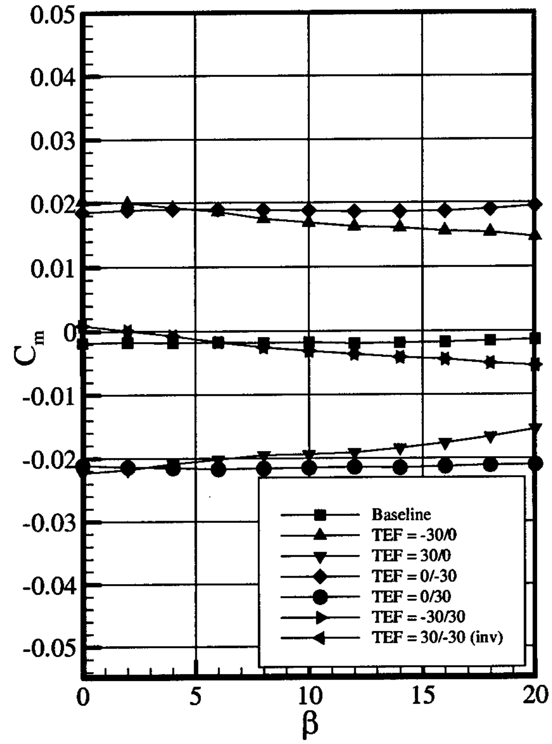

Figure D1b Pitching Moment Coefficient as a Function of β, α = 0°

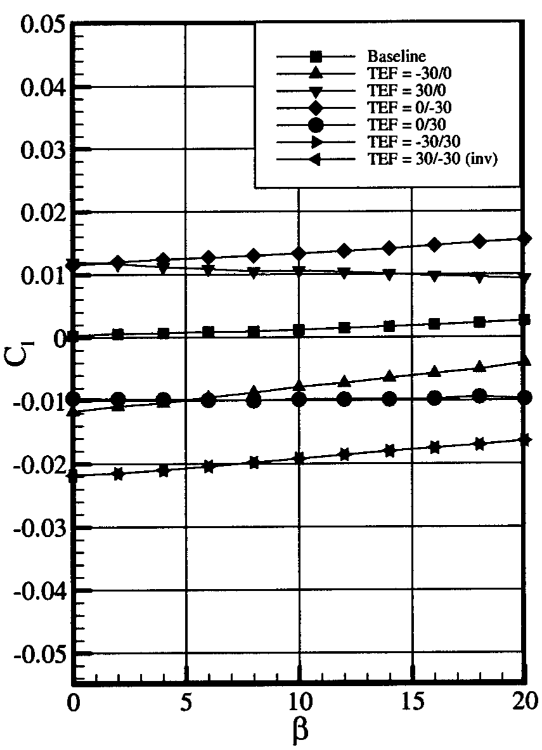

Figure D1c Rolling Moment Coefficient as a Function of β, α = 0°

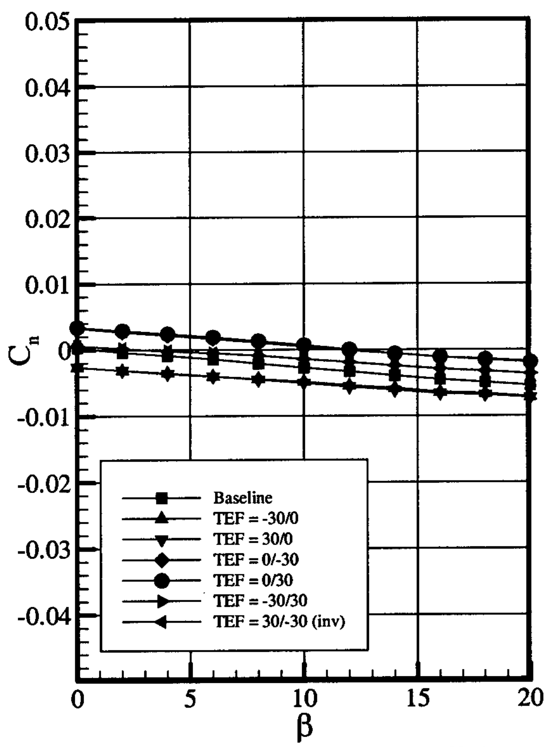

Figure D1d Yawing Moment Coefficient as a Function of β, α = 0°

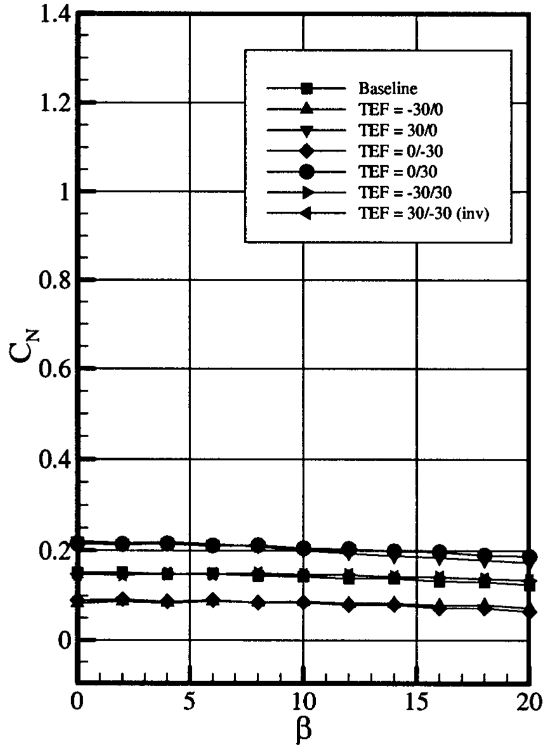

Figure D2a Normal Force Coefficient as a Function of β, α = 5°

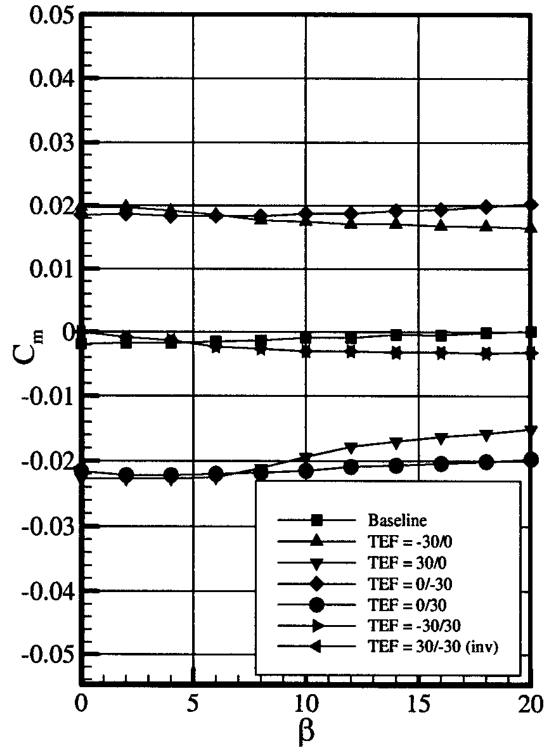

Figure D2b Pitching Moment Coefficient as a Function of β, α = 5°

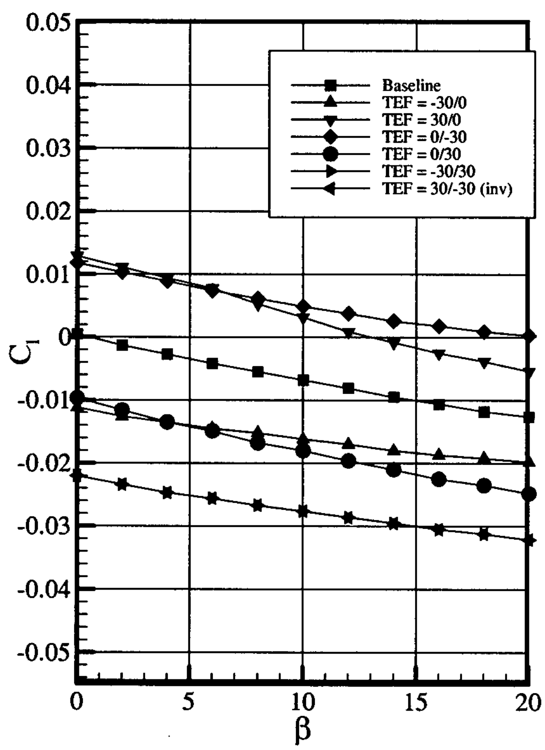

Figure D2c Rolling Moment Coefficient as a Function of β, α = 5°

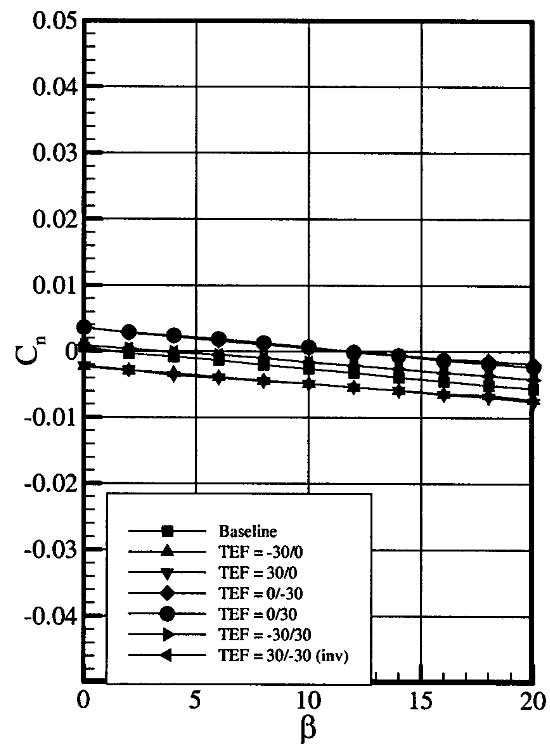

Figure D2d Yawing Moment Coefficient as a Function of β, α = 5°

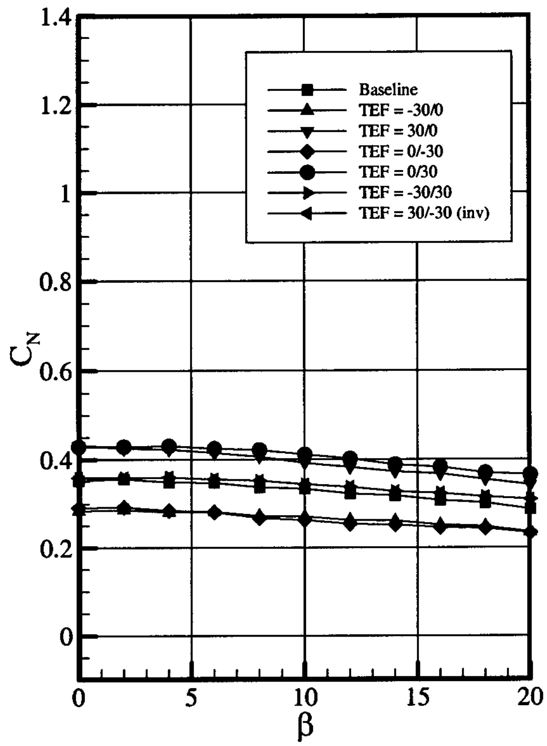

Figure D3a Normal Force Coefficient as a Function of β, α = 10°

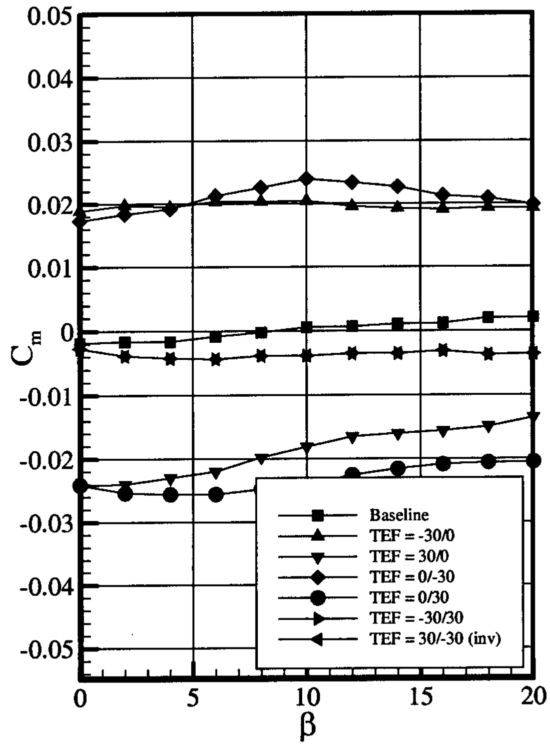

Figure D3b Pitching Moment Coefficient as a Function of β, α = 10°

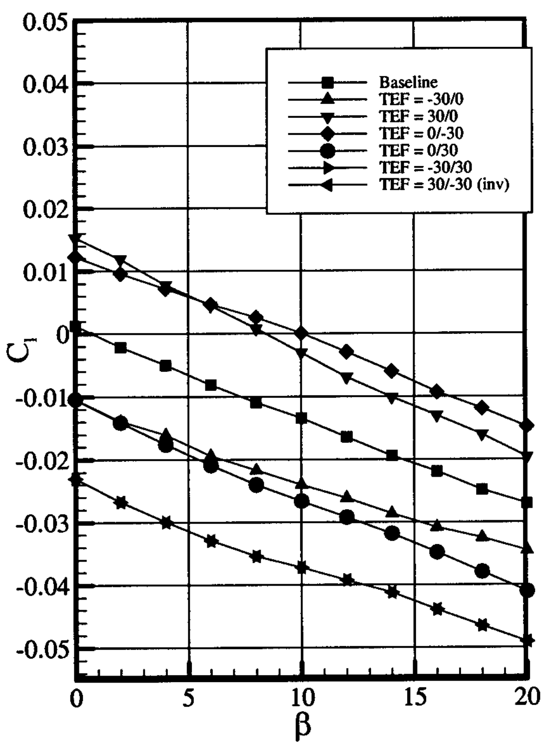

Figure D3c Rolling Moment Coefficient as a Function of β, α = 10°

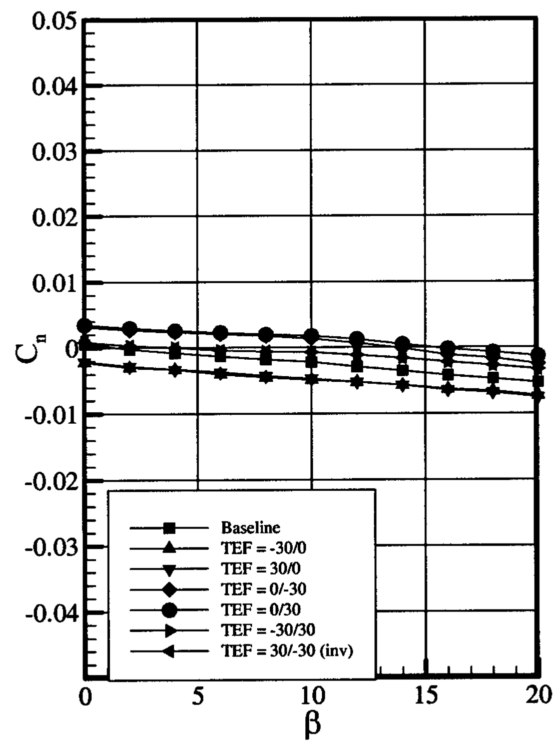

Figure D3d Yawing Moment Coefficient as a Function of β, α = 10°

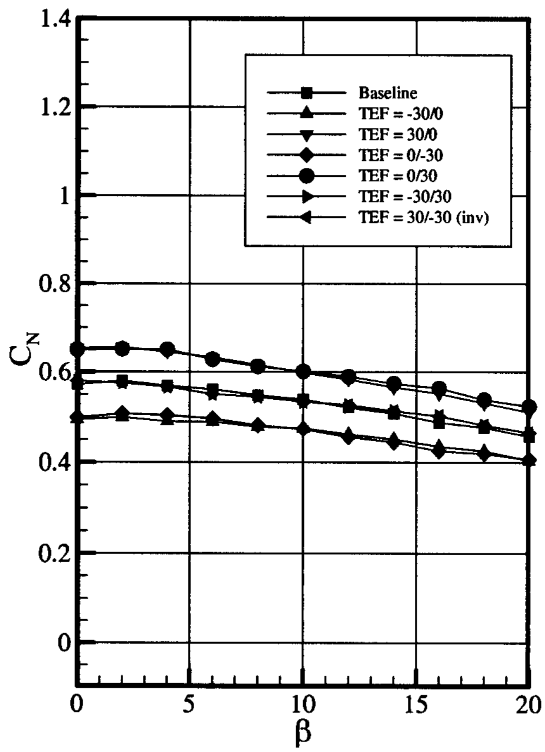

Figure D4a Normal Force Coefficient as a Function of β, α = 15°

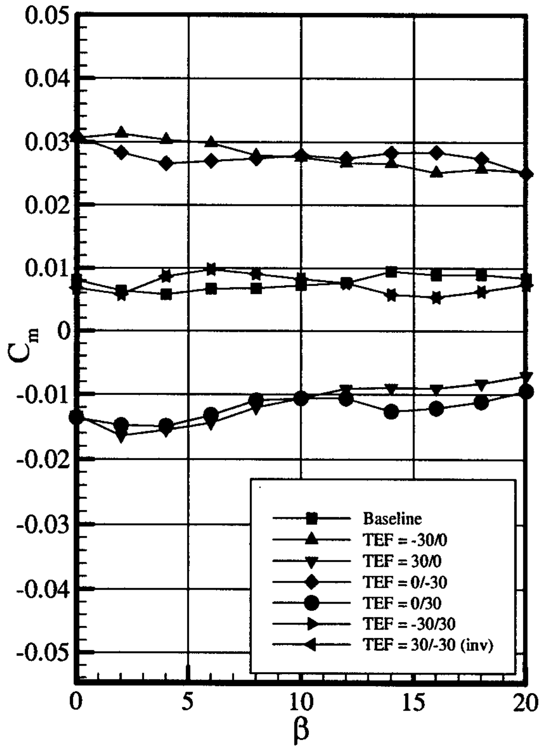

Figure D4b Pitching Moment Coefficient as a Function of β, α = 15°

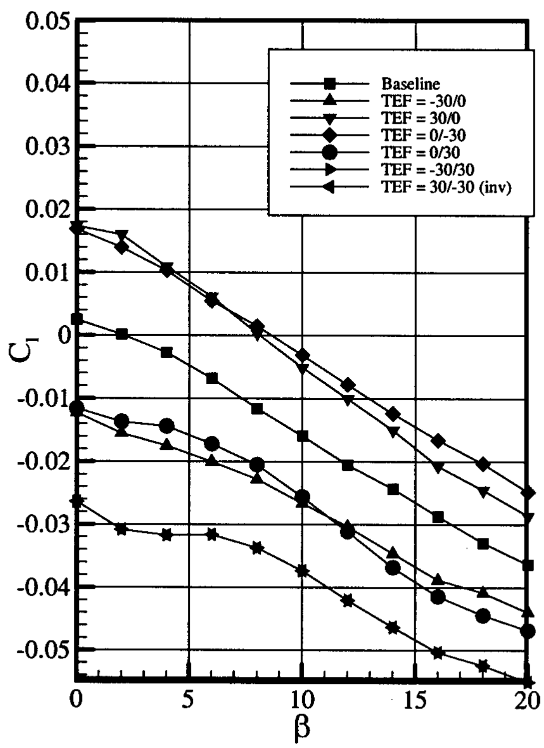

Figure D4c Rolling Moment Coefficient as a Function of β, α = 15°

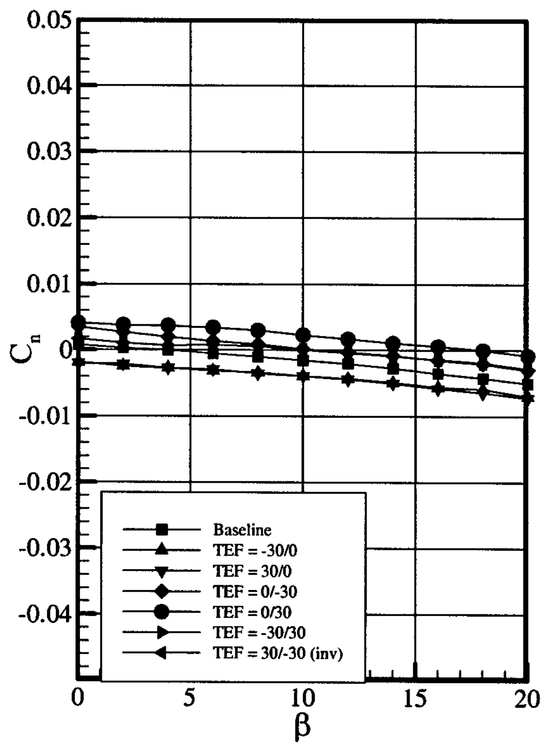

Figure D4d Yawing Moment Coefficient as a Function of β, α = 15°

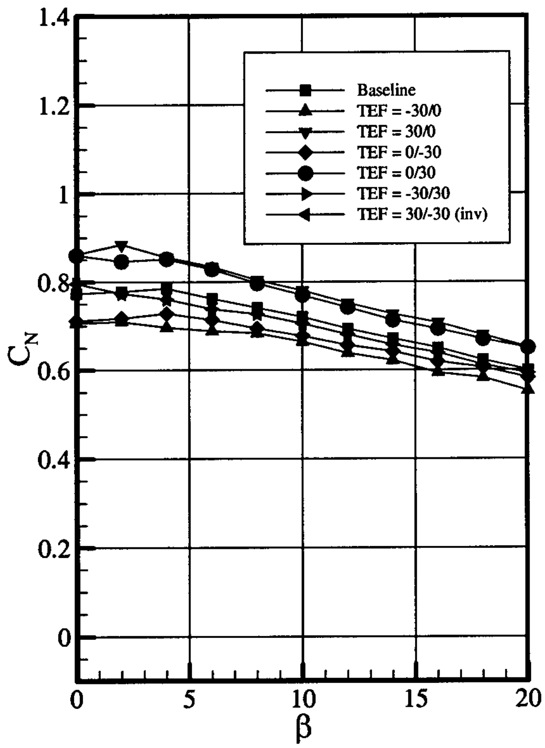

Figure D5a Normal Force Coefficient as a Function of β, $\alpha = 20^{\circ}$

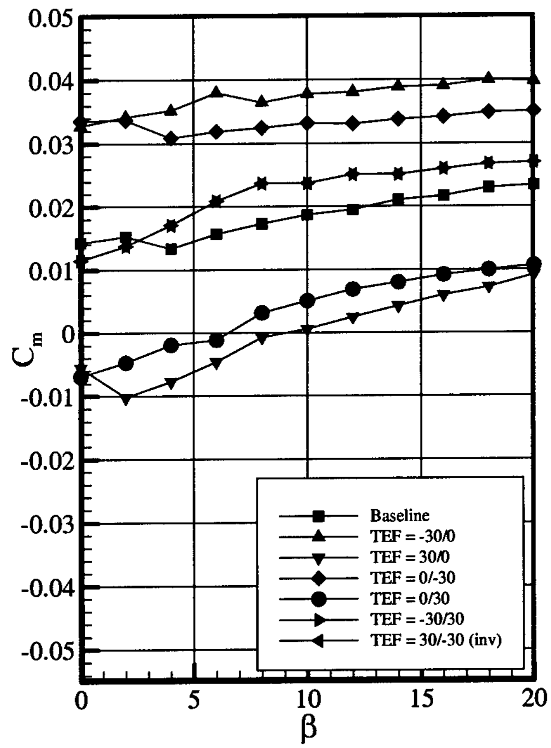

Figure D5b Pitching Moment Coefficient as a Function of β, $\alpha = 20^{\circ}$

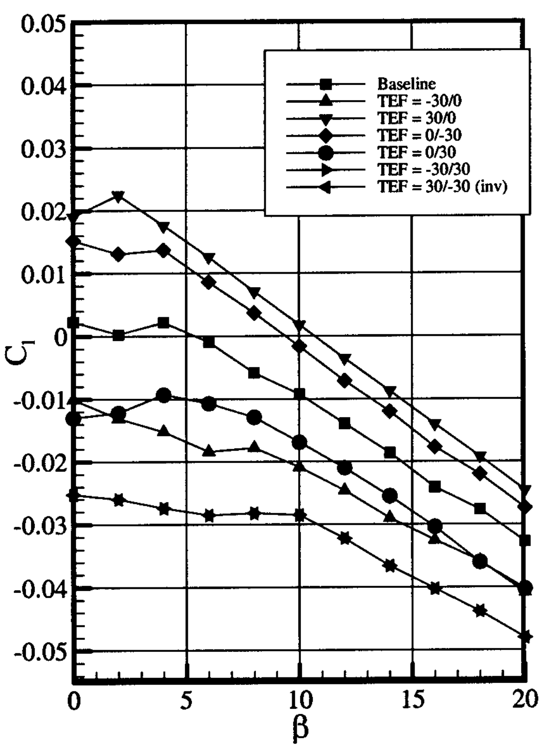

Figure D5c Rolling Moment Coefficient as a Function of β, $\alpha = 20^{\circ}$

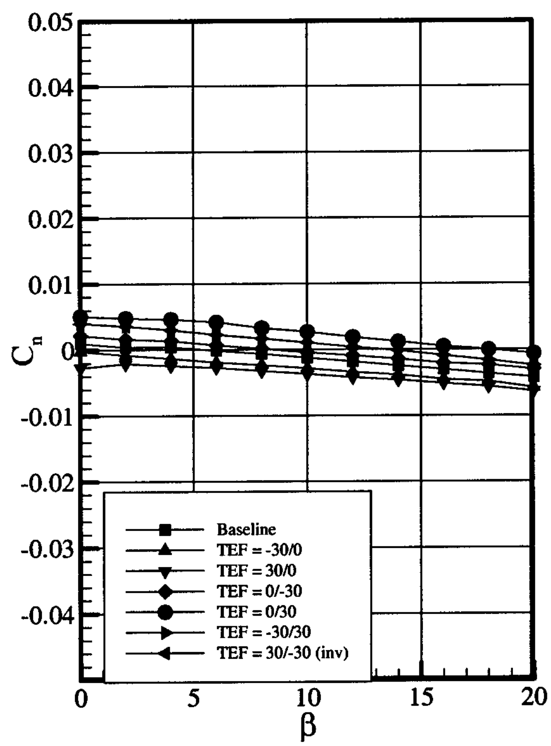

Figure D5d Yawing Moment Coefficient as a Function of β, $\alpha = 20^{\circ}$

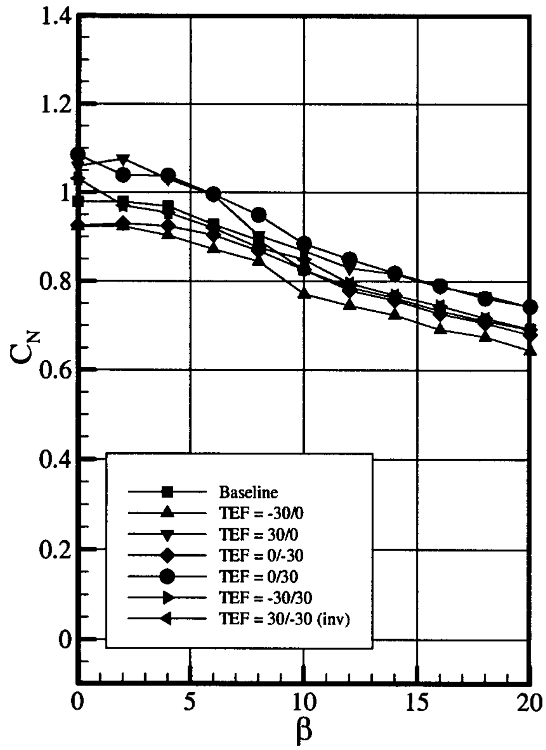

Figure D6a Normal Force Coefficient as a Function of β, α = 25°

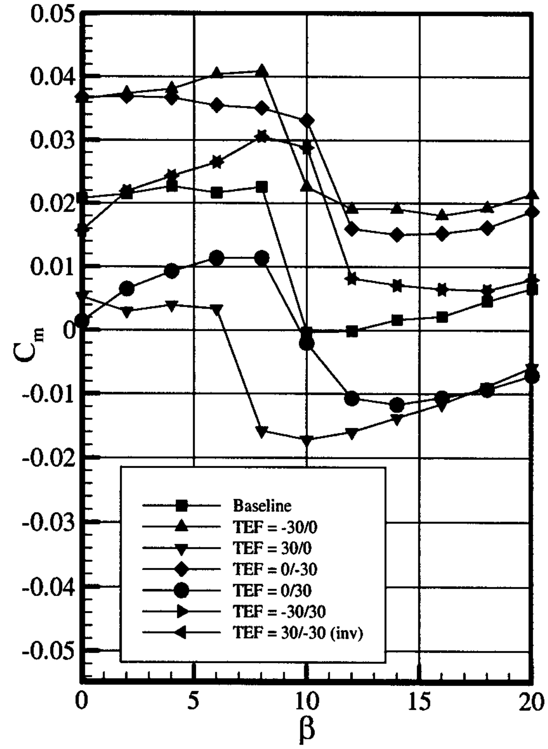

Figure D6b Pitching Moment Coefficient as a Function of β, α = 25°

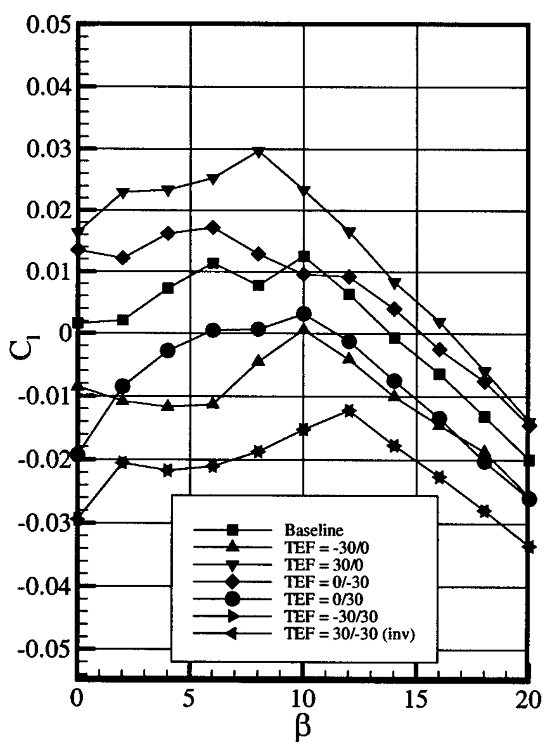

Figure D6c Rolling Moment Coefficient as a Function of β, α = 25°

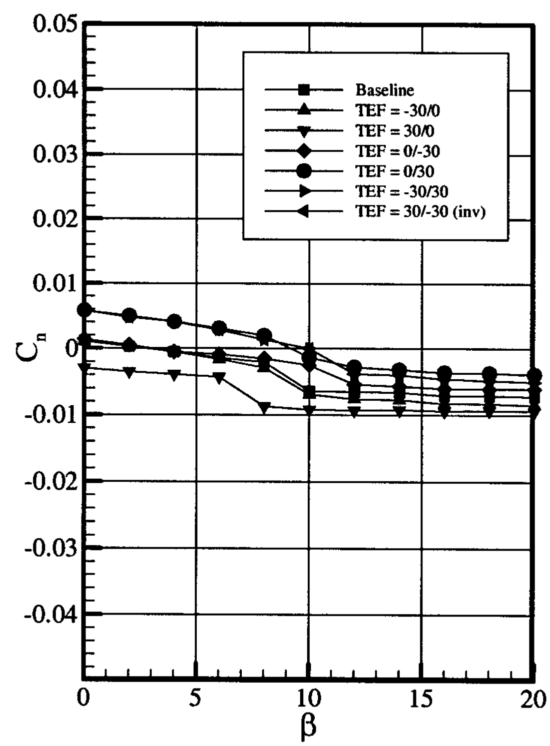

Figure D6d Yawing Moment Coefficient as a Function of β, α = 25°

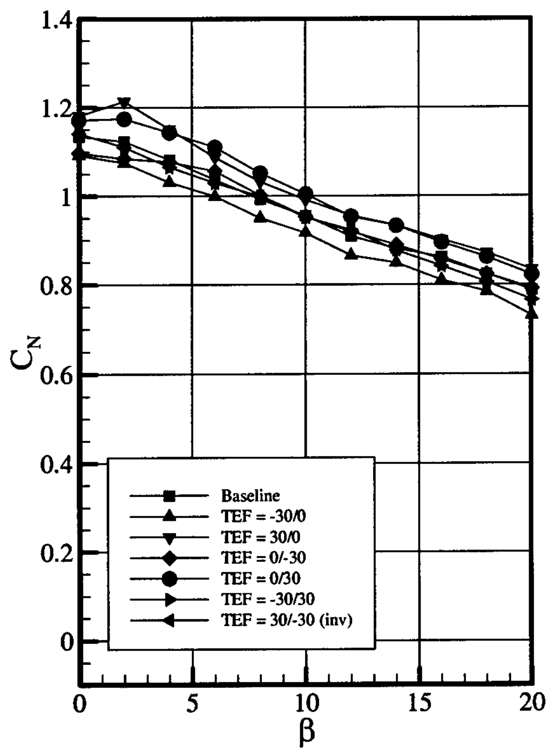

Figure D7a Normal Force Coefficient as a Function of β, α = 30°

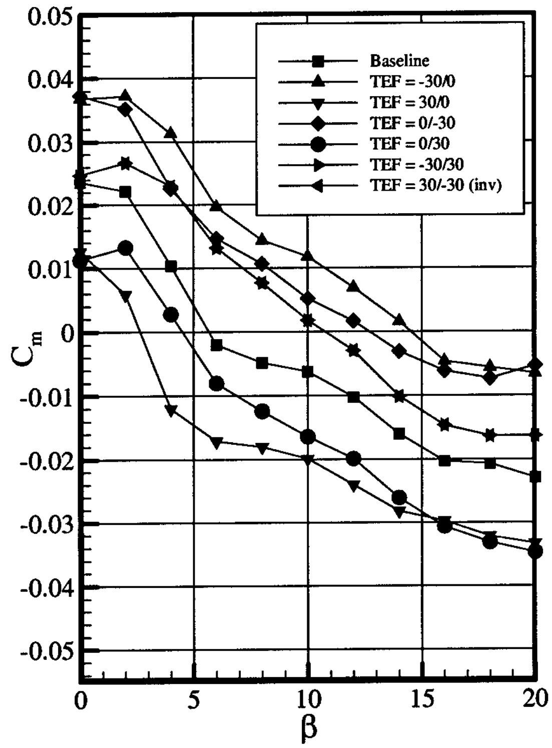

Figure D7b Pitching Moment Coefficient as a Function of β, α = 30°

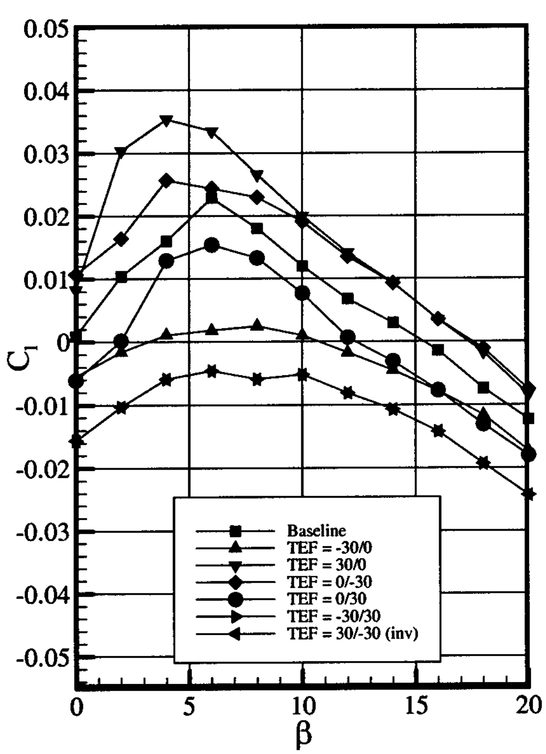

Figure D7c Rolling Moment Coefficient as a Function of β, α = 30°

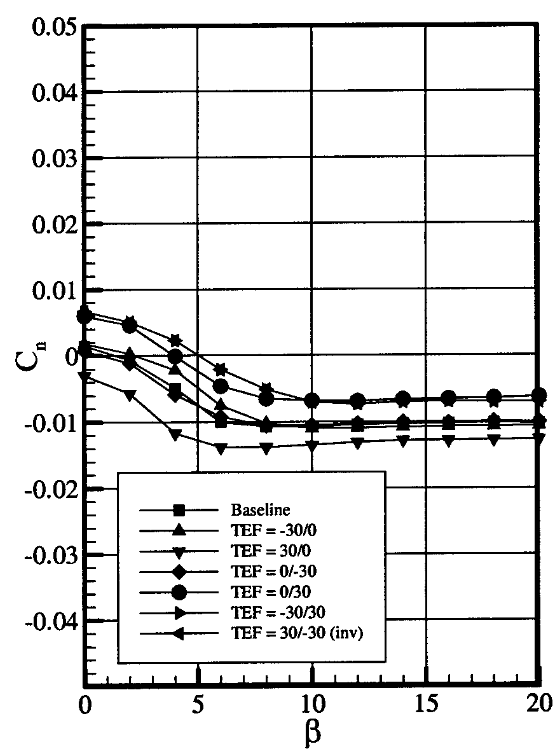

Figure D7d Yawing Moment Coefficient as a Function of β, α = 30°

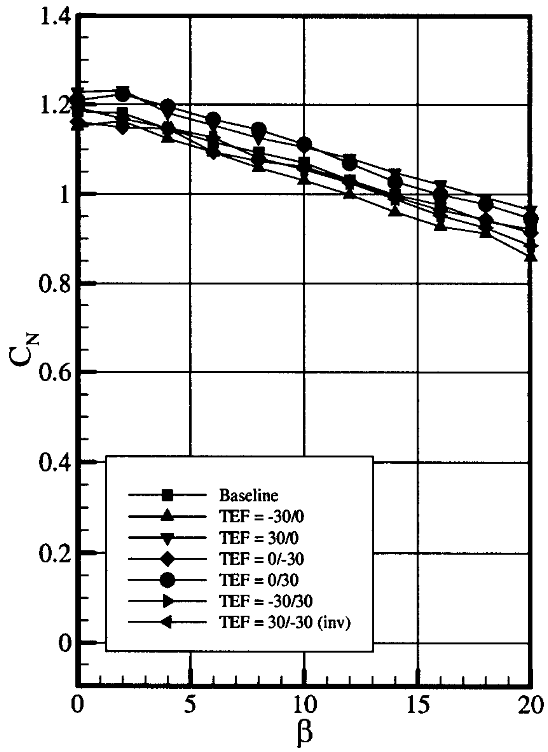

Figure D8a Normal Force Coefficient as a Function of β, α = 35°

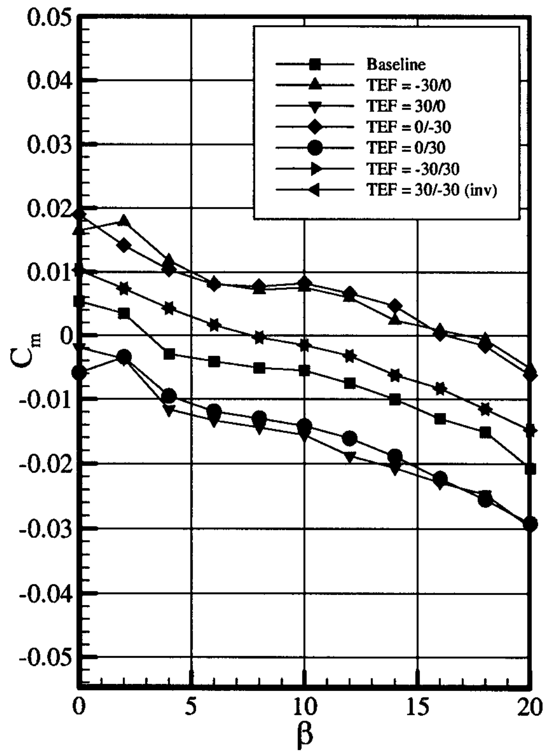

Figure D8b Pitching Moment Coefficient as a Function of β, α = 35°

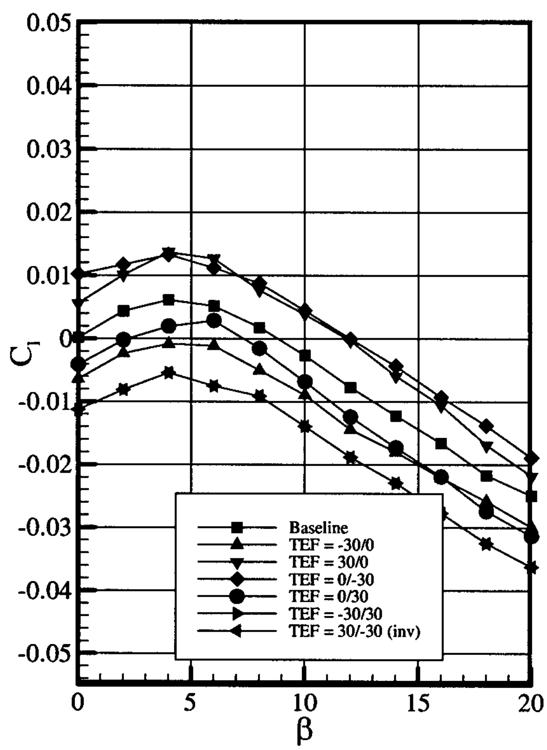

Figure D8c Rolling Moment Coefficient as a Function of β, α = 35°

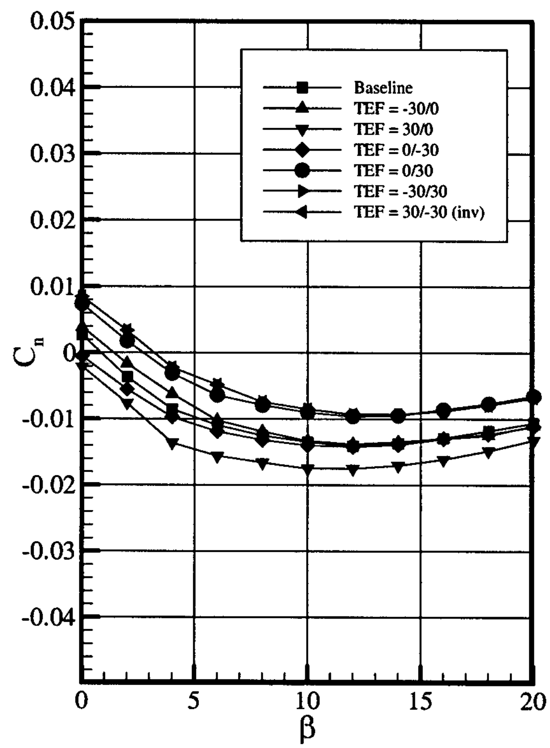

Figure D8d Yawing Moment Coefficient as a Function of β, α = 35°

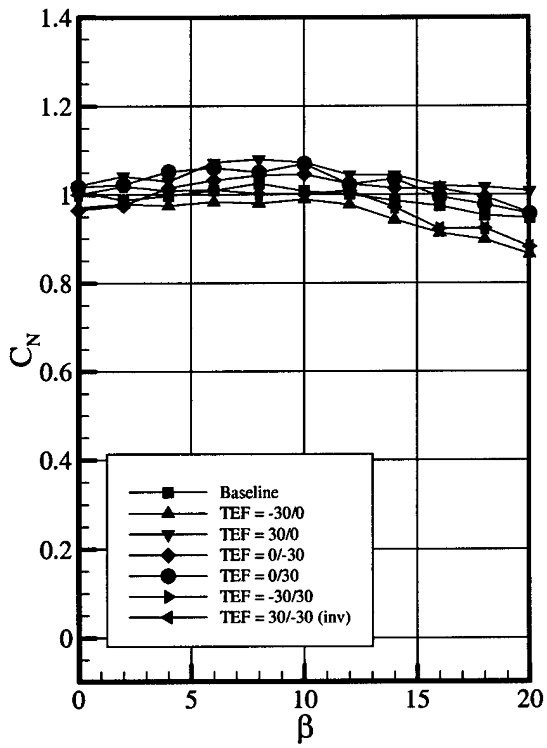

Figure D9a Normal Force Coefficient as a Function of β, α = 40°

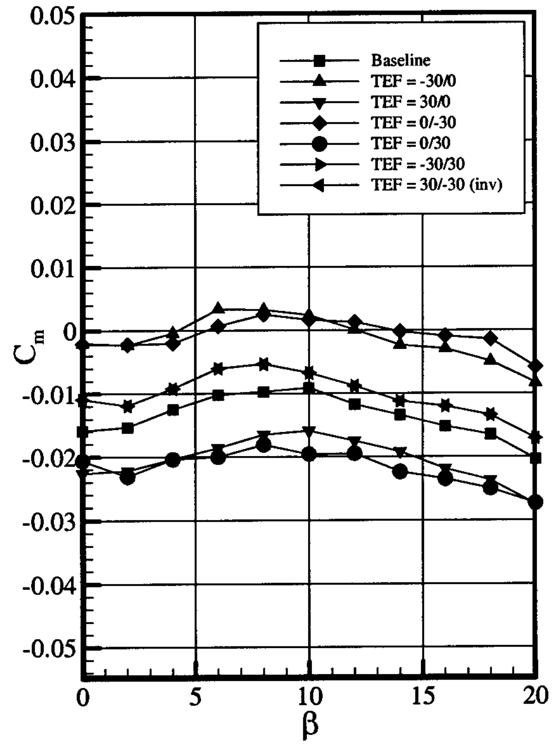

Figure D9b Pitching Moment Coefficient as a Function of β, α = 40°

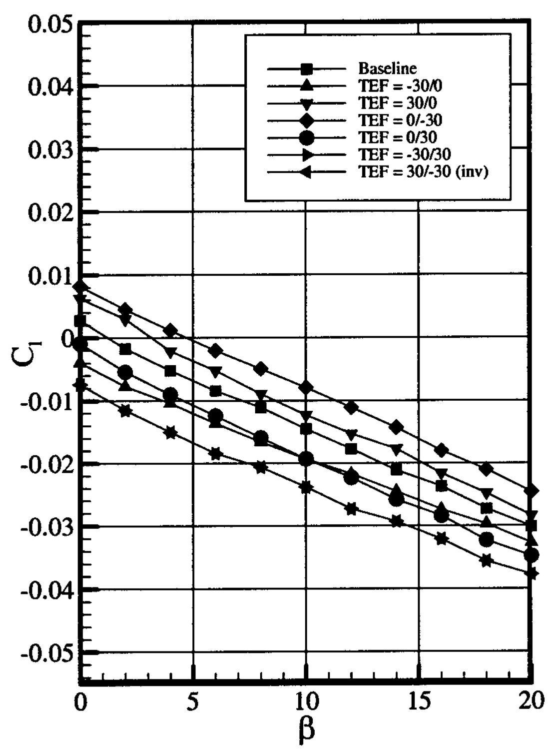

Figure D9c Rolling Moment Coefficient as a Function of β, α = 40°

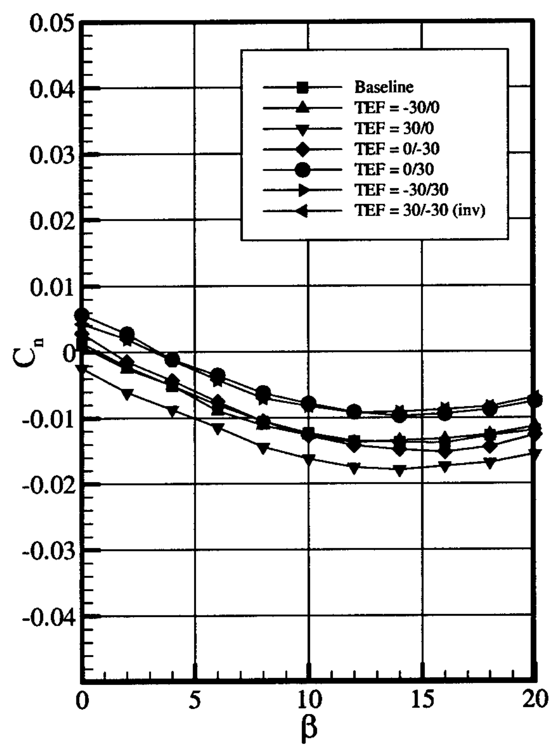

Figure D9d Yawing Moment Coefficient as a Function of β, α = 40°

Appendix E Pitch-Flap-Deflection Data as a Function of Angle of Attack

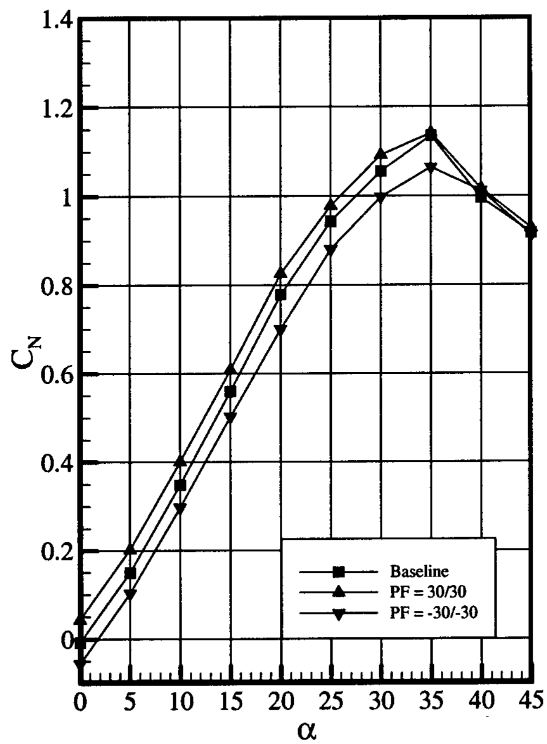

Figure E1a Normal Force Coefficient as a Function of α, β = -6°

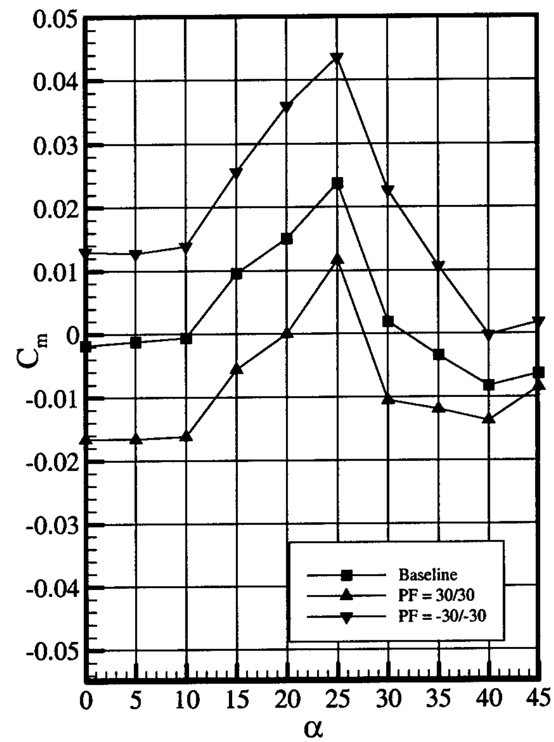

Figure E1b Pitching Moment Coefficient as a Function of α, β = -6°

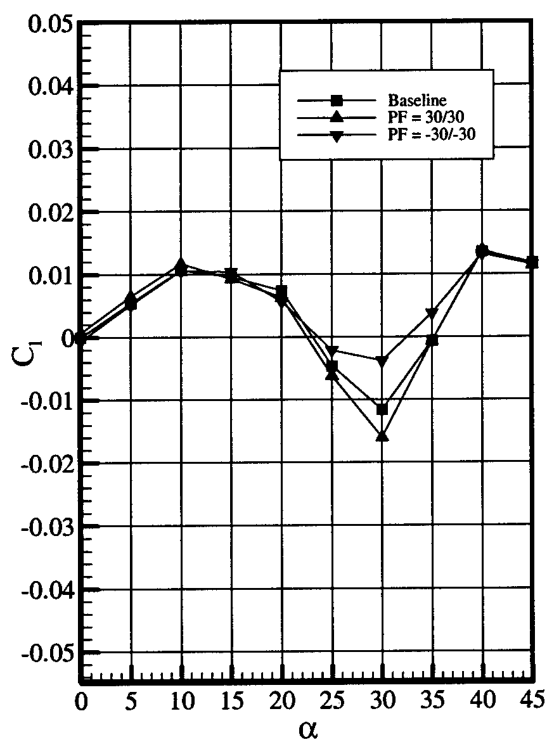

Figure E1c Rolling Moment Coefficient as a Function of α, β = -6°

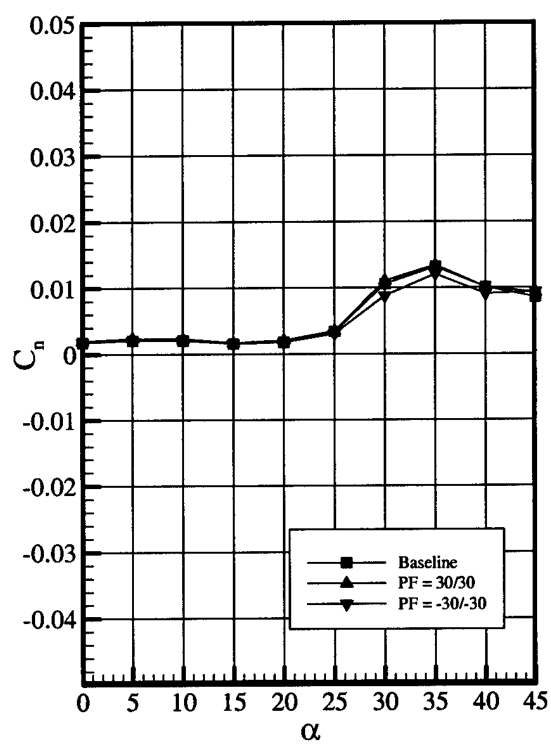

Figure E1d Yawing Moment Coefficient as a Function of α, β = -6°

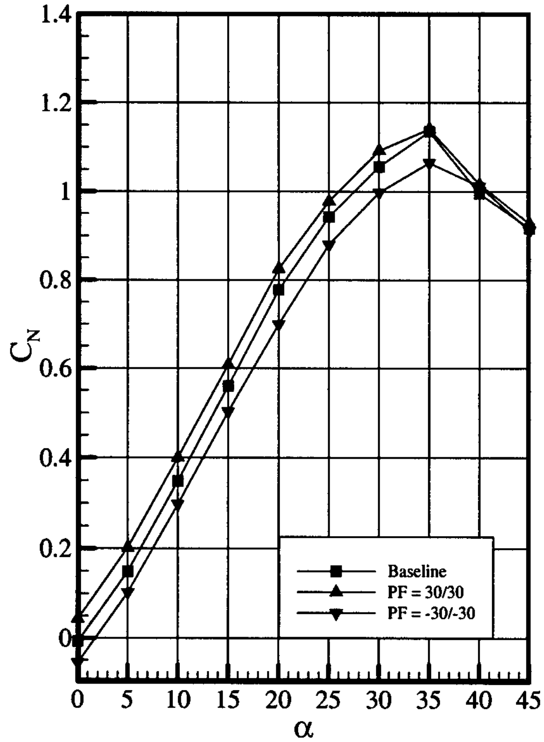

Figure E1a Normal Force Coefficient
as a Function of α, β = -6°

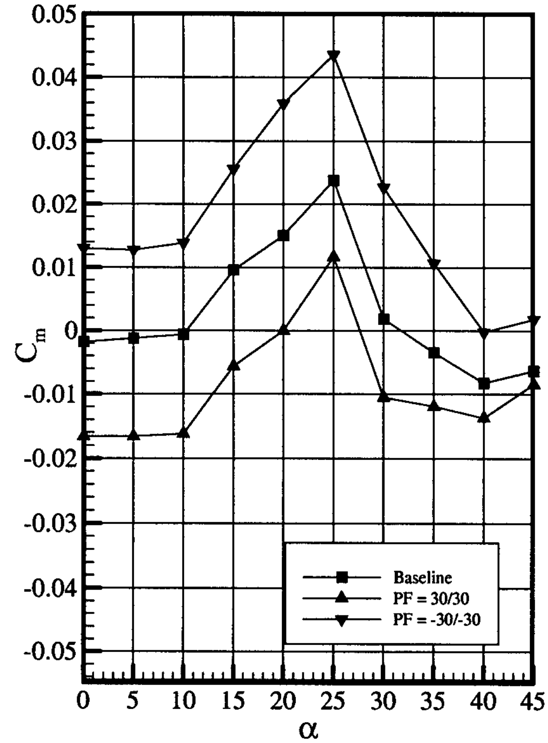

Figure E1b Pitching Moment Coefficient
as a Function of α, β = -6°

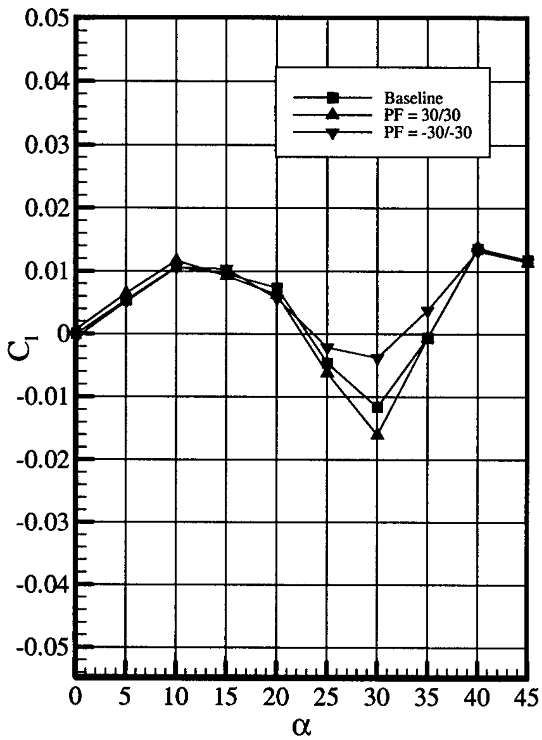

Figure E1c Rolling Moment Coefficient
as a Function of α, β = -6°

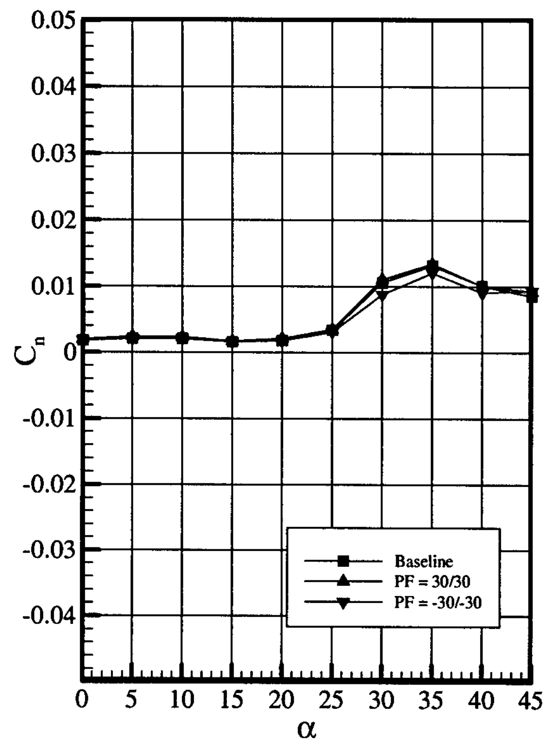

Figure E1d Yawing Moment Coefficient
as a Function of α, β = -6°

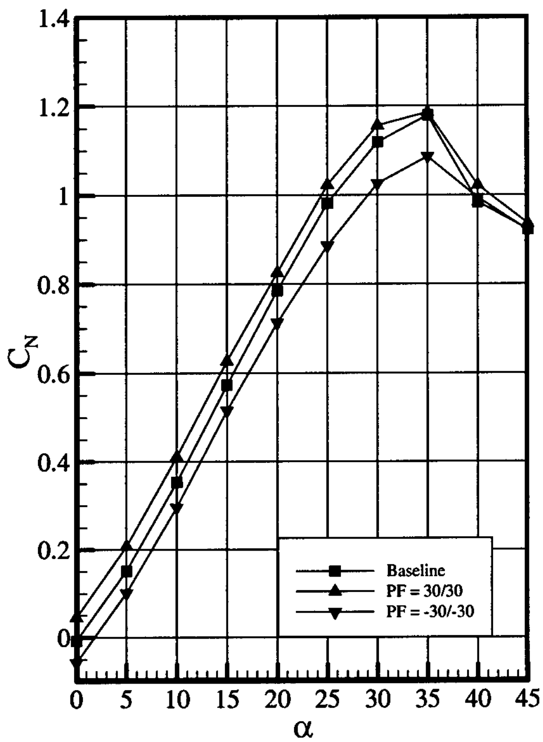

Figure E3a Normal Force Coefficient as a Function of α, β = -2°

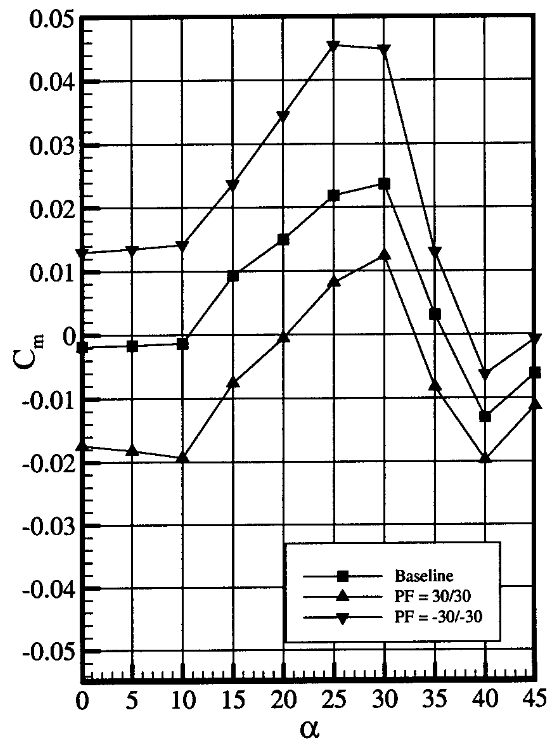

Figure E3b Pitching Moment Coefficient as a Function of α, β = -2°

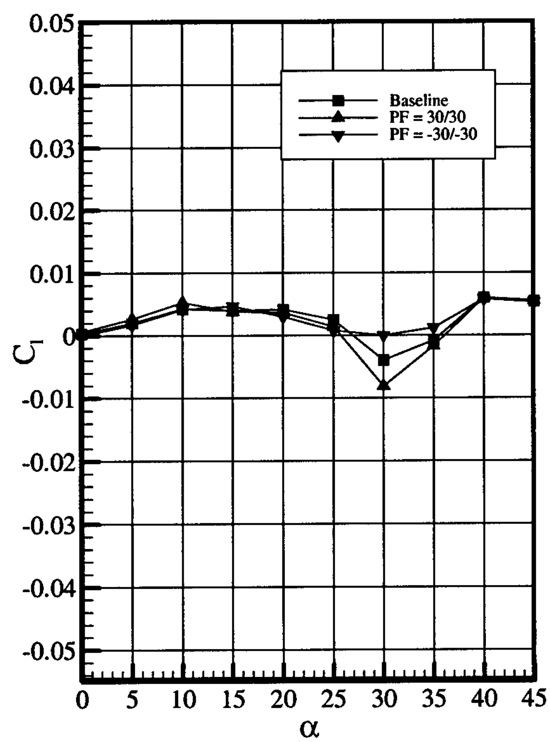

Figure E3c Rolling Moment Coefficient as a Function of α, β = -2°

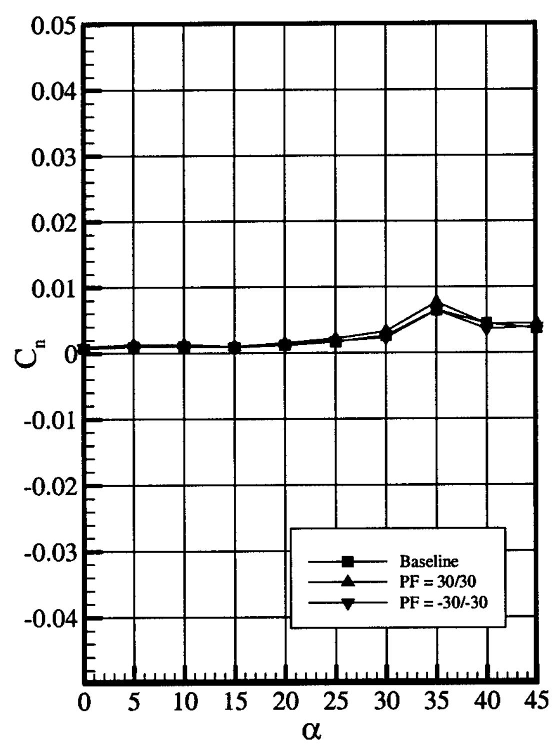

Figure E3d Yawing Moment Coefficient as a Function of α, β = -2°

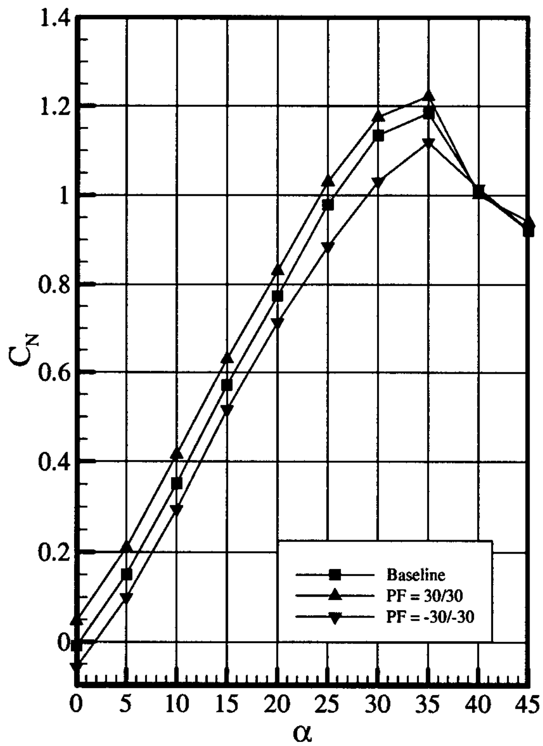

Figure E4a Normal Force Coefficient as a Function of α, β = 0°

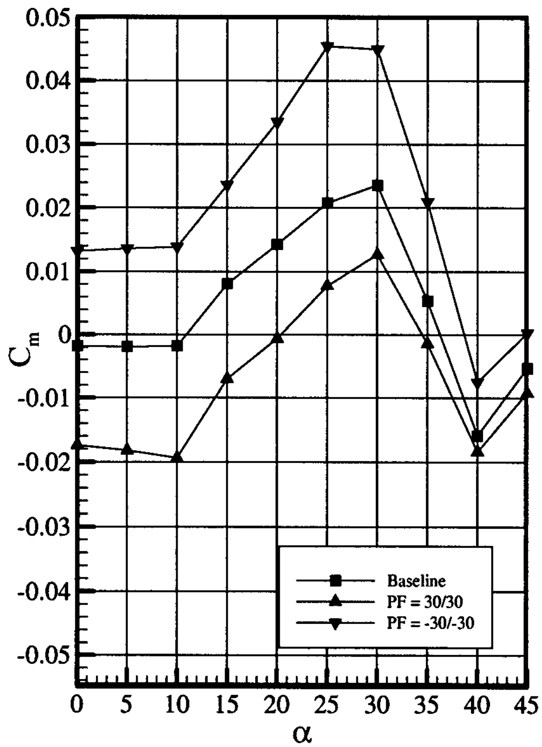

Figure E4b Pitching Moment Coefficient as a Function of α, β = 0°

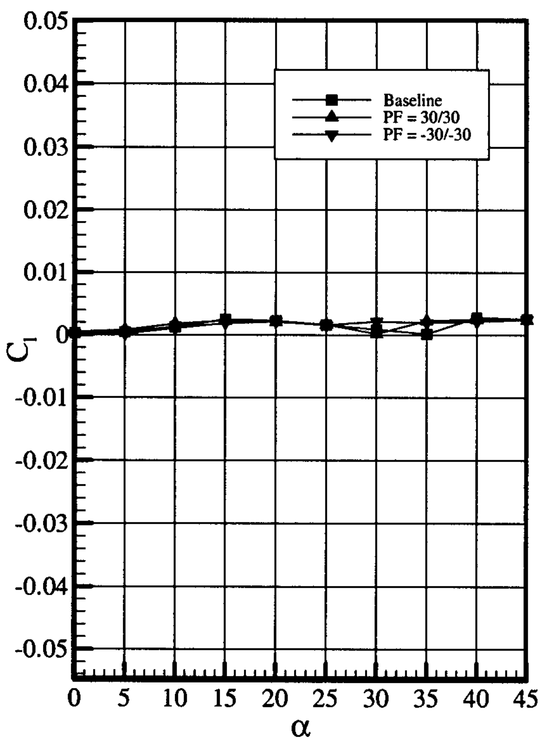

Figure E4c Rolling Moment Coefficient as a Function of α, β = 0°

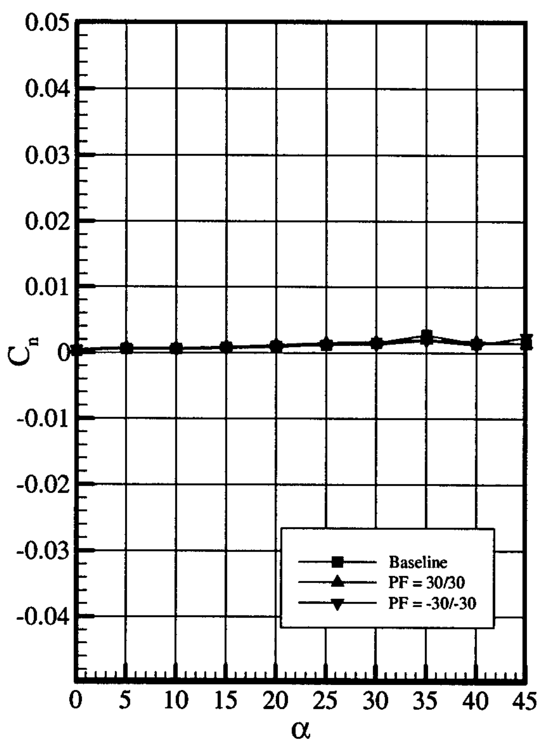

Figure E4d Yawing Moment Coefficient as a Function of α, β = 0°

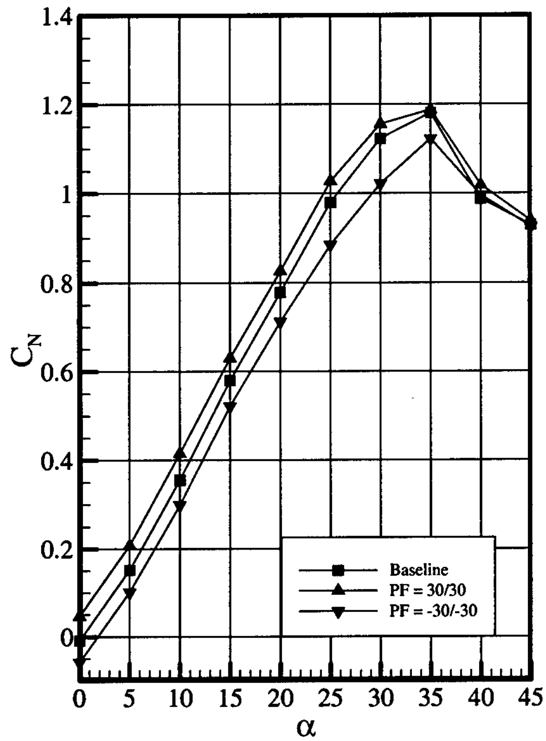

Figure E5a Normal Force Coefficient as a Function of α, $\beta = 2^{\circ}$

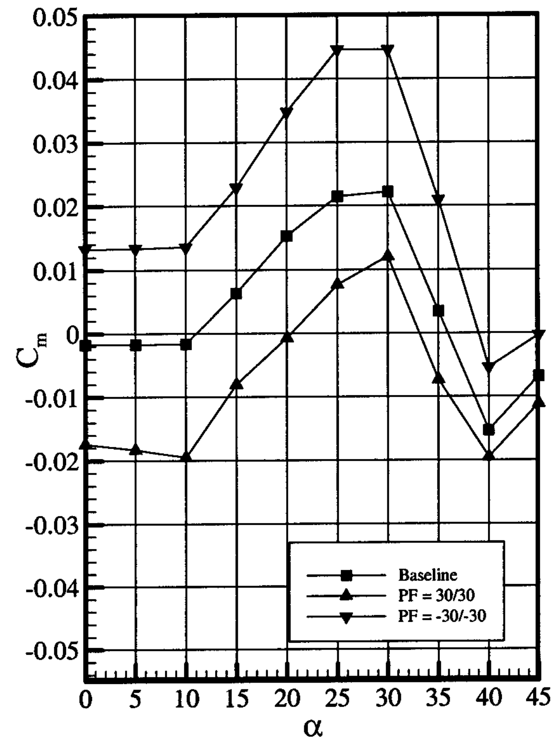

Figure E5b Pitching Moment Coefficient as a Function of α, $\beta = 2^{\circ}$

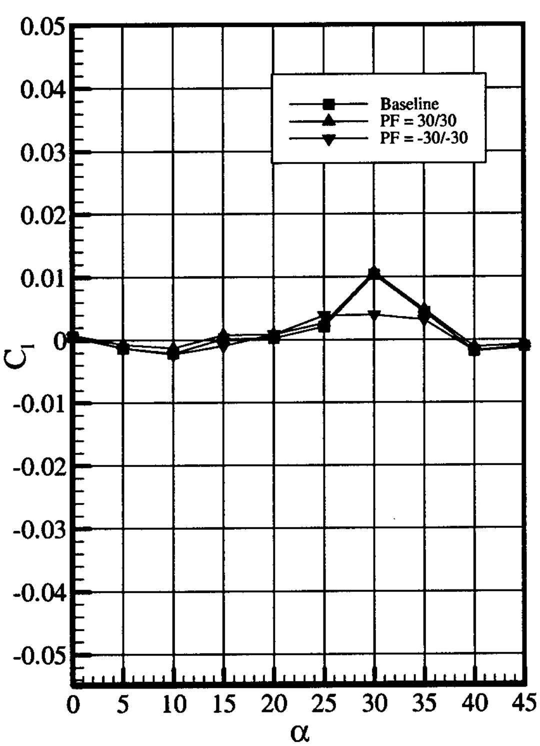

Figure E5c Rolling Moment Coefficient as a Function of α, $\beta = 2^{\circ}$

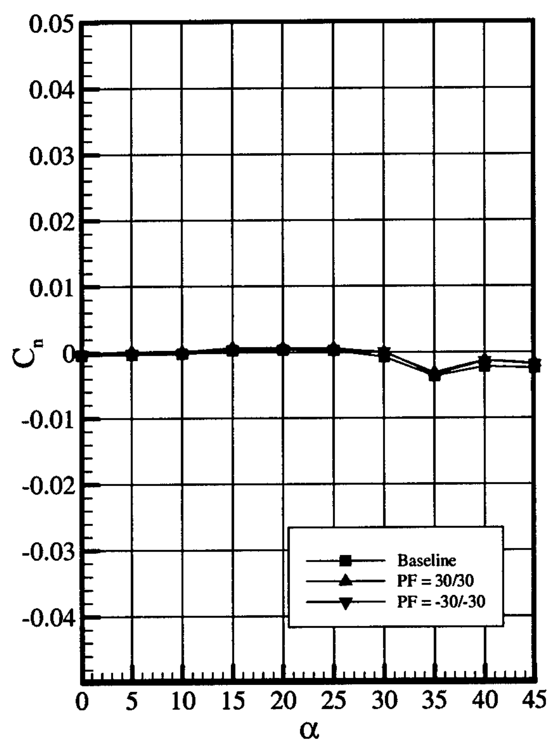

Figure E5d Yawing Moment Coefficient as a Function of α, $\beta = 2^{\circ}$

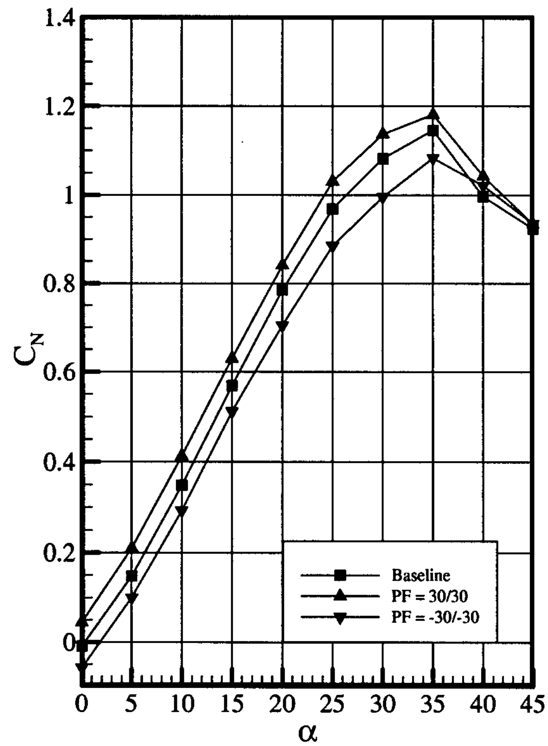

Figure E6a Normal Force Coefficient as a Function of α, β = 4°

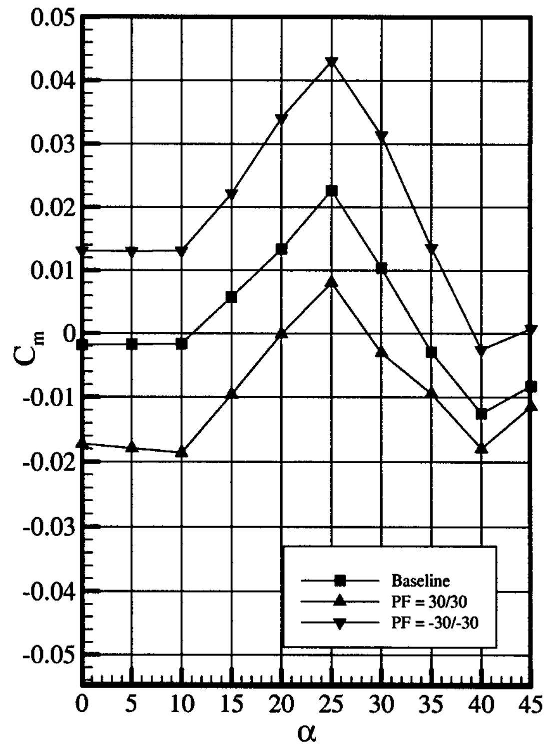

Figure E6b Pitching Moment Coefficient as a Function of α, β = 4°

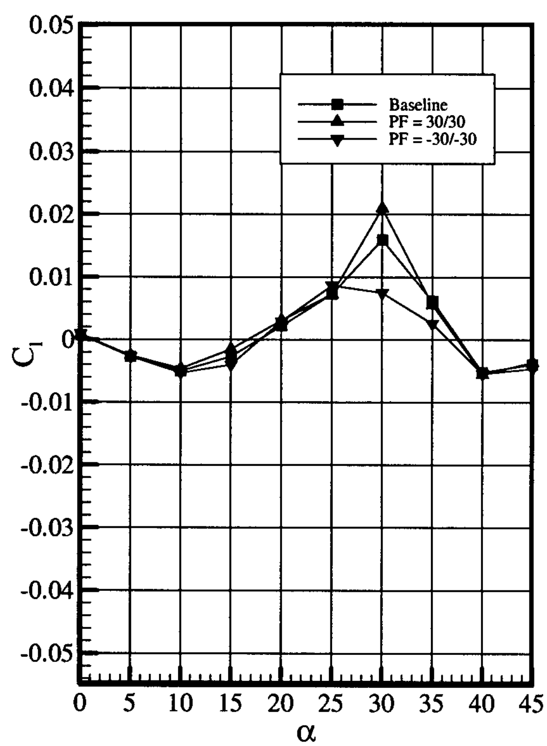

Figure E6c Rolling Moment Coefficient as a Function of α, β = 4°

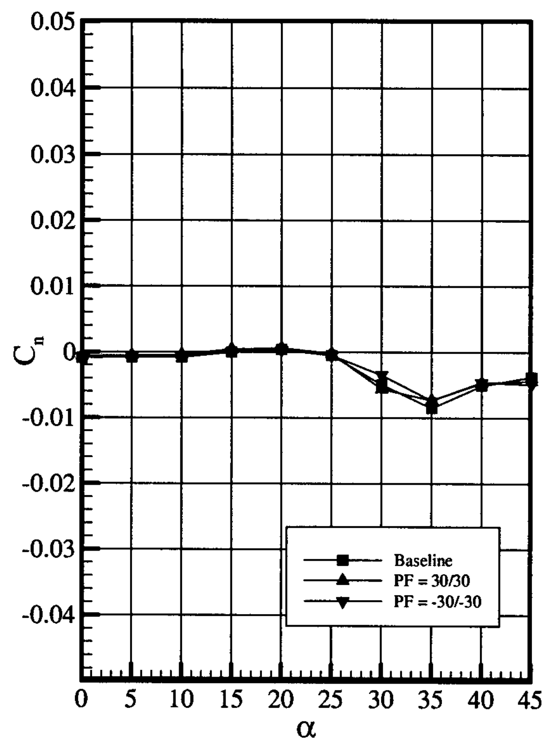

Figure E6d Yawing Moment Coefficient as a Function of α, β = 4°

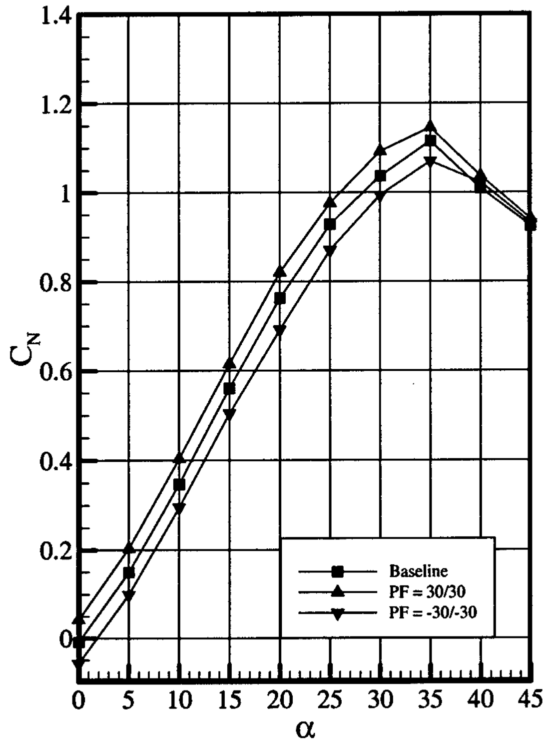

Figure E7a Normal Force Coefficient as a Function of α, β = 6°

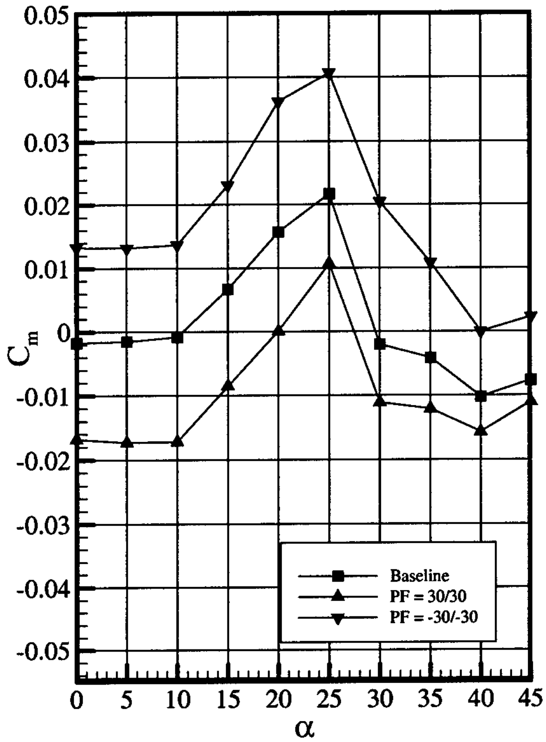

Figure E7b Pitching Moment Coefficient as a Function of α, β = 6°

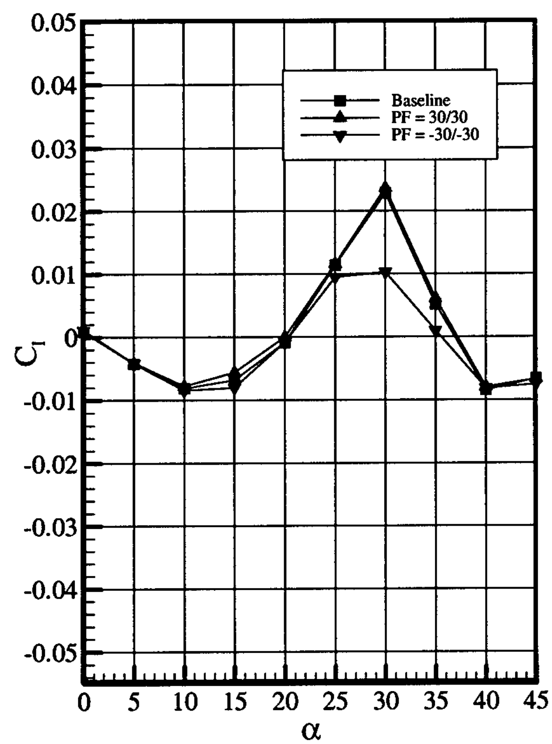

Figure E7c Rolling Moment Coefficient as a Function of α, β = 6°

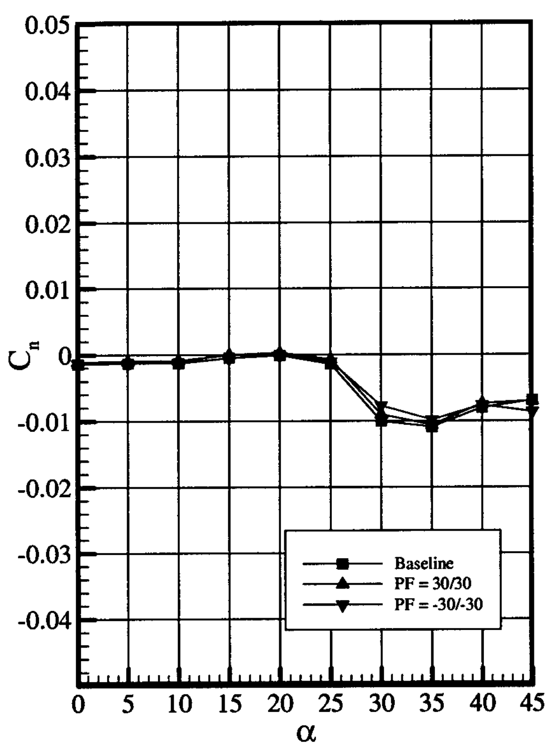

Figure E7d Yawing Moment Coefficient as a Function of α, β = 6°

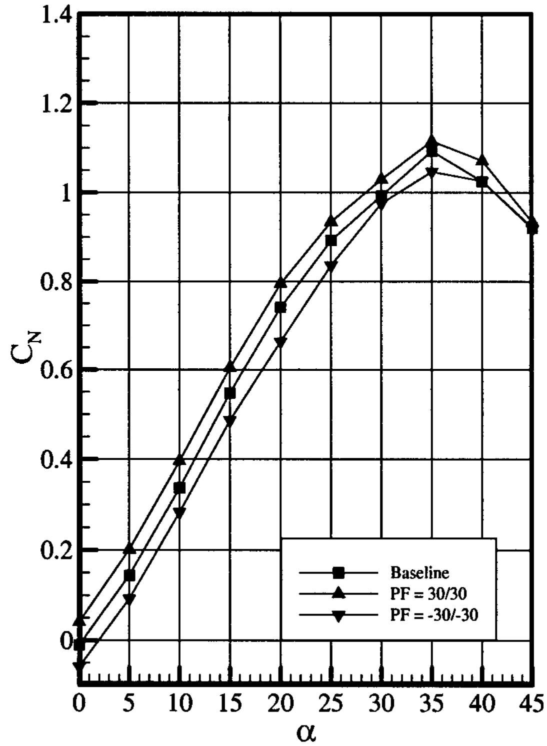

Figure E8a Normal Force Coefficient as a Function of α, β = 8°

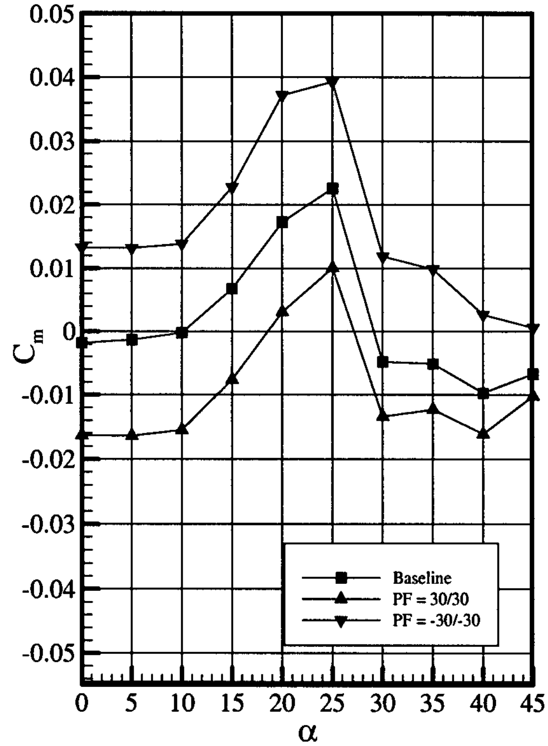

Figure E8b Pitching Moment Coefficient as a Function of α, β = 8°

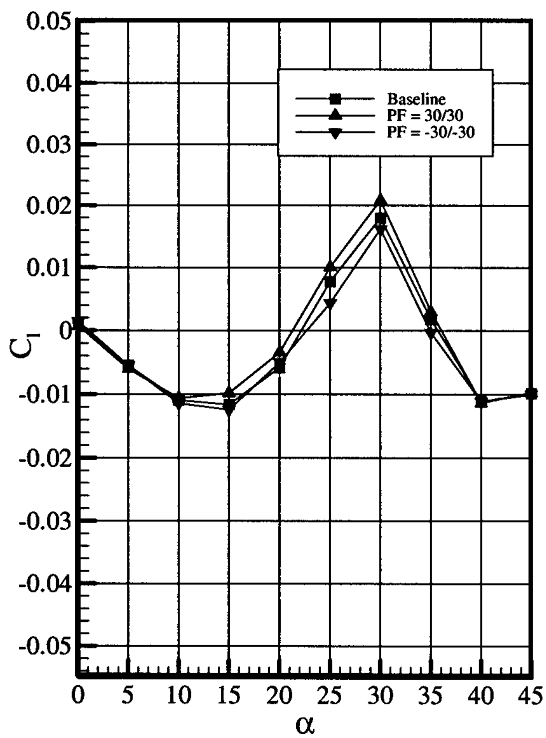

Figure E8c Rolling Moment Coefficient as a Function of α, β = 8°

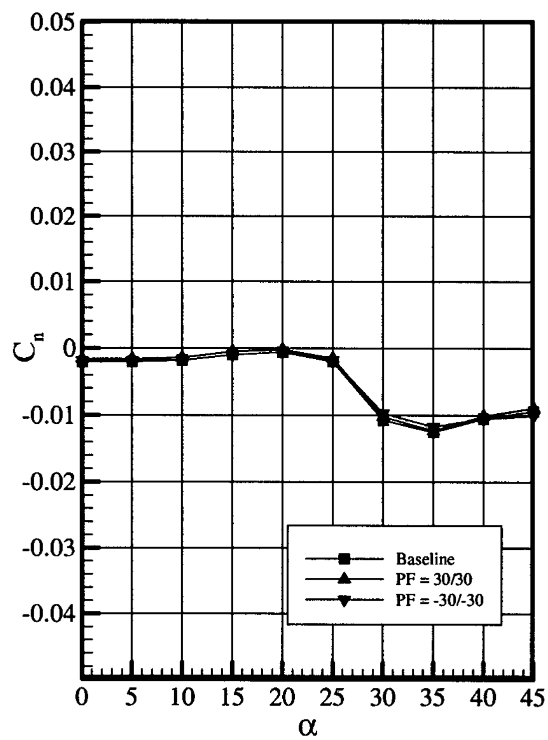

Figure E8d Yawing Moment Coefficient as a Function of α, β = 8°

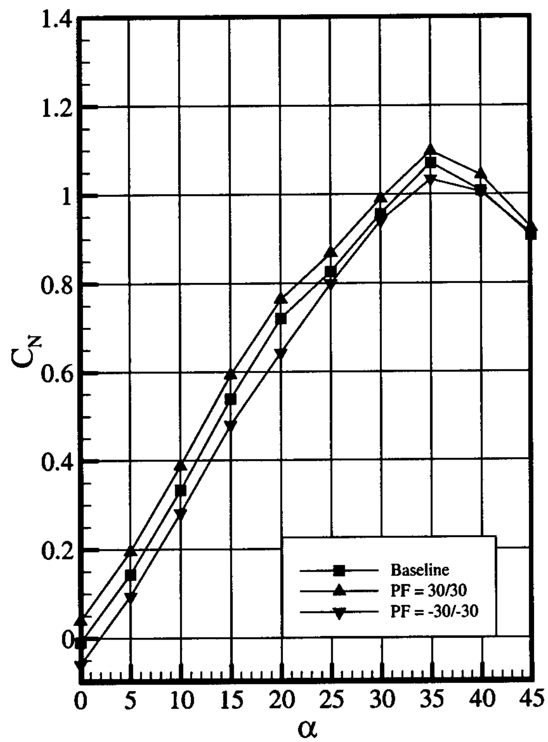

Figure E9a Normal Force Coefficient as a Function of α, β = 10°

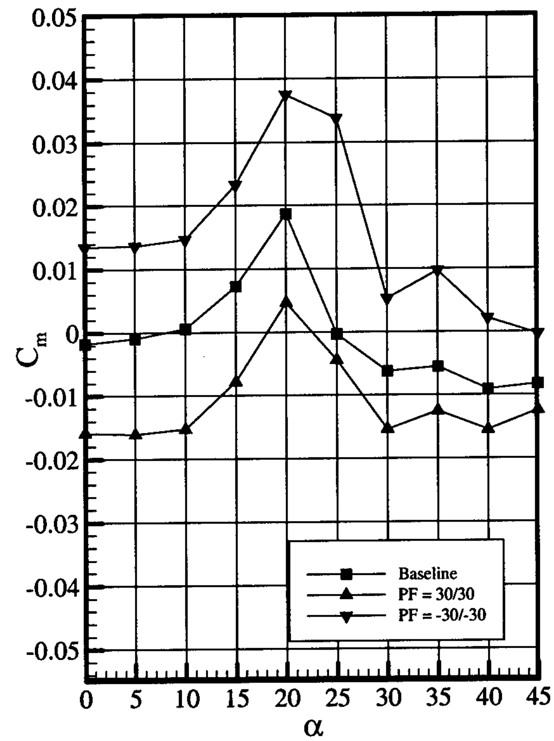

Figure E9b Pitching Moment Coefficient as a Function of α, β = 10°

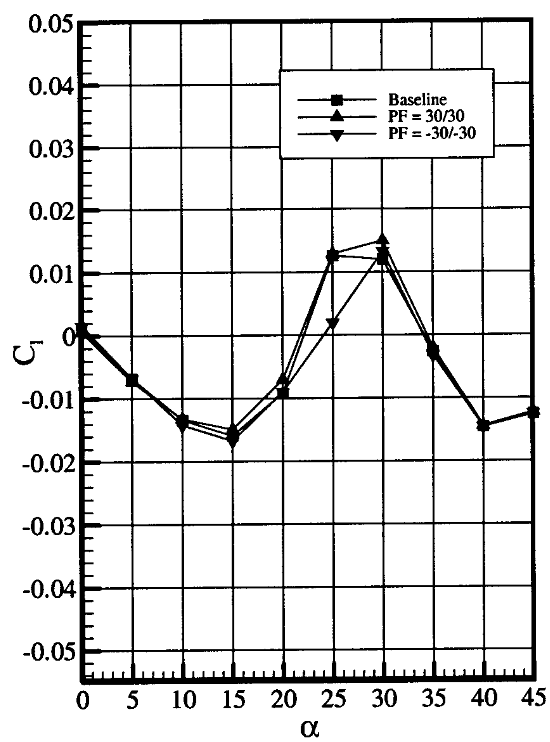

Figure E9c Rolling Moment Coefficient as a Function of α, β = 10°

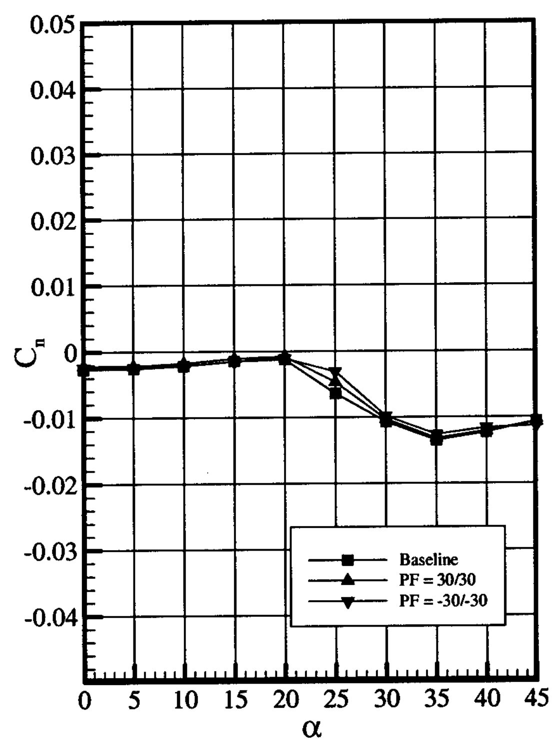

Figure E9d Yawing Moment Coefficient as a Function of α, β = 10°

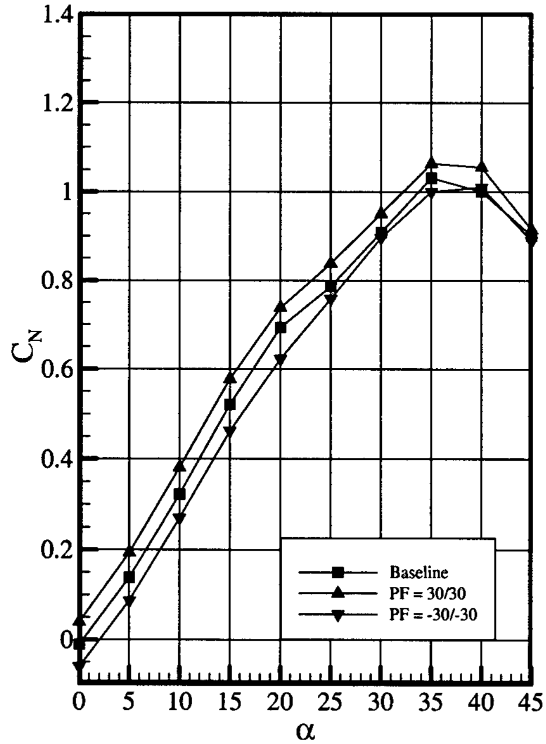

Figure E10a Normal Force Coefficient as a Function of α, β = 12°

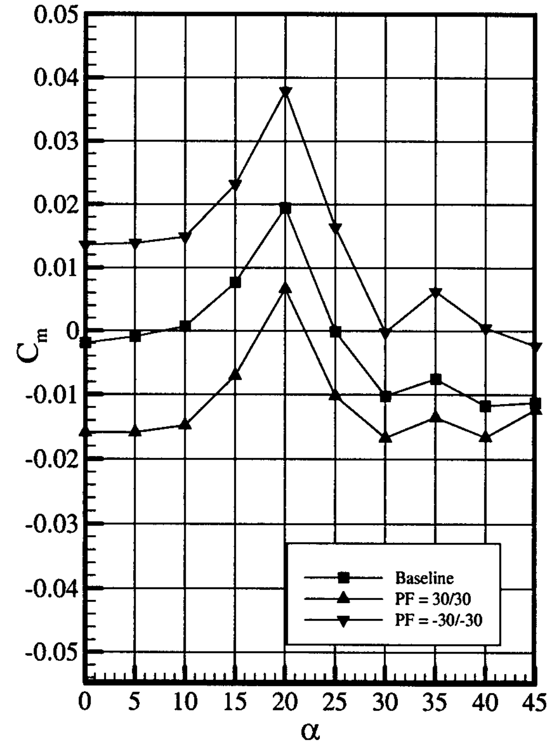

Figure E10b Pitching Moment Coefficient as a Function of α, β = 12°

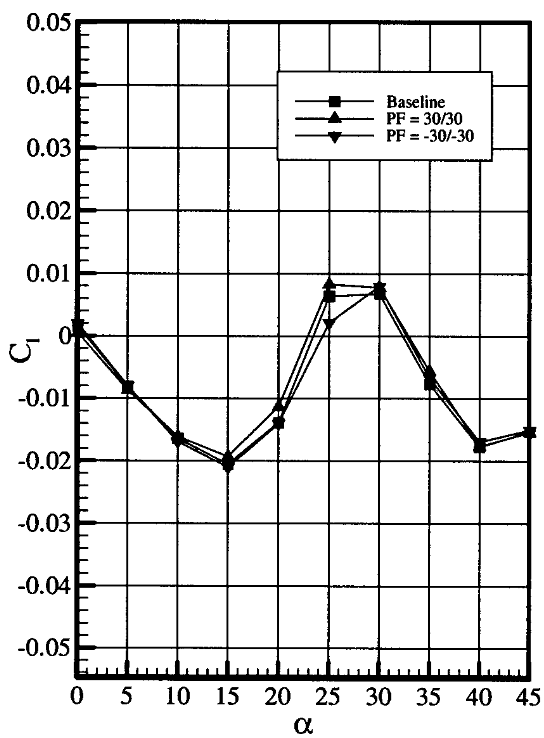

Figure E10c Rolling Moment Coefficient as a Function of α, β = 12°

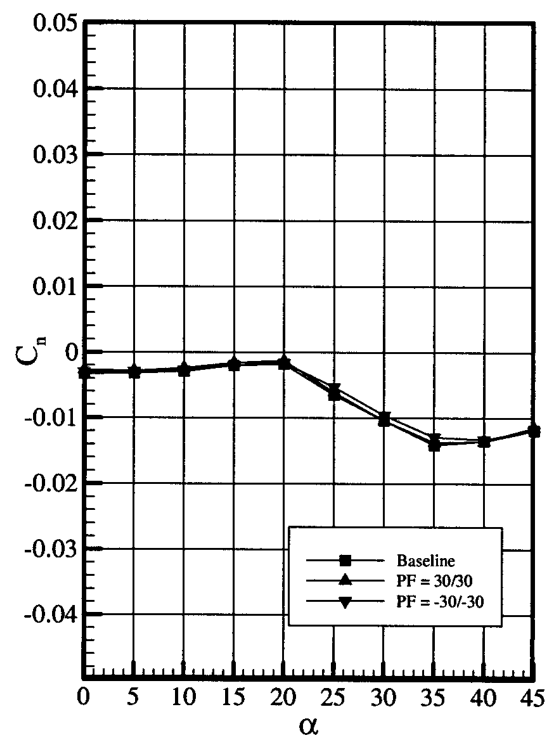

Figure E10d Yawing Moment Coefficient as a Function of α, β = 12°

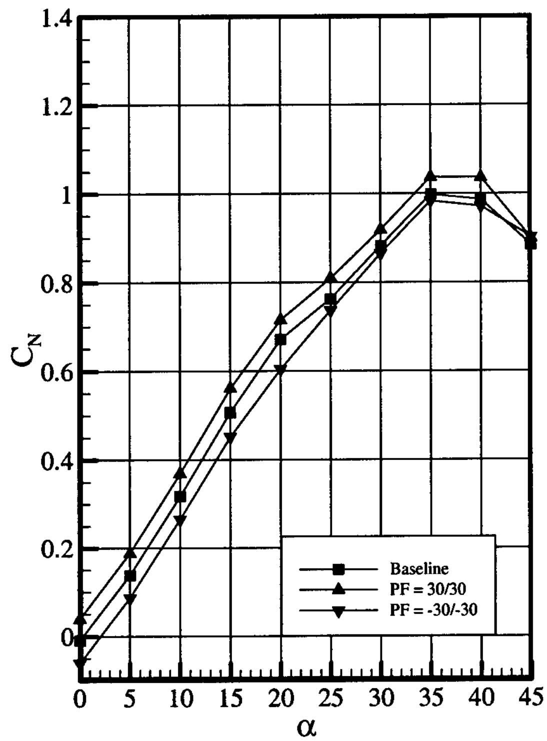

Figure E11a Normal Force Coefficient as a Function of α, β = 14°

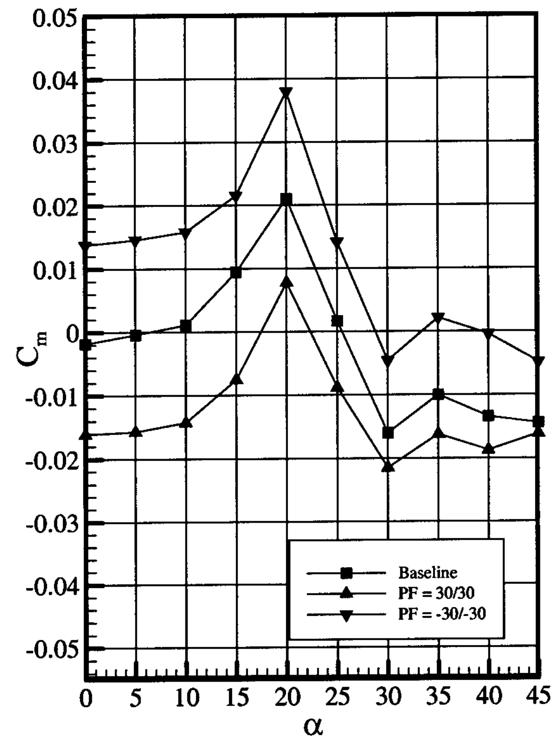

Figure E11b Pitching Moment Coefficient as a Function of α, β = 14°

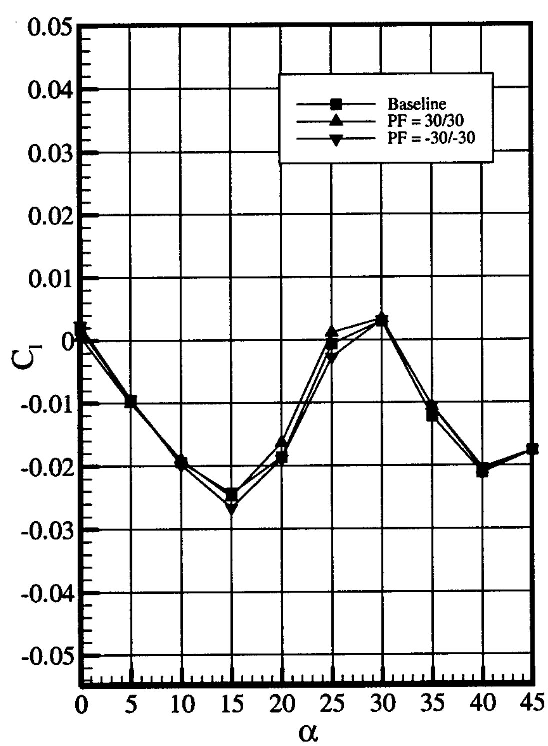

Figure E11c Rolling Moment Coefficient as a Function of α, β = 14°

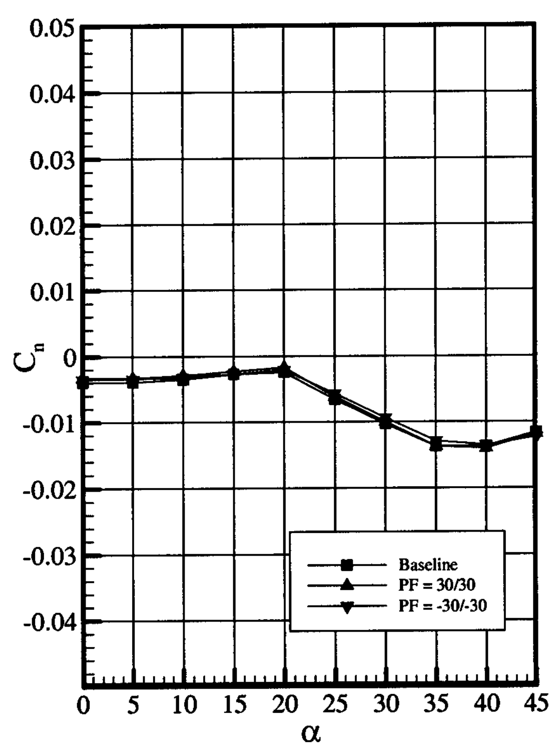

Figure E11d Yawing Moment Coefficient as a Function of α, β = 14°

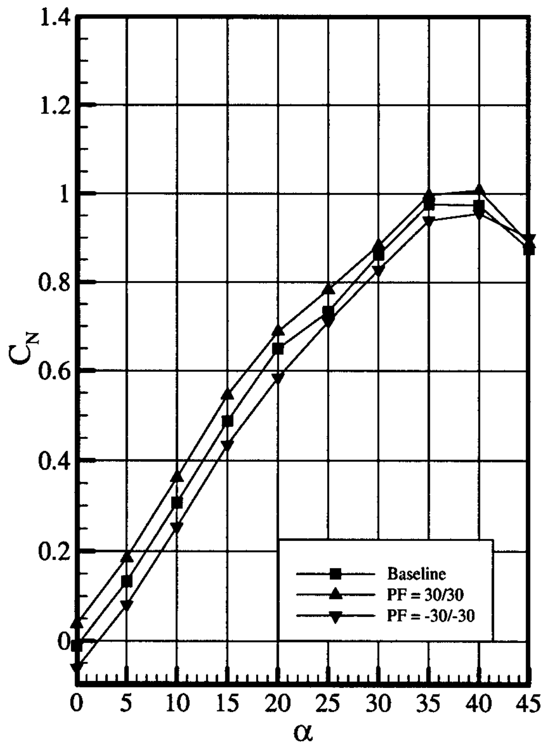

Figure E12a Normal Force Coefficient as a Function of α, β = 16°

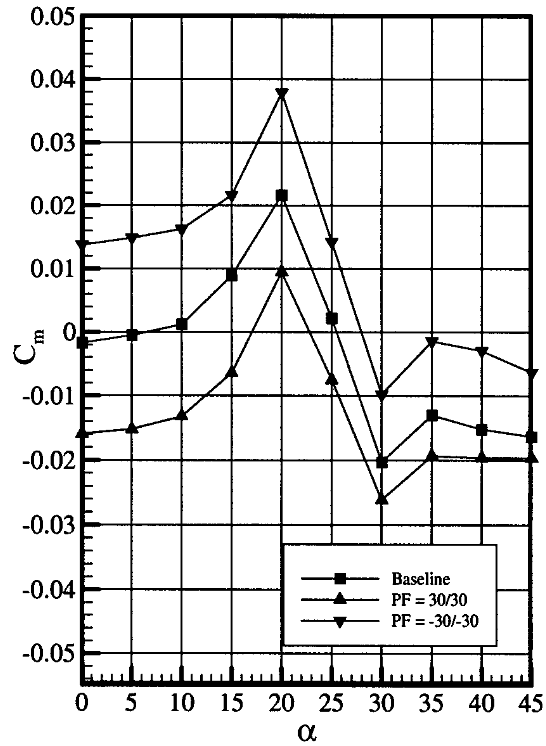

Figure E12b Pitching Moment Coefficient as a Function of α, β = 16°

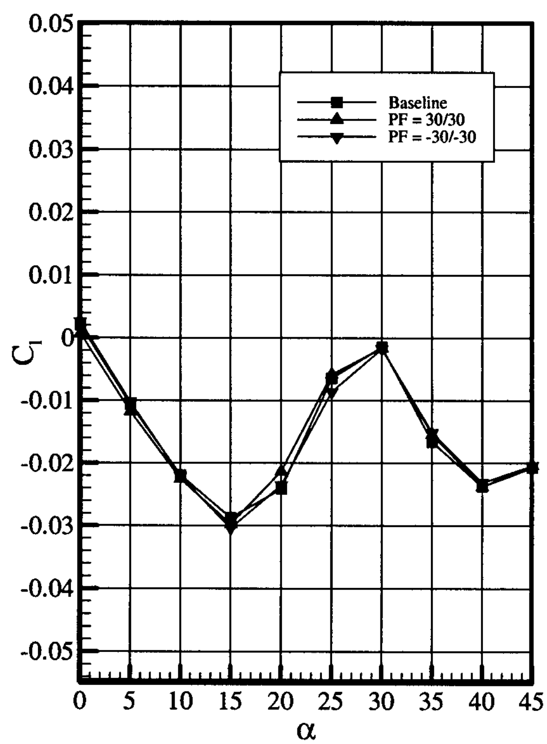

Figure E12c Rolling Moment Coefficient as a Function of α, β = 16°

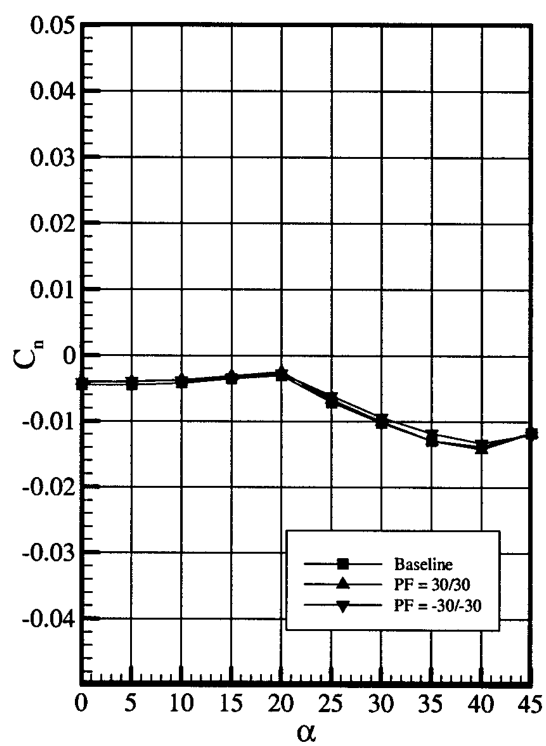

Figure E12d Yawing Moment Coefficient as a Function of α, β = 16°

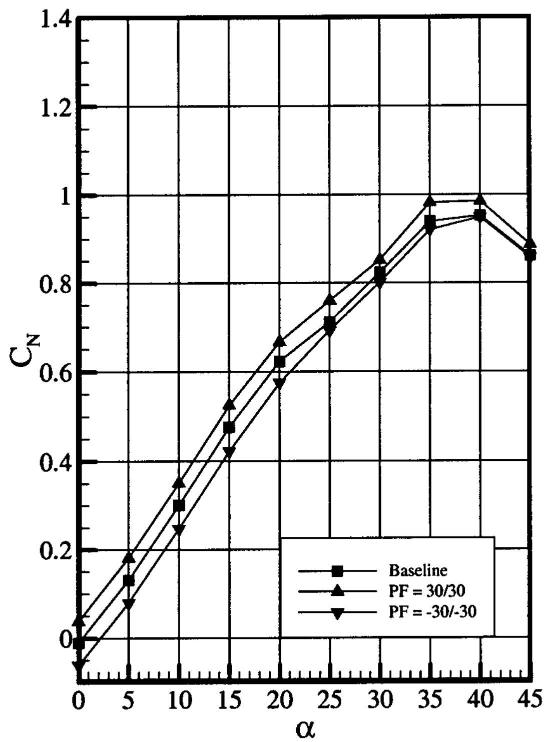

Figure E13a Normal Force Coefficient as a Function of α, $\beta = 18^{\circ}$

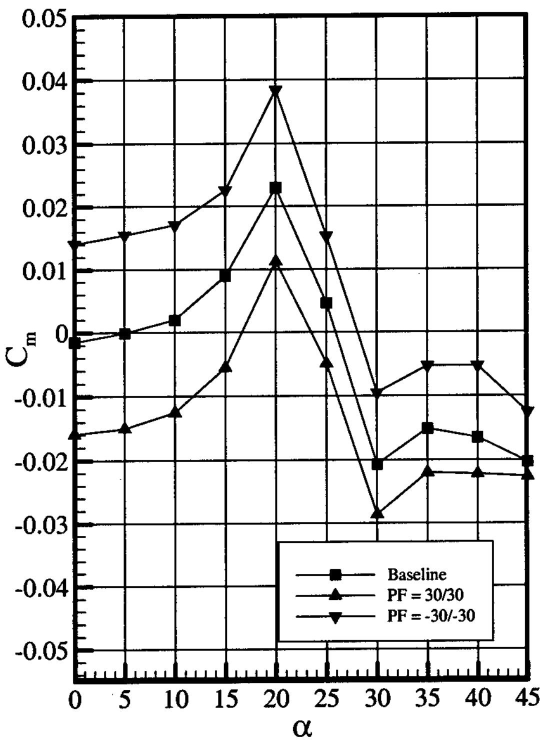

Figure E13b Pitching Moment Coefficient as a Function of α, $\beta = 18^{\circ}$

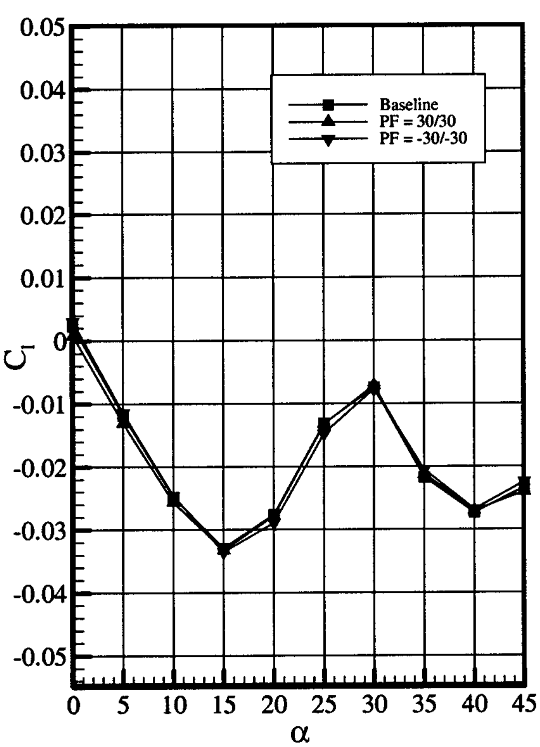

Figure E13c Rolling Moment Coefficient as a Function of α, $\beta = 18^{\circ}$

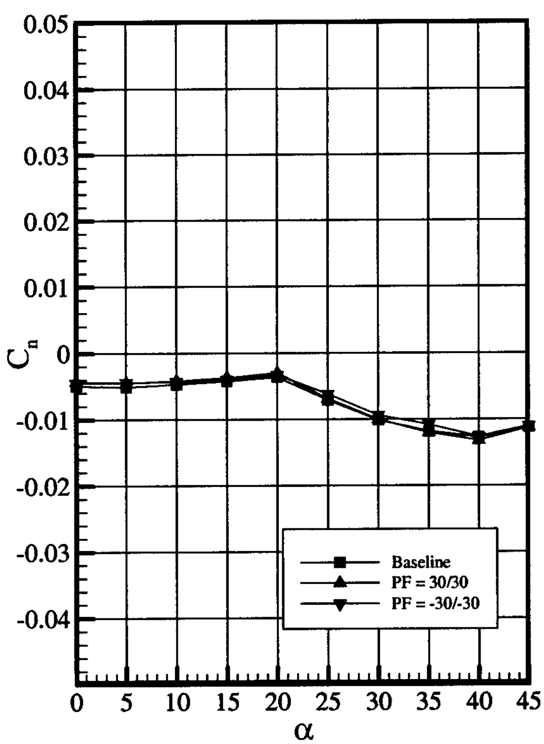

Figure E13d Yawing Moment Coefficient as a Function of α, $\beta = 18^{\circ}$

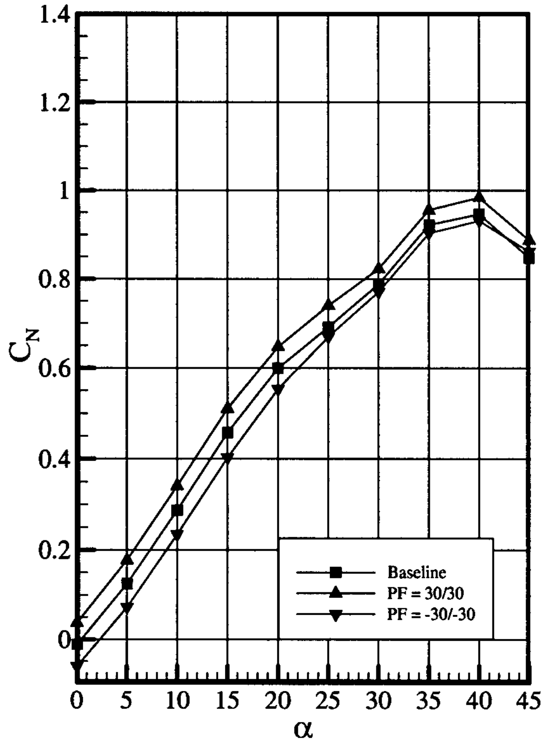

Figure E14a Normal Force Coefficient as a Function of α, β = 20°

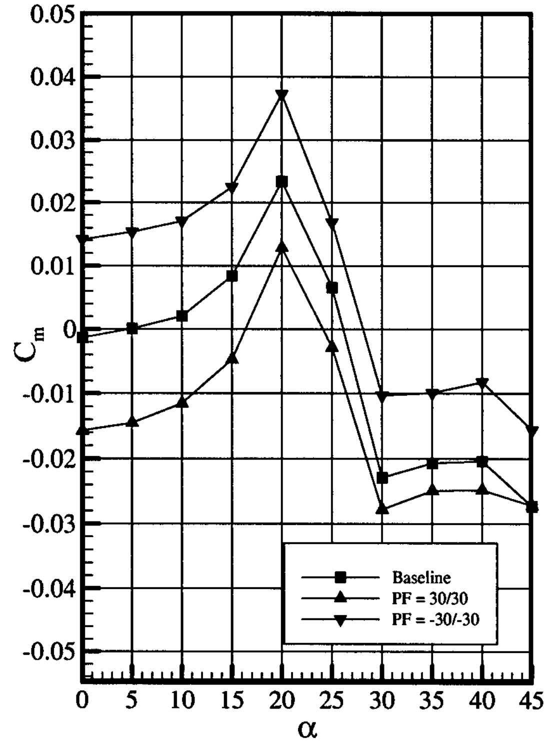

Figure E14b Pitching Moment Coefficient as a Function of α, β = 20°

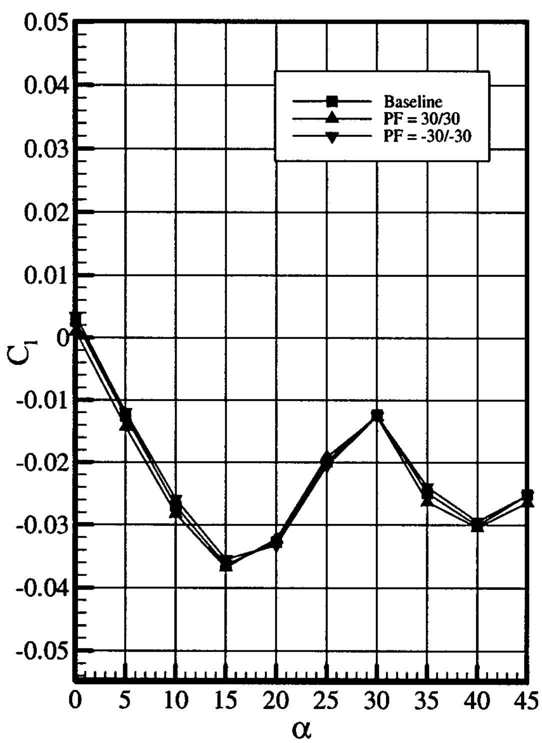

Figure E14c Rolling Moment Coefficient as a Function of α, β = 20°

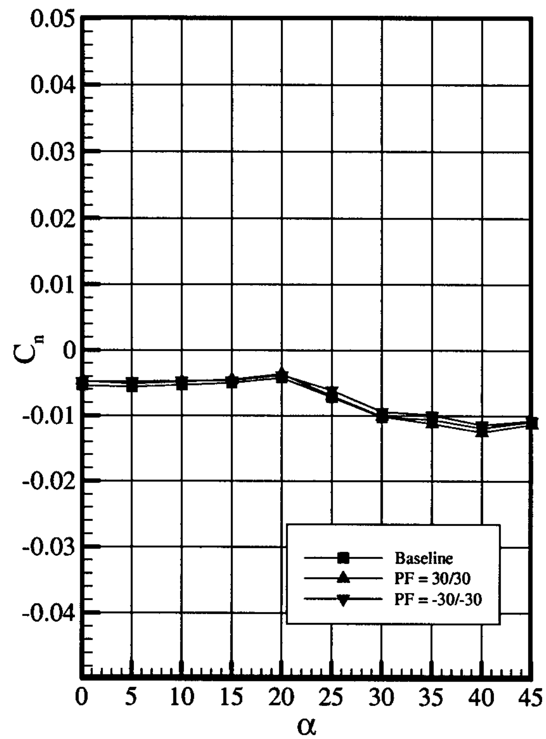

Figure E14d Yawing Moment Coefficient as a Function of α, β = 20°

Appendix F Pitch-Flap-Deflection Deflection Data as a Function of Sideslip Angle

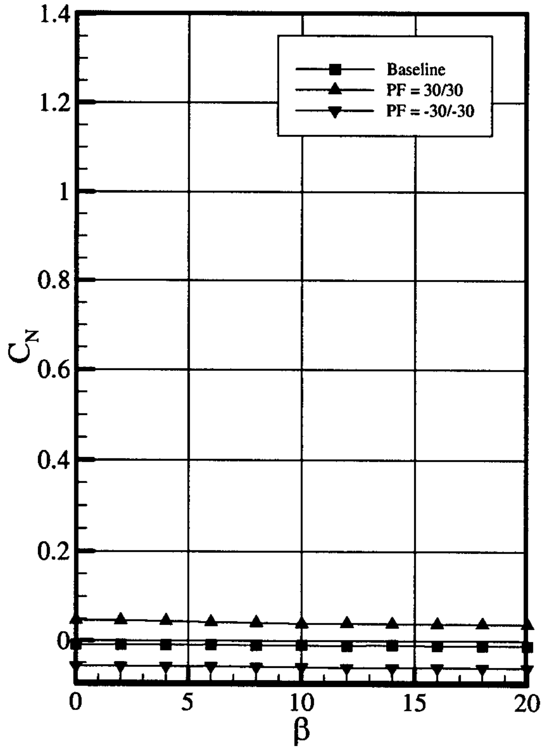

Figure F1a Normal Force Coefficient
as a Function of β, $\alpha = 0^\circ$

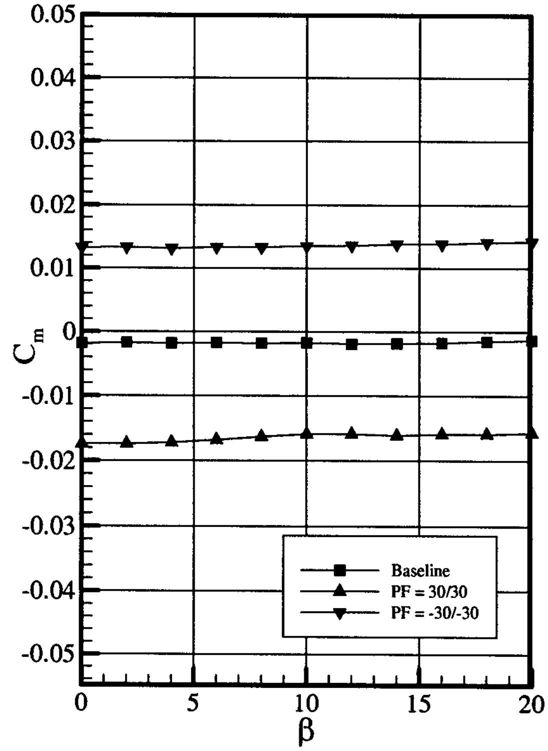

Figure F1b Pitching Moment Coefficient
as a Function of β, $\alpha = 0^\circ$

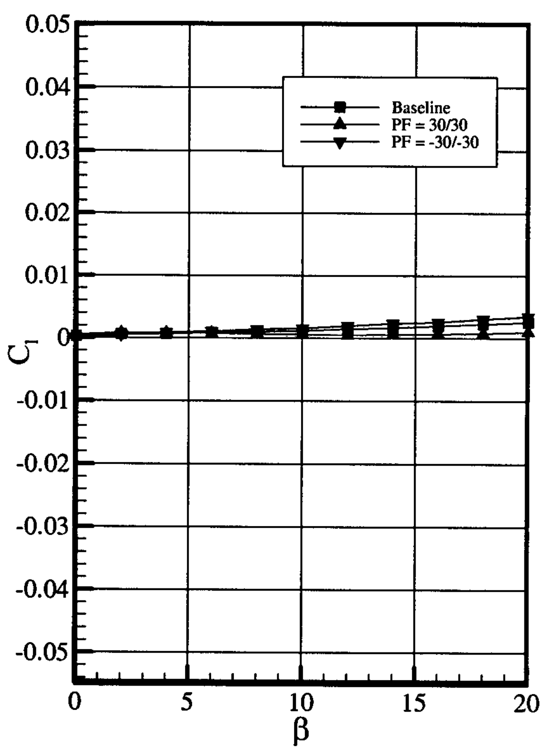

Figure F1c Rolling Moment Coefficient
as a Function of β, $\alpha = 0^\circ$

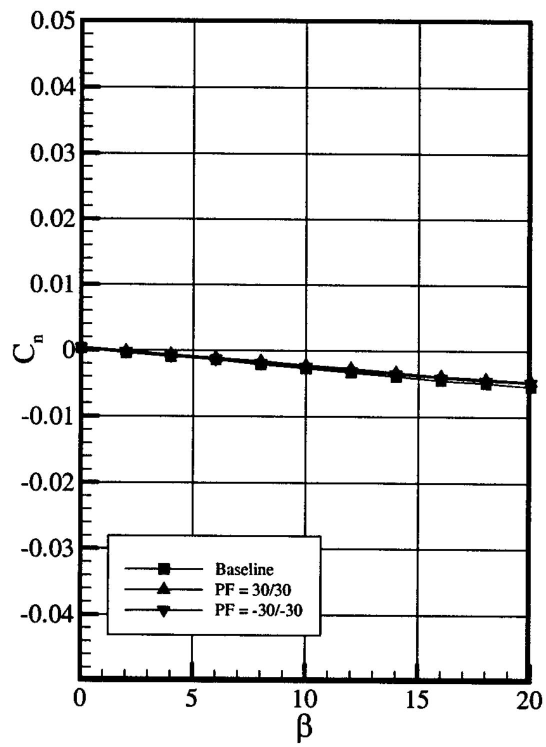

Figure F1d Yawing Moment Coefficient
as a Function of β, $\alpha = 0^\circ$

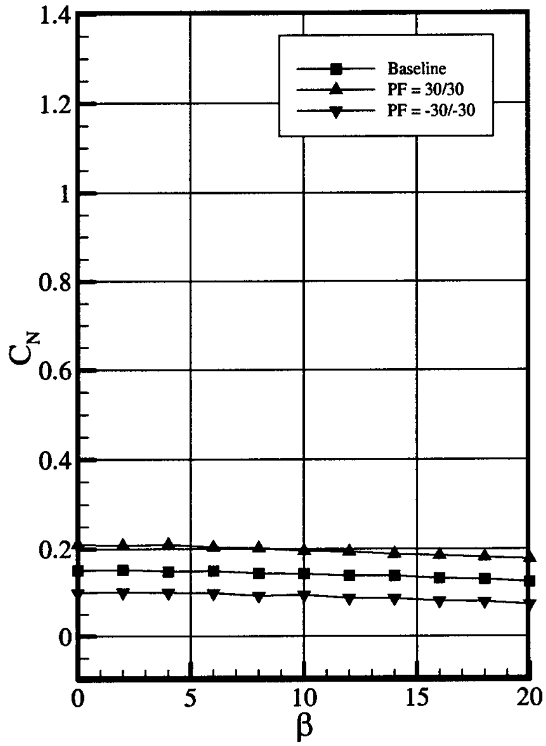

Figure F2a Normal Force Coefficient as a Function of β, α = 5°

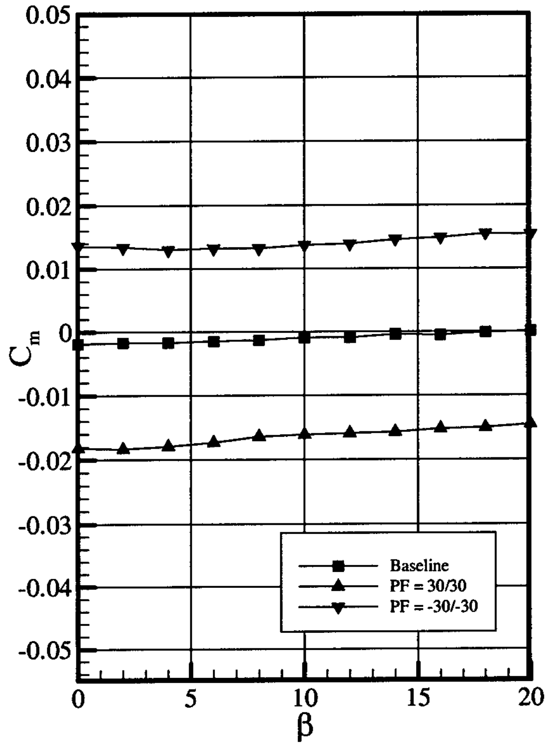

Figure F2b Pitching Moment Coefficient as a Function of β, α = 5°

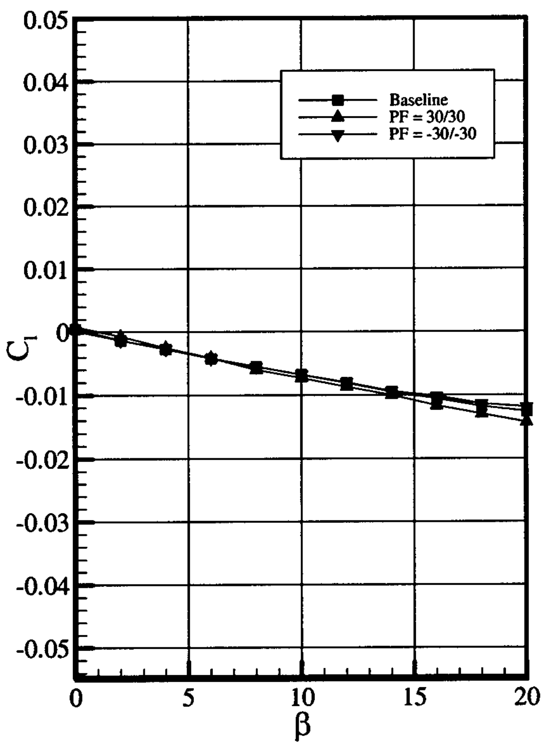

Figure F2c Rolling Moment Coefficient as a Function of β, α = 5°

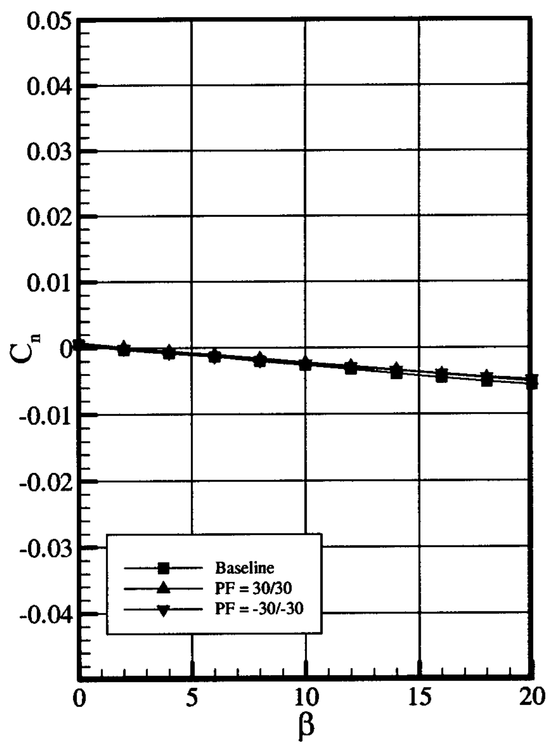

Figure F2d Yawing Moment Coefficient as a Function of β, α = 5°

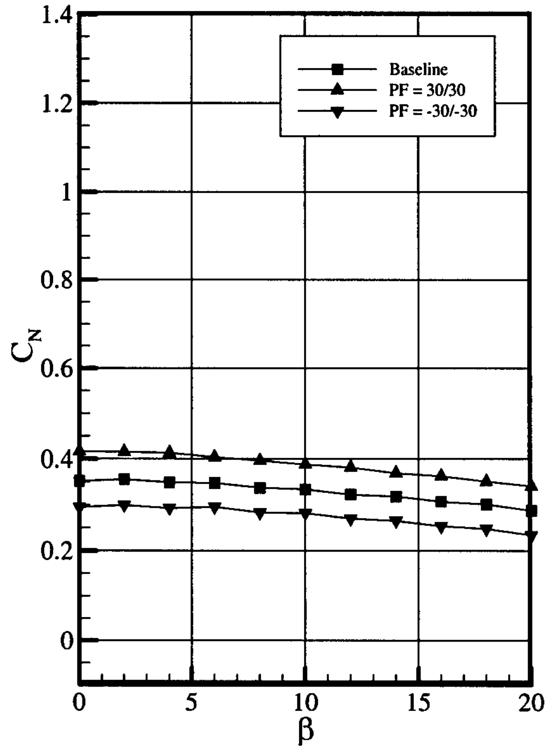

Figure F3a Normal Force Coefficient as a Function of β, α = 10°

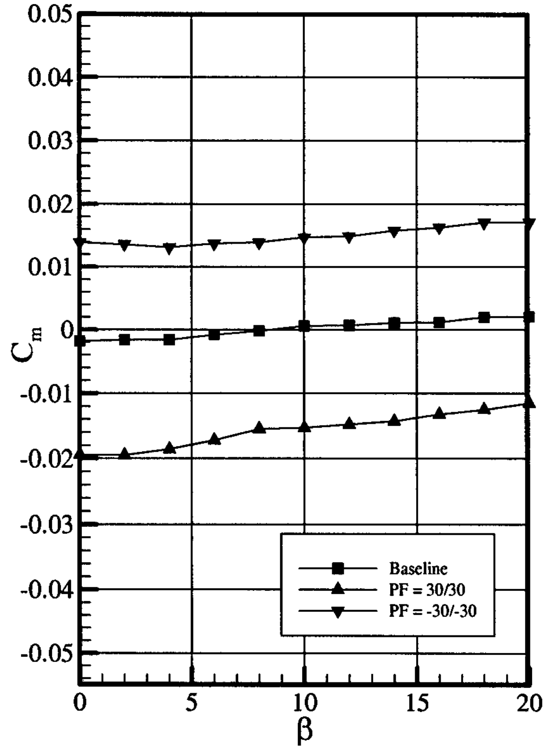

Figure F3b Pitching Moment Coefficient as a Function of β, α = 10°

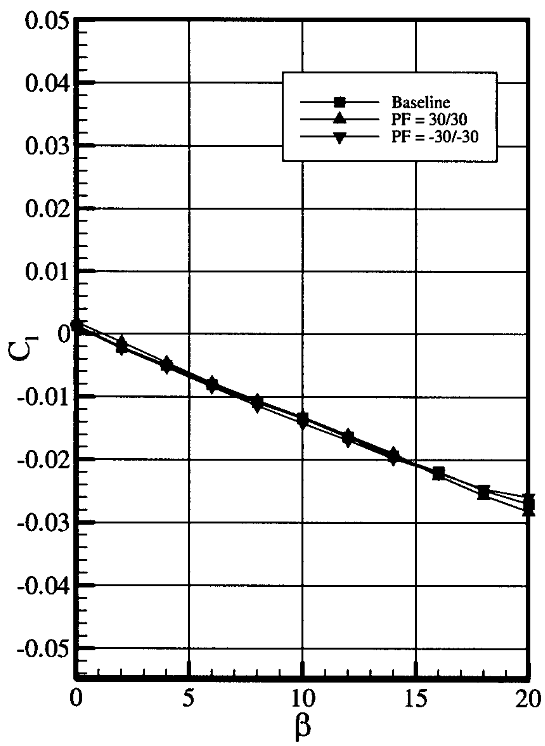

Figure F3c Rolling Moment Coefficient as a Function of β, α = 10°

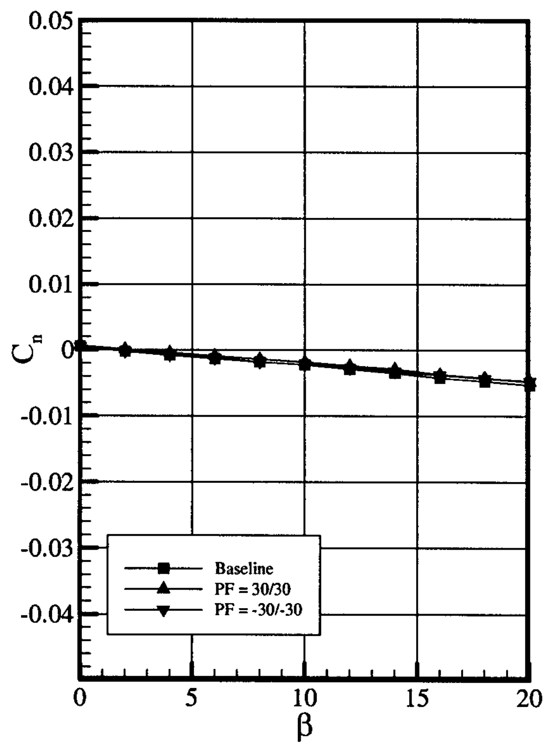

Figure F3d Yawing Moment Coefficient as a Function of β, α = 10°

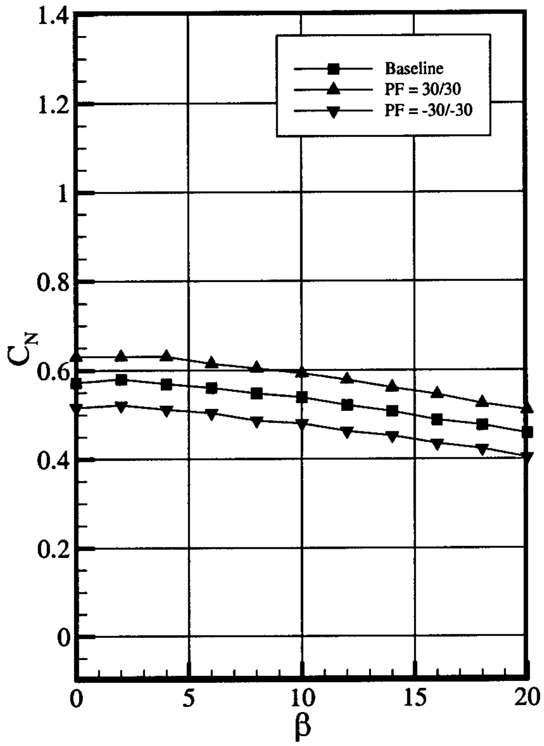

Figure F4a Normal Force Coefficient
as a Function of β, α = 15°

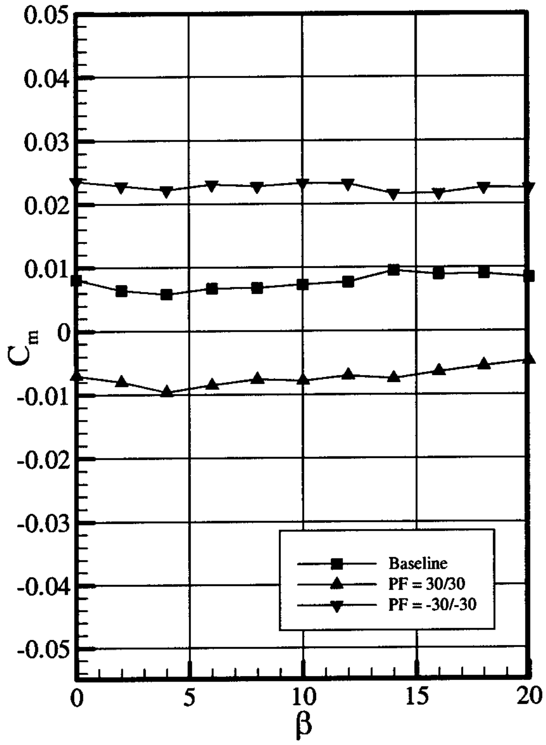

Figure F4b Pitching Moment Coefficient
as a Function of β, α = 15°

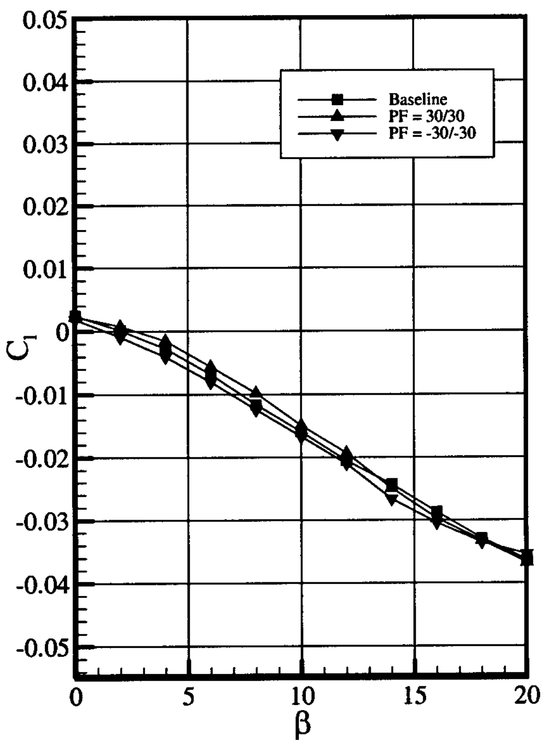

Figure F4c Rolling Moment Coefficient
as a Function of β, α = 15°

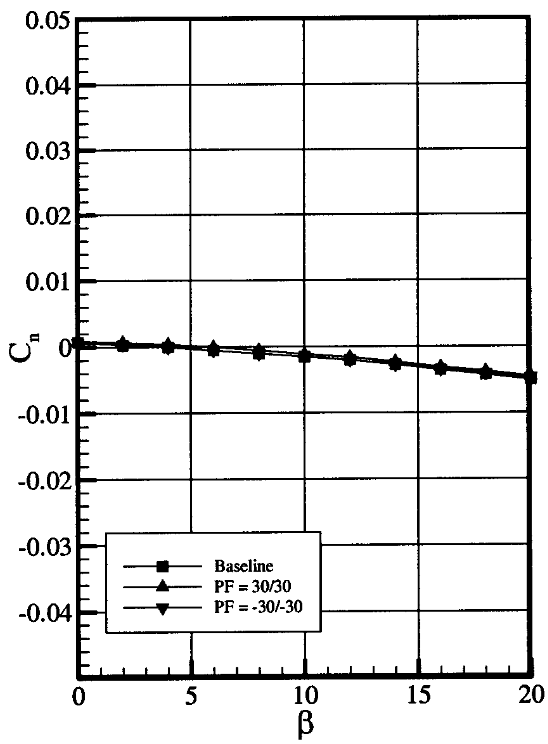

Figure F4d Yawing Moment Coefficient
as a Function of β, α = 15°

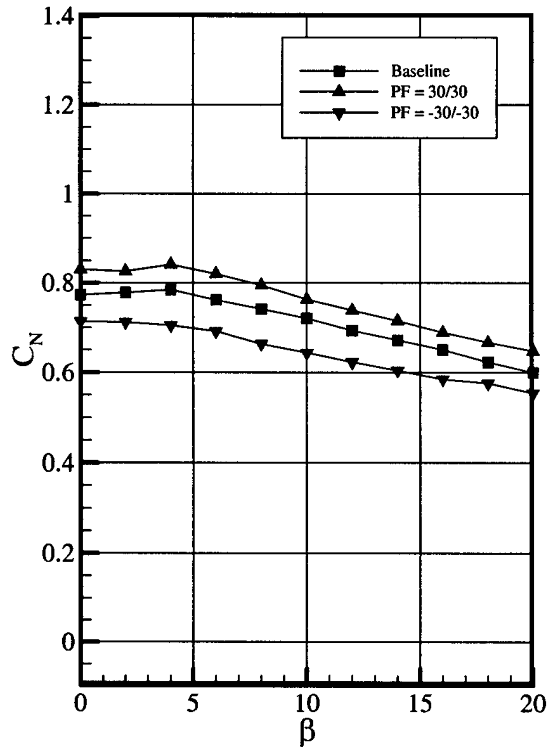

Figure F5a Normal Force Coefficient
as a Function of β, α = 20°

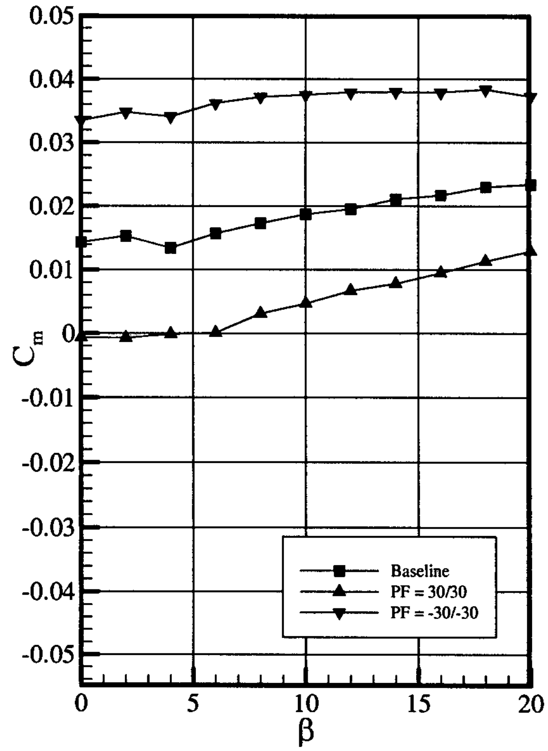

Figure F5b Pitching Moment Coefficient
as a Function of β, α = 20°

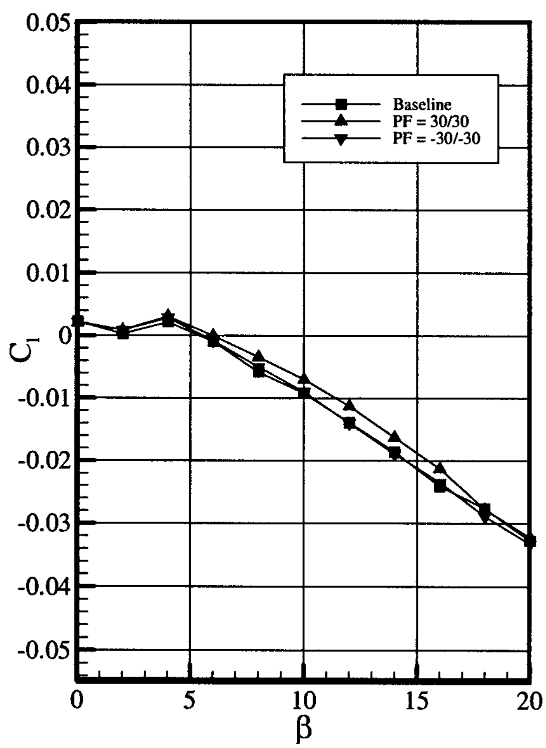

Figure F5c Rolling Moment Coefficient
as a Function of β, α = 20°

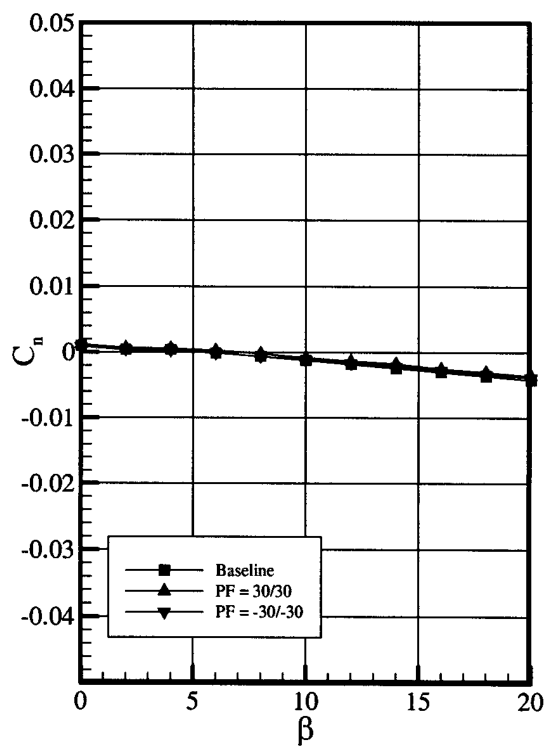

Figure F5d Yawing Moment Coefficient
as a Function of β, α = 20°

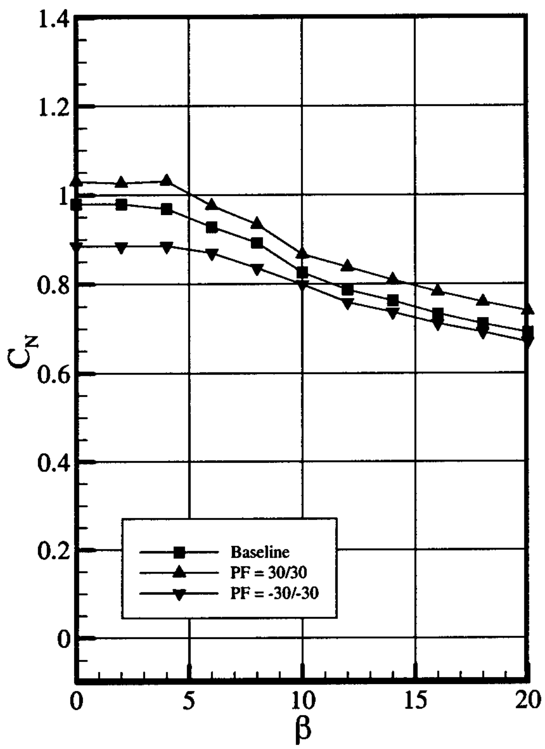

Figure F6a Normal Force Coefficient as a Function of β, α = 25°

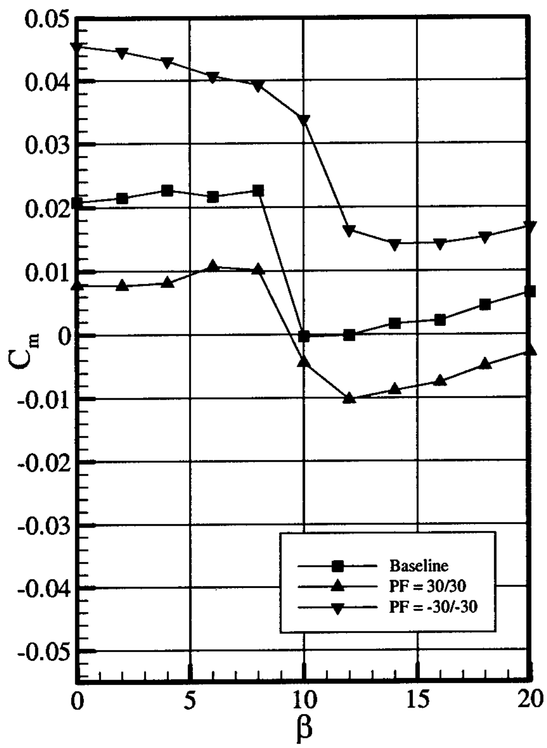

Figure F6b Pitching Moment Coefficient as a Function of β, α = 25°

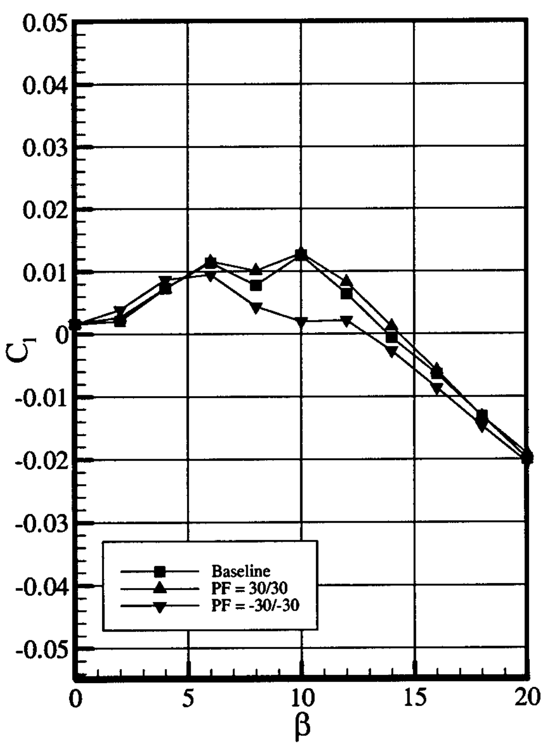

Figure F6c Rolling Moment Coefficient as a Function of β, α = 25°

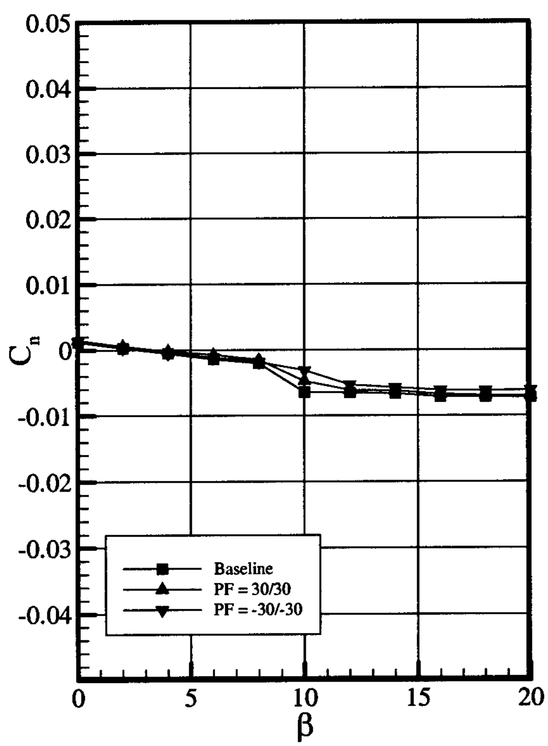

Figure F6d Yawing Moment Coefficient as a Function of β, α = 25°

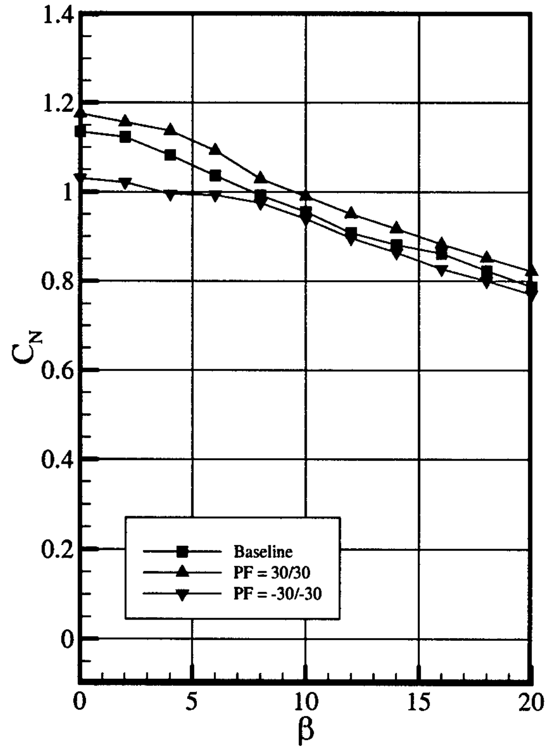

Figure F7a Normal Force Coefficient as a Function of β, α = 30°

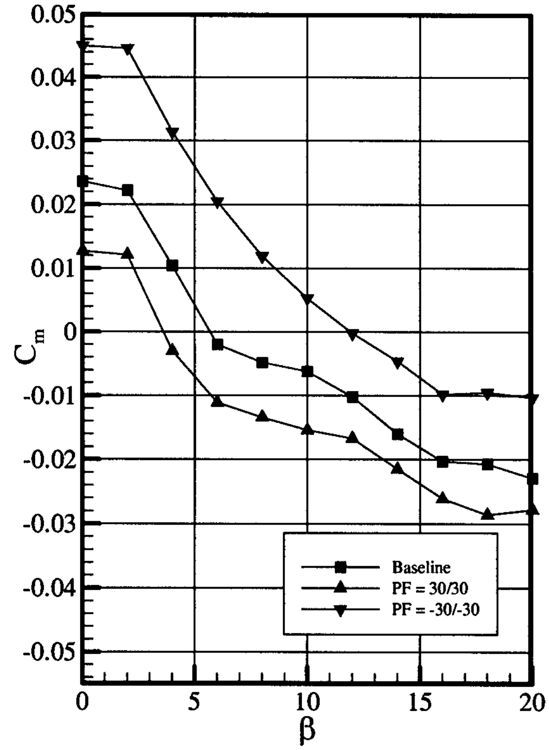

Figure F7b Pitching Moment Coefficient as a Function of β, α = 30°

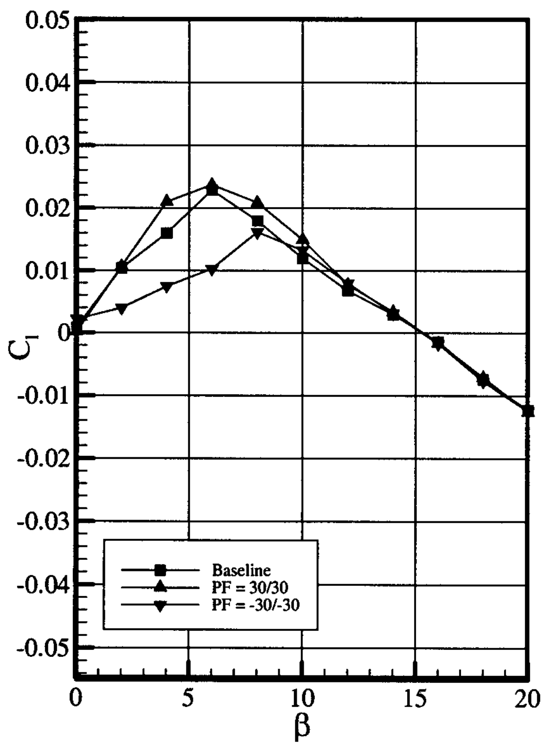

Figure F7c Rolling Moment Coefficient as a Function of β, α = 30°

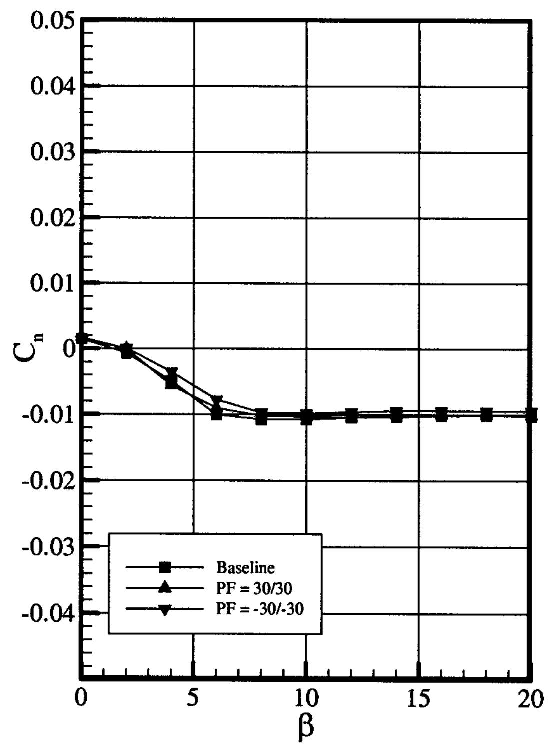

Figure F7d Yawing Moment Coefficient as a Function of β, α = 30°

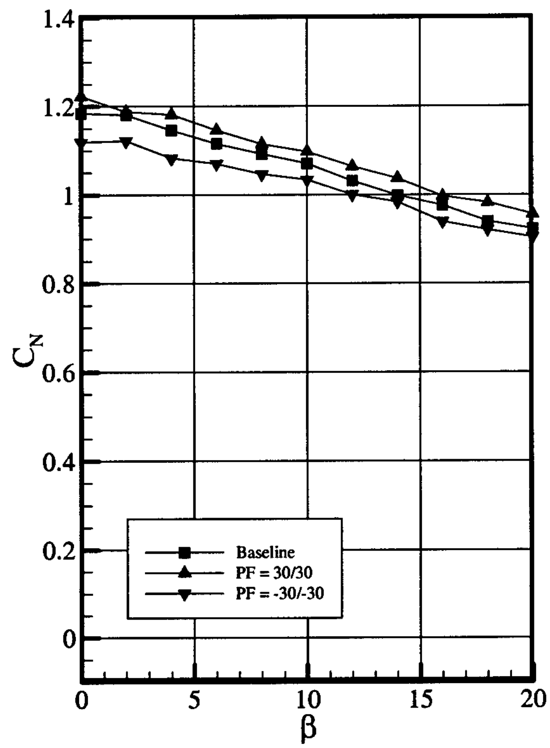

Figure F8a Normal Force Coefficient
as a Function of β, α = 35°

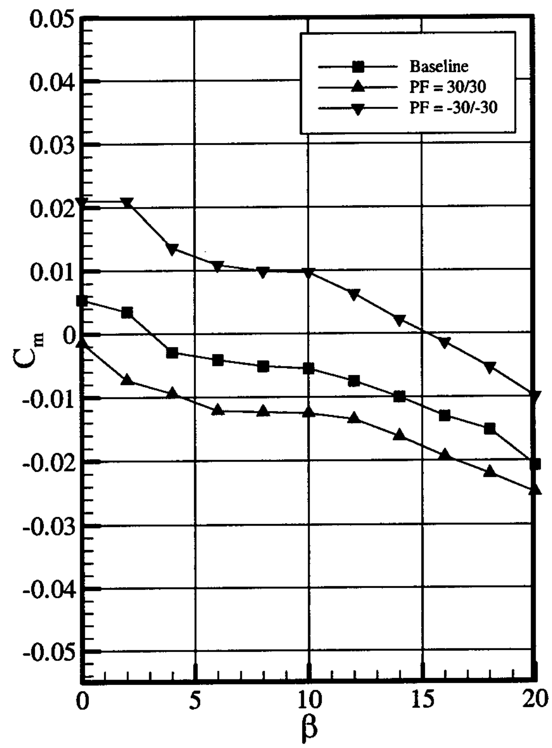

Figure F8b Pitching Moment Coefficient
as a Function of β, α = 35°

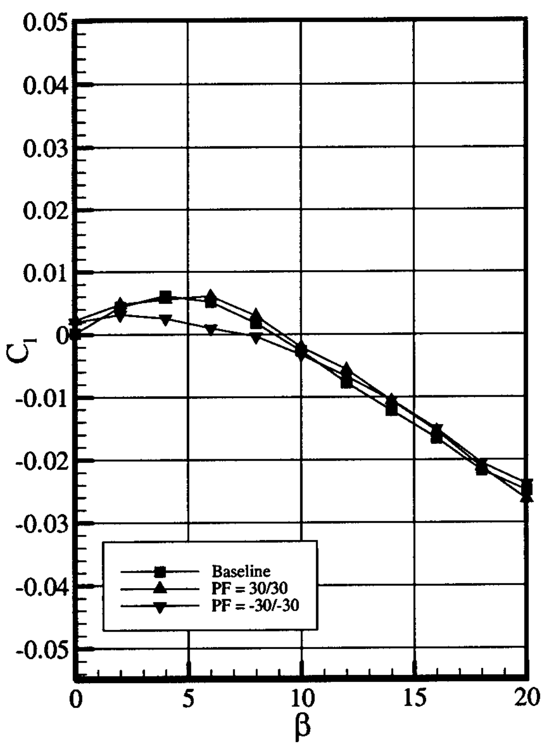

Figure F8c Rolling Moment Coefficient
as a Function of β, α = 35°

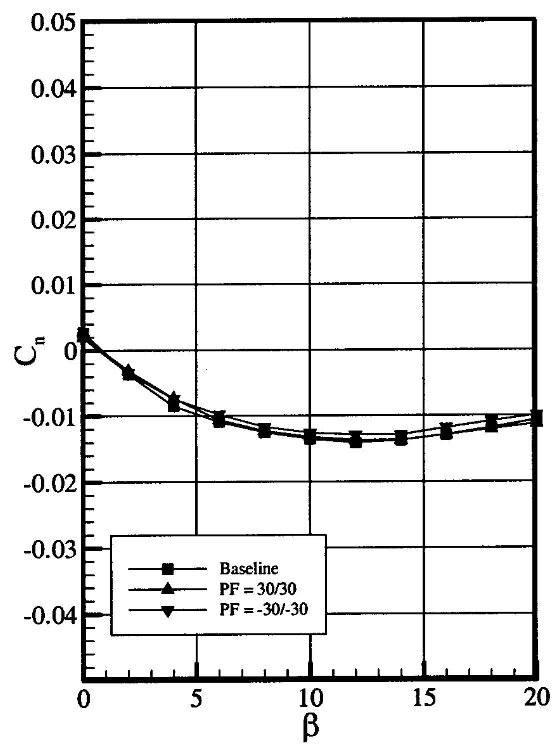

Figure F8d Yawing Moment Coefficient
as a Function of β, α = 35°

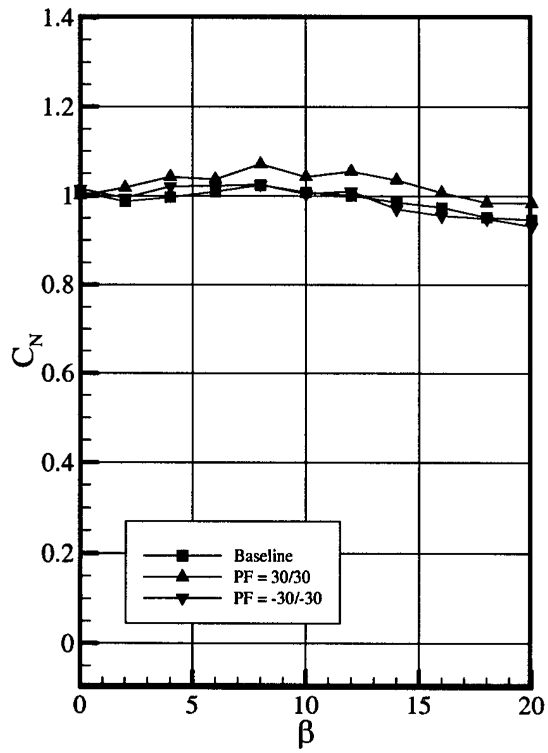

Figure F9a Normal Force Coefficient as a Function of β, α = 40°

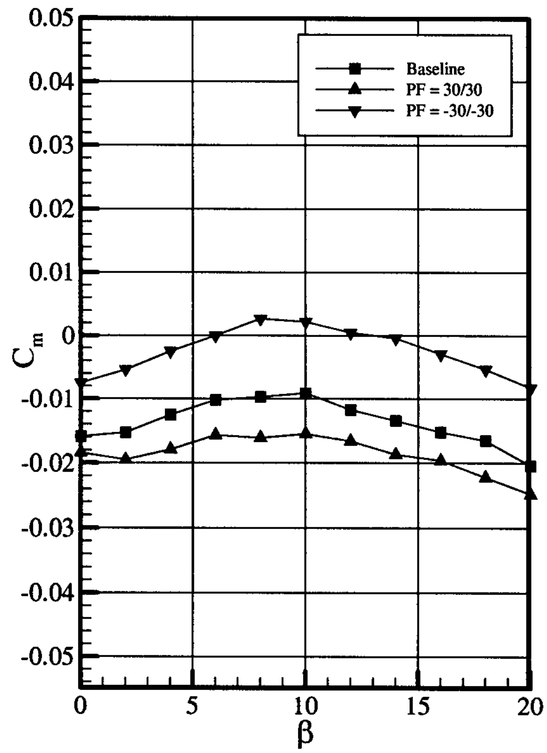

Figure F9b Pitching Moment Coefficient as a Function of β, α = 40°

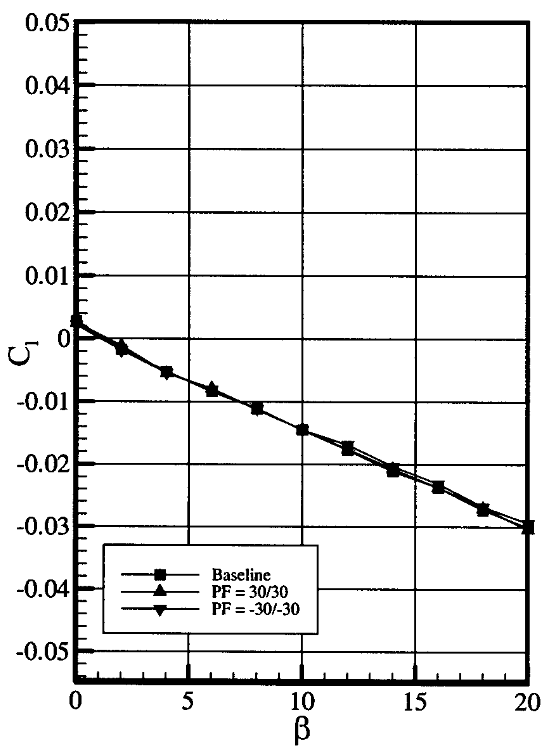

Figure F9c Rolling Moment Coefficient as a Function of β, α = 40°

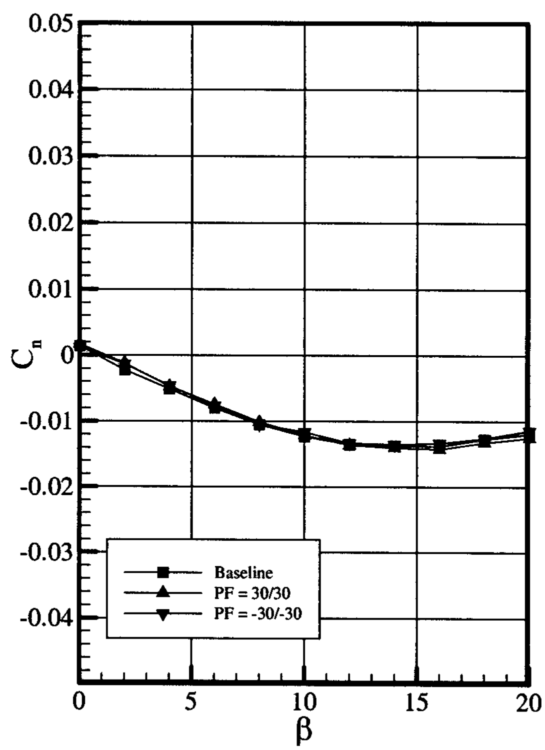

Figure F9d Yawing Moment Coefficient as a Function of β, α = 40°

Appendix G All-Moving-Tip Deflection Data as a Function of Angle of Attack

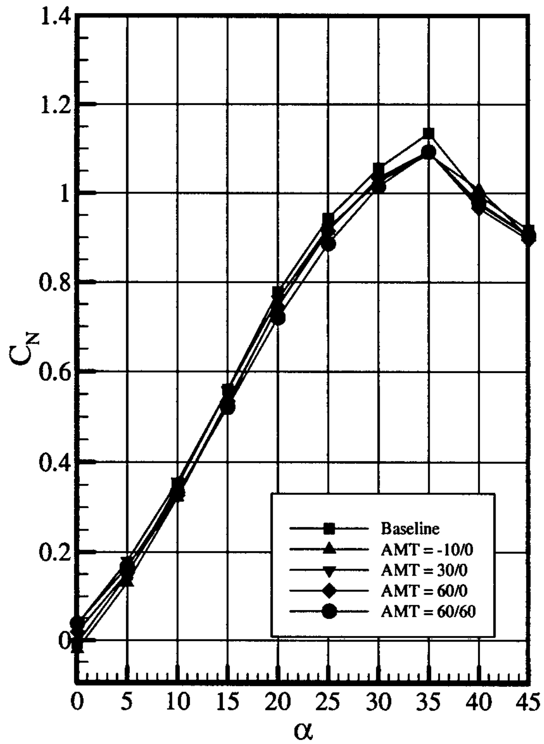

Figure G1a Normal Force Coefficient as a Function of α, β = -6°

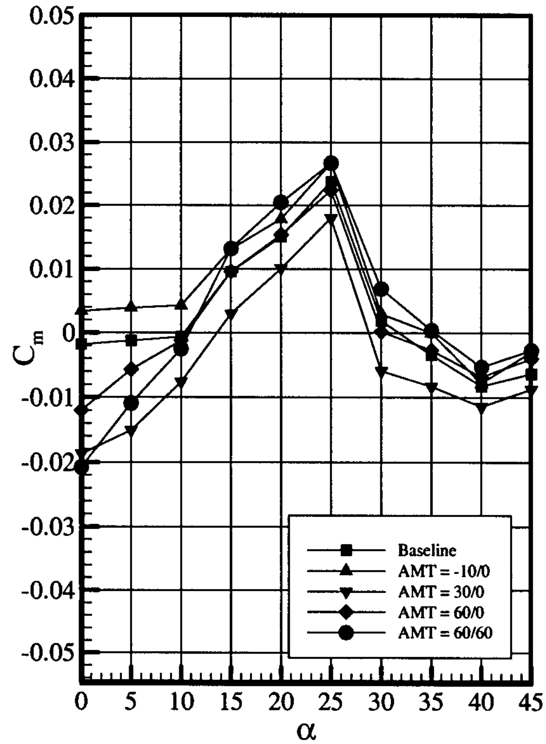

Figure G1b Pitching Moment Coefficient as a Function of α, β = -6°

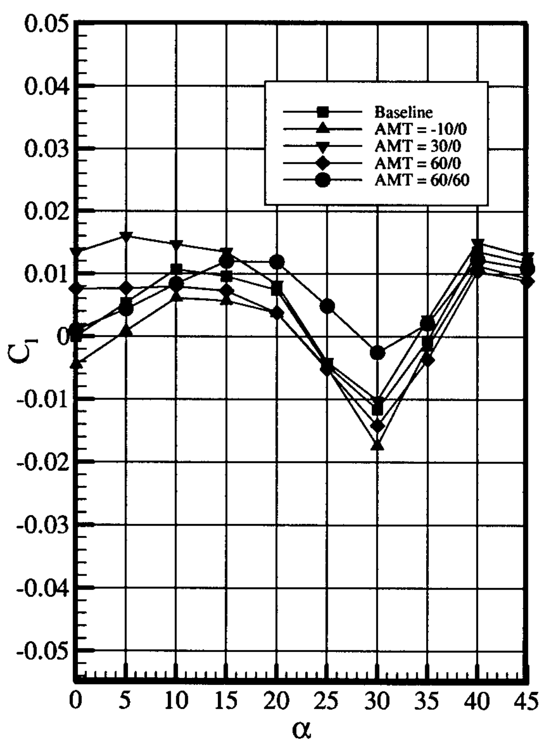

Figure G1c Rolling Moment Coefficient as a Function of α, β = -6°

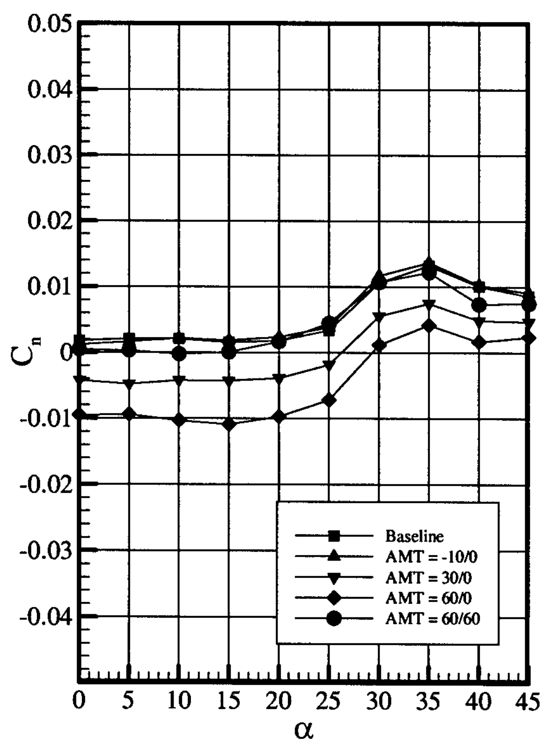

Figure G1d Yawing Moment Coefficient as a Function of α, β = -6°

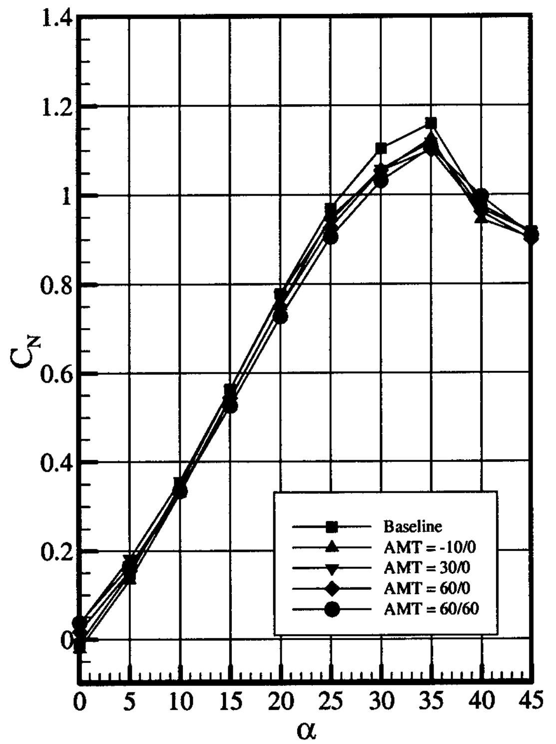

Figure G2a Normal Force Coefficient
as a Function of α, β = -4°

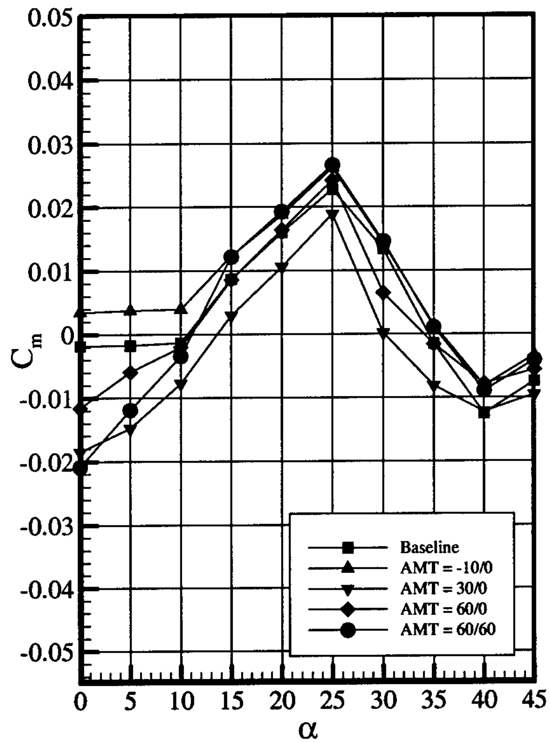

Figure G2b Pitching Moment Coefficient
as a Function of α, β = -4°

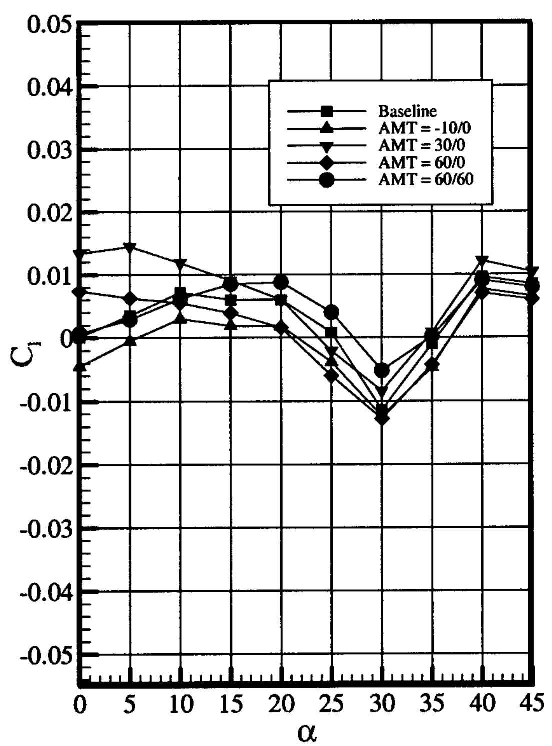

Figure G2c Rolling Moment Coefficient
as a Function of α, β = -4°

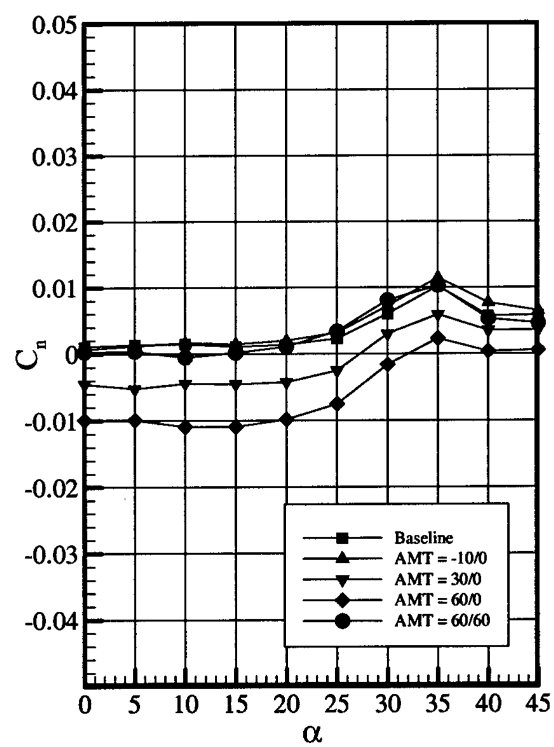

Figure G2d Yawing Moment Coefficient
as a Function of α, β = -4°

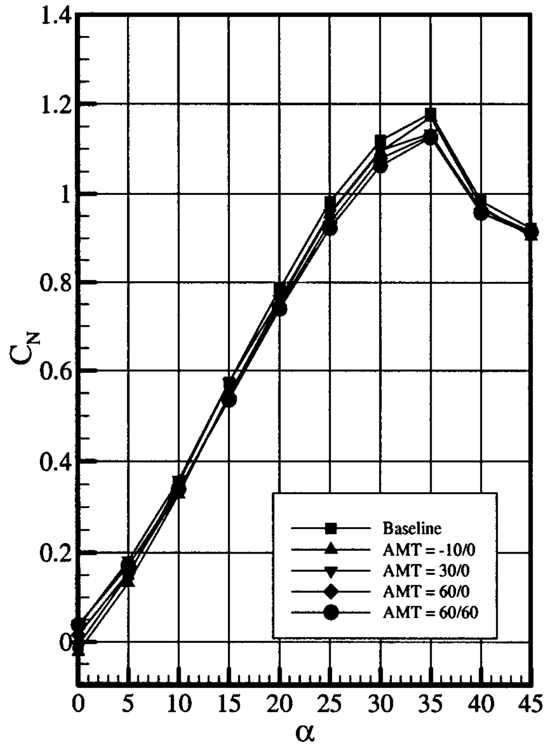

Figure G3a Normal Force Coefficient as a Function of α, β = -2°

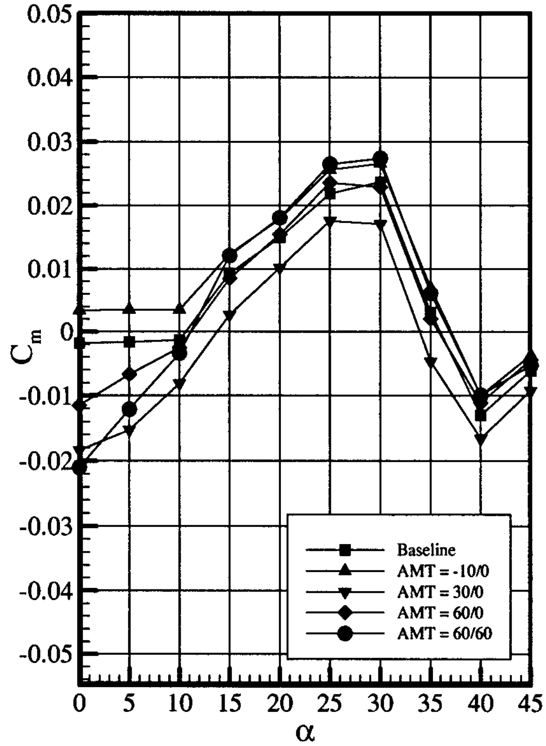

Figure G3b Pitching Moment Coefficient as a Function of α, β = -2°

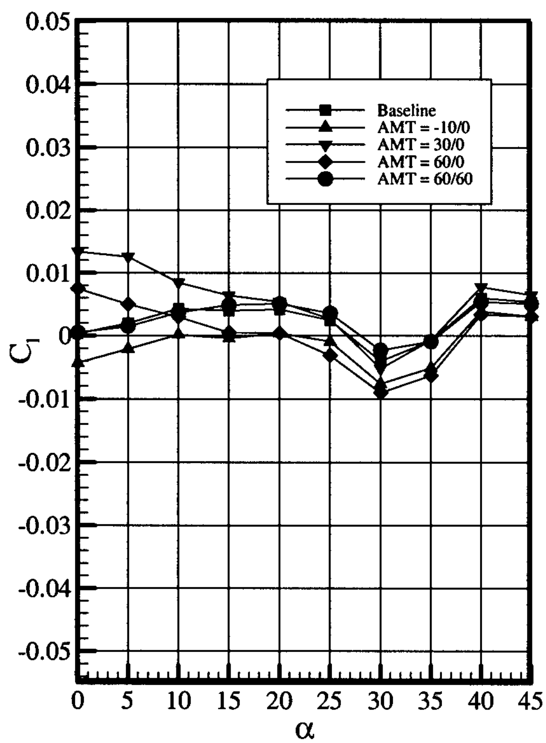

Figure G3c Rolling Moment Coefficient as a Function of α, β = -2°

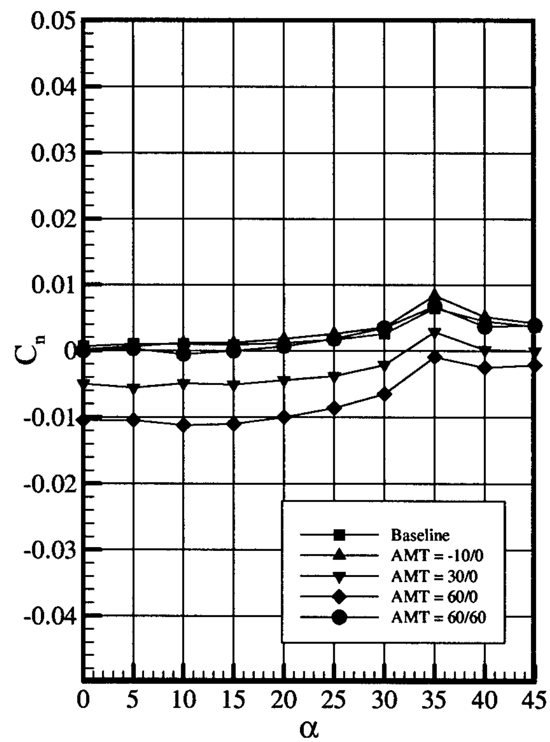

Figure G3d Yawing Moment Coefficient as a Function of α, β = -2°

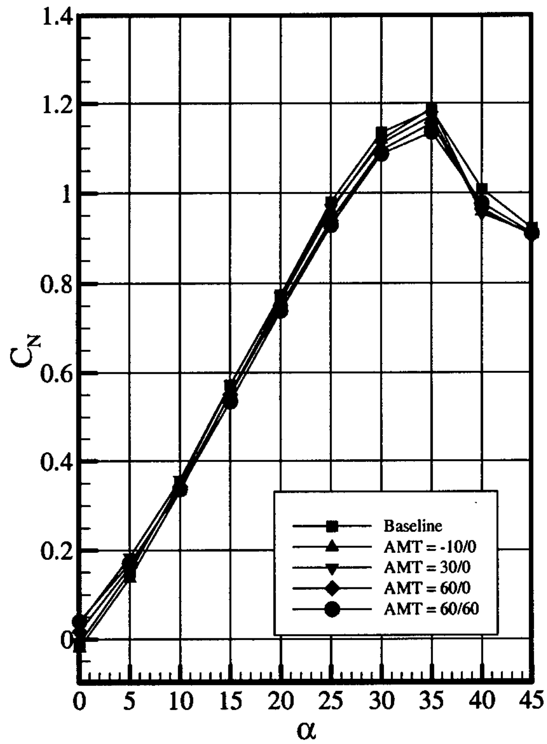

Figure G4a Normal Force Coefficient as a Function of α, $\beta = 0^{\circ}$

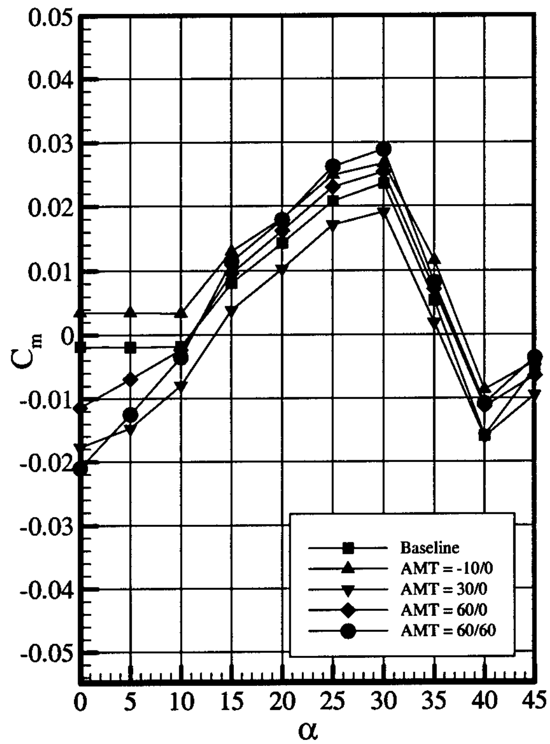

Figure G4b Pitching Moment Coefficient as a Function of α, $\beta = 0^{\circ}$

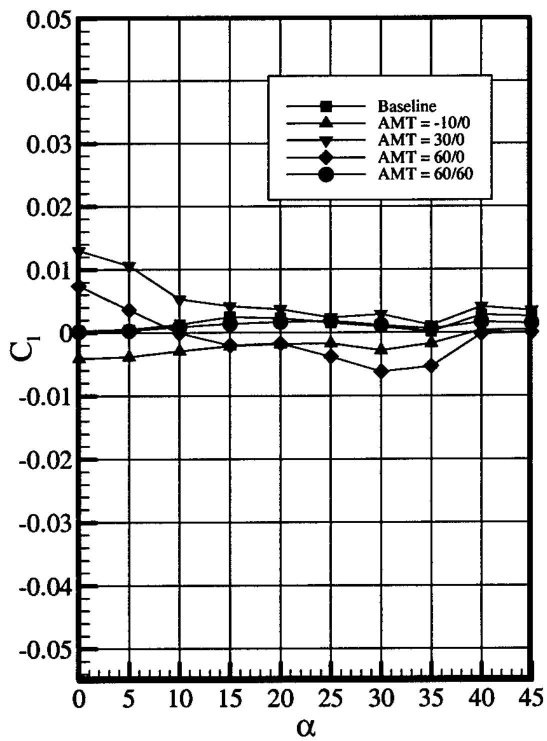

Figure G4c Rolling Moment Coefficient as a Function of α, $\beta = 0^{\circ}$

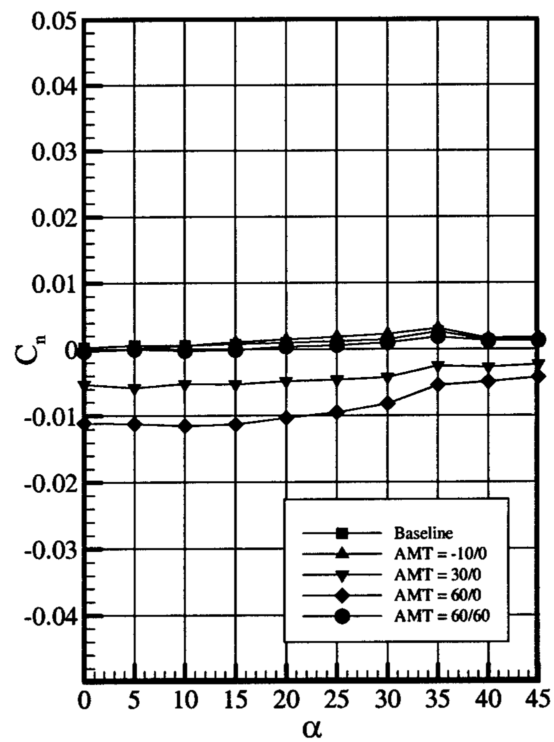

Figure G4d Yawing Moment Coefficient as a Function of α, $\beta = 0^{\circ}$

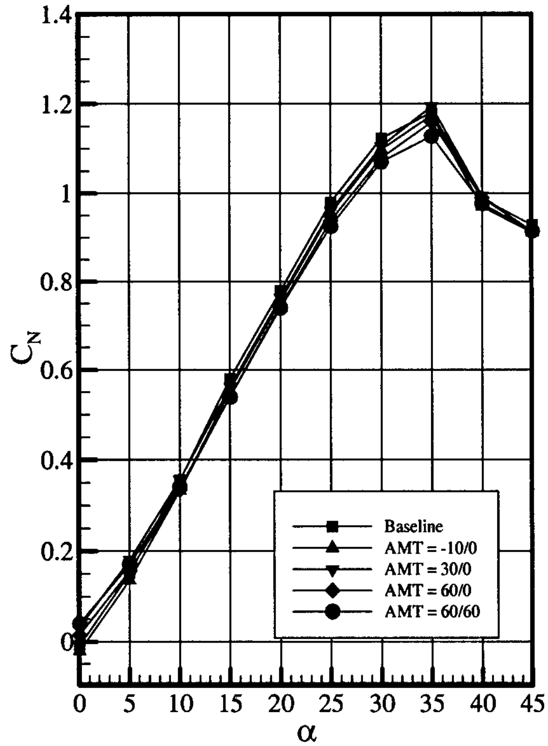

Figure G5a Normal Force Coefficient as a Function of α, $\beta = 2^{\circ}$

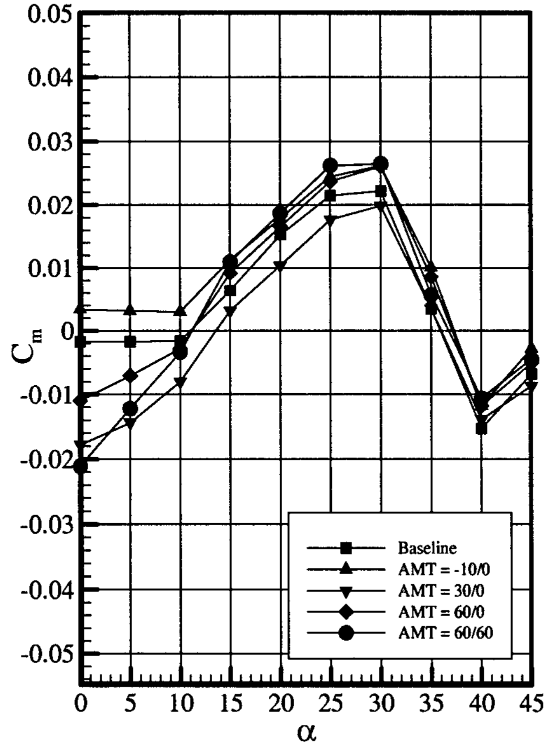

Figure G5b Pitching Moment Coefficient as a Function of α, $\beta = 2^{\circ}$

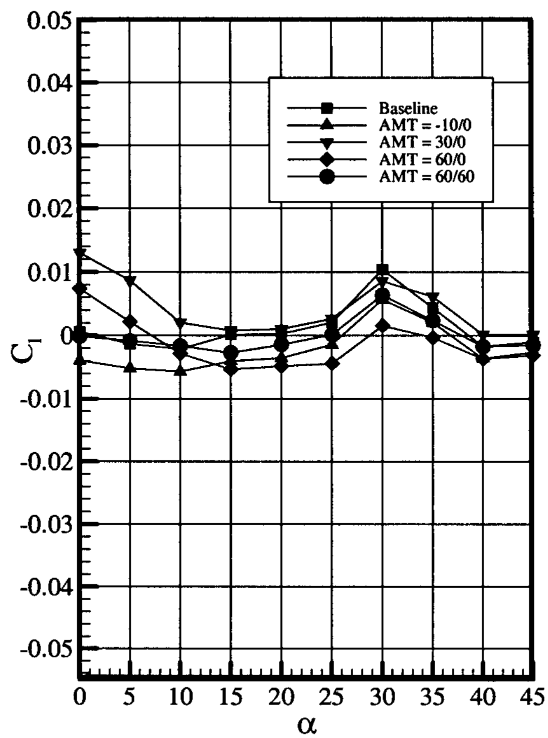

Figure G5c Rolling Moment Coefficient as a Function of α, $\beta = 2^{\circ}$

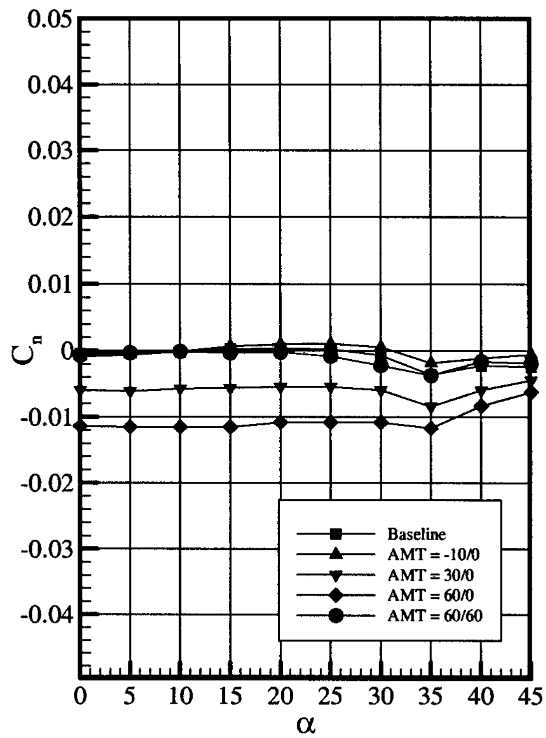

Figure G5d Yawing Moment Coefficient as a Function of α, $\beta = 2^{\circ}$

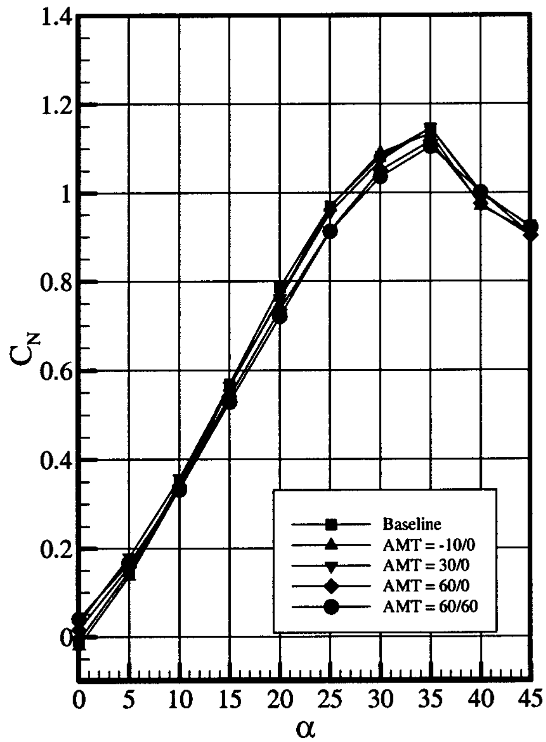

Figure G6a Normal Force Coefficient as a Function of α, β = 4°

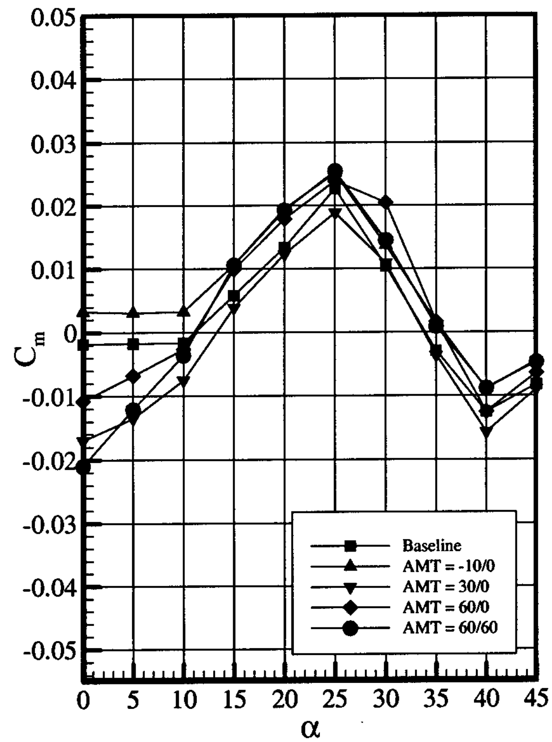

Figure G6b Pitching Moment Coefficient as a Function of α, β = 4°

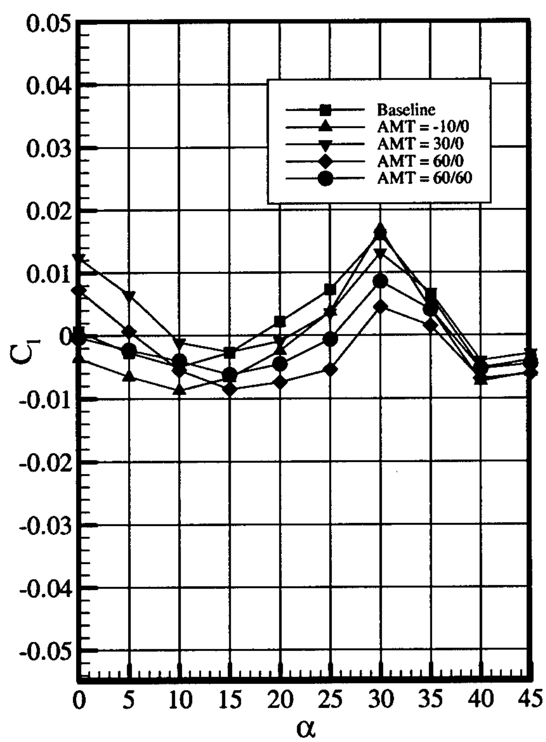

Figure G6c Rolling Moment Coefficient as a Function of α, β = 4°

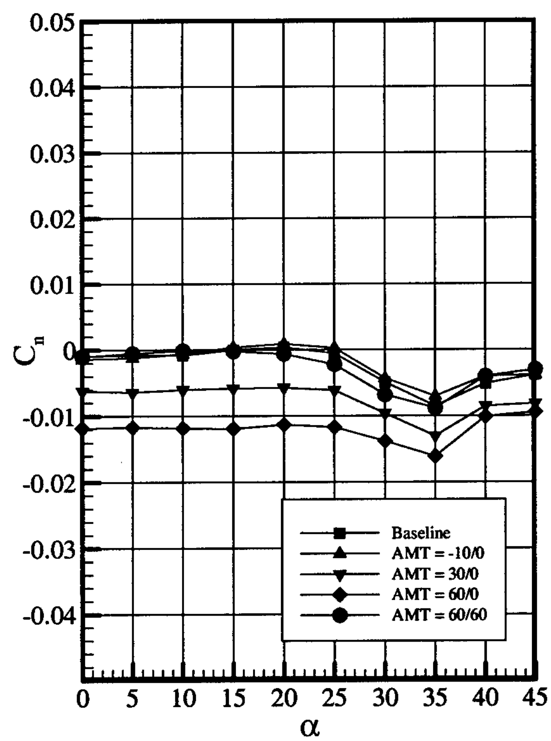

Figure G6d Yawing Moment Coefficient as a Function of α, β = 4°

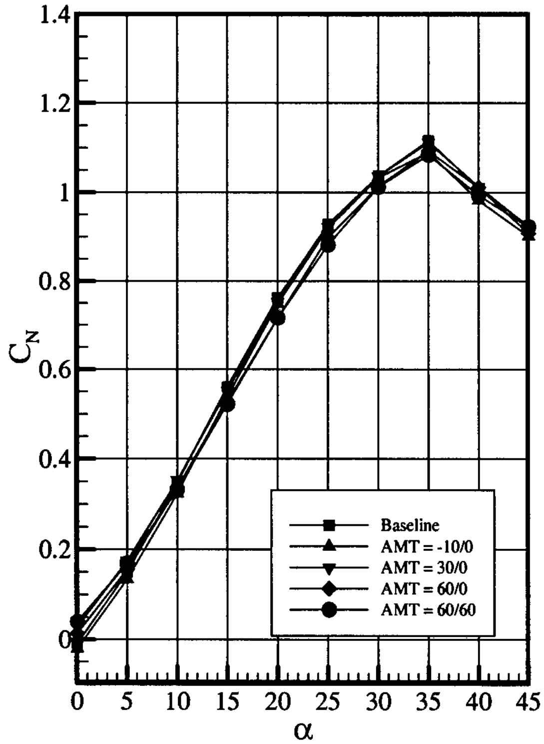

Figure G7a Normal Force Coefficient as a Function of α, β = 6°

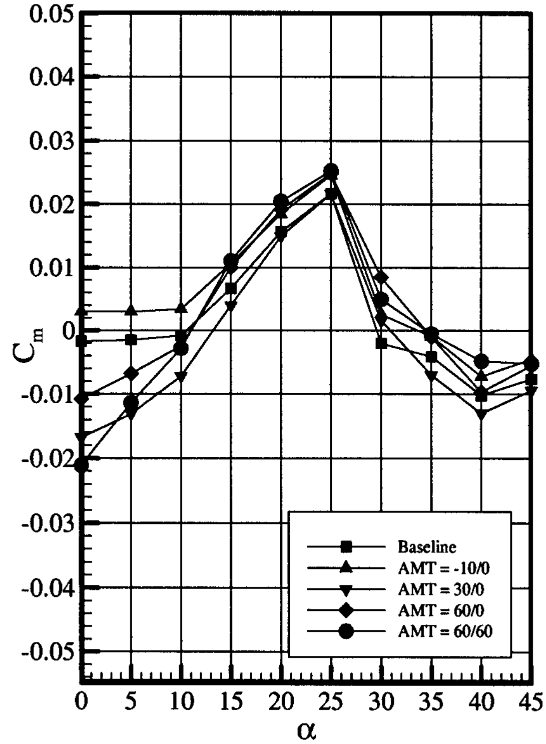

Figure G7b Pitching Moment Coefficient as a Function of α, β = 6°

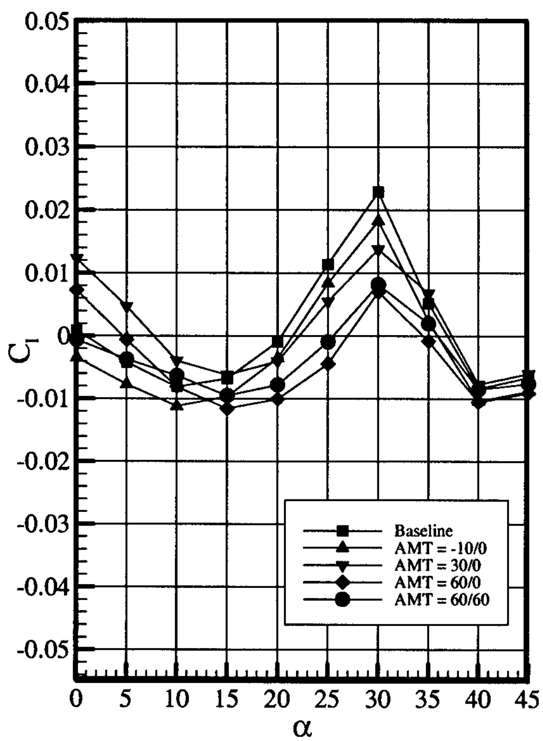

Figure G7c Rolling Moment Coefficient as a Function of α, β = 6°

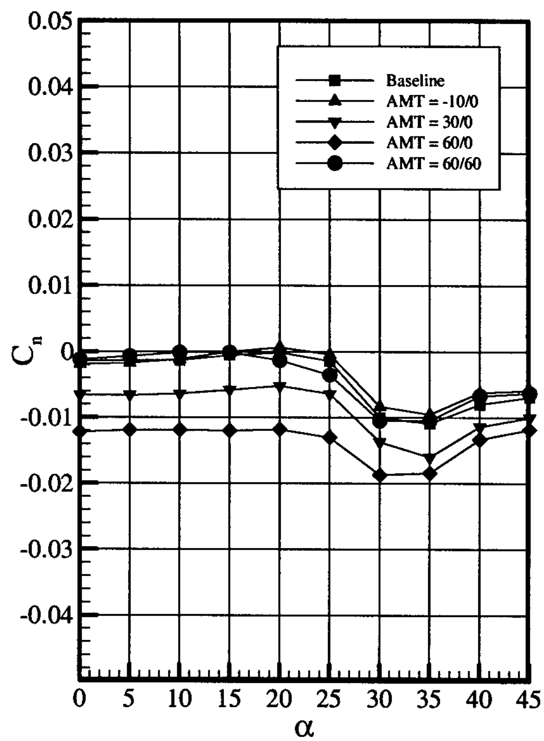

Figure G7d Yawing Moment Coefficient as a Function of α, β = 6°

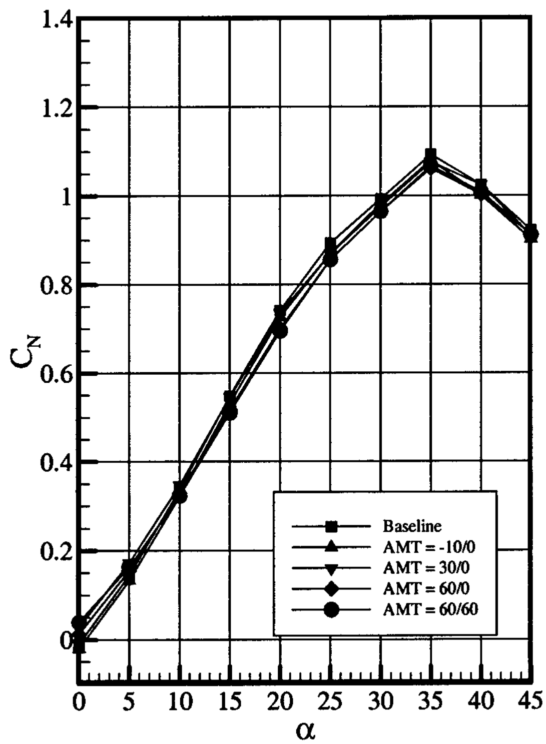

Figure G8a Normal Force Coefficient as a Function of α, $\beta = 8^{\circ}$

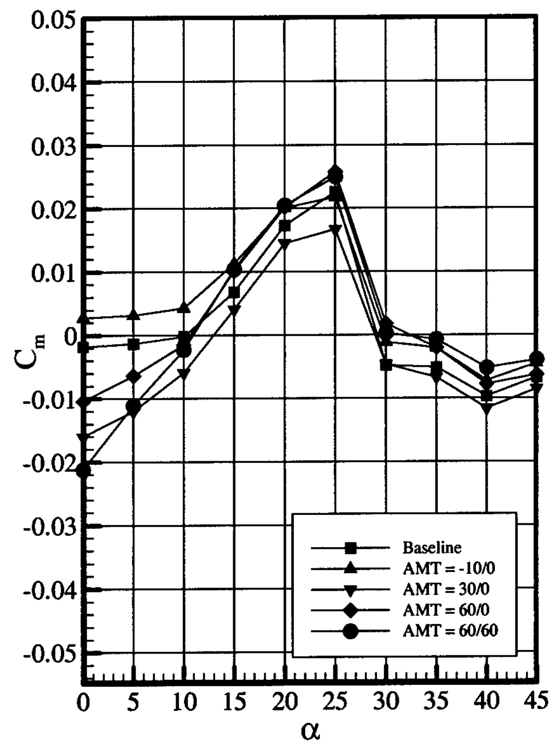

Figure G8b Pitching Moment Coefficient as a Function of α, $\beta = 8^{\circ}$

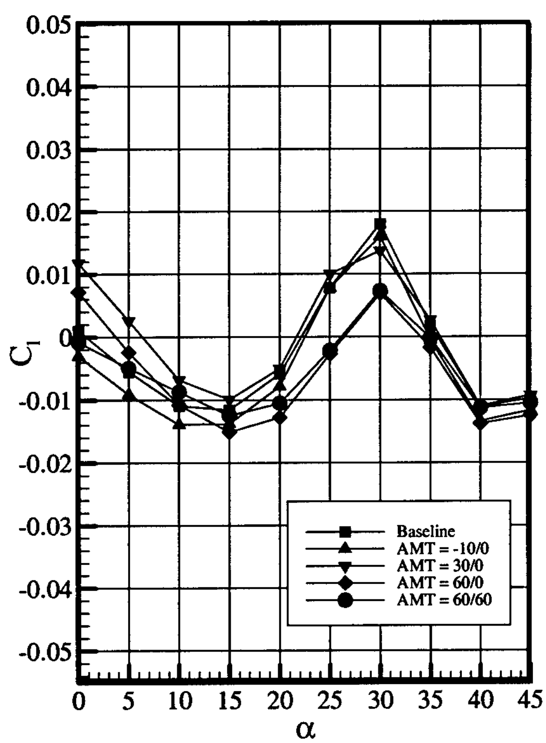

Figure G8c Rolling Moment Coefficient as a Function of α, $\beta = 8^{\circ}$

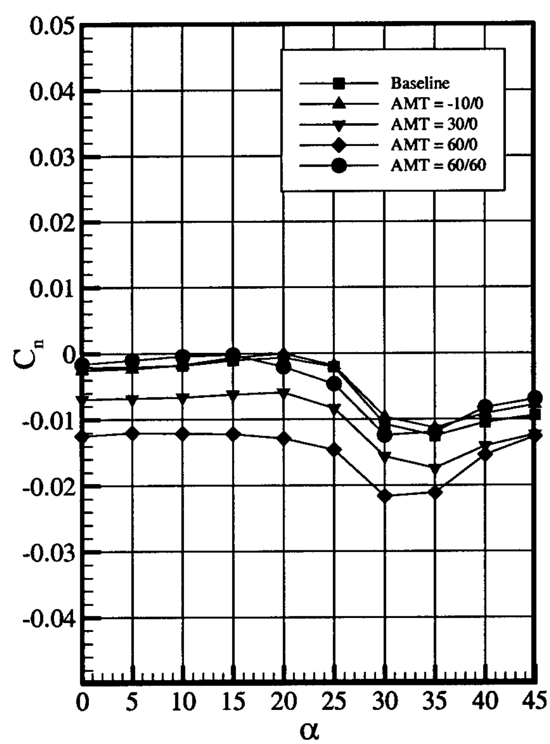

Figure G8d Yawing Moment Coefficient as a Function of α, $\beta = 8^{\circ}$

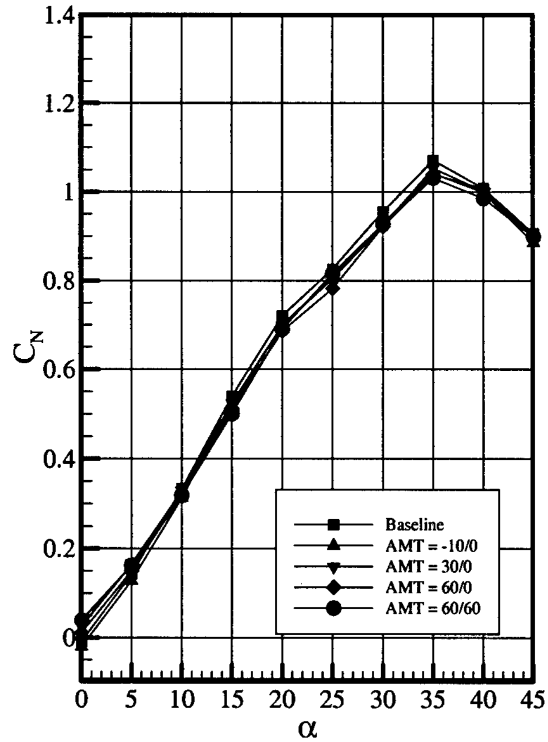

Figure G9a Normal Force Coefficient as a Function of α, β = 10°

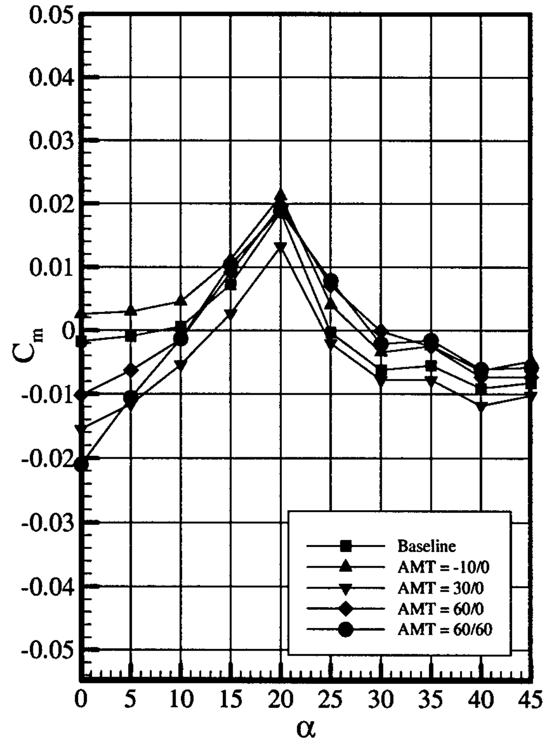

Figure G9b Pitching Moment Coefficient as a Function of α, β = 10°

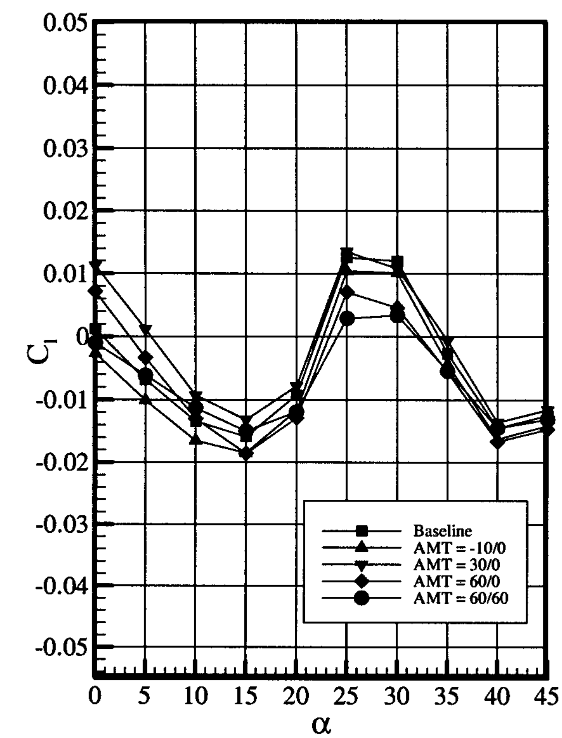

Figure G9c Rolling Moment Coefficient as a Function of α, β = 10°

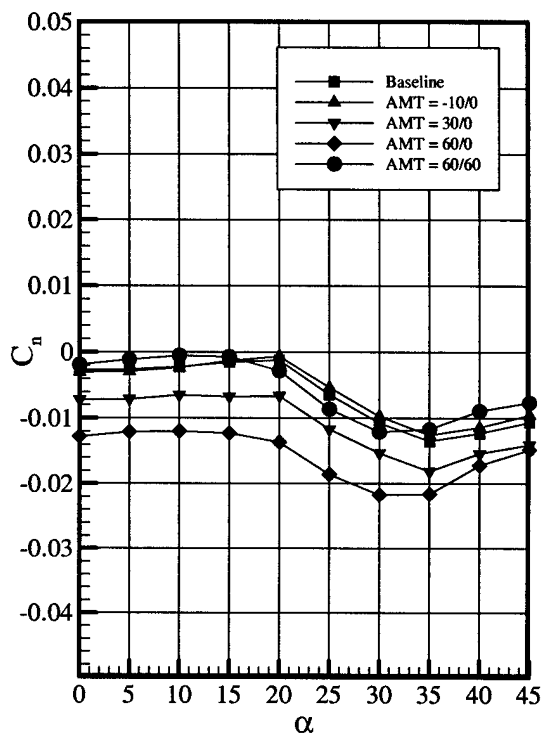

Figure G9d Yawing Moment Coefficient as a Function of α, β = 10°

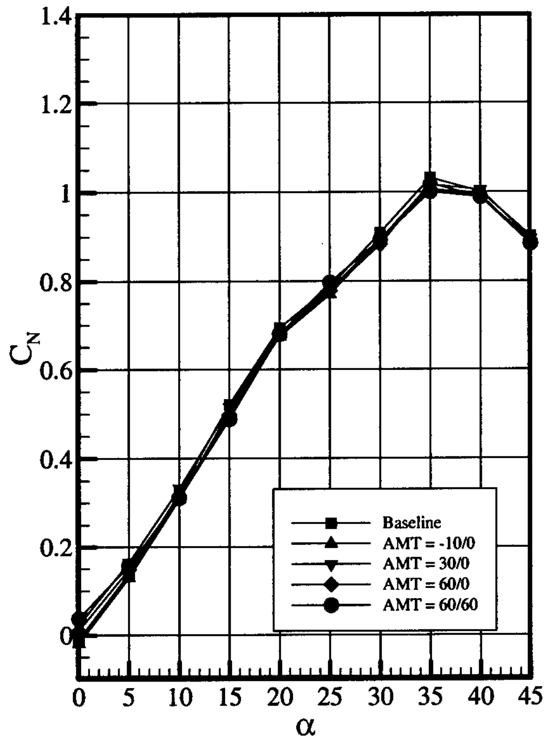

Figure G10a Normal Force Coefficient as a Function of α, β = 12°

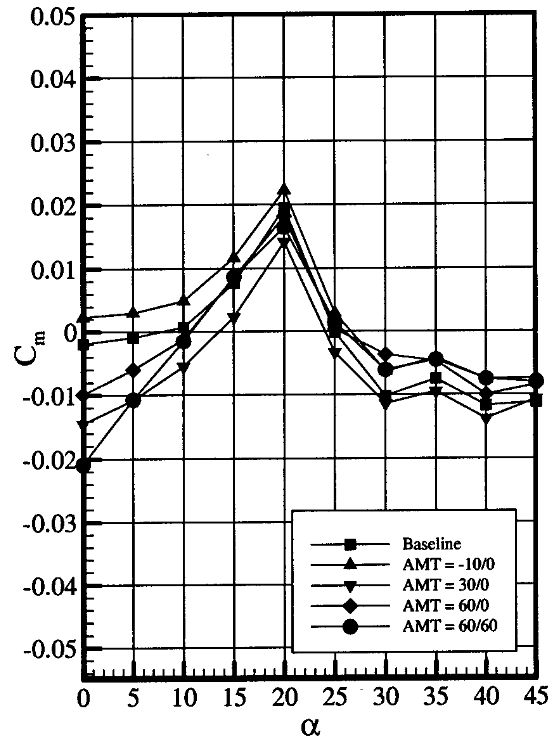

Figure G10b Pitching Moment Coefficient as a Function of α, β = 12°

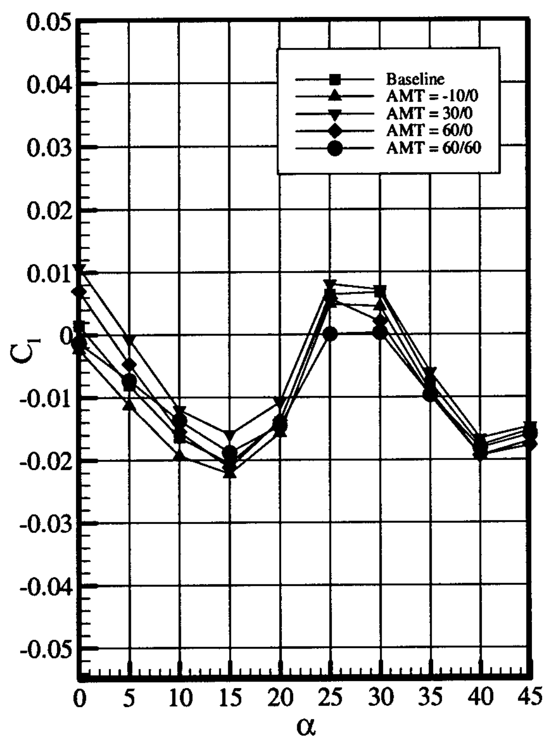

Figure G10c Rolling Moment Coefficient as a Function of α, β = 12°

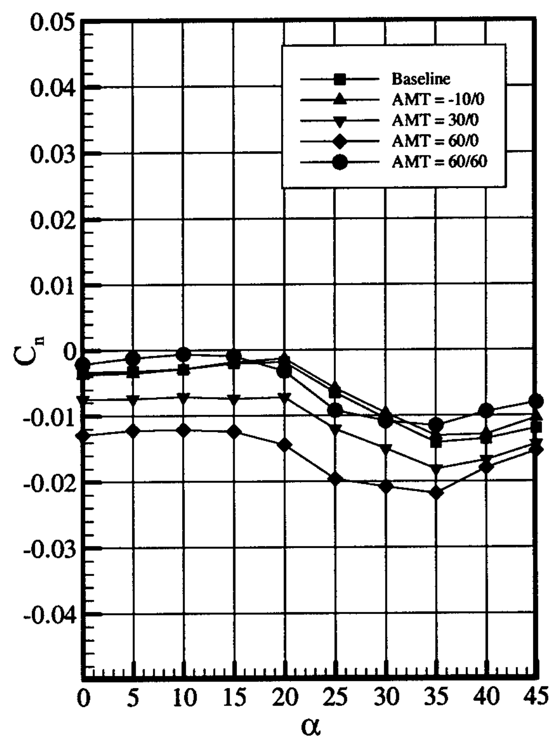

Figure G10d Yawing Moment Coefficient as a Function of α, β = 12°

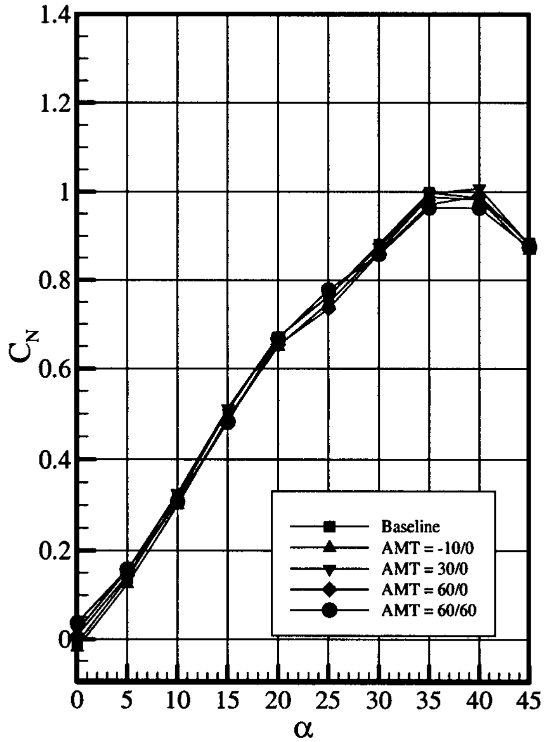

Figure G11a Normal Force Coefficient as a Function of α, β = 14°

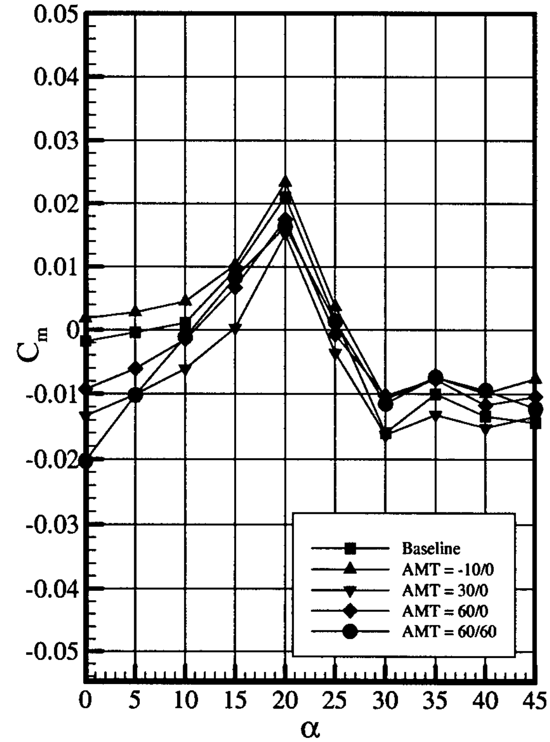

Figure G11b Pitching Moment Coefficient as a Function of α, β = 14°

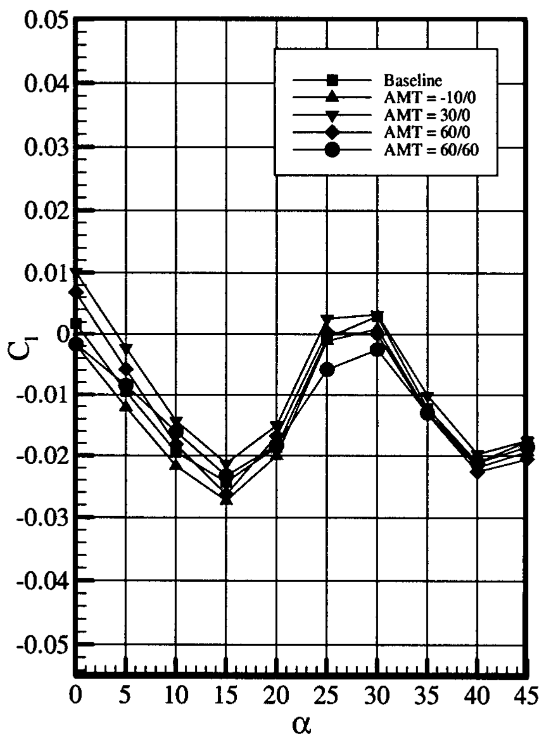

Figure G11c Rolling Moment Coefficient as a Function of α, β = 14°

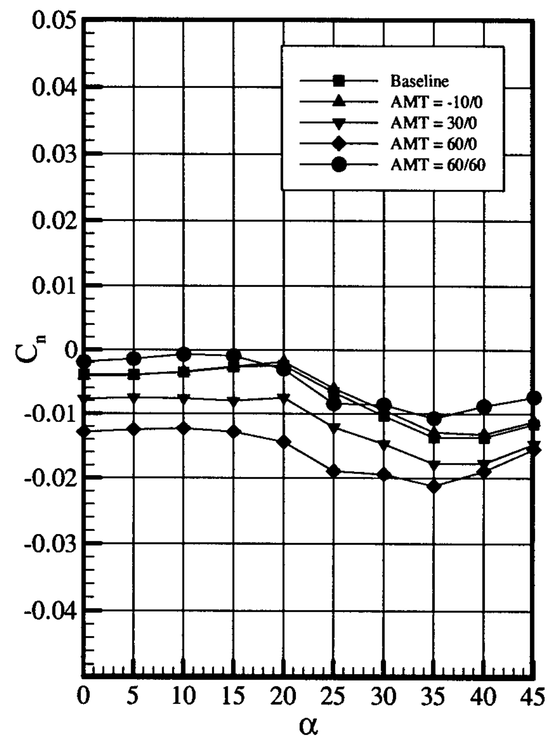

Figure G11d Yawing Moment Coefficient as a Function of α, β = 14°

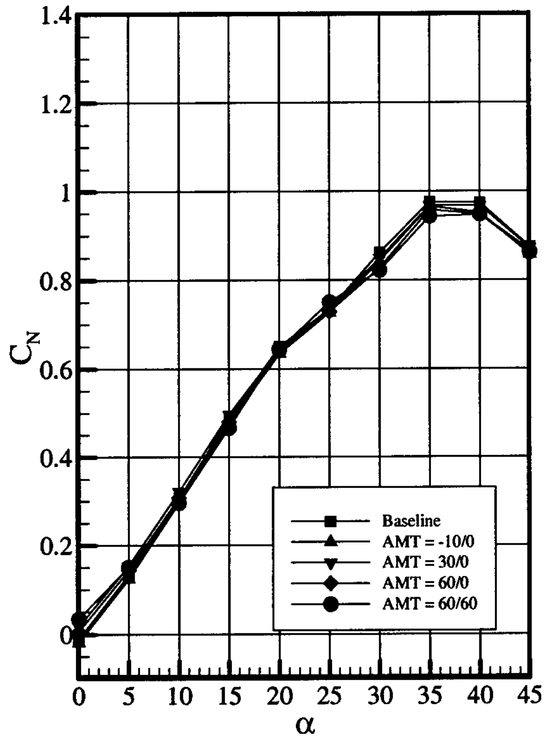

Figure G12a Normal Force Coefficient as a Function of α, β = 16°

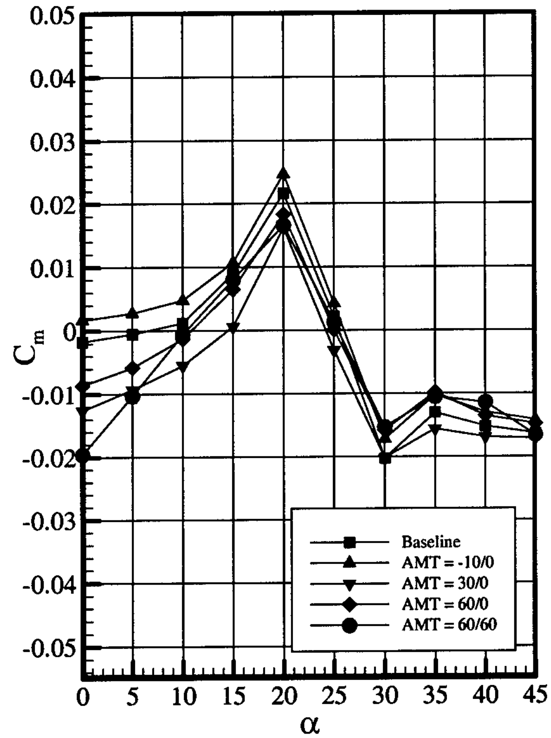

Figure G12b Pitching Moment Coefficient as a Function of α, β = 16°

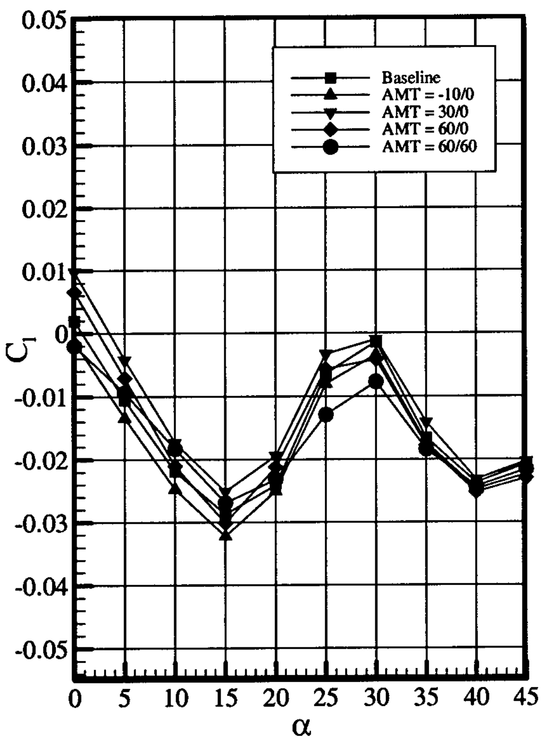

Figure G12c Rolling Moment Coefficient as a Function of α, β = 16°

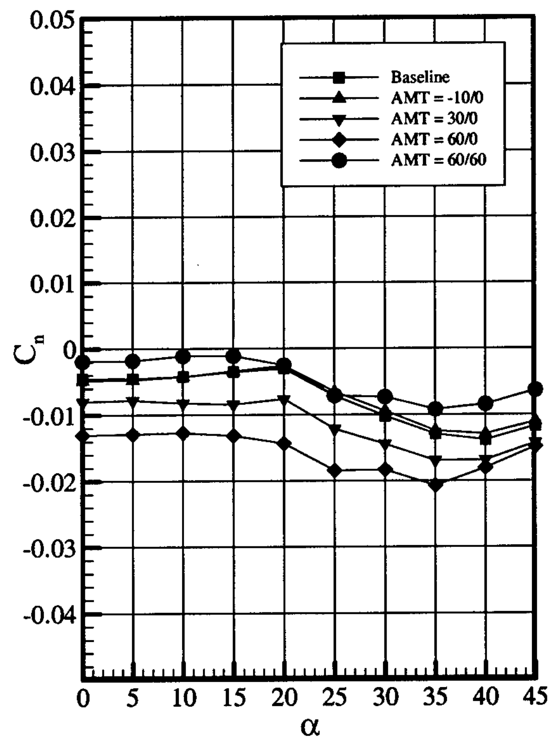

Figure G12d Yawing Moment Coefficient as a Function of α, β = 16°

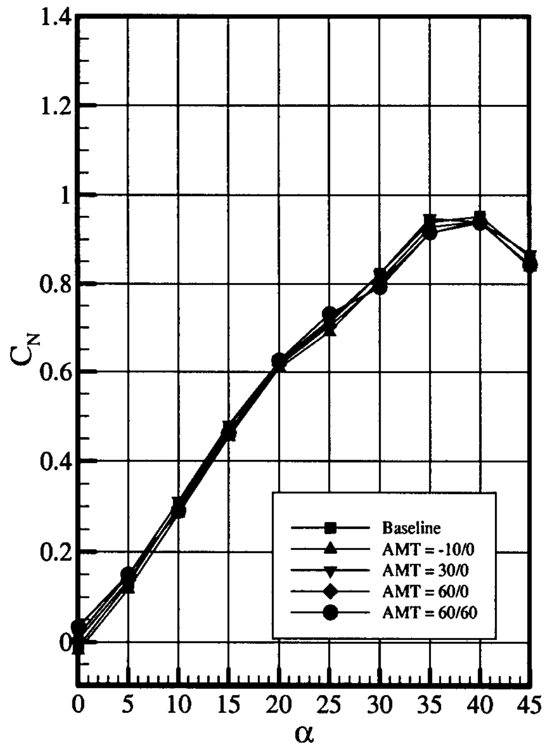

Figure G13a Normal Force Coefficient as a Function of α, β = 18°

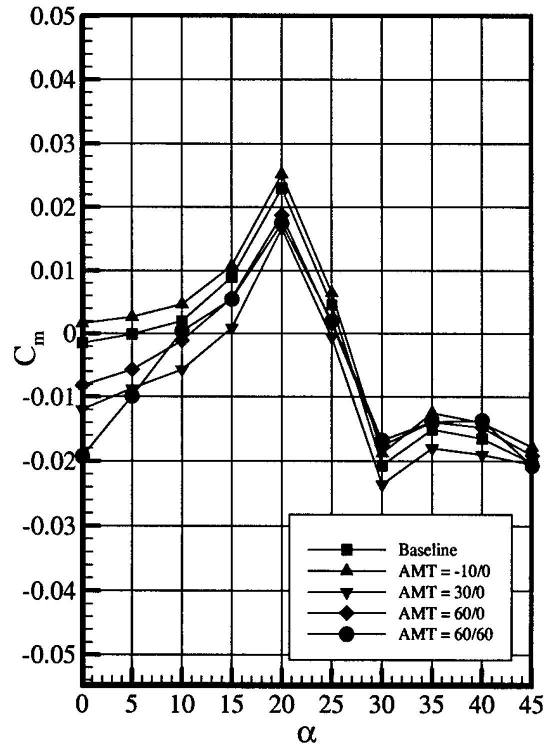

Figure G13b Pitching Moment Coefficient as a Function of α, β = 18°

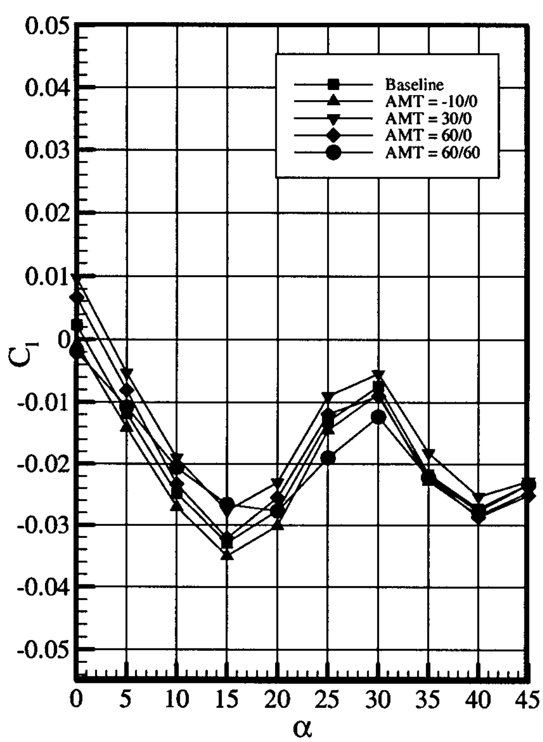

Figure G13c Rolling Moment Coefficient as a Function of α, β = 18°

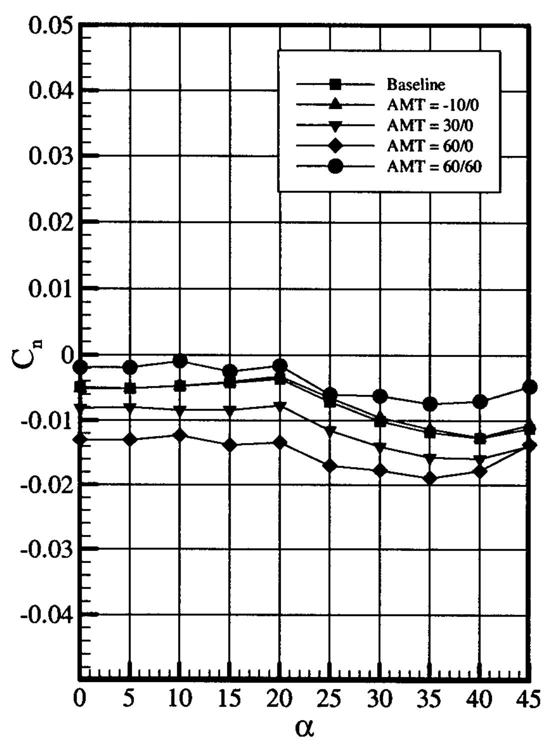

Figure G13d Yawing Moment Coefficient as a Function of α, β = 18°

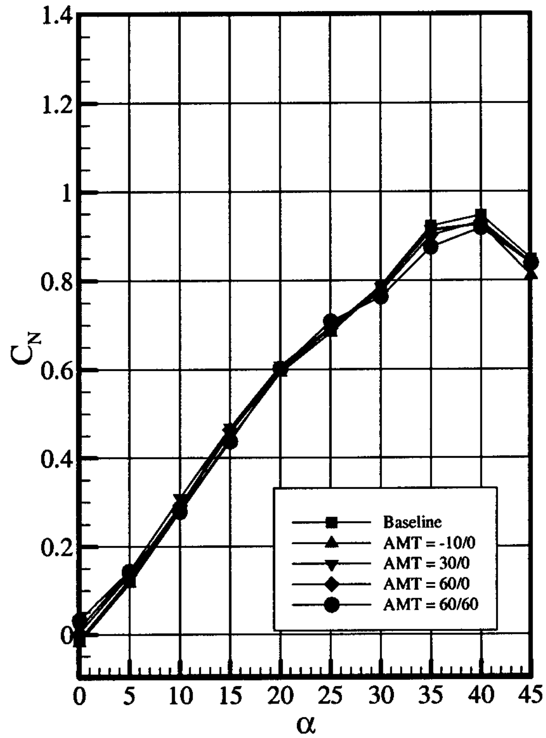

Figure G14a Normal Force Coefficient as a Function of α, $\beta = 20^{\circ}$

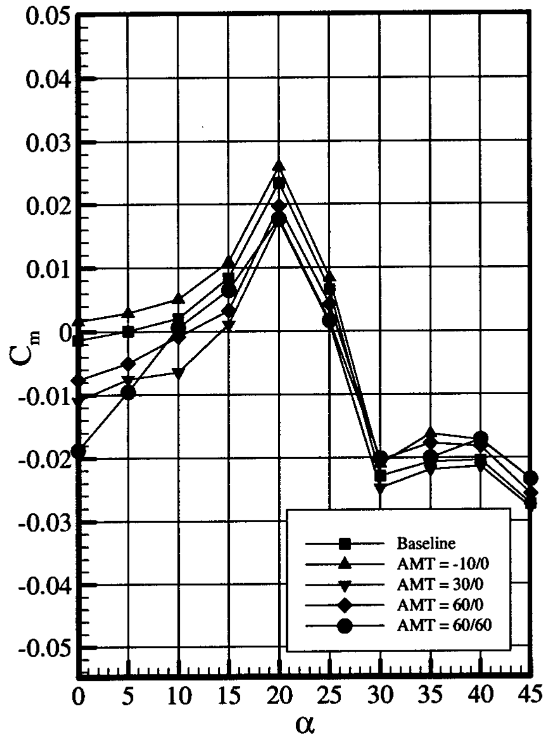

Figure G14b Pitching Moment Coefficient as a Function of α, $\beta = 20^{\circ}$

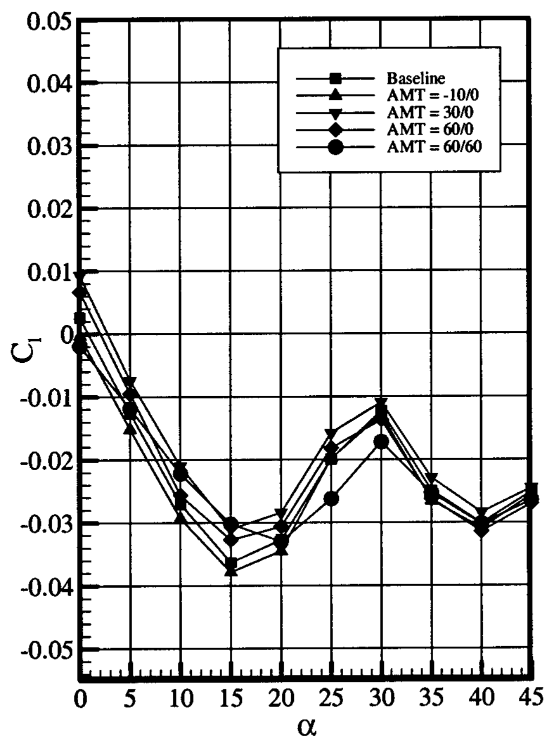

Figure G14c Rolling Moment Coefficient as a Function of α, $\beta = 20^{\circ}$

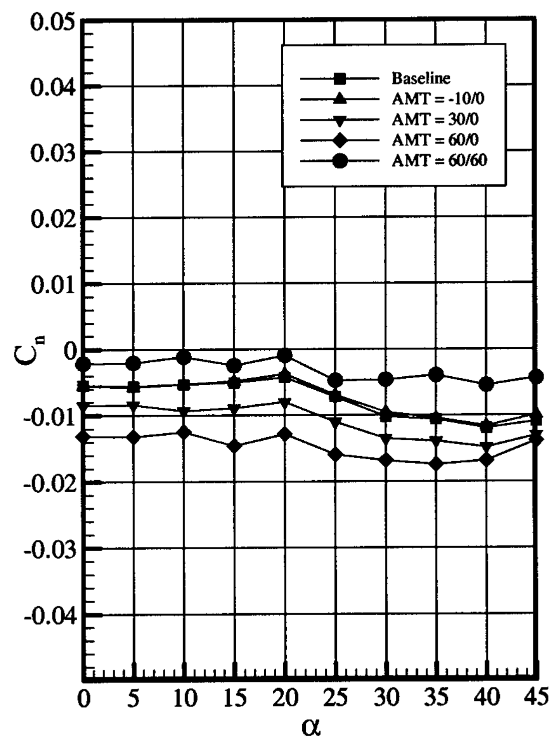

Figure G14d Yawing Moment Coefficient as a Function of α, $\beta = 20^{\circ}$

Appendix H All-Moving-Tip Deflection Data as a Function of Sideslip Angle

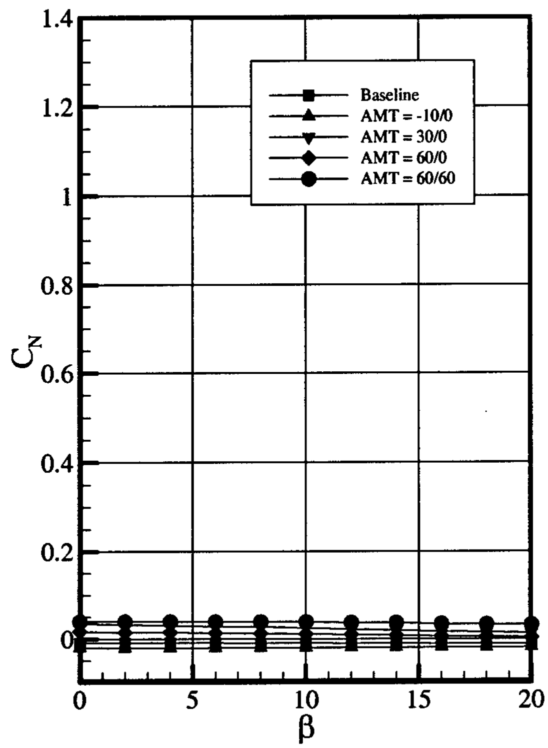

Figure H1a Normal Force Coefficient as a Function of β, α = 0°

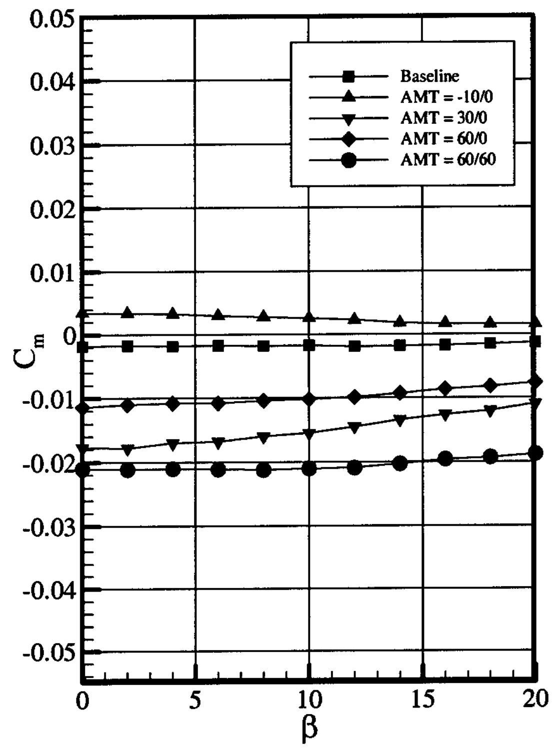

Figure H1b Pitching Moment Coefficient as a Function of β, α = 0°

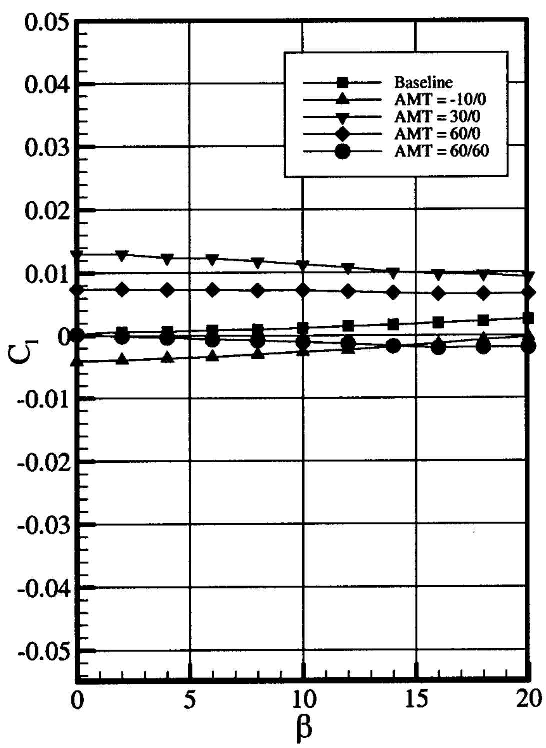

Figure H1c Rolling Moment Coefficient as a Function of β, α = 0°

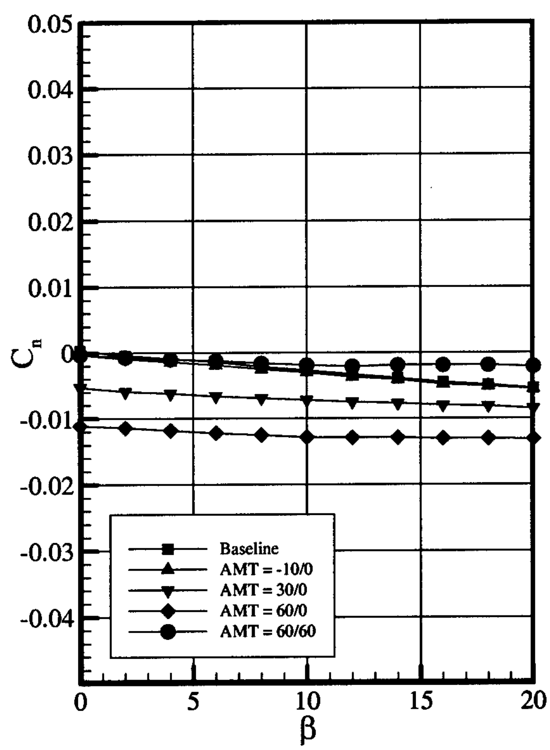

Figure H1d Yawing Moment Coefficient as a Function of β, α = 0°

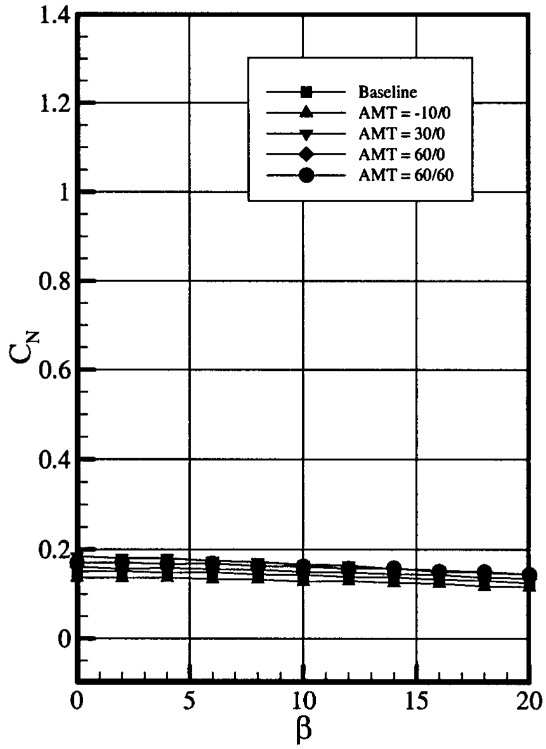

Figure H2a Normal Force Coefficient as a Function of β, α = 5°

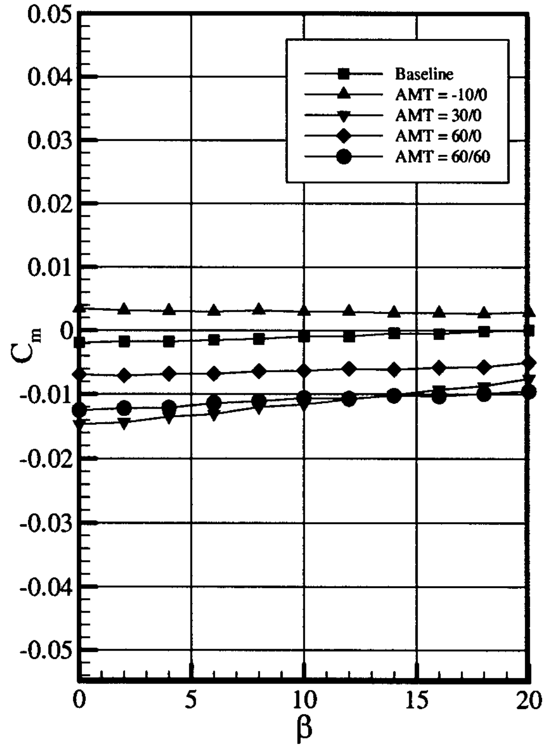

Figure H2b Pitching Moment Coefficient as a Function of β, α = 5°

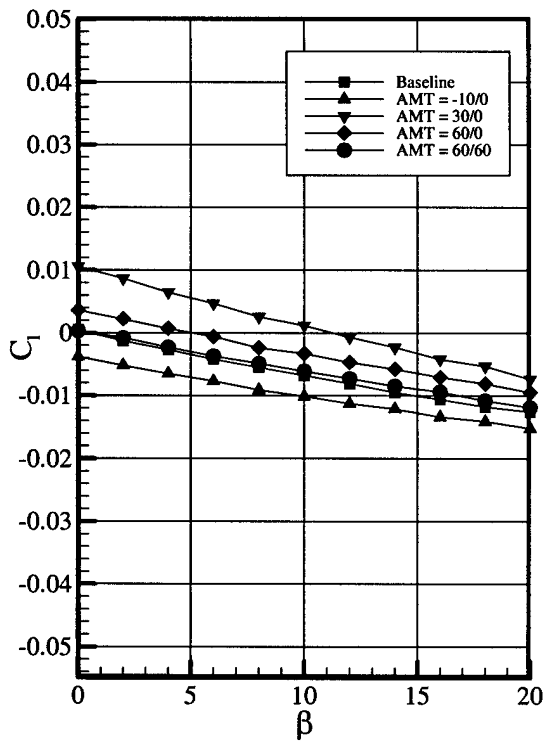

Figure H2c Rolling Moment Coefficient as a Function of β, α = 5°

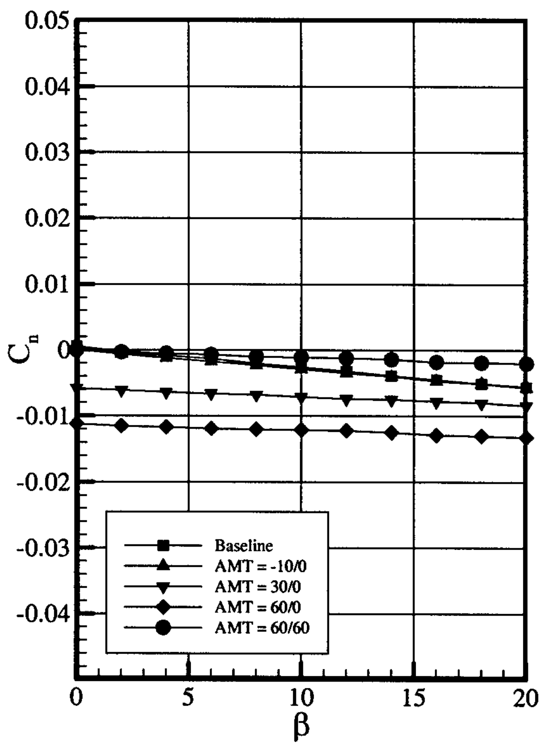

Figure H2d Yawing Moment Coefficient as a Function of β, α = 5°

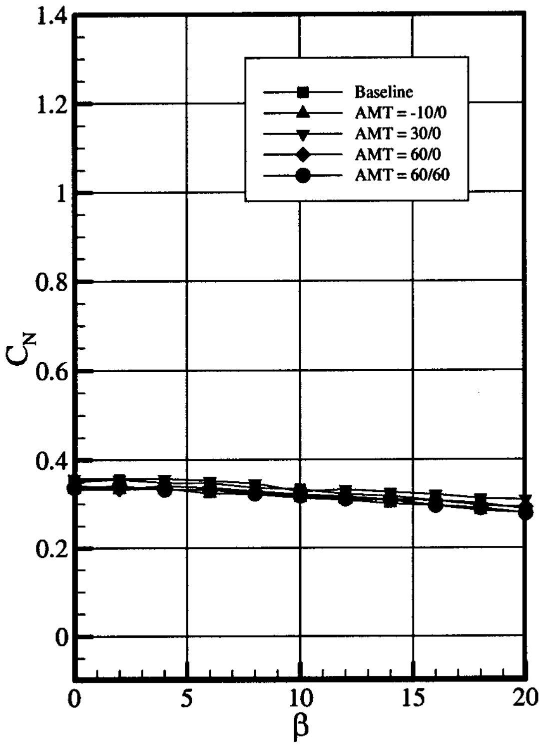

Figure H3a Normal Force Coefficient as a Function of β, α = 10°

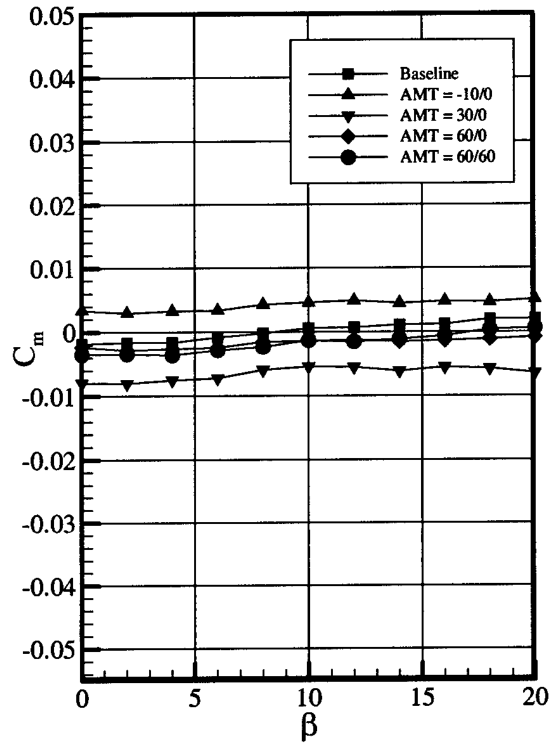

Figure H3b Pitching Moment Coefficient as a Function of β, α = 10°

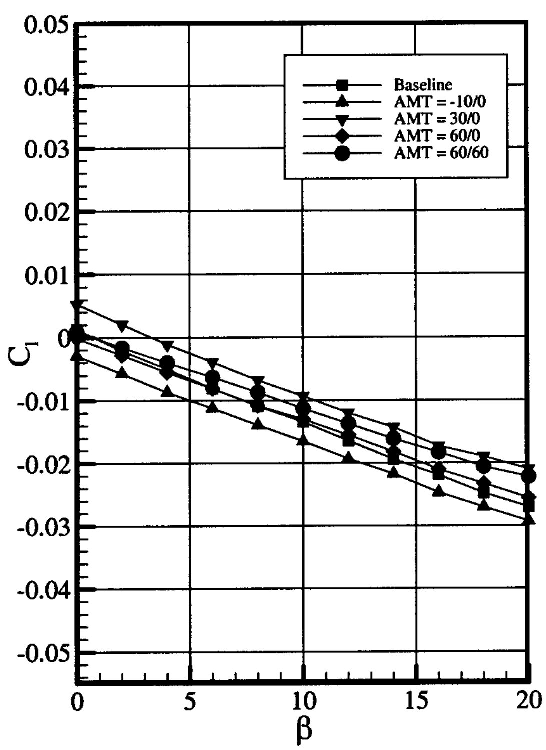

Figure H3c Rolling Moment Coefficient as a Function of β, α = 10°

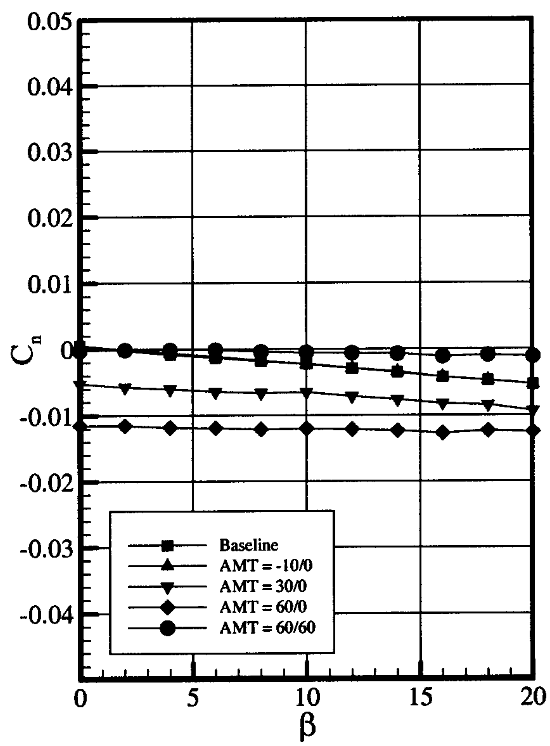

Figure H3d Yawing Moment Coefficient as a Function of β, α = 10°

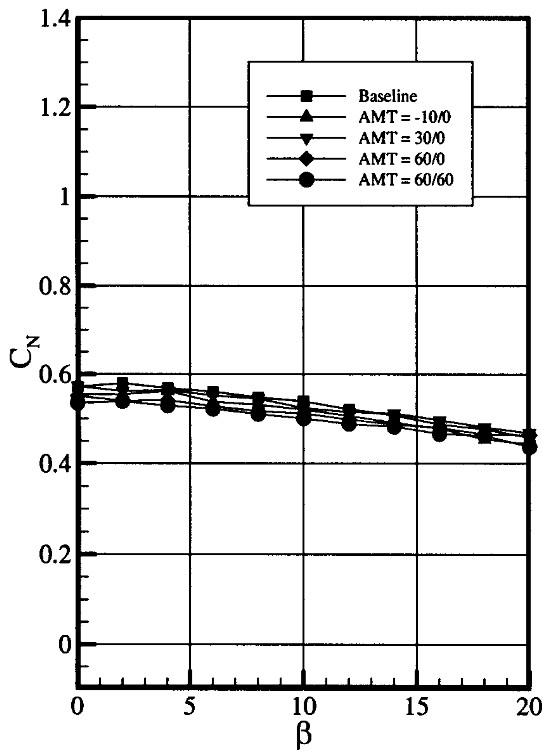

Figure H4a Normal Force Coefficient as a Function of β, α = 15°

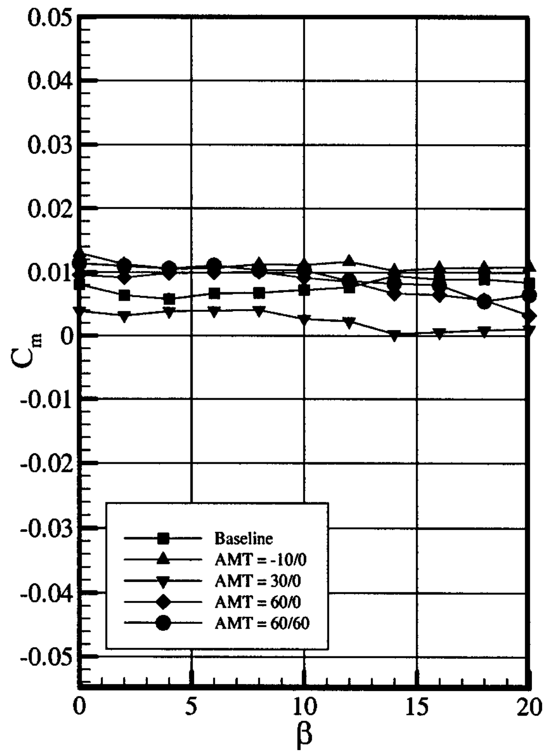

Figure H4b Pitching Moment Coefficient as a Function of β, α = 15°

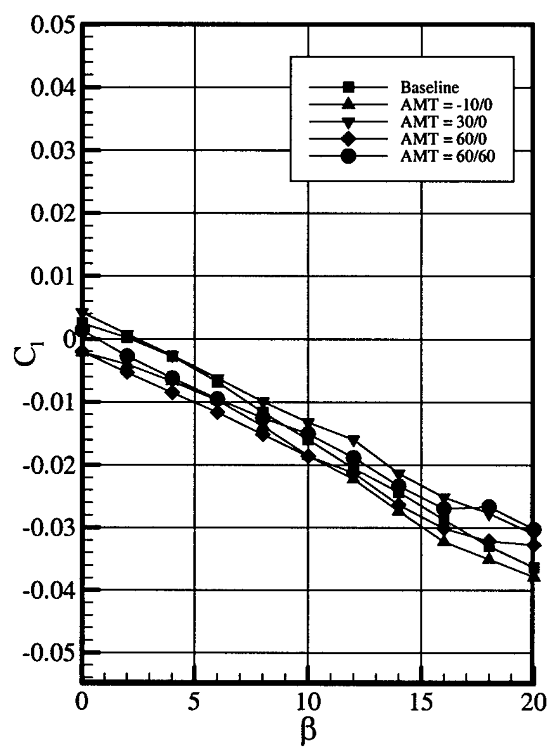

Figure H4c Rolling Moment Coefficient as a Function of β, α = 15°

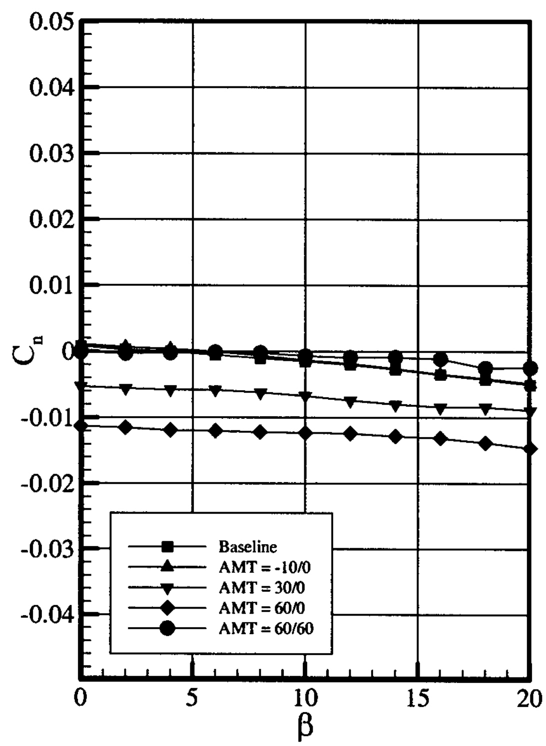

Figure H4d Yawing Moment Coefficient as a Function of β, α = 15°

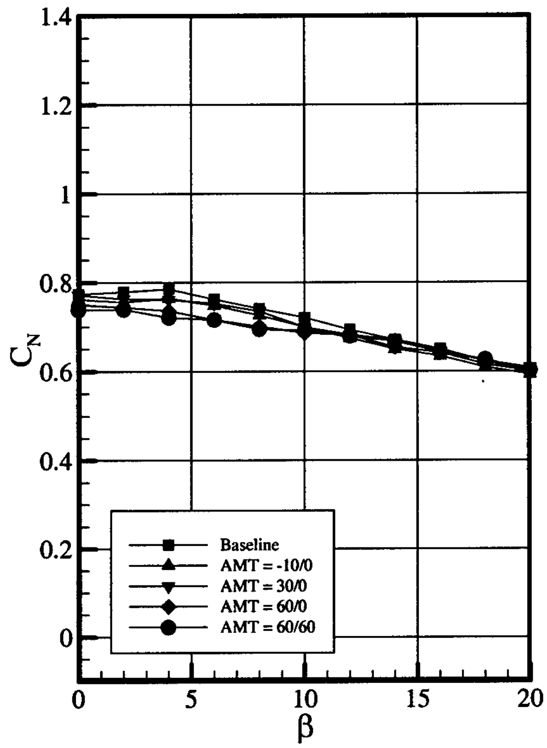

Figure H5a Normal Force Coefficient as a Function of β, α = 20°

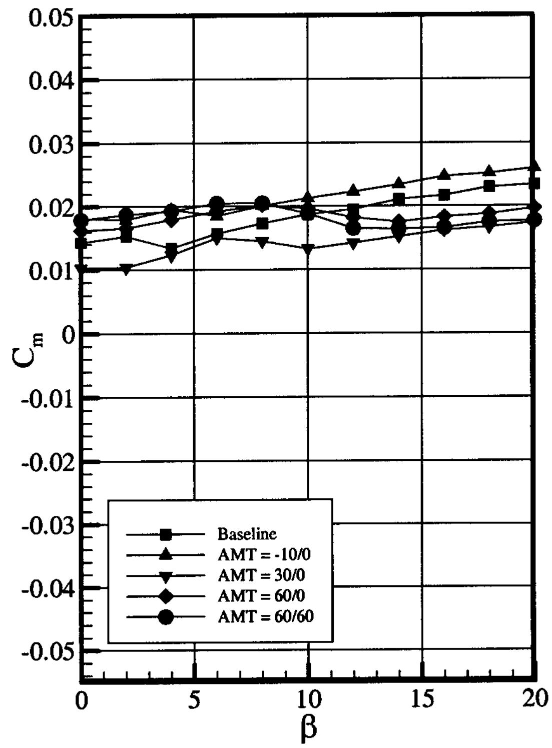

Figure H5b Pitching Moment Coefficient as a Function of β, α = 20°

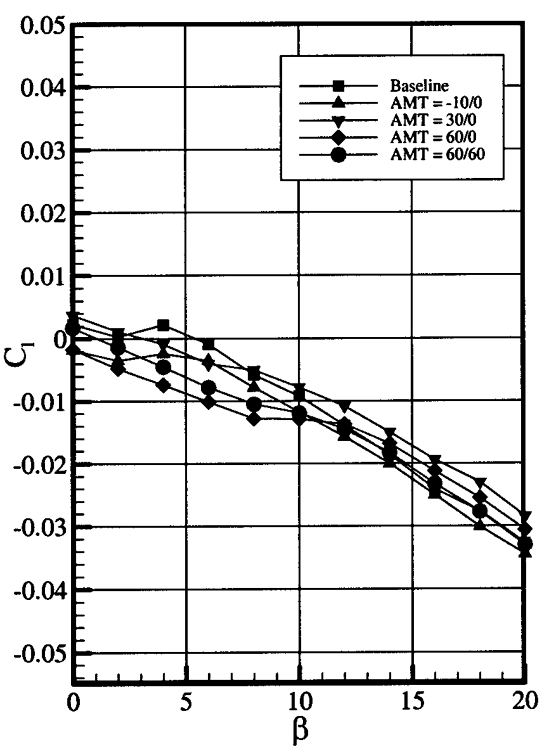

Figure H5c Rolling Moment Coefficient as a Function of β, α = 20°

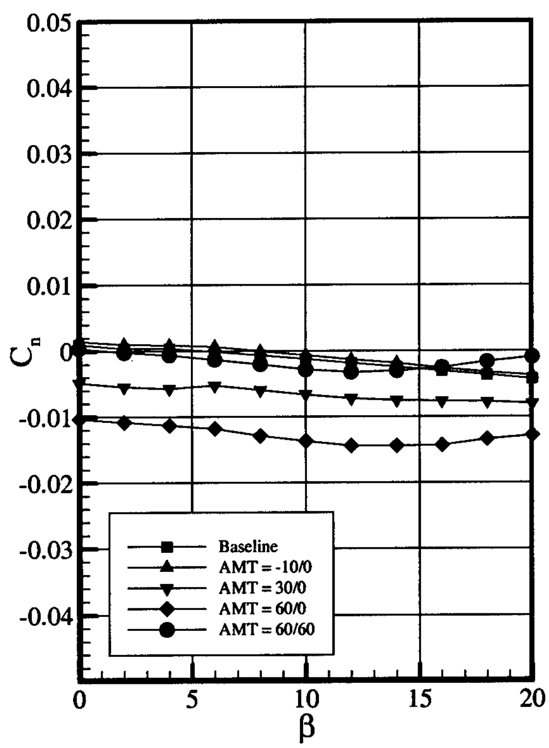

Figure H5d Yawing Moment Coefficient as a Function of β, α = 20°

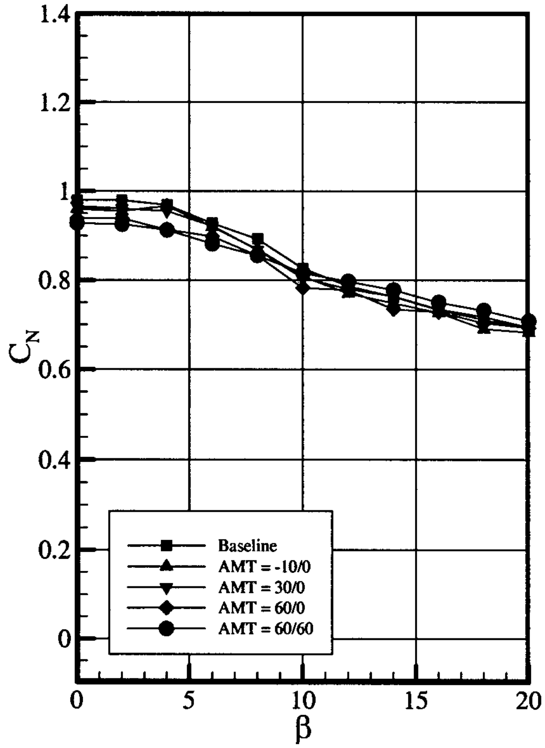

Figure H6a Normal Force Coefficient
as a Function of β, α = 25°

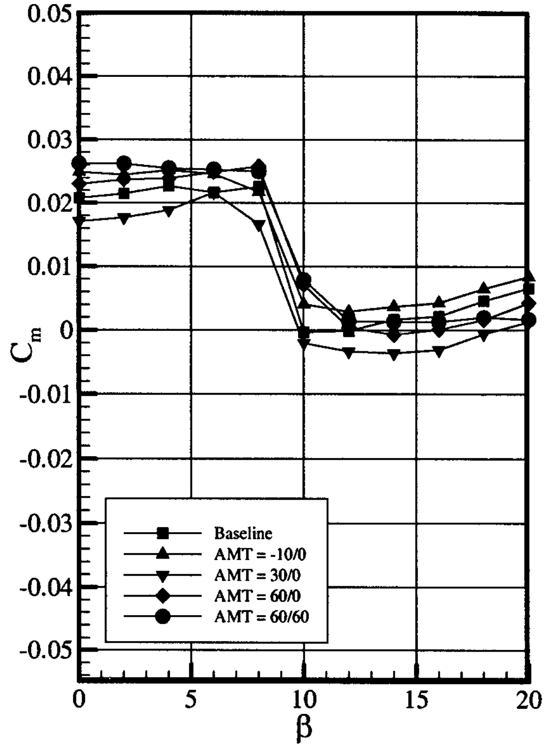

Figure H6b Pitching Moment Coefficient
as a Function of β, α = 25°

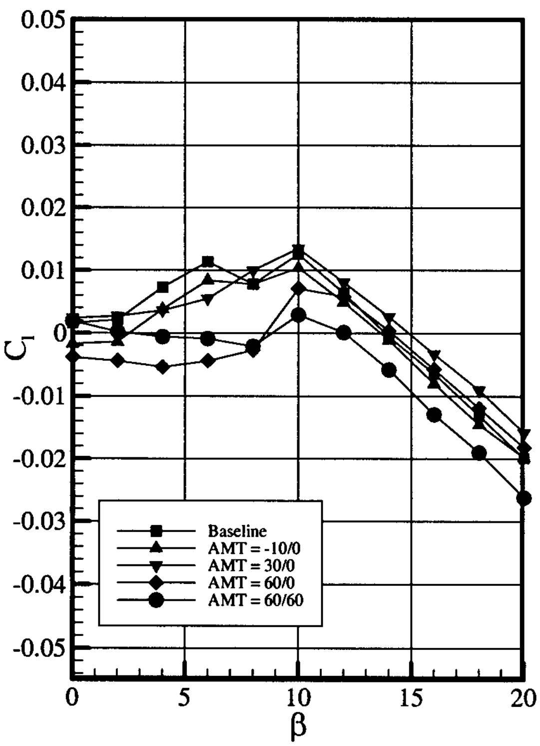

Figure H6c Rolling Moment Coefficient
as a Function of β, α = 25°

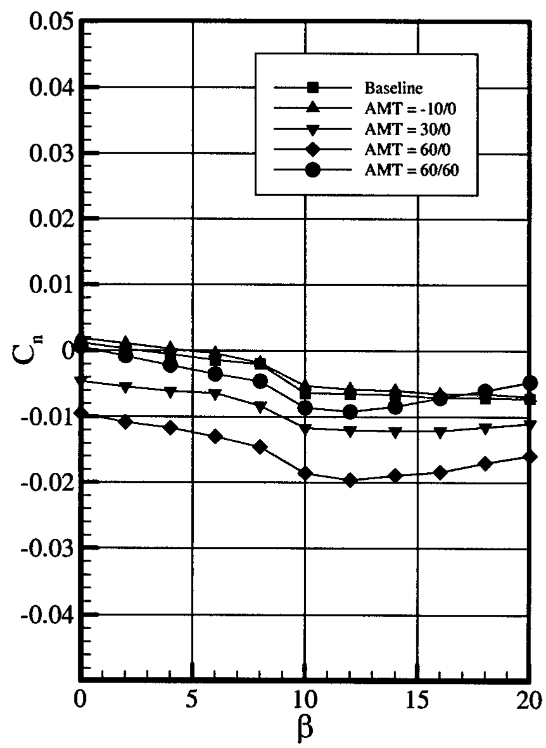

Figure H6d Yawing Moment Coefficient
as a Function of β, α = 25°

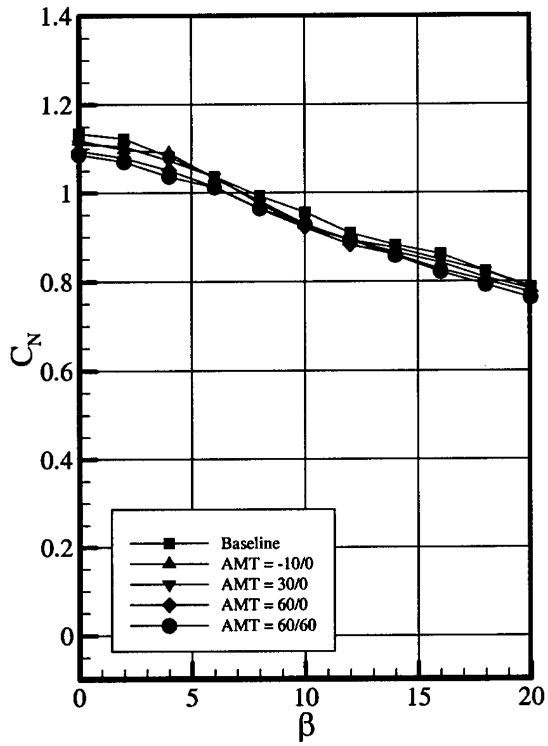

Figure H7a Normal Force Coefficient as a Function of β, α = 30°

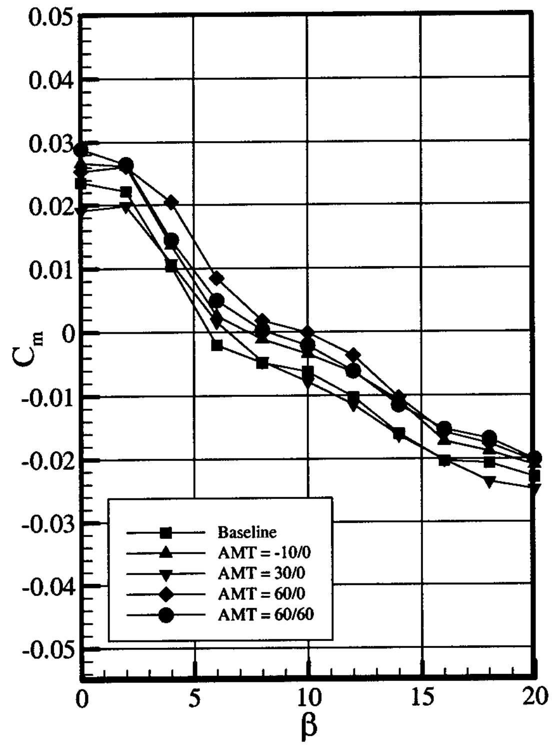

Figure H7b Pitching Moment Coefficient as a Function of β, α = 30°

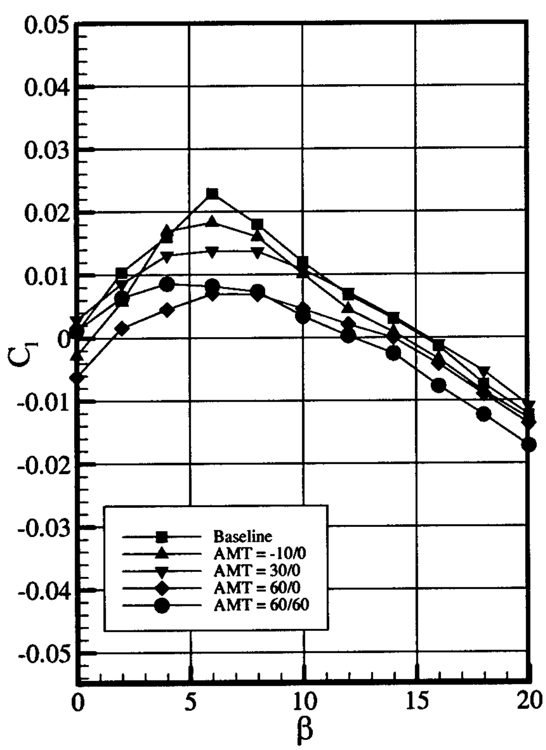

Figure H7c Rolling Moment Coefficient as a Function of β, α = 30°

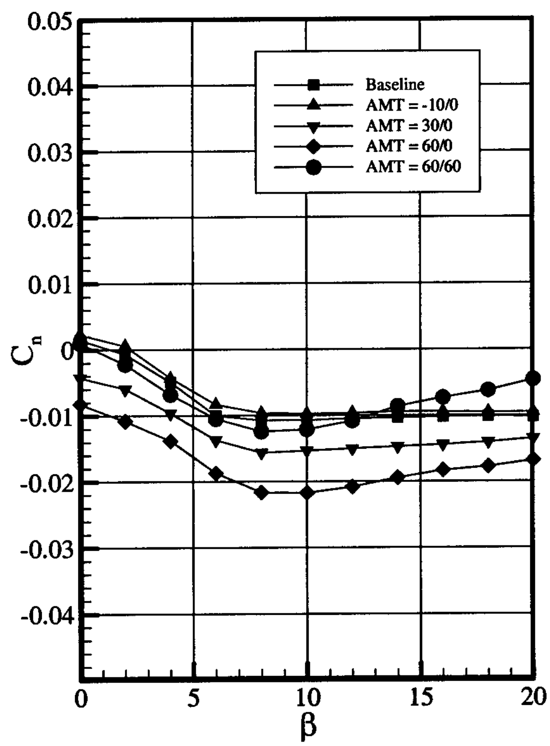

Figure H7d Yawing Moment Coefficient as a Function of β, α = 30°

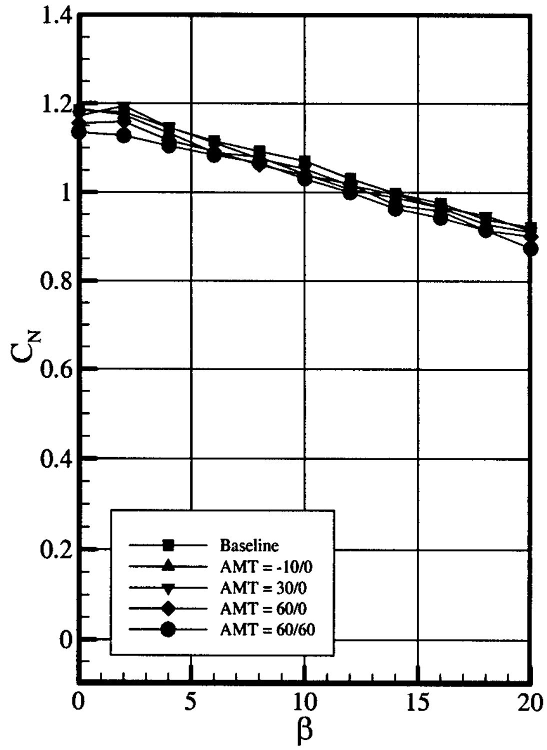

Figure H8a Normal Force Coefficient as a Function of β, α = 35°

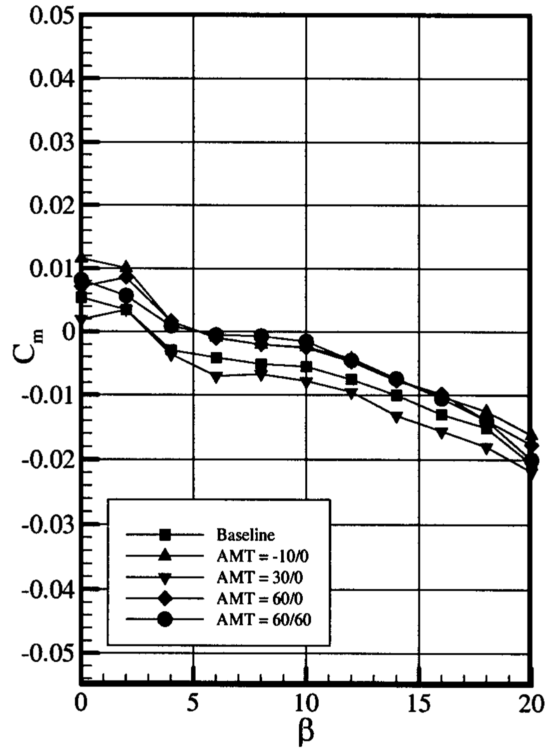

Figure H8b Pitching Moment Coefficient as a Function of β, α = 35°

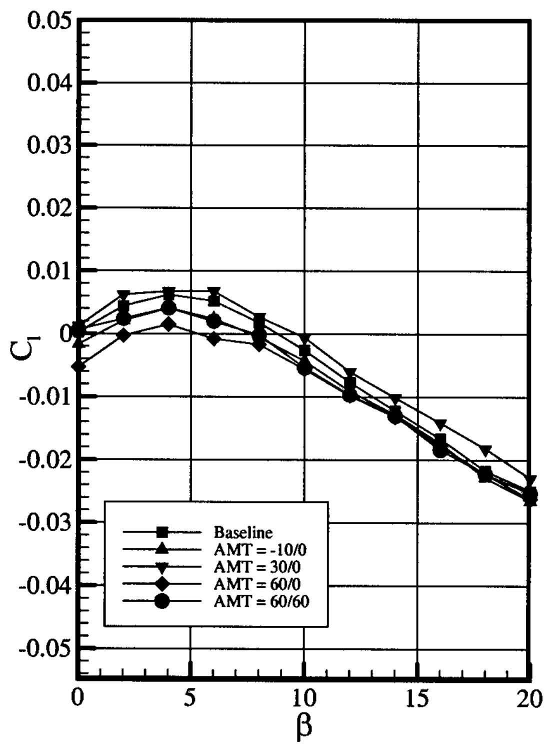

Figure H8c Rolling Moment Coefficient as a Function of β, α = 35°

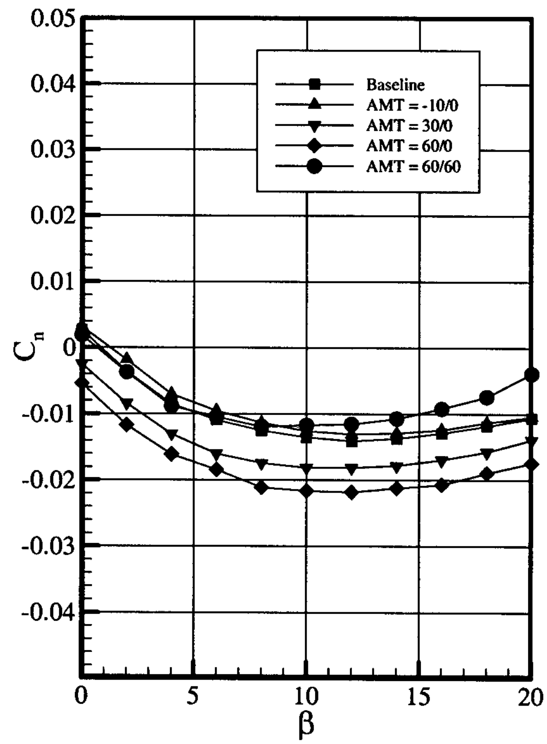

Figure H8d Yawing Moment Coefficient as a Function of β, α = 35°

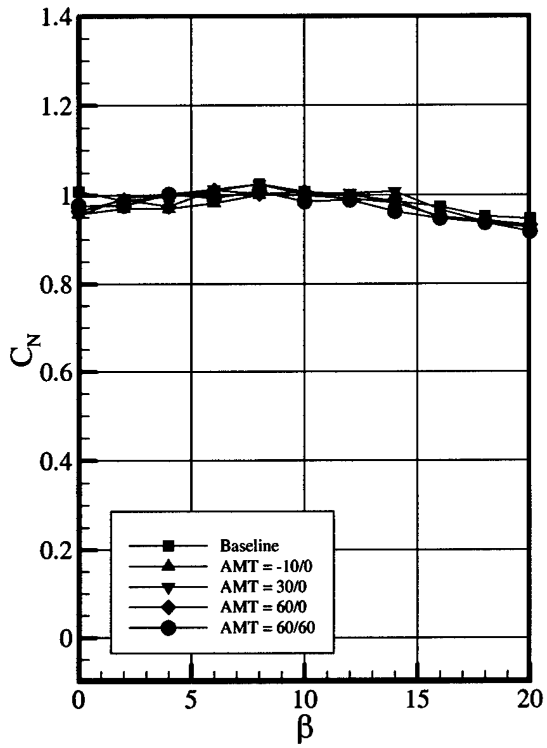

Figure H9a Normal Force Coefficient as a Function of β, α = 40°

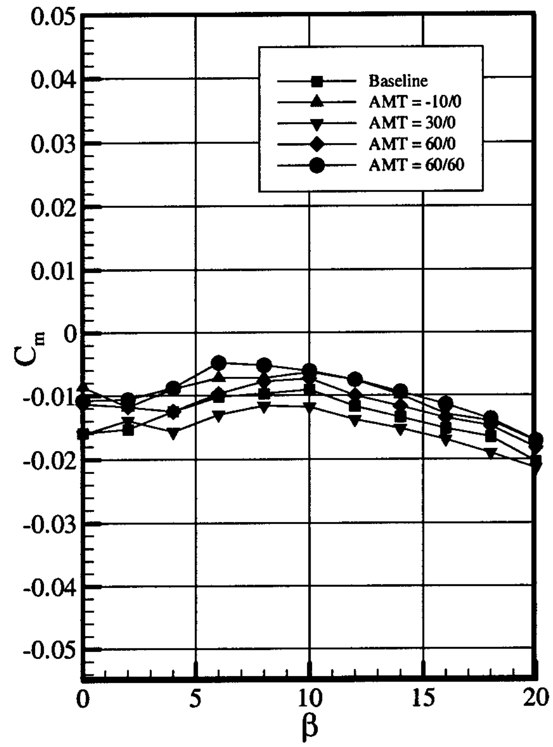

Figure H9b Pitching Moment Coefficient as a Function of β, α = 40°

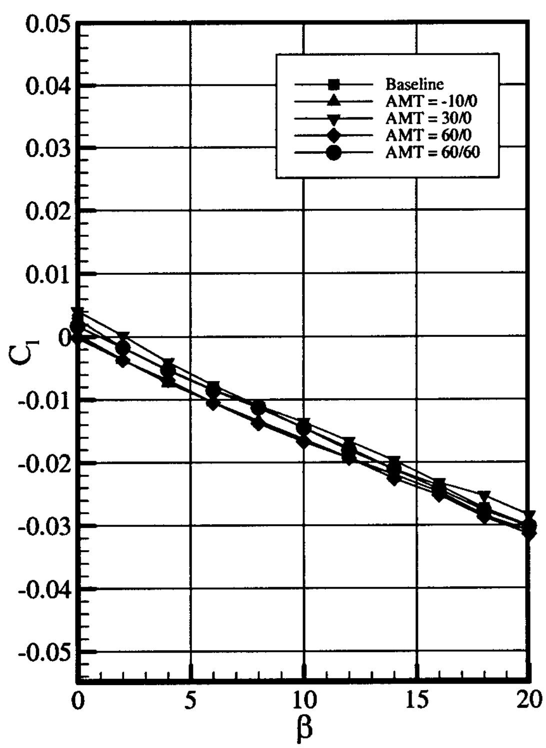

Figure H9c Rolling Moment Coefficient as a Function of β, α = 40°

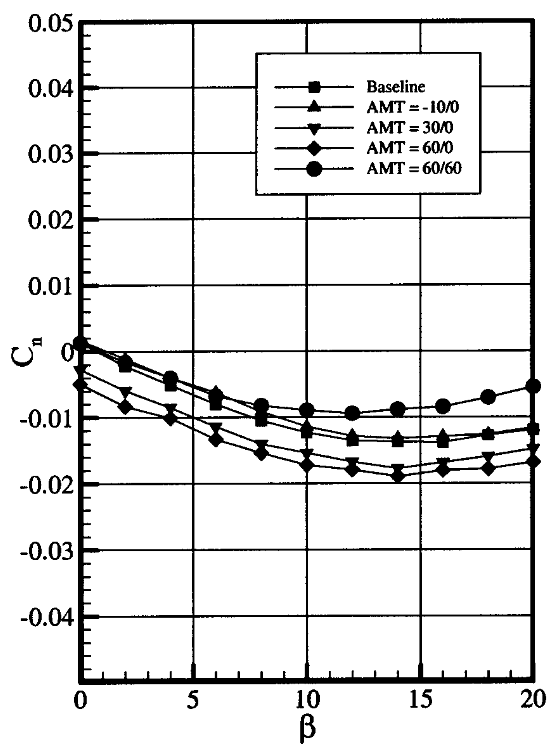

Figure H9d Yawing Moment Coefficient as a Function of β, α = 40°

Appendix I Spoiler Deflection Data as a Function of Angle of Attack

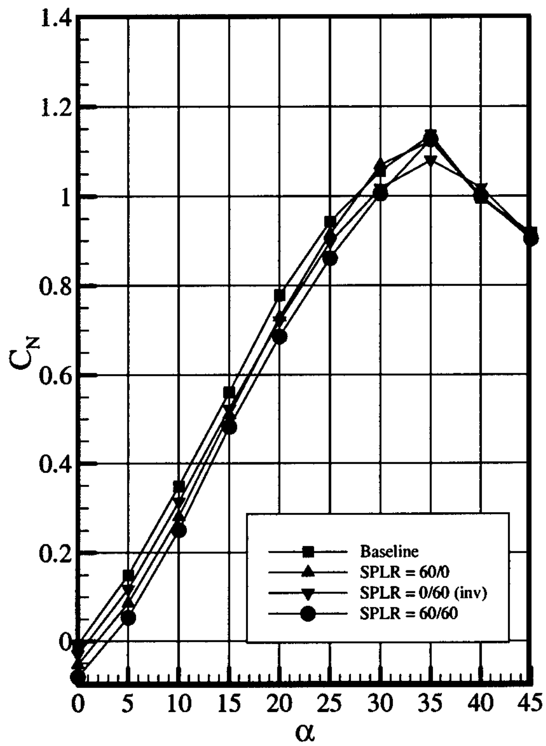

Figure I1a Normal Force Coefficient as a Function of α, β = -6°

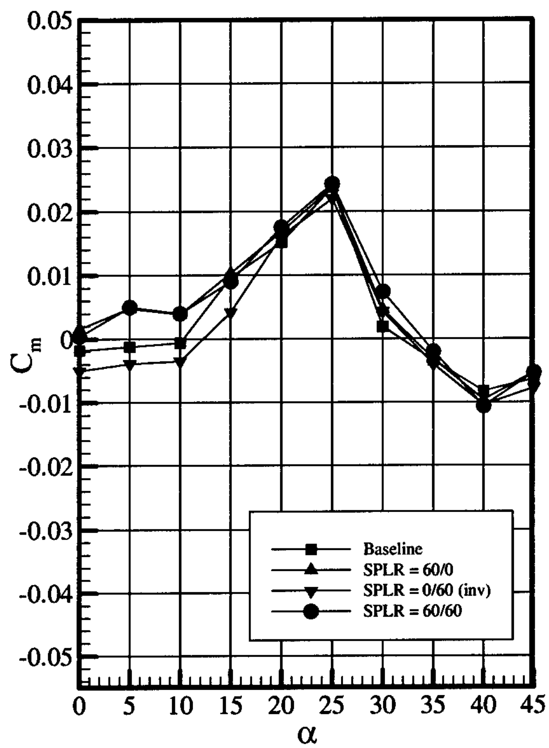

Figure I1b Pitching Moment Coefficient as a Function of α, β = -6°

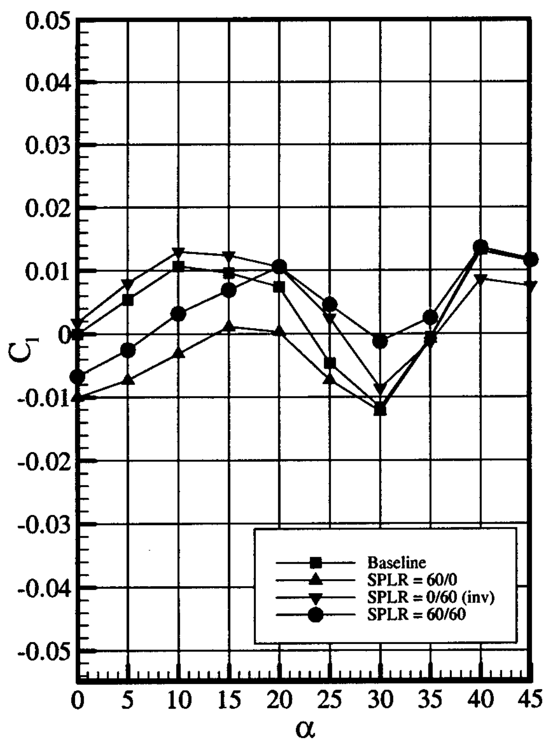

Figure I1c Rolling Moment Coefficient as a Function of α, β = -6°

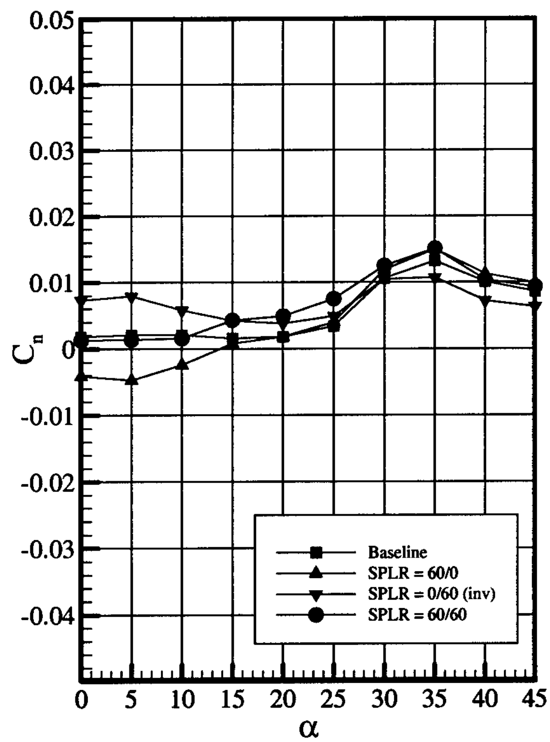

Figure I1d Yawing Moment Coefficient as a Function of α, β = -6°

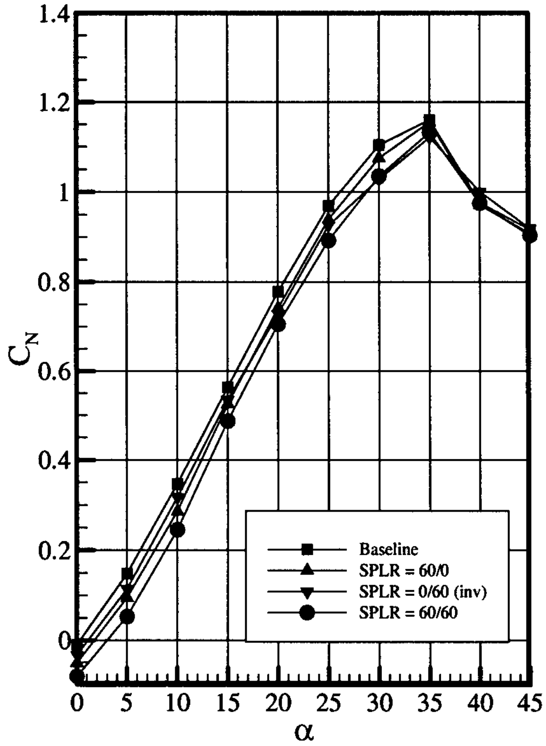

Figure I2a Normal Force Coefficient
as a Function of α, β = -4°

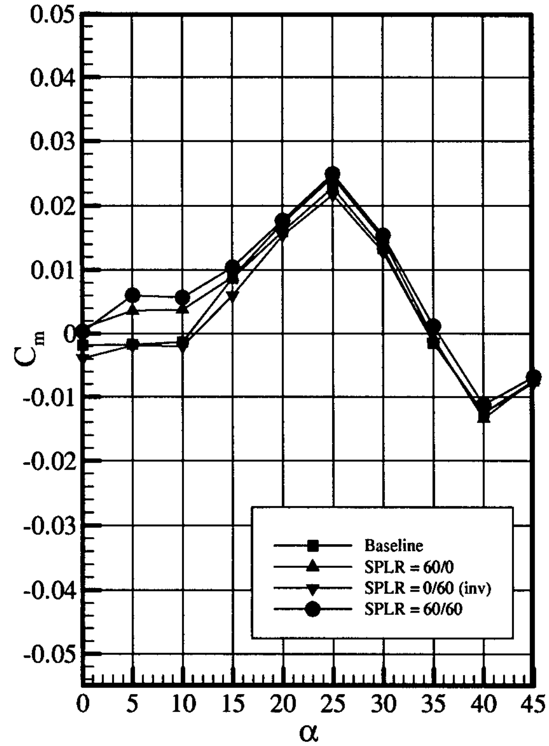

Figure I2b Pitching Moment Coefficient
as a Function of α, β = -4°

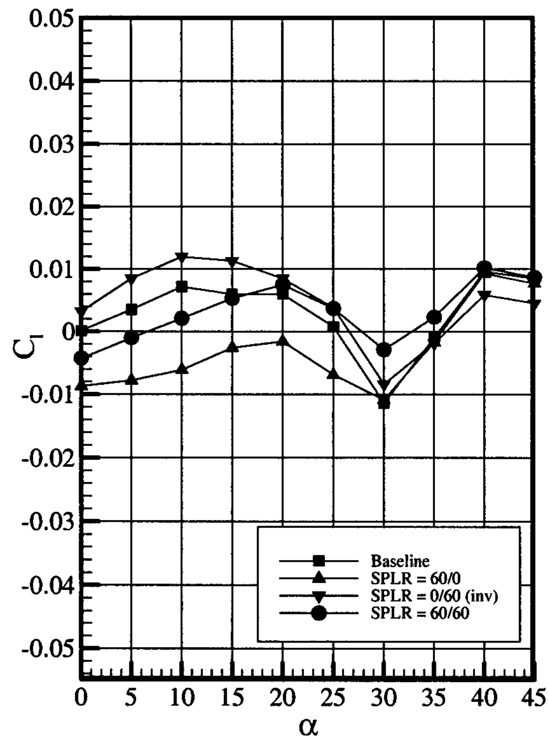

Figure I2c Rolling Moment Coefficient
as a Function of α, β = -4°

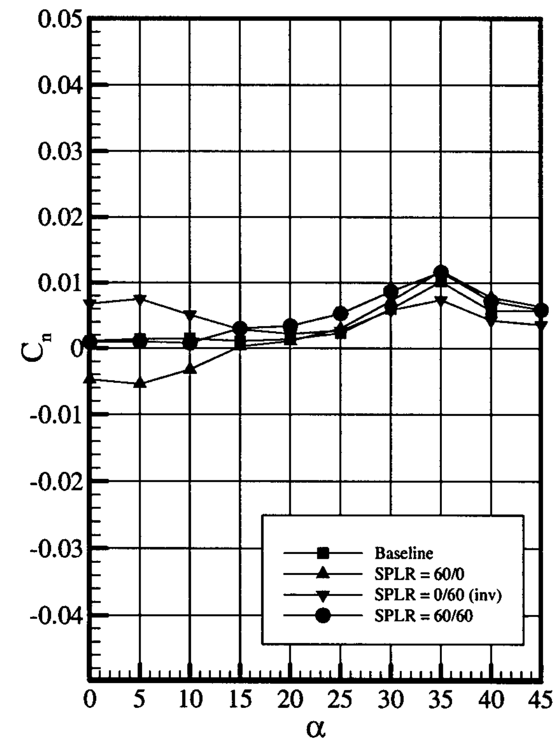

Figure I2d Yawing Moment Coefficient
as a Function of α, β = -4°

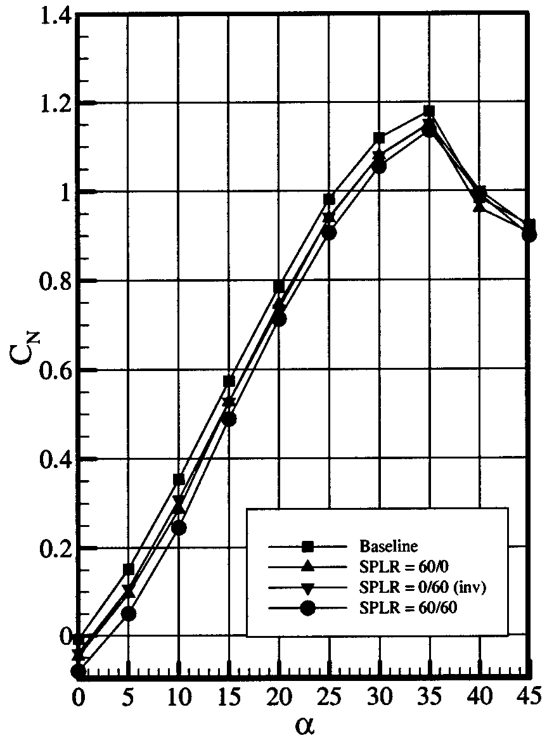

Figure I3a Normal Force Coefficient as a Function of α, β = -2°

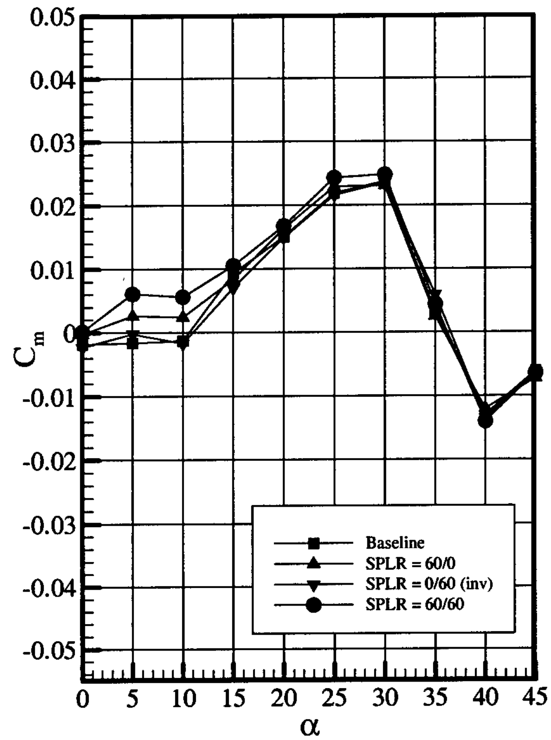

Figure I3b Pitching Moment Coefficient as a Function of α, β = -2°

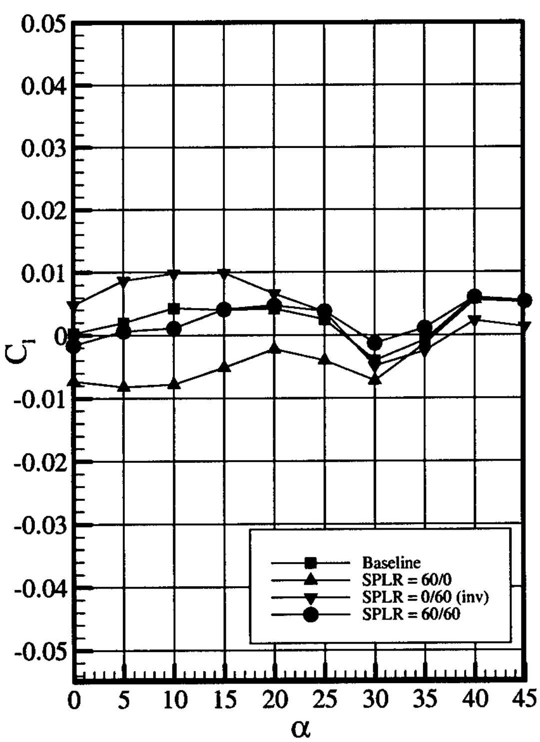

Figure I3c Rolling Moment Coefficient as a Function of α, β = -2°

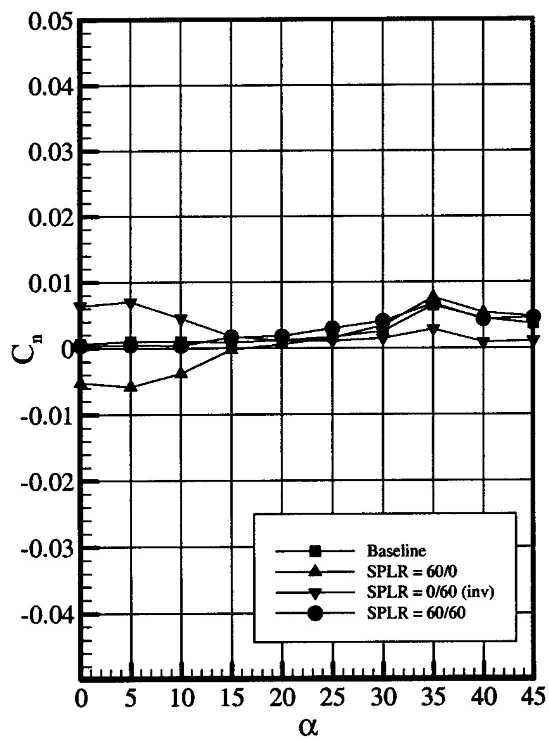

Figure I3d Yawing Moment Coefficient as a Function of α, β = -2°

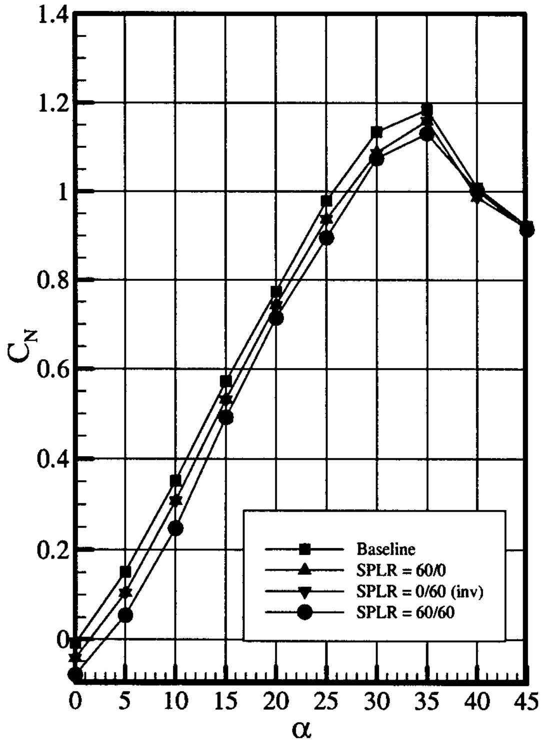

Figure I4a Normal Force Coefficient
as a Function of α, β = 0°

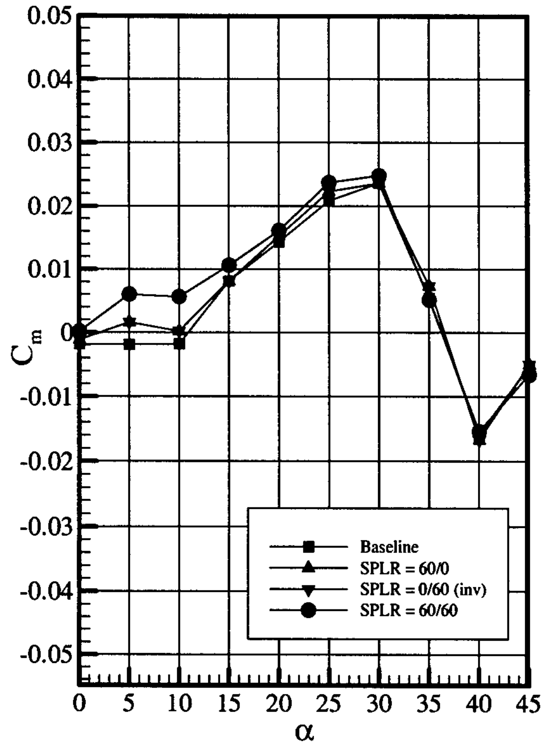

Figure I4b Pitching Moment Coefficient
as a Function of α, β = 0°

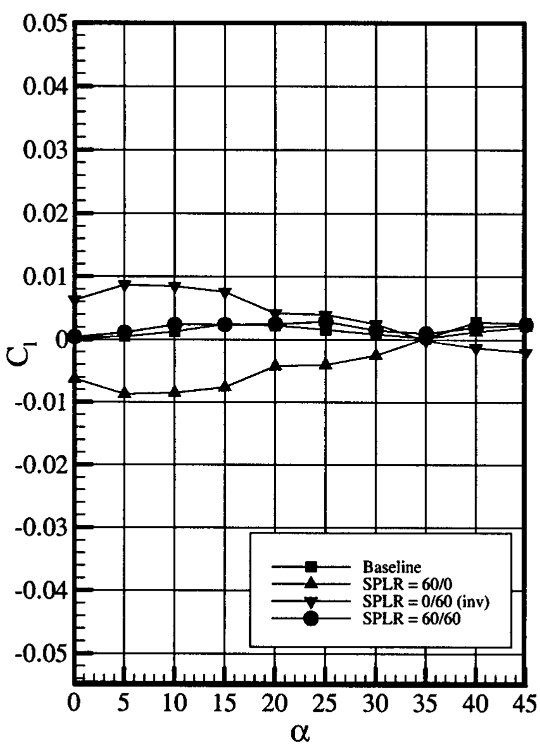

Figure I4c Rolling Moment Coefficient
as a Function of α, β = 0°

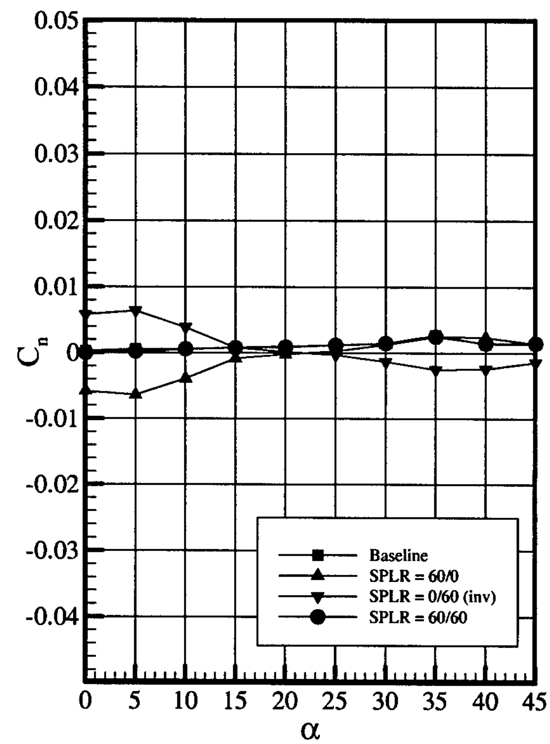

Figure I4d Yawing Moment Coefficient
as a Function of α, β = 0°

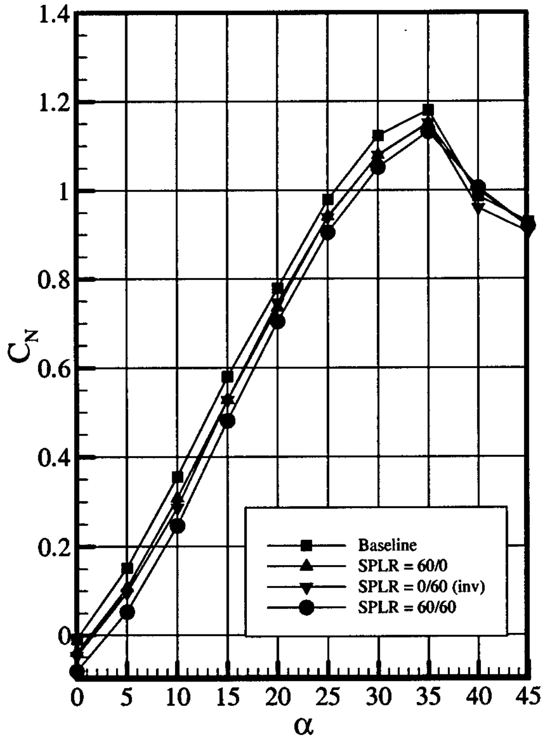

Figure I5a Normal Force Coefficient as a Function of α, β = 2°

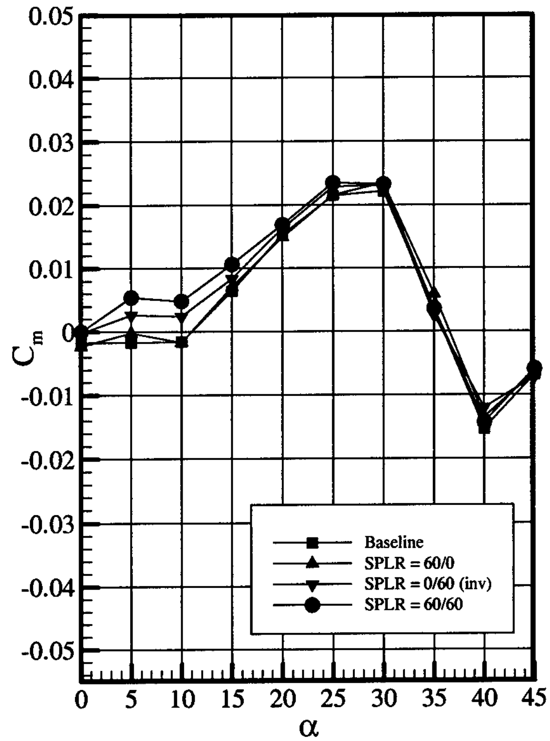

Figure I5b Pitching Moment Coefficient as a Function of α, β = 2°

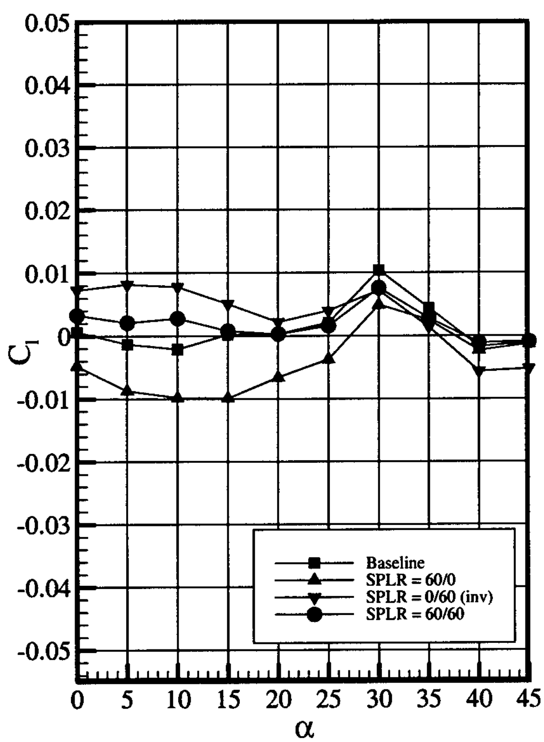

Figure I5c Rolling Moment Coefficient as a Function of α, β = 2°

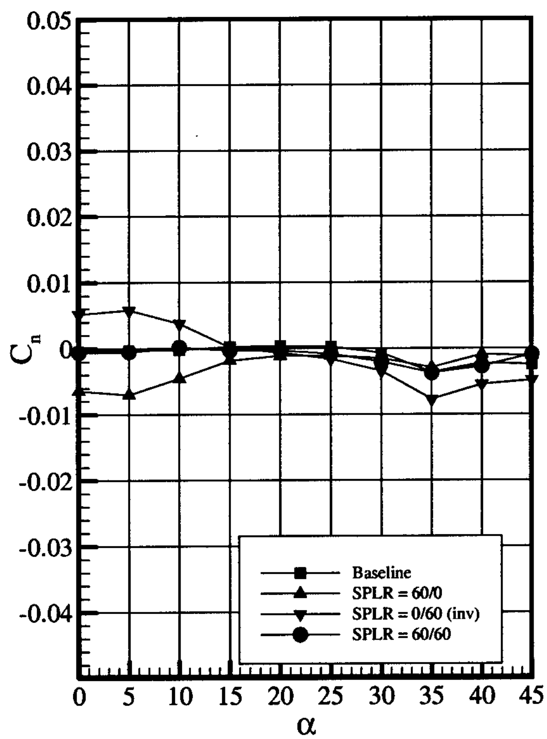

Figure I5d Yawing Moment Coefficient as a Function of α, β = 2°

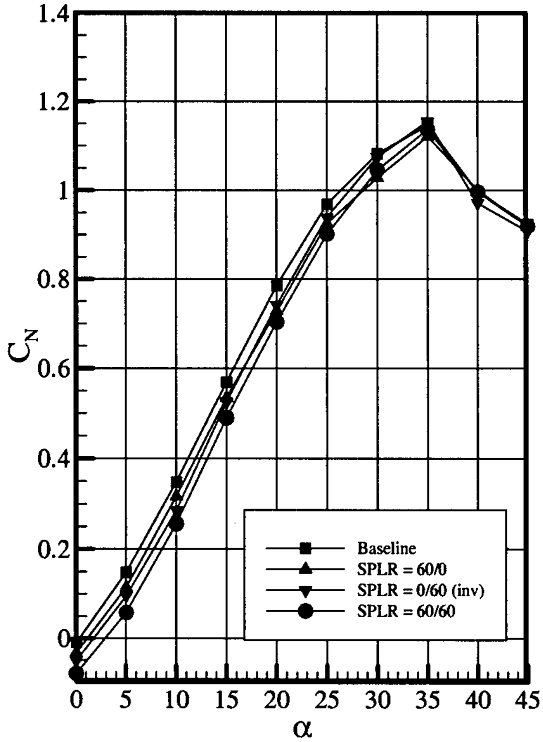

Figure I6a Normal Force Coefficient as a Function of α, β = 4°

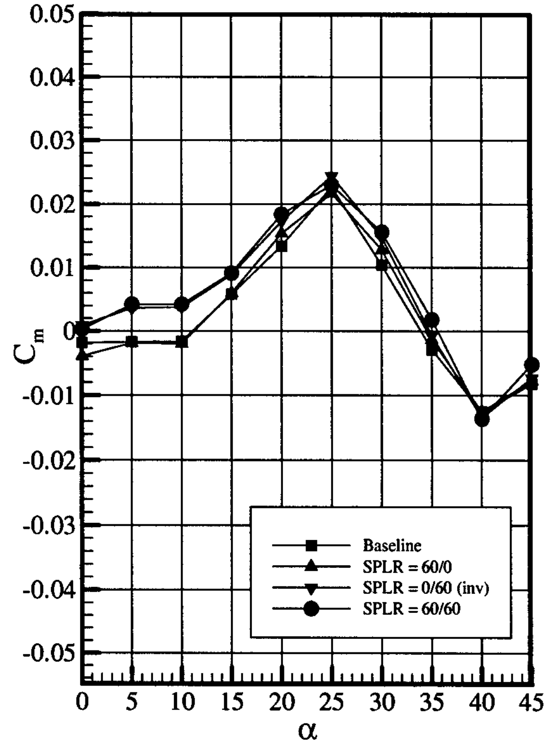

Figure I6b Pitching Moment Coefficient as a Function of α, β = 4°

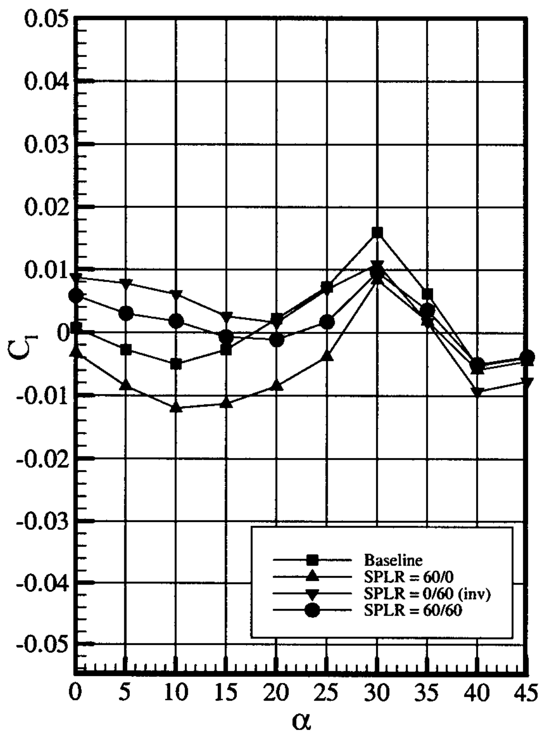

Figure I6c Rolling Moment Coefficient as a Function of α, β = 4°

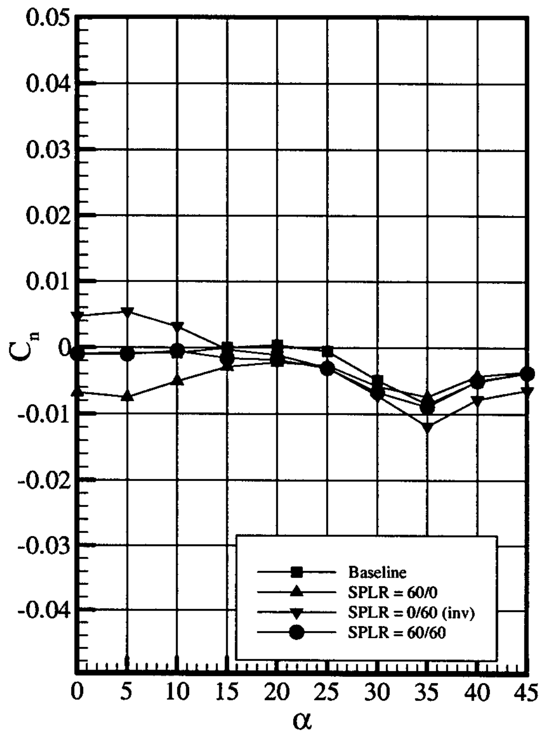

Figure I6d Yawing Moment Coefficient as a Function of α, β = 4°

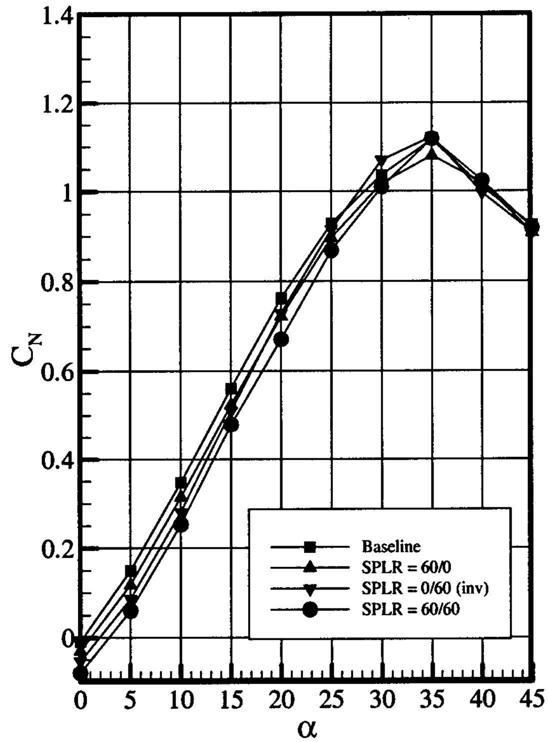

Figure I7a Normal Force Coefficient as a Function of α, $\beta = 6^{\circ}$

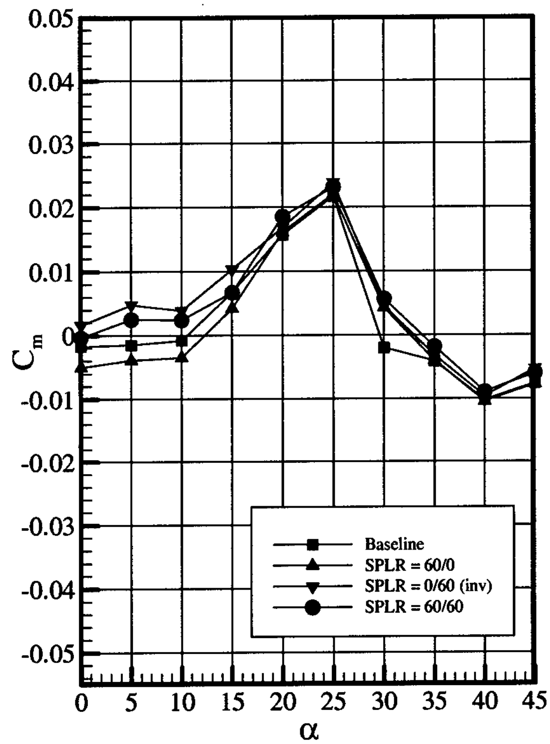

Figure I7b Pitching Moment Coefficient as a Function of α, $\beta = 6^{\circ}$

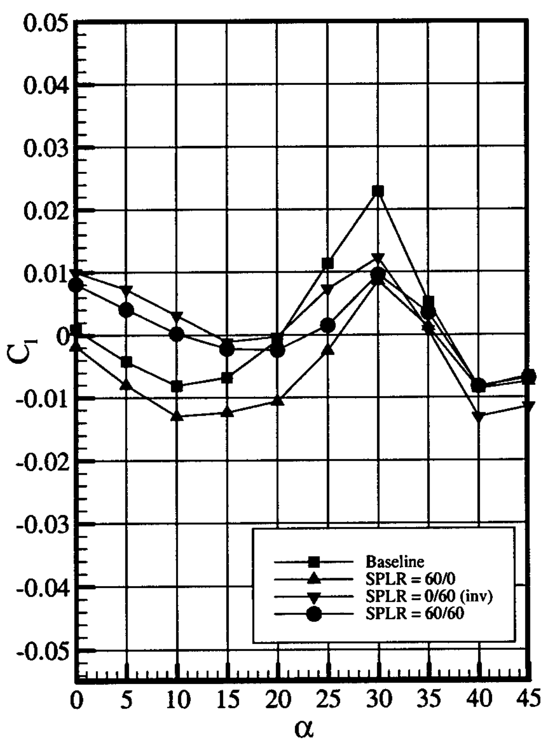

Figure I7c Rolling Moment Coefficient as a Function of α, $\beta = 6^{\circ}$

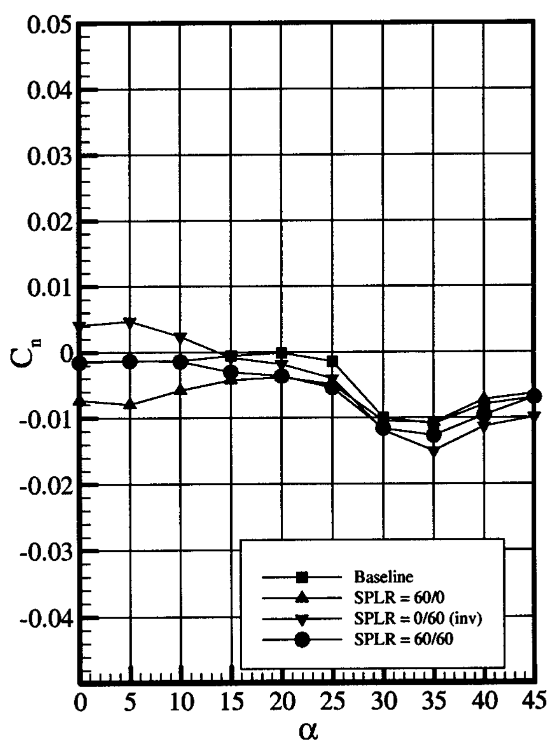

Figure I7d Yawing Moment Coefficient as a Function of α, $\beta = 6^{\circ}$

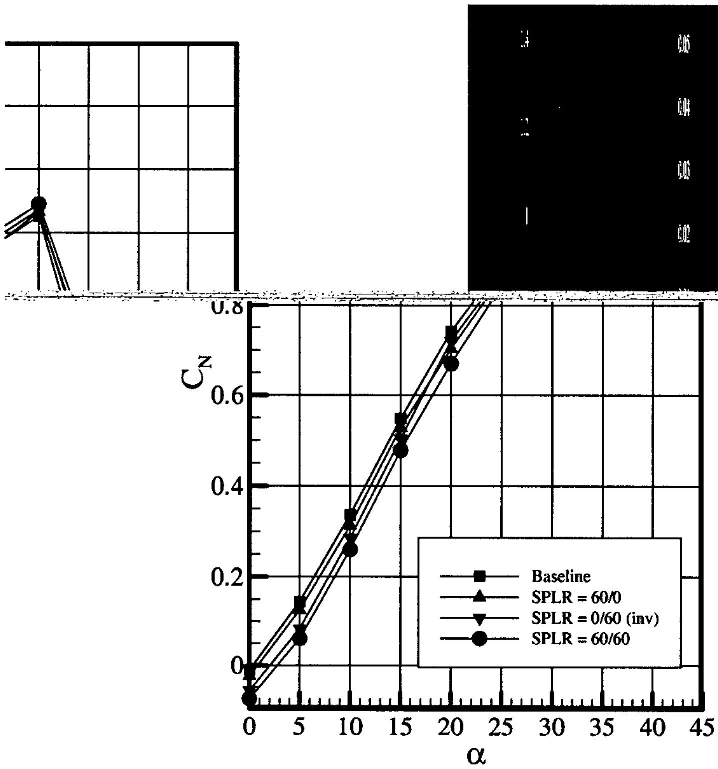

Figure I8a Normal Force Coefficient
as a Function of α, β = 8°

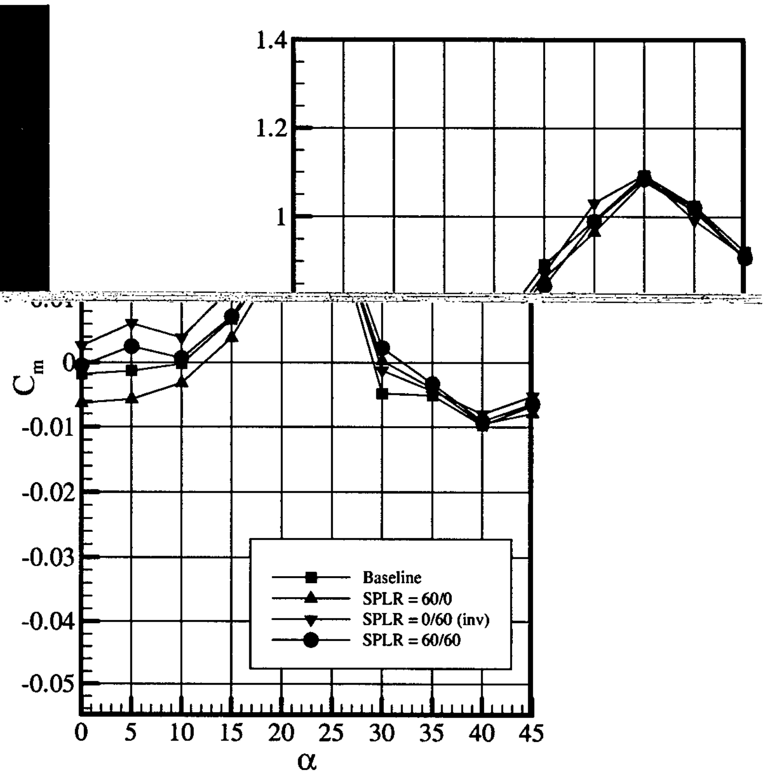

Figure I8b Pitching Moment Coefficient
as a Function of α, β = 8°

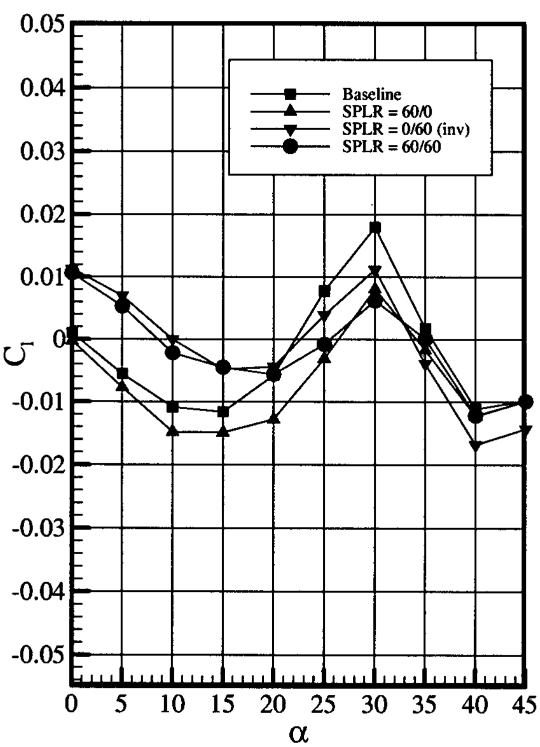

Figure I8c Rolling Moment Coefficient
as a Function of α, β = 8°

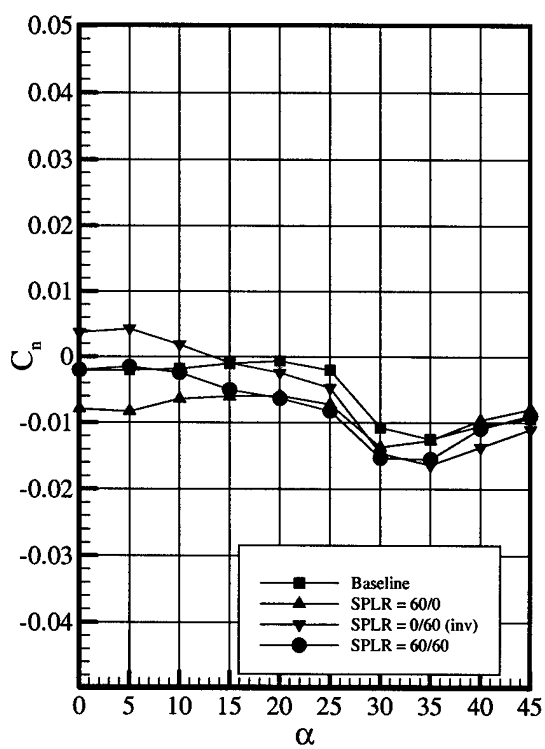

Figure I8d Yawing Moment Coefficient
as a Function of α, β = 8°

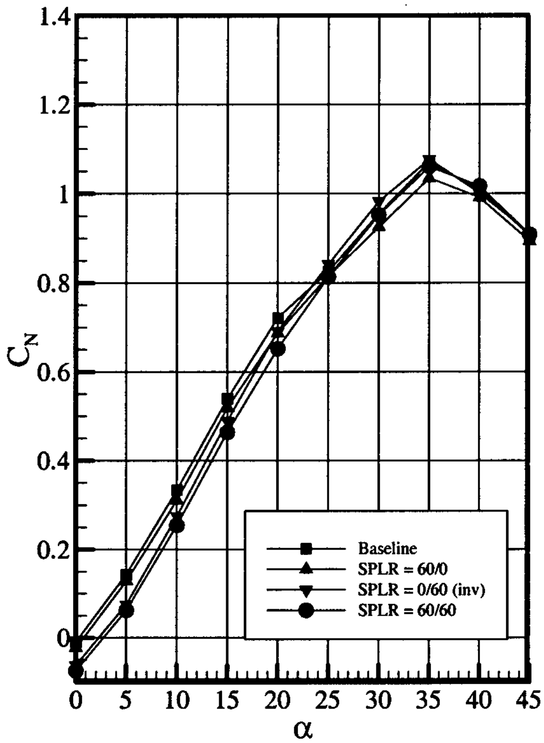

Figure I9a Normal Force Coefficient as a Function of α, β = 10°

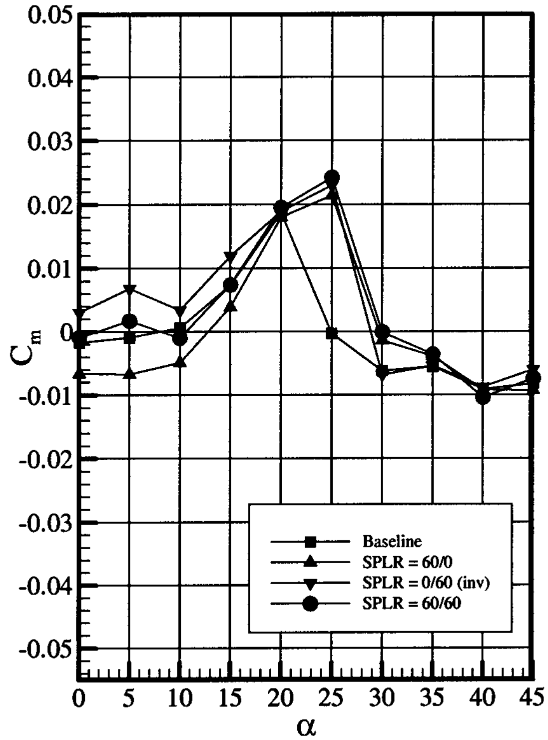

Figure I9b Pitching Moment Coefficient as a Function of α, β = 10°

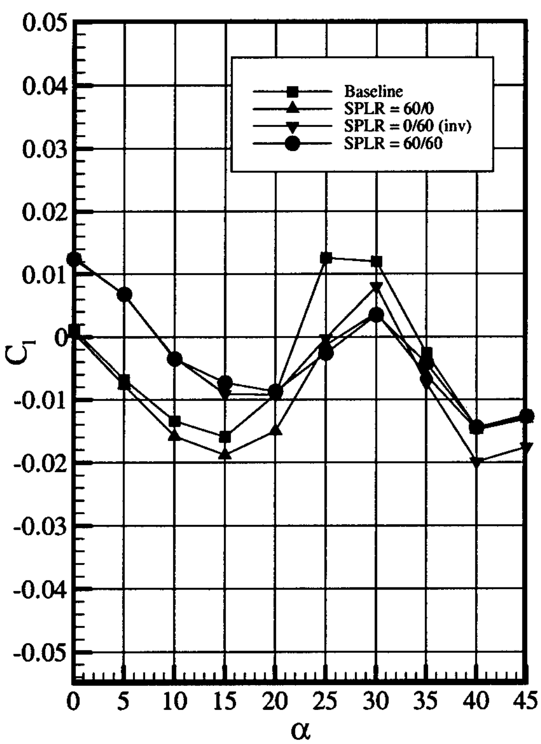

Figure I9c Rolling Moment Coefficient as a Function of α, β = 10°

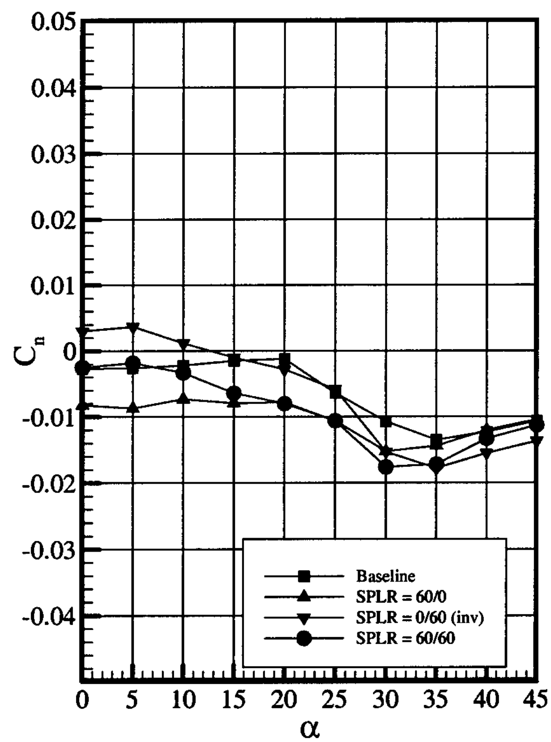

Figure I9d Yawing Moment Coefficient as a Function of α, β = 10°

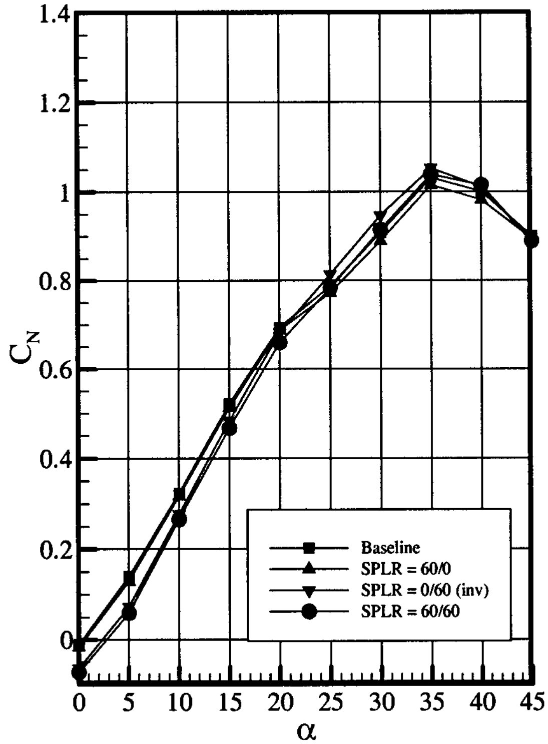

Figure I10a Normal Force Coefficient
as a Function of α, β = 12°

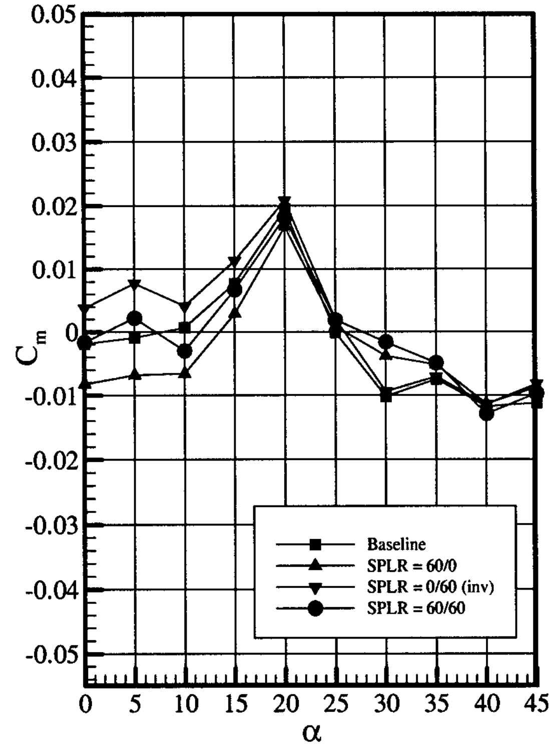

Figure I10b Pitching Moment Coefficient
as a Function of α, β = 12°

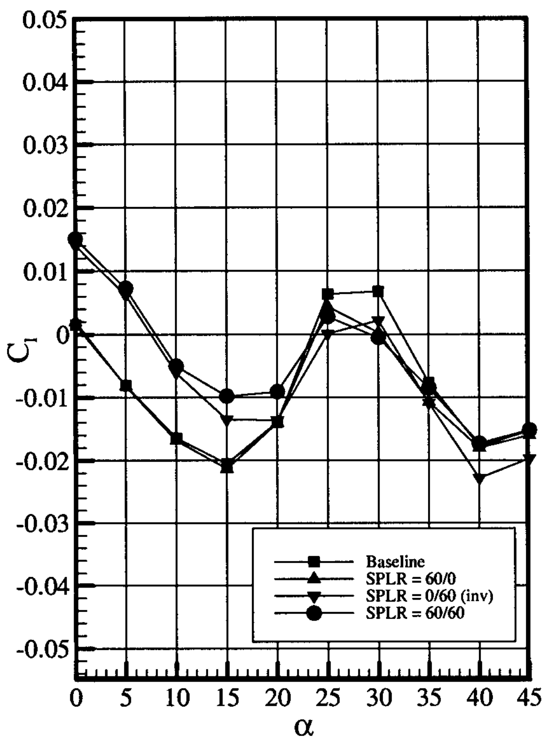

Figure I10c Rolling Moment Coefficient
as a Function of α, β = 12°

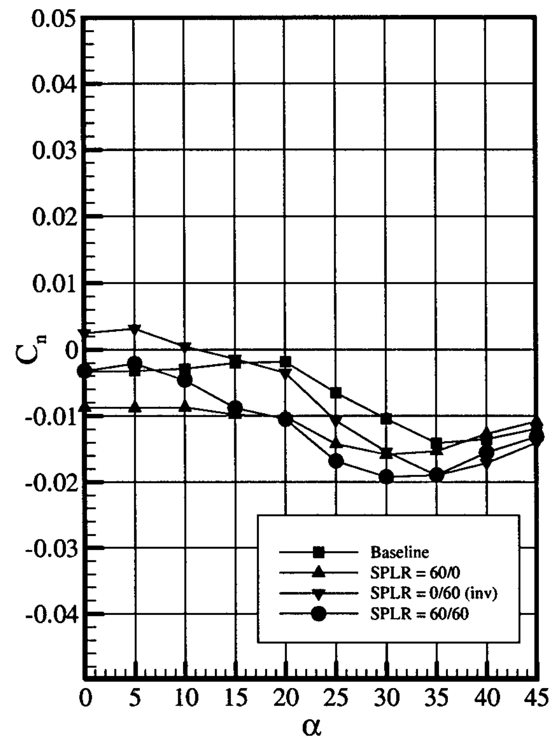

Figure I10d Yawing Moment Coefficient
as a Function of α, β = 12°

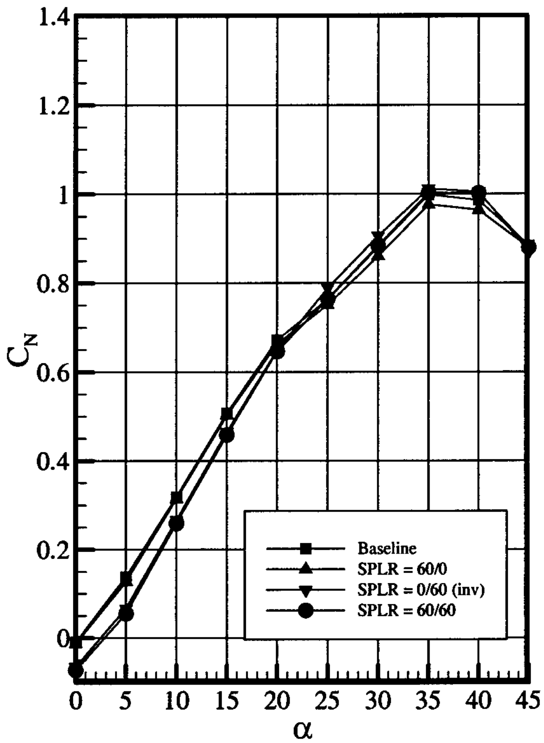

Figure I1 1a Normal Force Coefficient as a Function of α, β = 14°

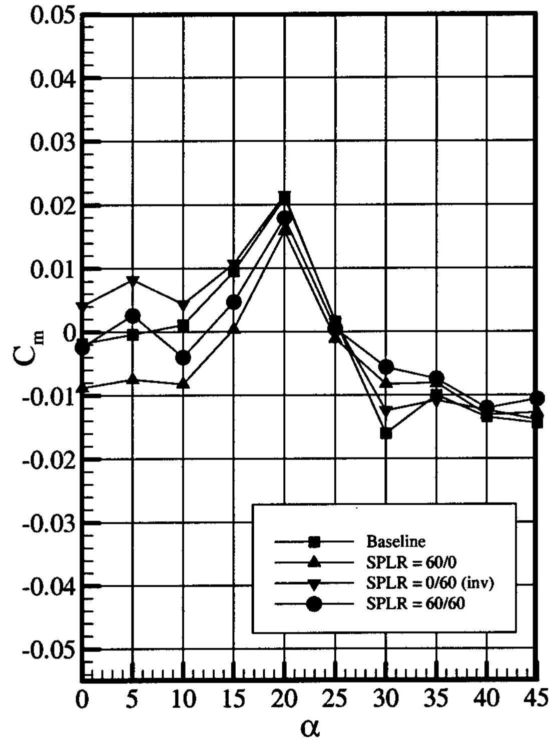

Figure I1 1b Pitching Moment Coefficient as a Function of α, β = 14°

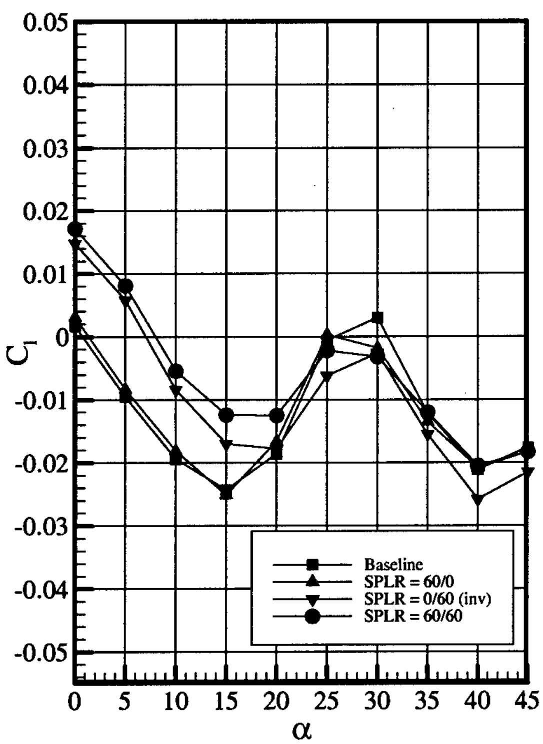

Figure I1 1c Rolling Moment Coefficient as a Function of α, β = 14°

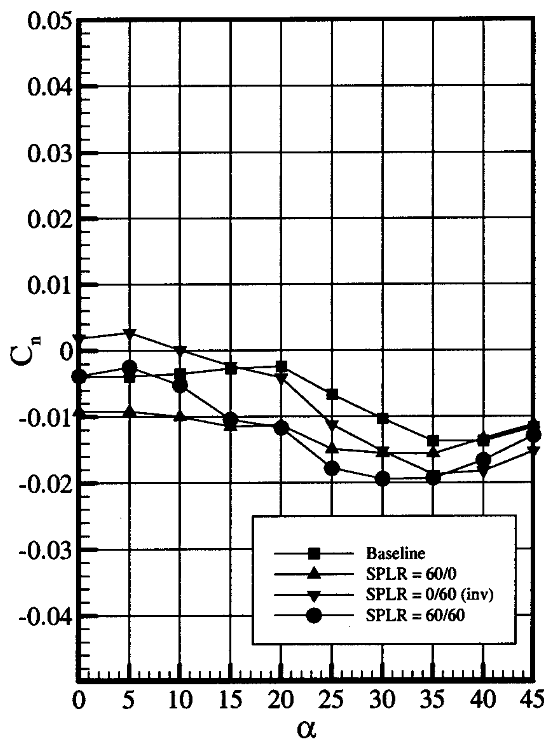

Figure I1 1d Yawing Moment Coefficient as a Function of α, β = 14°

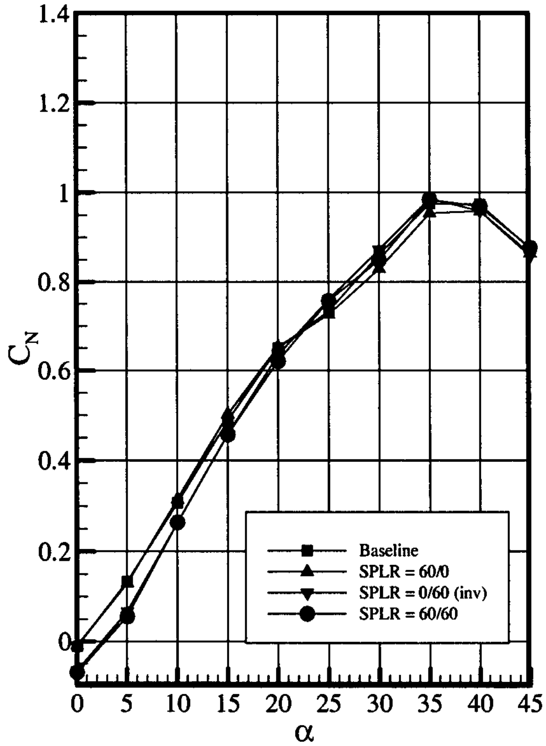

Figure I12a Normal Force Coefficient as a Function of α, β = 16°

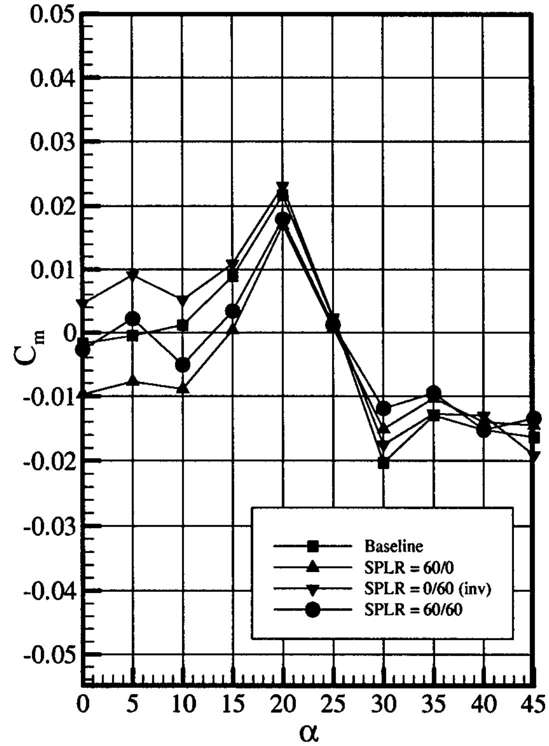

Figure I12b Pitching Moment Coefficient as a Function of α, β = 16°

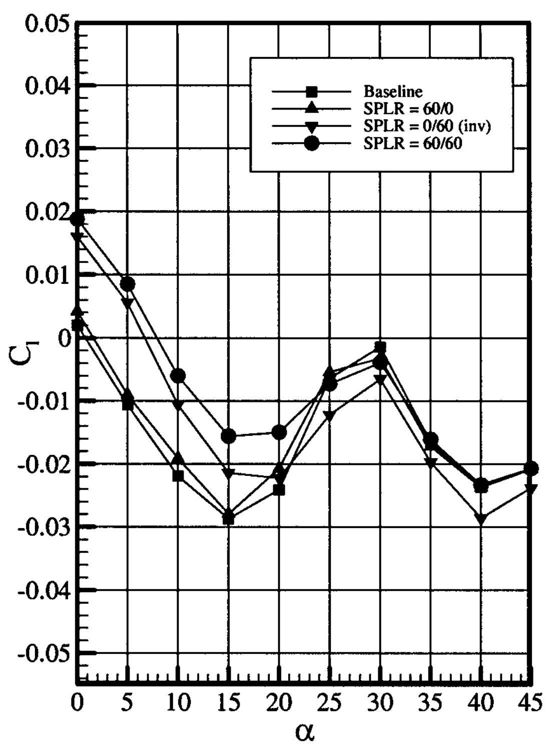

Figure I12c Rolling Moment Coefficient as a Function of α, β = 16°

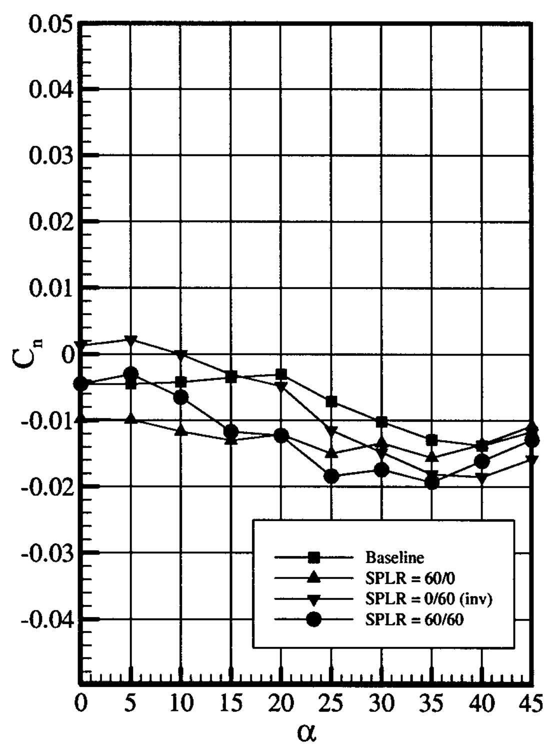

Figure I12d Yawing Moment Coefficient as a Function of α, β = 16°

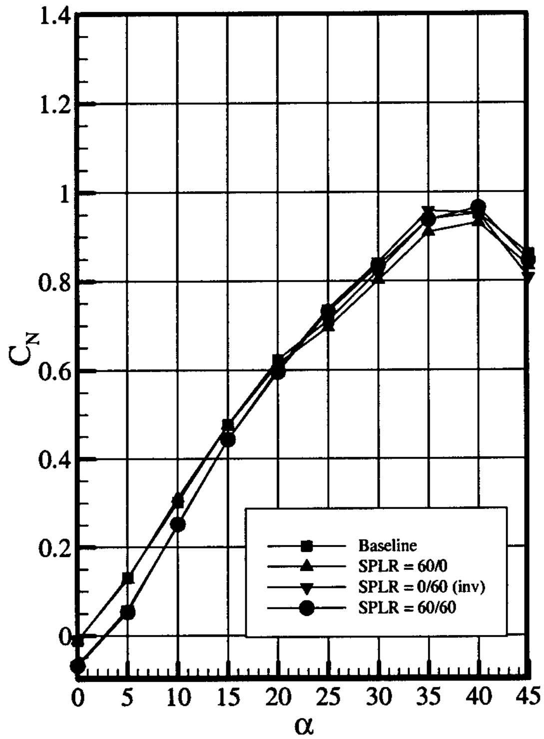

Figure I13a Normal Force Coefficient as a Function of α, β = 18°

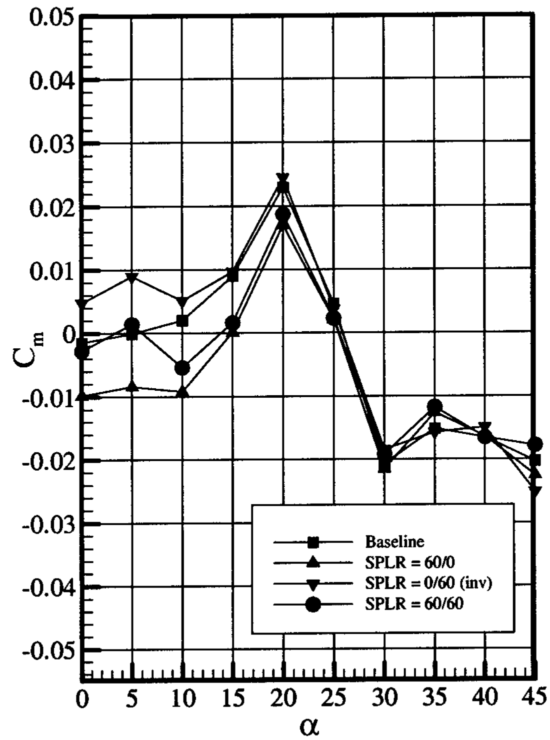

Figure I13b Pitching Moment Coefficient as a Function of α, β = 18°

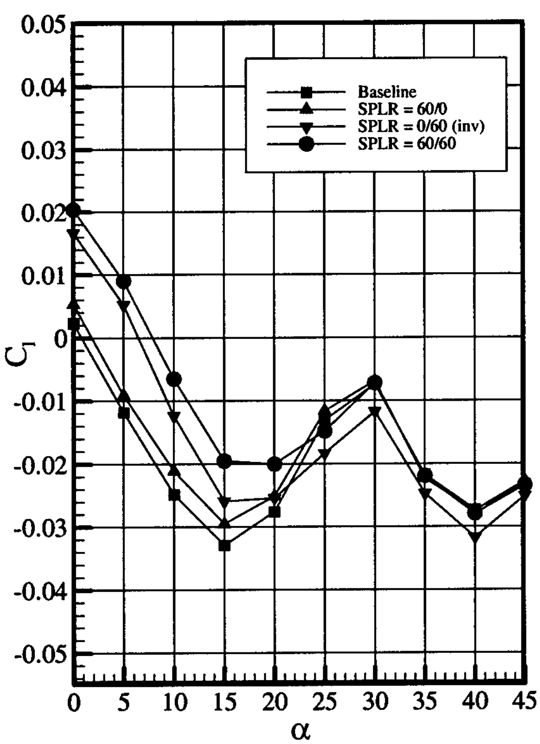

Figure I13c Rolling Moment Coefficient as a Function of α, β = 18°

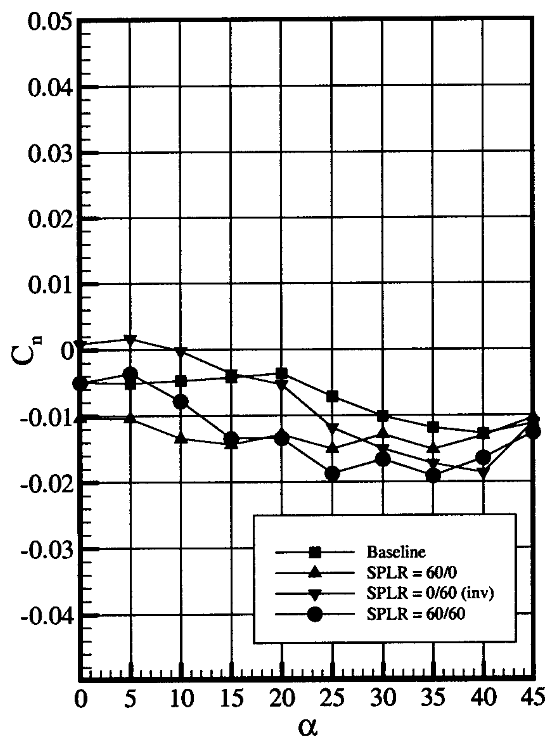

Figure I13d Yawing Moment Coefficient as a Function of α, β = 18°

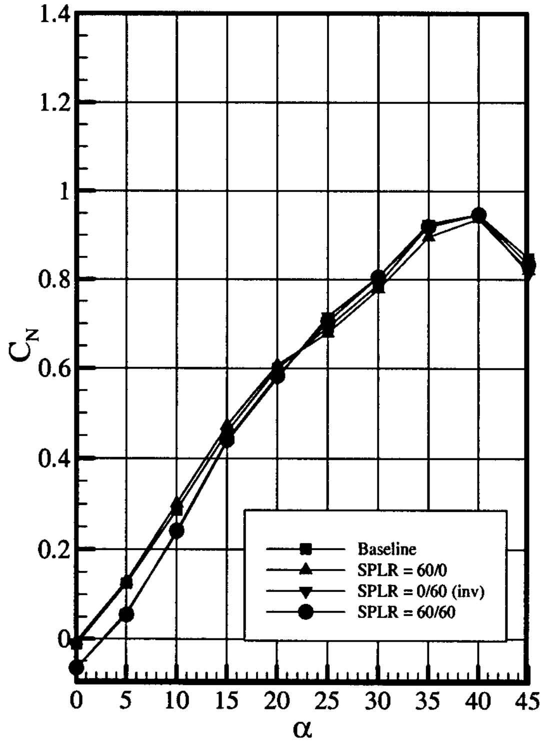

Figure I14a Normal Force Coefficient as a Function of α, β = 20°

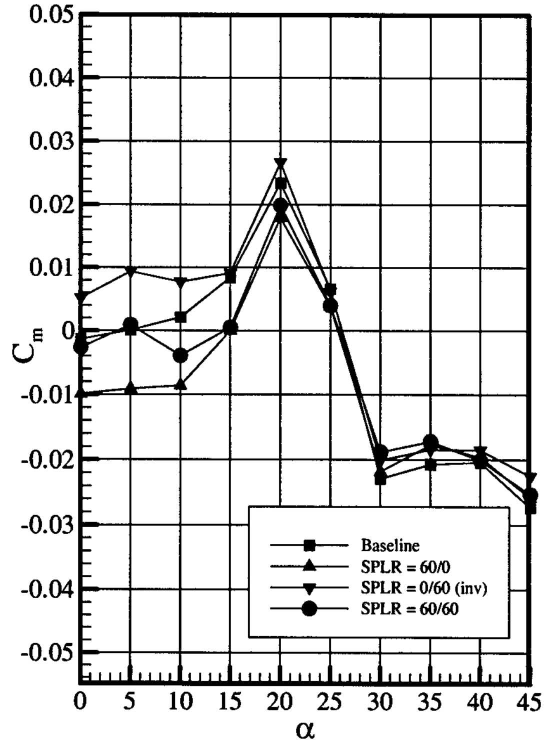

Figure I14b Pitching Moment Coefficient as a Function of α, β = 20°

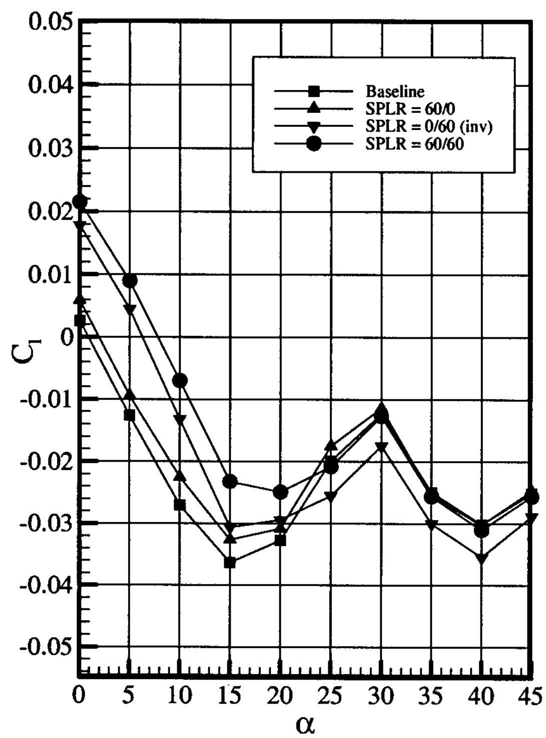

Figure I14c Rolling Moment Coefficient as a Function of α, β = 20°

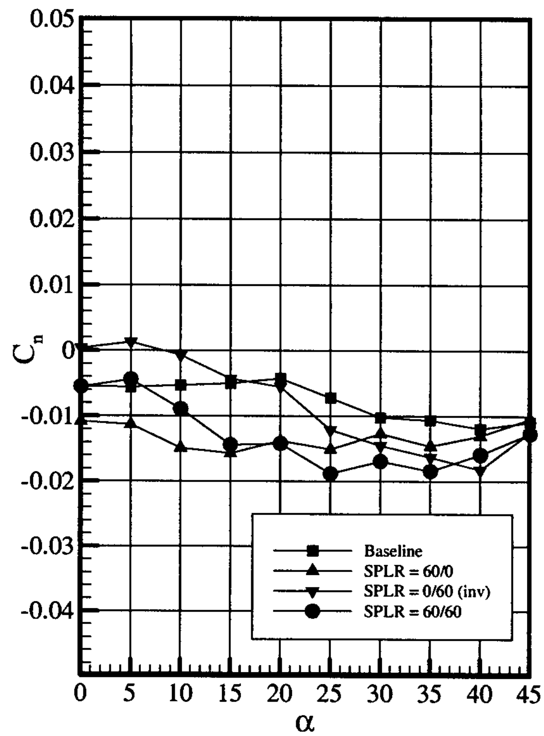

Figure I14d Yawing Moment Coefficient as a Function of α, β = 20°

Appendix J Spoiler Deflection Data as a Function of Sideslip Angle

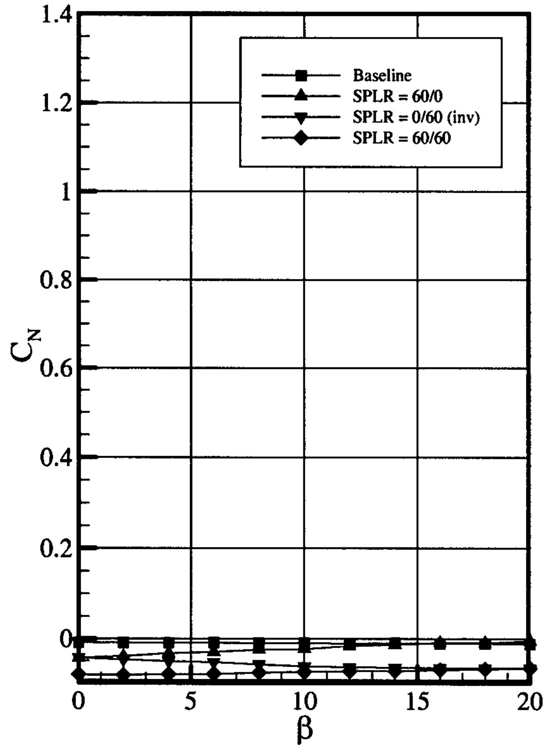

Figure J1a Normal Force Coefficient as a Function of β, α = 0°

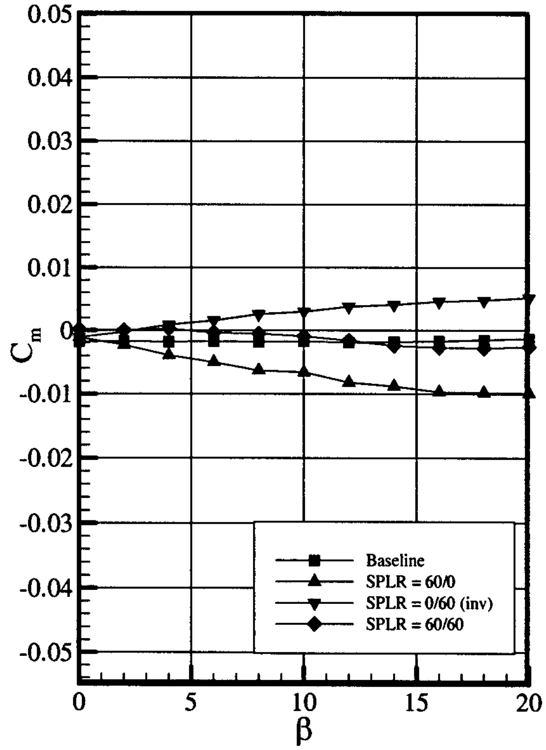

Figure J1b Pitching Moment Coefficient as a Function of β, α = 0°

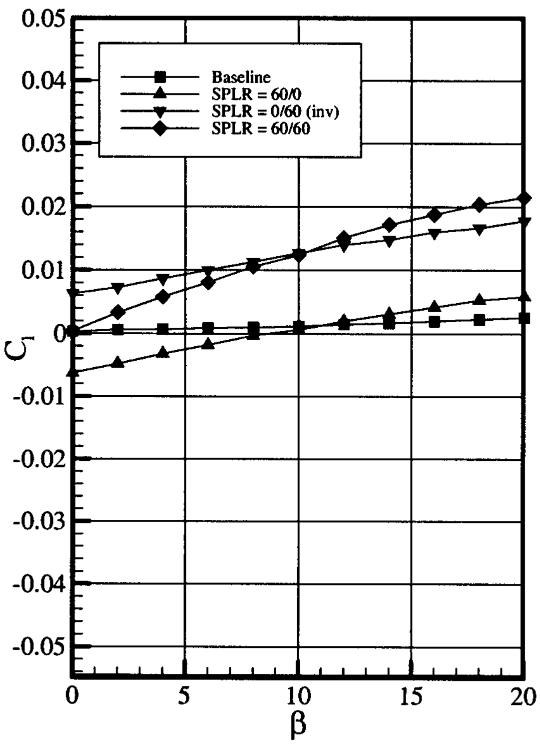

Figure J1c Rolling Moment Coefficient as a Function of β, α = 0°

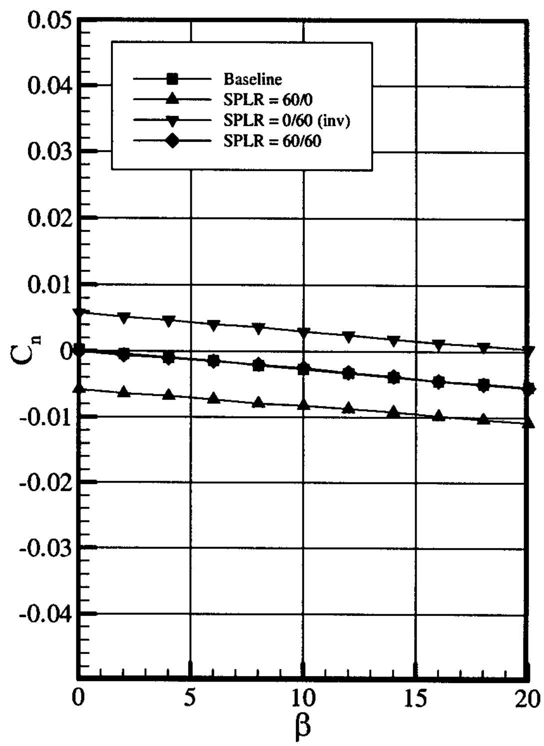

Figure J1d Yawing Moment Coefficient as a Function of β, α = 0°

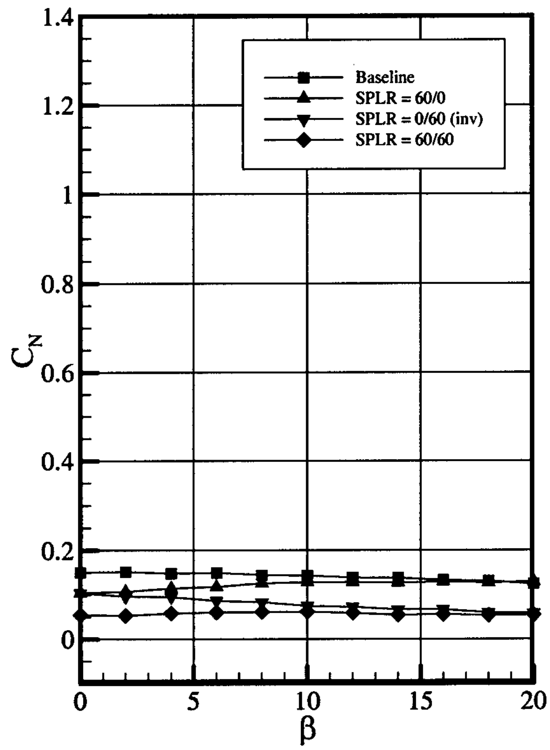

Figure J2a Normal Force Coefficient as a Function of β, $\alpha = 5^{\circ}$

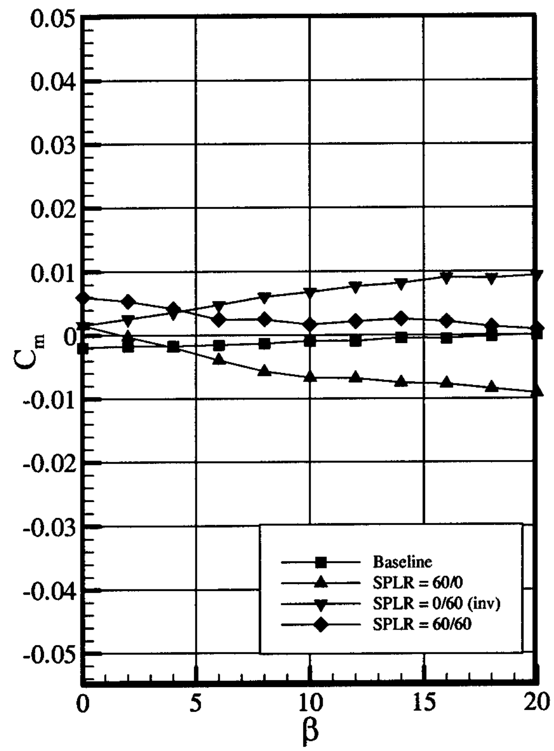

Figure J2b Pitching Moment Coefficient as a Function of β, $\alpha = 5^{\circ}$

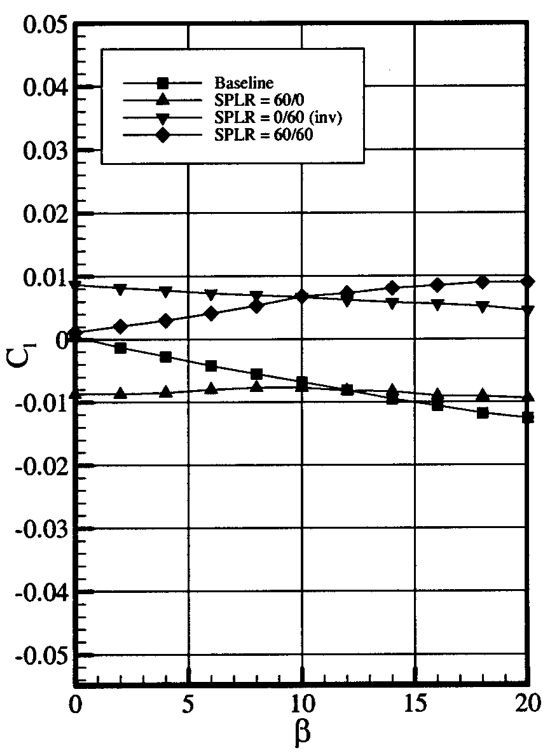

Figure J2c Rolling Moment Coefficient as a Function of β, $\alpha = 5^{\circ}$

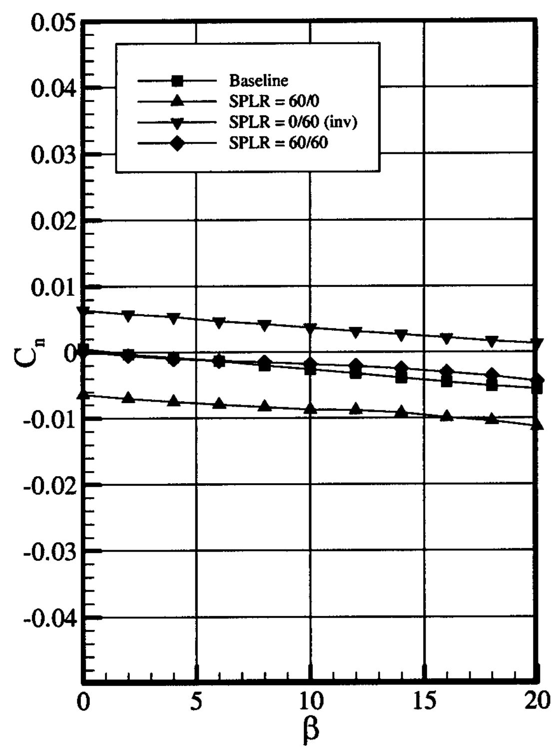

Figure J2d Yawing Moment Coefficient as a Function of β, $\alpha = 5^{\circ}$

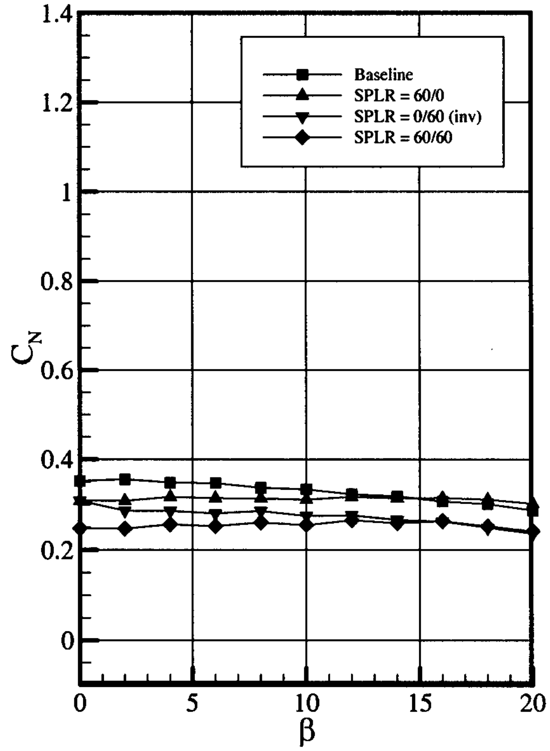

Figure J3a Normal Force Coefficient as a Function of β, α = 10°

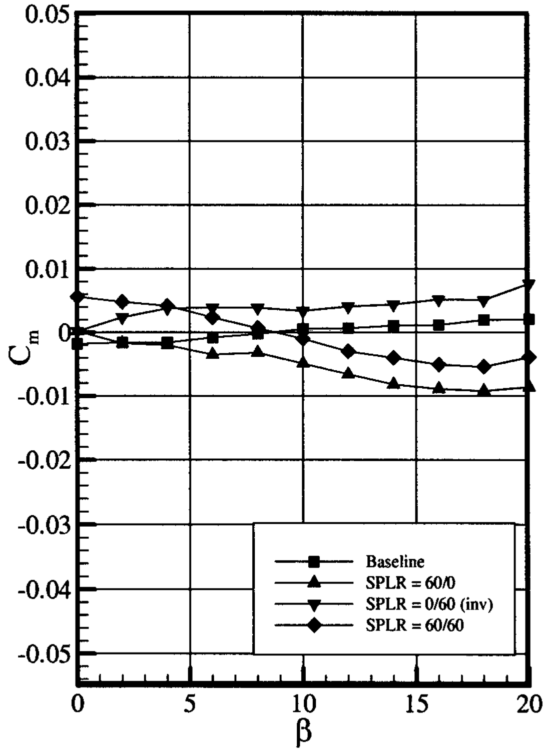

Figure J3b Pitching Moment Coefficient as a Function of β, α = 10°

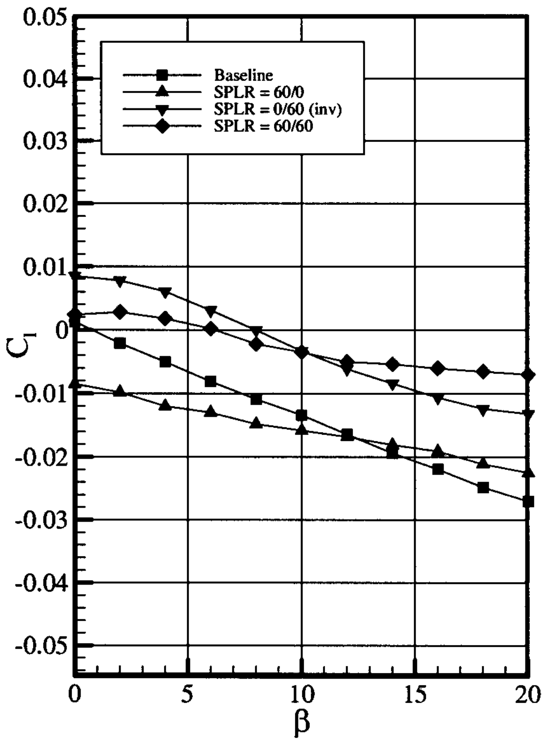

Figure J3c Rolling Moment Coefficient as a Function of β, α = 10°

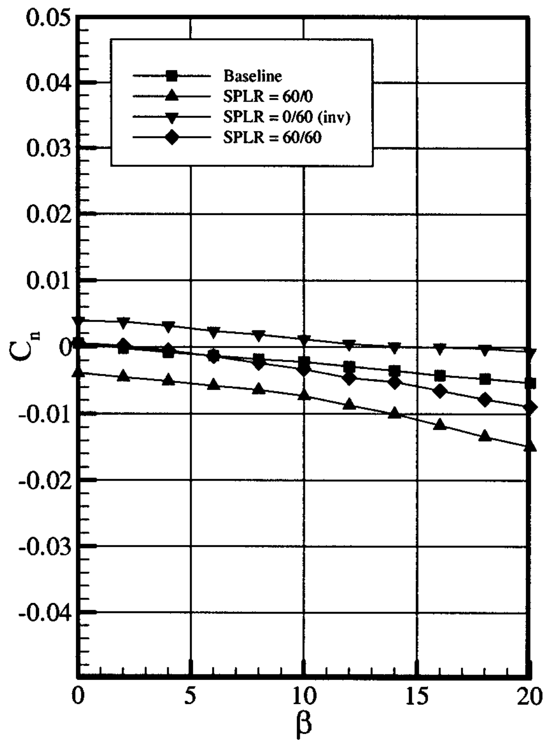

Figure J3d Yawing Moment Coefficient as a Function of β, α = 10°

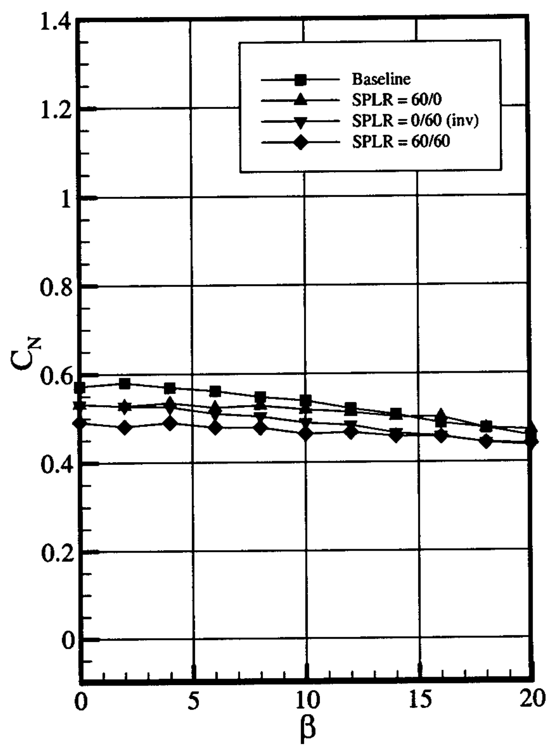

Figure J4a Normal Force Coefficient as a Function of β, α = 15°

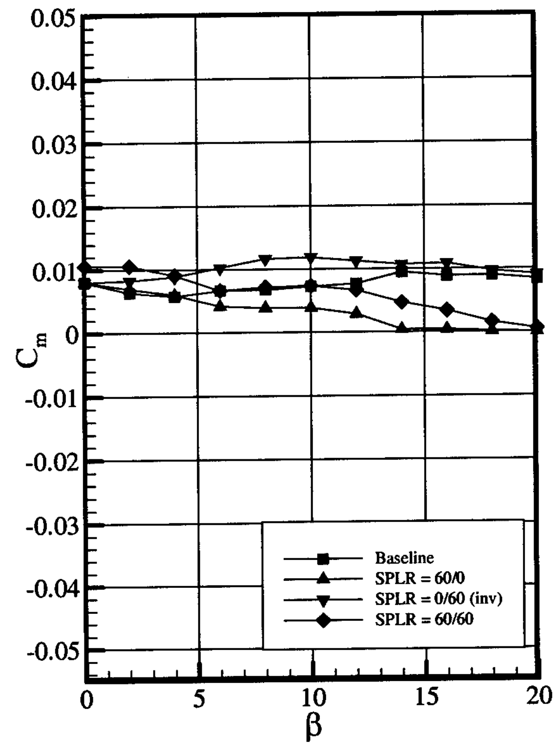

Figure J4b Pitching Moment Coefficient as a Function of β, α = 15°

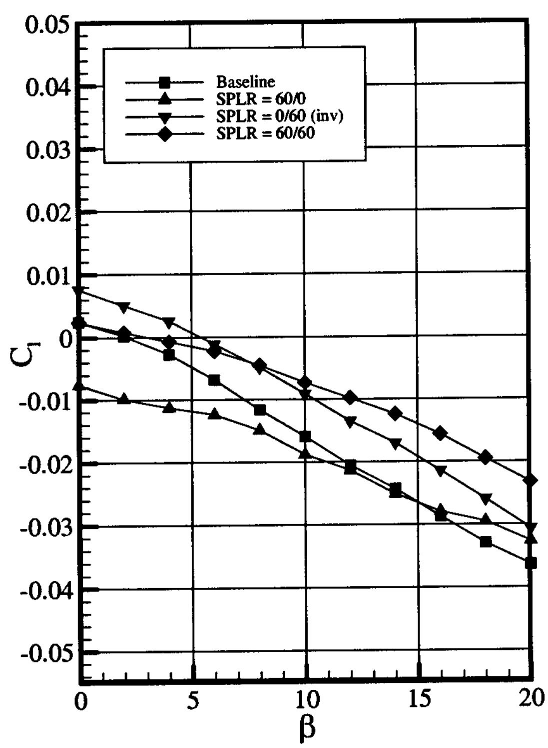

Figure J4c Rolling Moment Coefficient as a Function of β, α = 15°

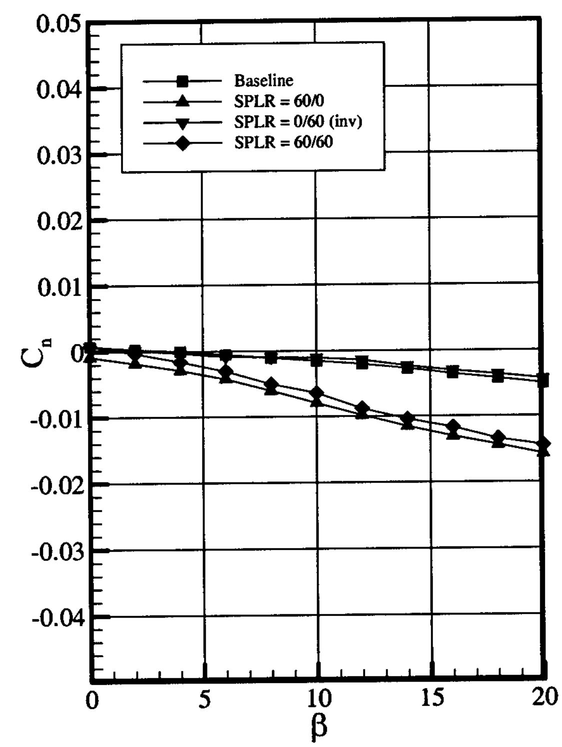

Figure J4d Yawing Moment Coefficient as a Function of β, α = 15°

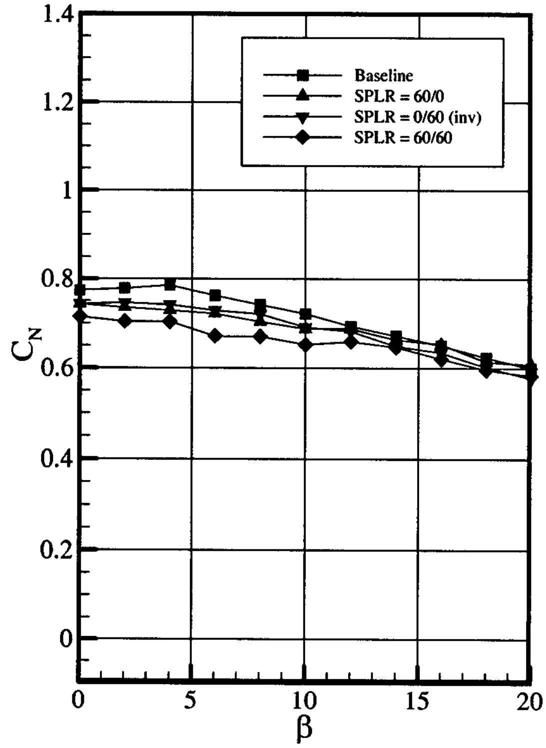

Figure J5a Normal Force Coefficient as a Function of β, $\alpha = 20^\circ$

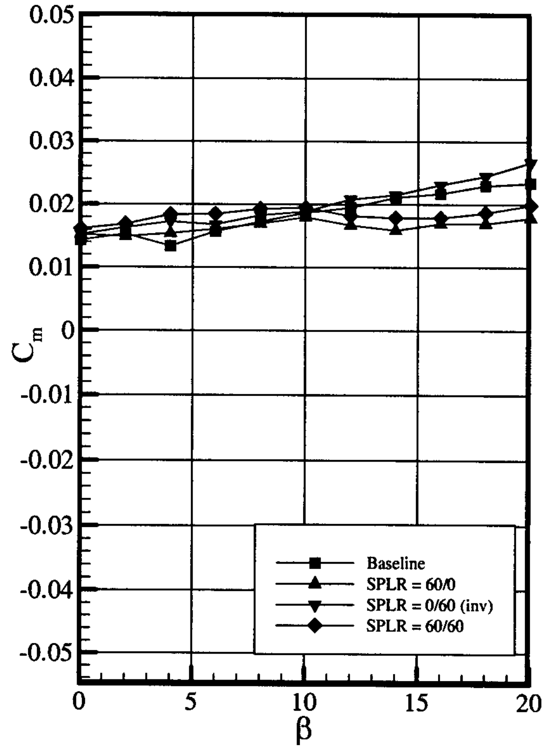

Figure J5b Pitching Moment Coefficient as a Function of β, $\alpha = 20^\circ$

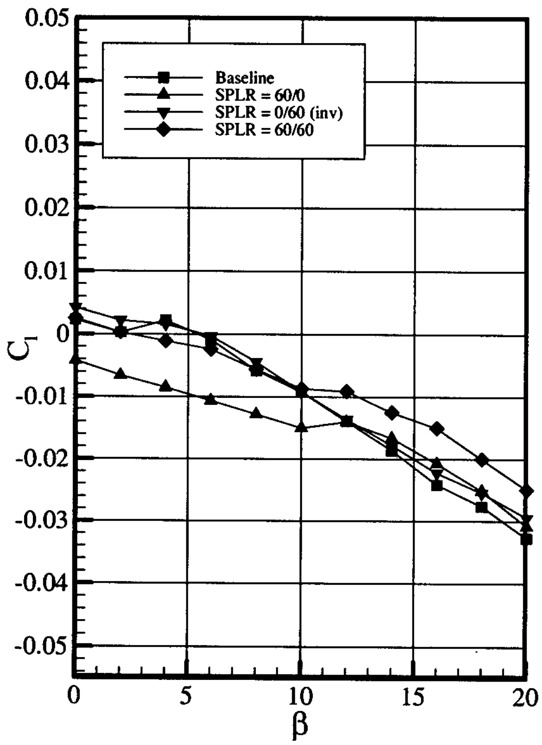

Figure J5c Rolling Moment Coefficient as a Function of β, $\alpha = 20^\circ$

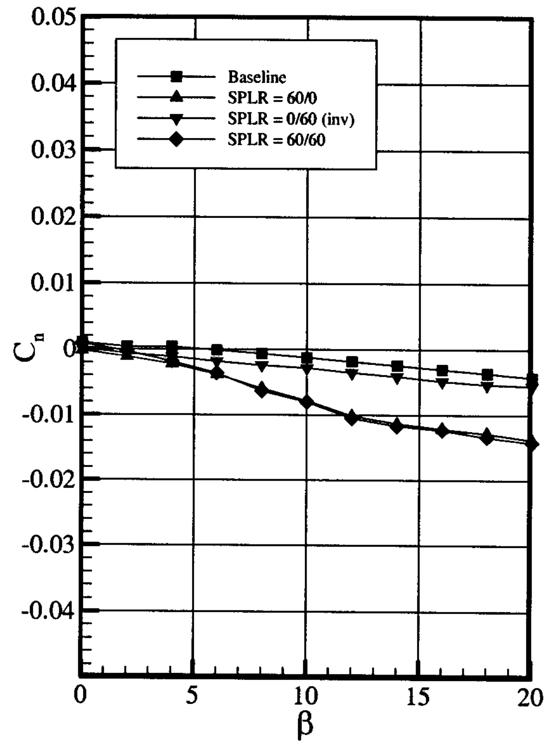

Figure J5d Yawing Moment Coefficient as a Function of β, $\alpha = 20^\circ$

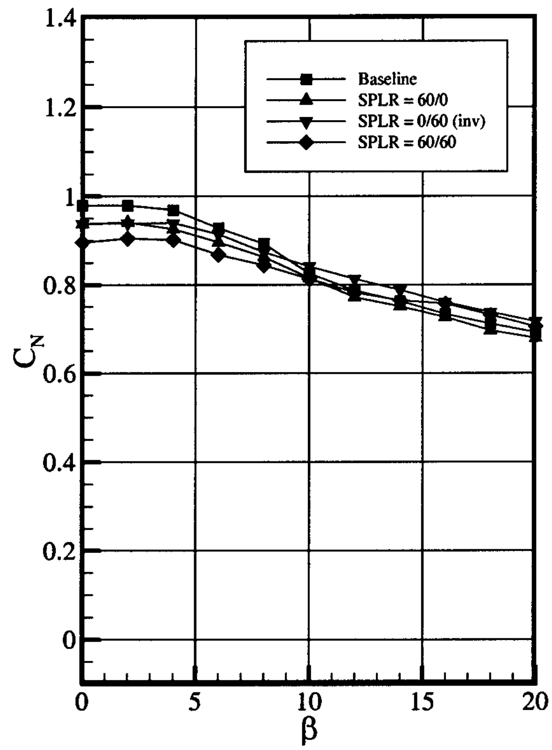

Figure J6a Normal Force Coefficient as a Function of β, $\alpha = 25^{\circ}$

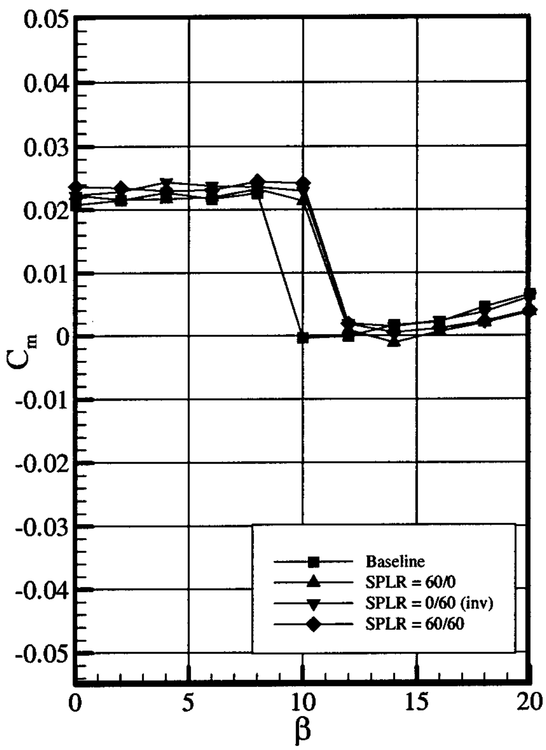

Figure J6b Pitching Moment Coefficient as a Function of β, $\alpha = 25^{\circ}$

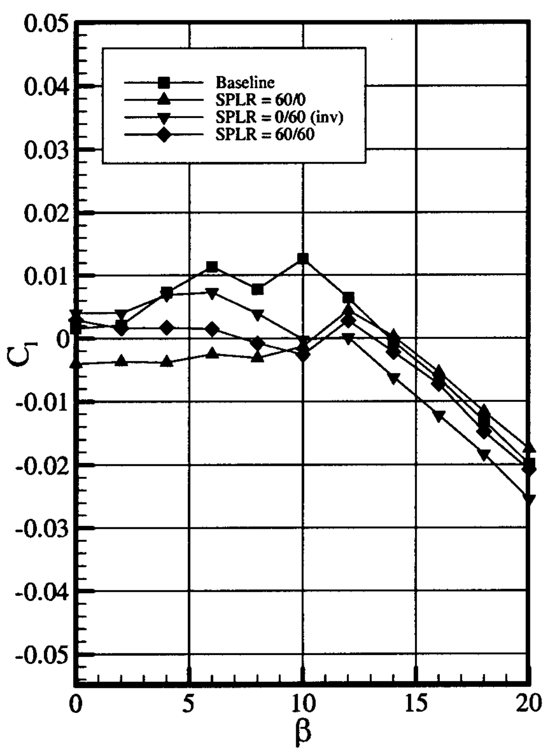

Figure J6c Rolling Moment Coefficient as a Function of β, $\alpha = 25^{\circ}$

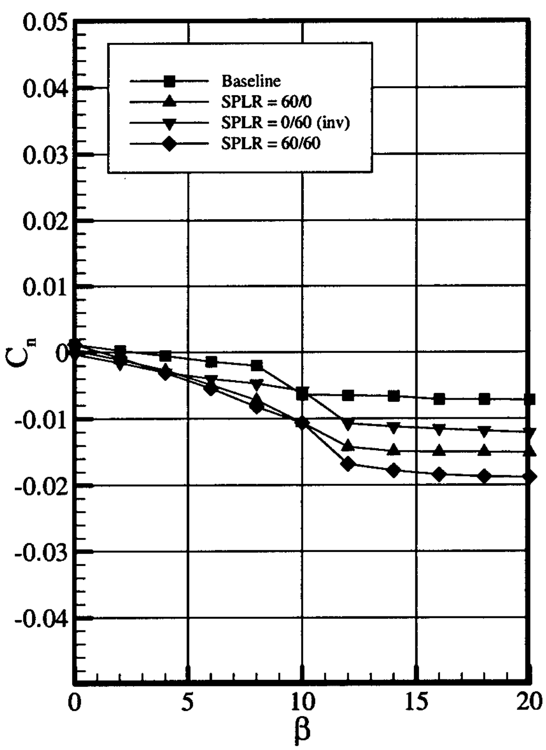

Figure J6d Yawing Moment Coefficient as a Function of β, $\alpha = 25^{\circ}$

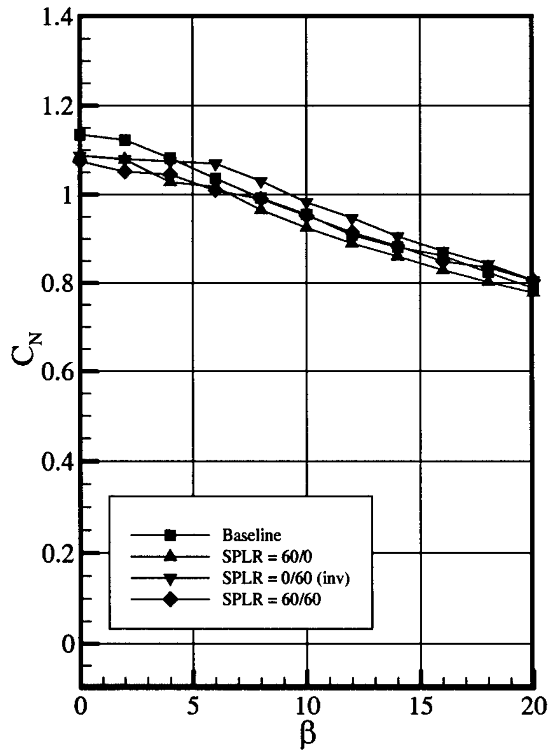

Figure J7a Normal Force Coefficient as a Function of β, α = 30°

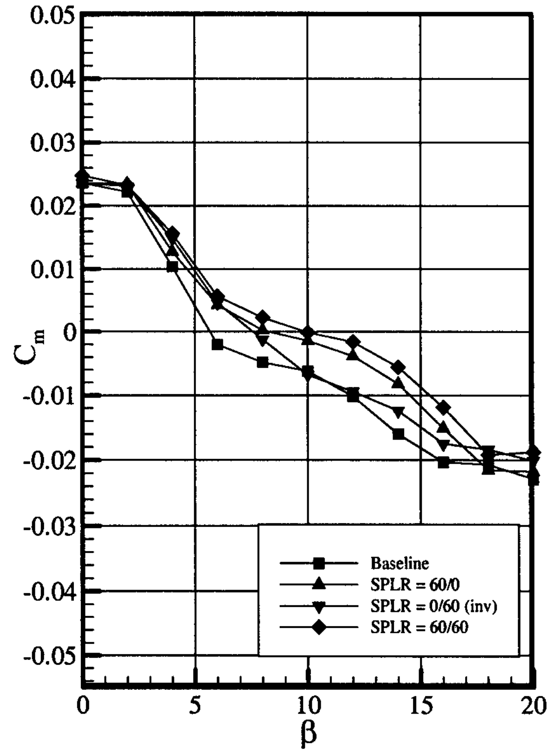

Figure J7b Pitching Moment Coefficient as a Function of β, α = 30°

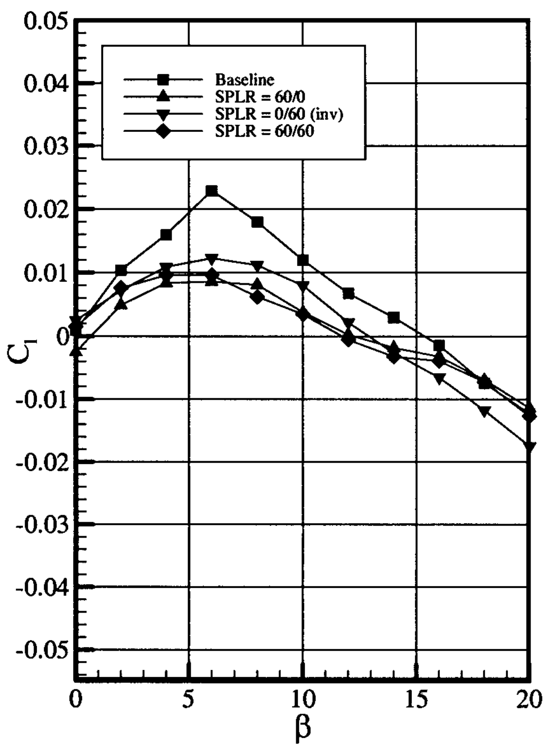

Figure J7c Rolling Moment Coefficient as a Function of β, α = 30°

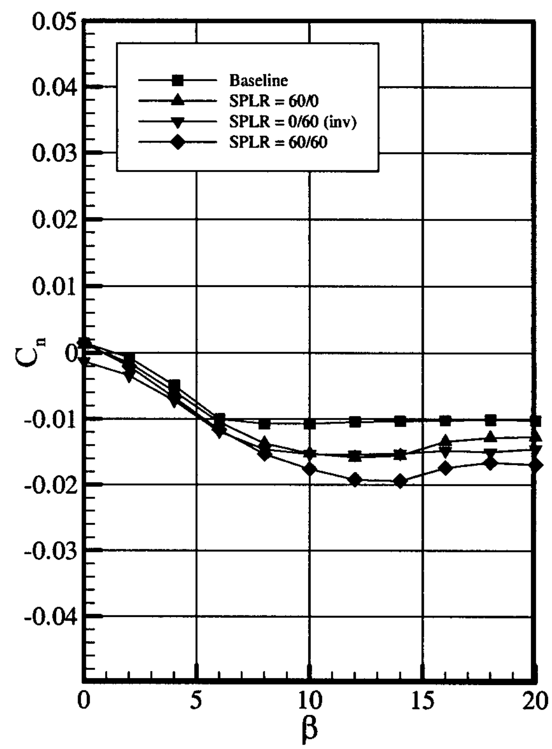

Figure J7d Yawing Moment Coefficient as a Function of β, α = 30°

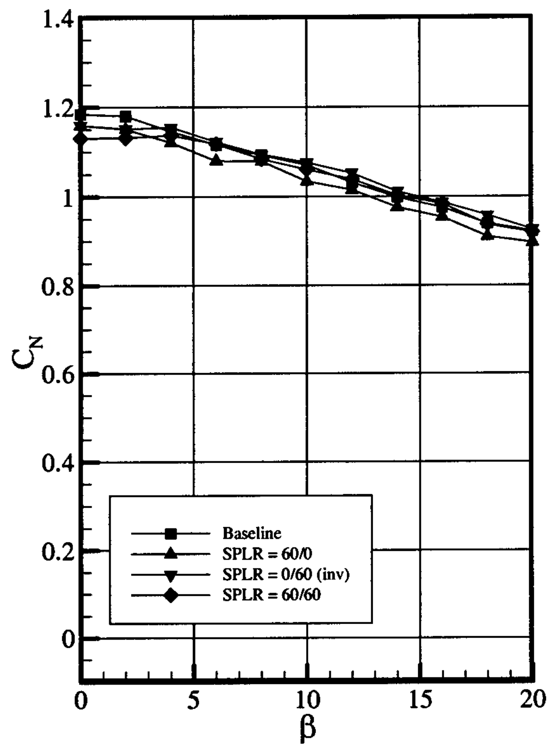

Figure J8a Normal Force Coefficient as a Function of β, α = 35°

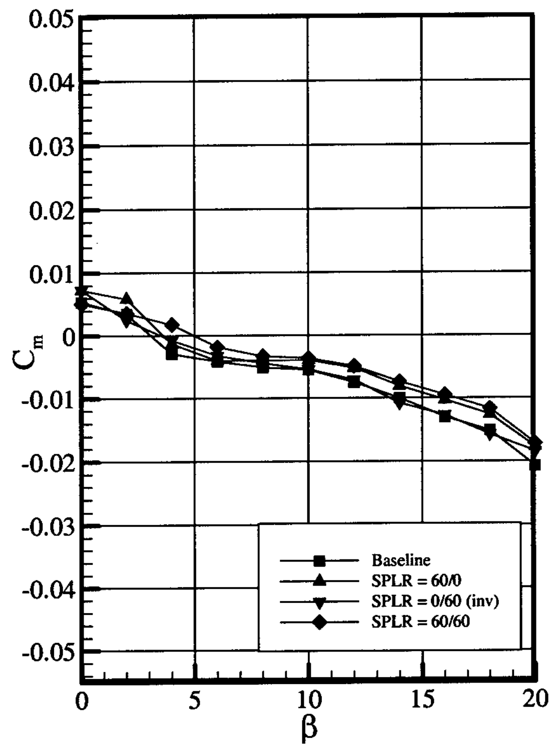

Figure J8b Pitching Moment Coefficient as a Function of β, α = 35°

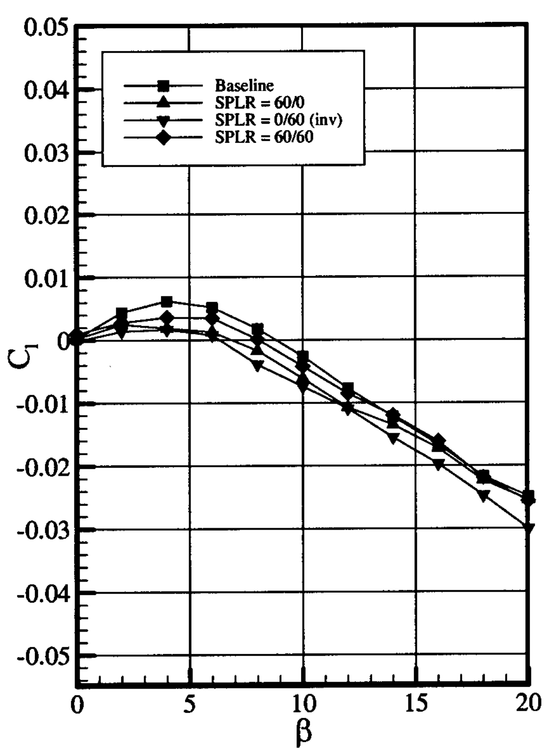

Figure J8c Rolling Moment Coefficient as a Function of β, α = 35°

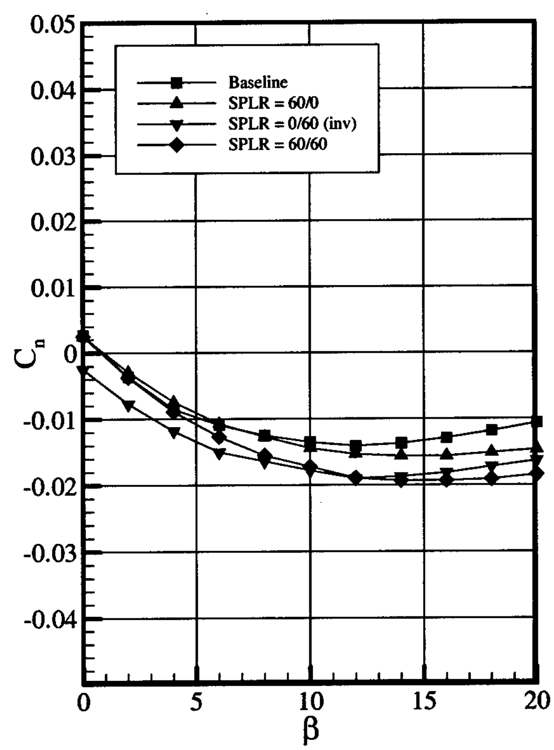

Figure J8d Yawing Moment Coefficient as a Function of β, α = 35°

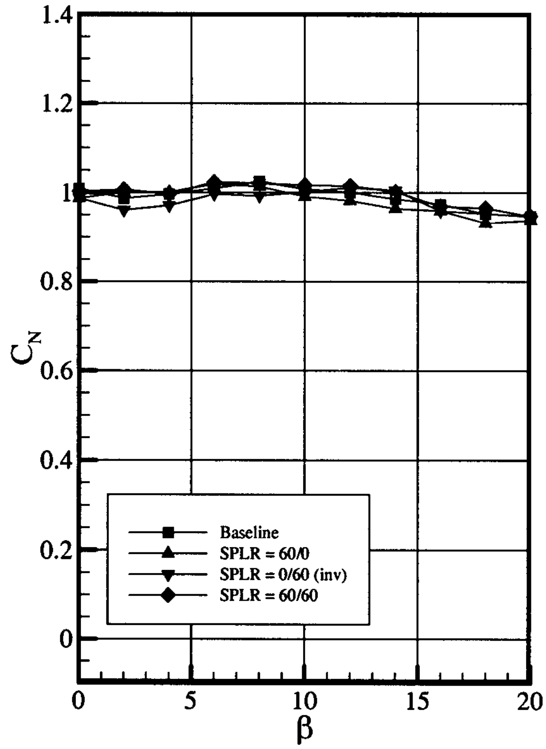

Figure J9a Normal Force Coefficient as a Function of β, α = 40°

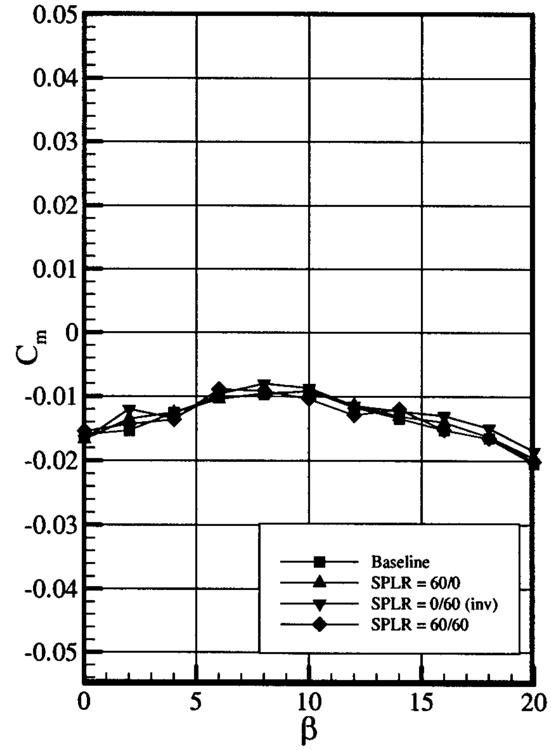

Figure J9b Pitching Moment Coefficient as a Function of β, α = 40°

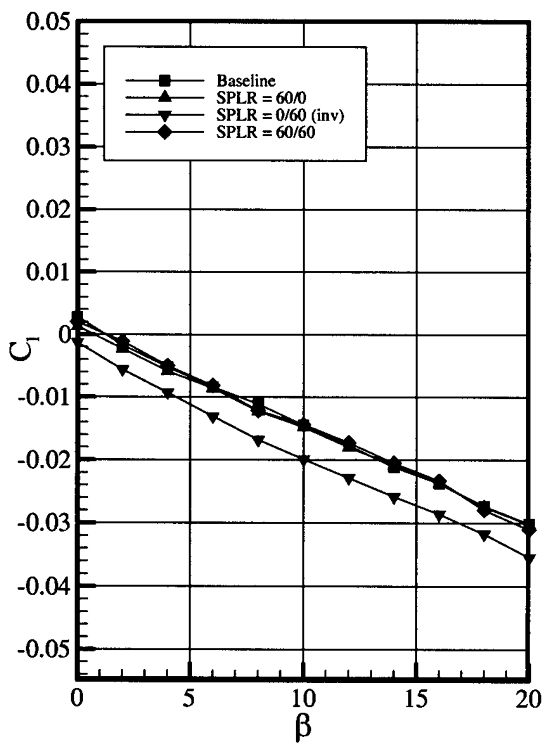

Figure J9c Rolling Moment Coefficient as a Function of β, α = 40°

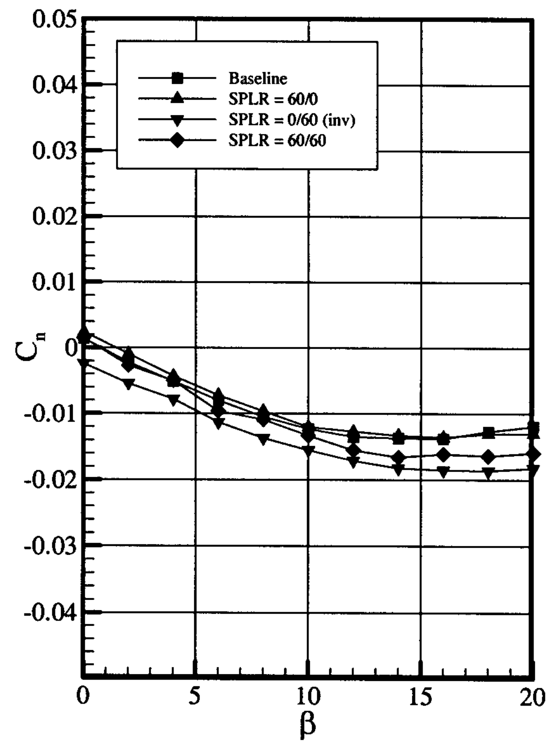

Figure J9d Yawing Moment Coefficient as a Function of β, α = 40°

Appendix K Spoiler-Slot-Deflector Deflection Data as a Function of Angle of Attack

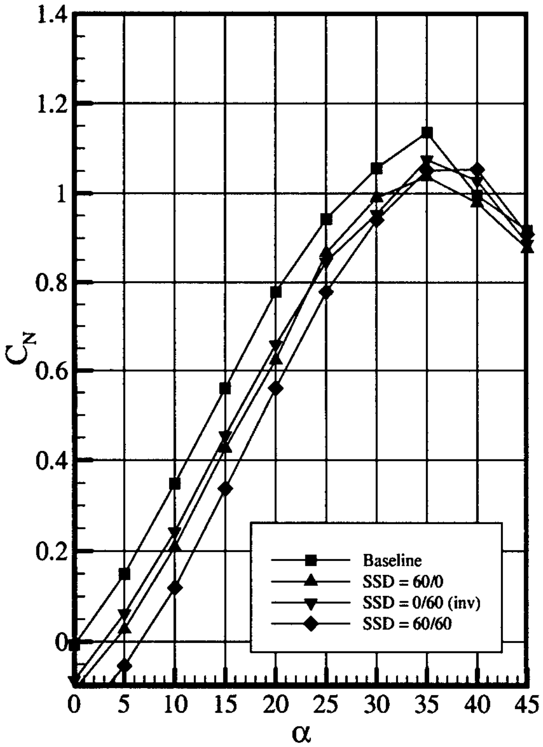

Figure K1a Normal Force Coefficient
as a Function of α, β = -6°

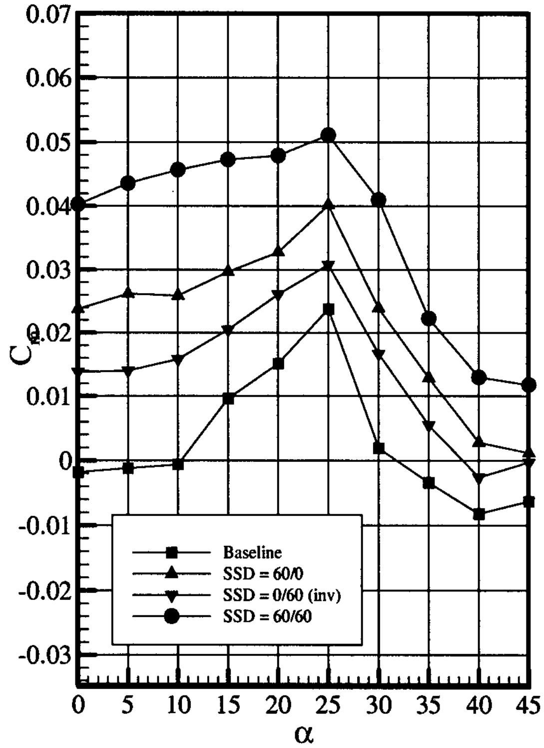

Figure K1b Pitching Moment Coefficient
as a Function of α, β = -6°

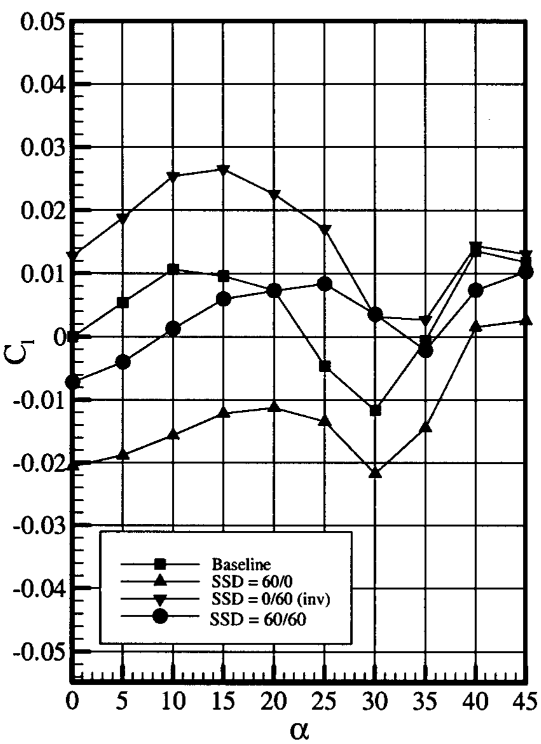

Figure K1c Rolling Moment Coefficient
as a Function of α, β = -6°

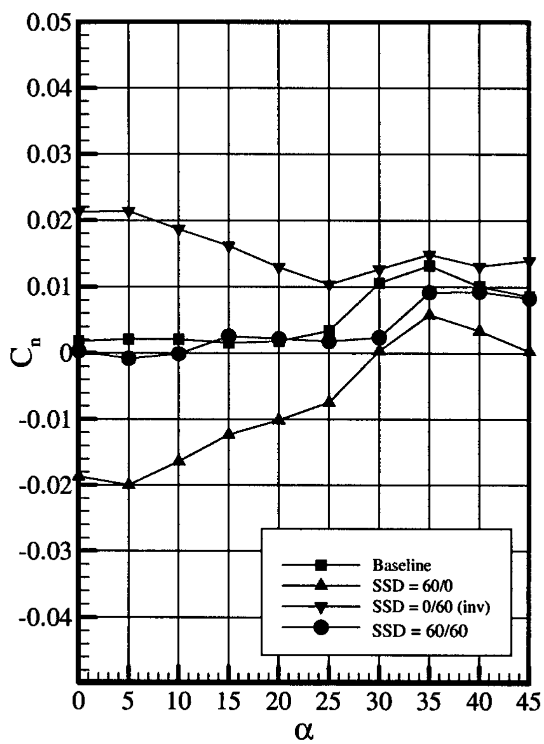

Figure K1d Yawing Moment Coefficient
as a Function of α, β = -6°

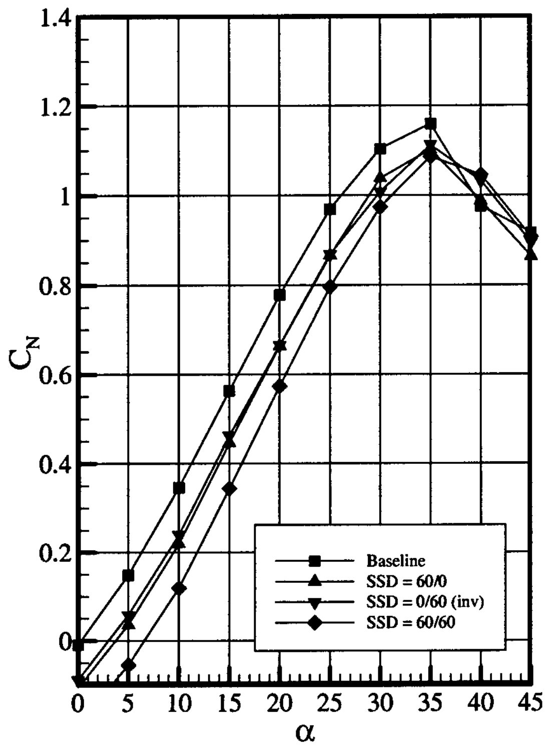

Figure K2a Normal Force Coefficient
as a Function of α, β = -4°

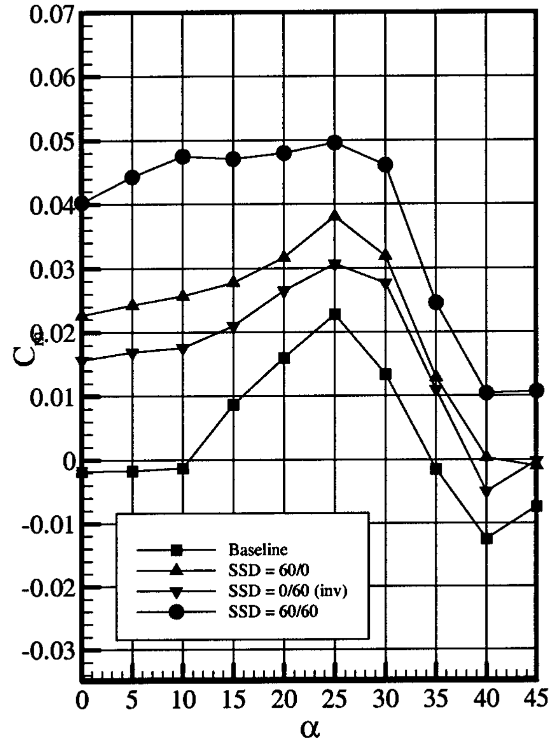

Figure K2b Pitching Moment Coefficient
as a Function of α, β = -4°

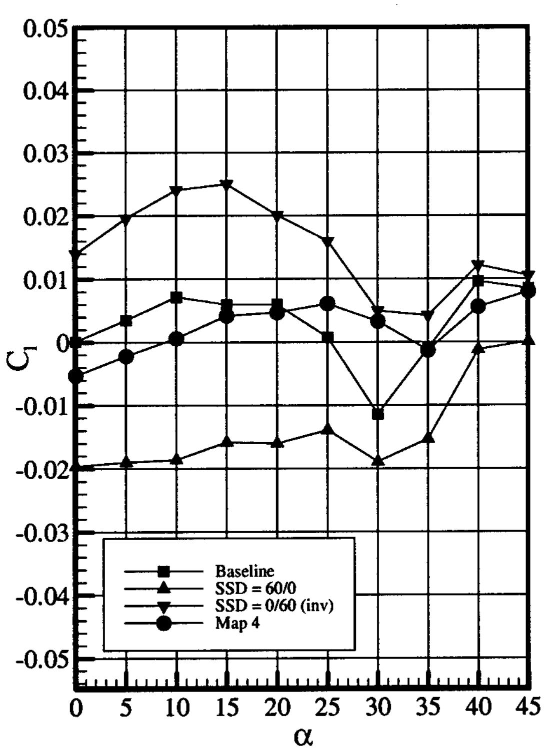

Figure K2c Rolling Moment Coefficient
as a Function of α, β = -4°

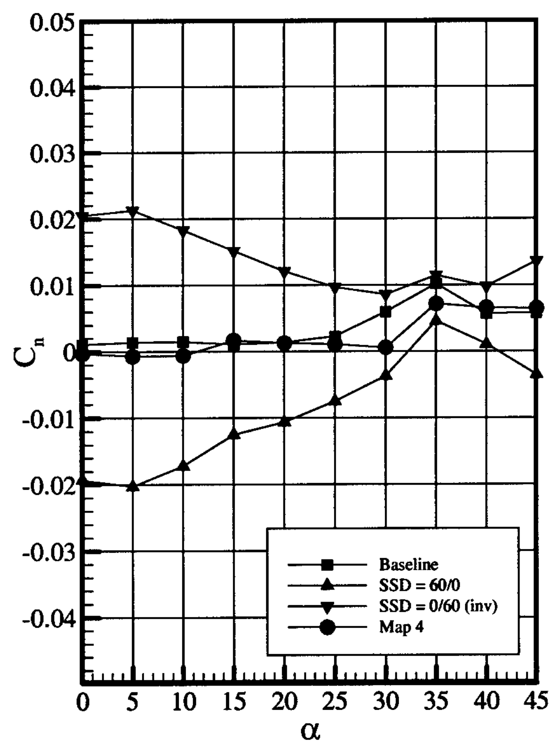

Figure K2d Yawing Moment Coefficient
as a Function of α, β = -4°

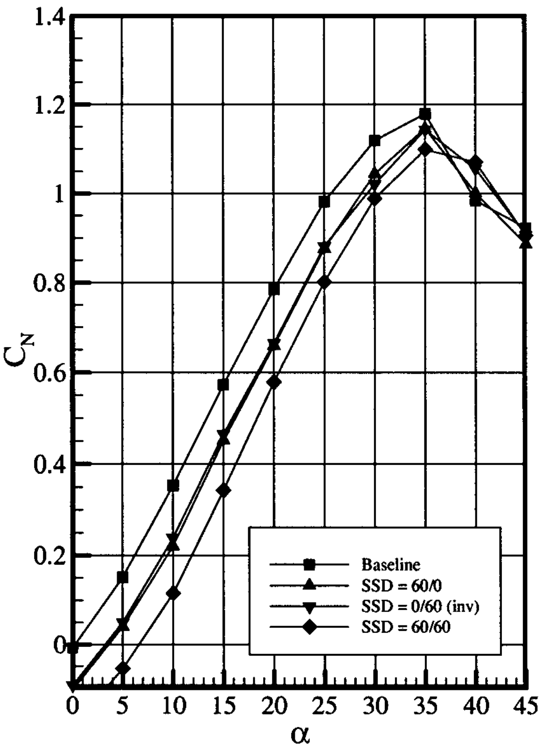

Figure K3a Normal Force Coefficient as a Function of α, $\beta = -2^\circ$

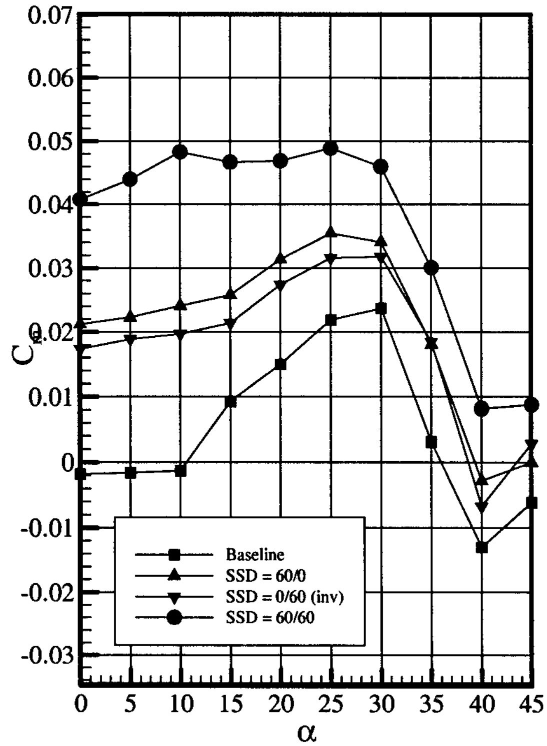

Figure K3b Pitching Moment Coefficient as a Function of α, $\beta = -2^\circ$

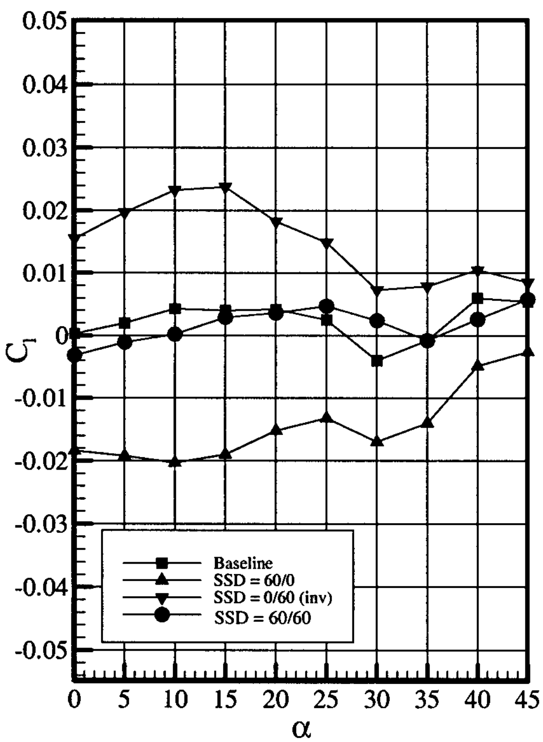

Figure K3c Rolling Moment Coefficient as a Function of α, $\beta = -2^\circ$

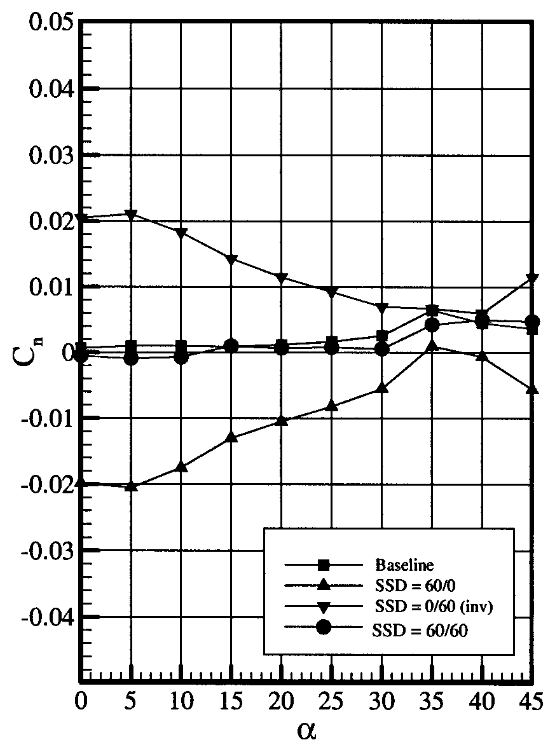

Figure K3d Yawing Moment Coefficient as a Function of α, $\beta = -2^\circ$

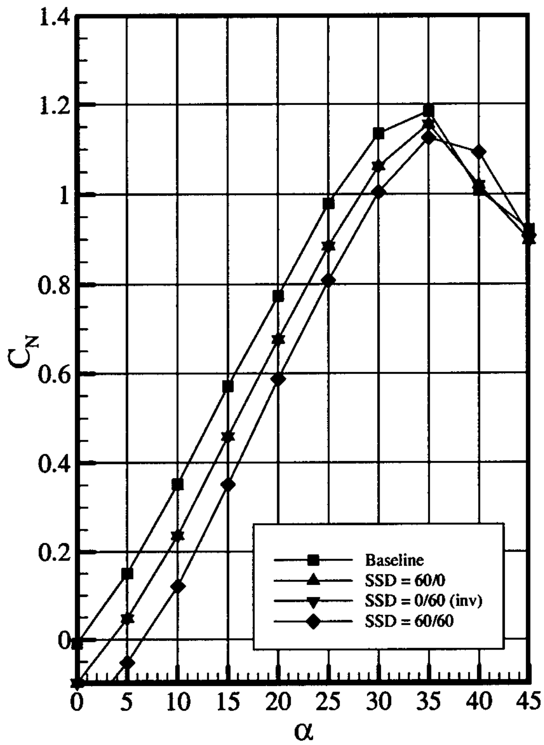

Figure K4a Normal Force Coefficient
as a Function of α, β = 0°

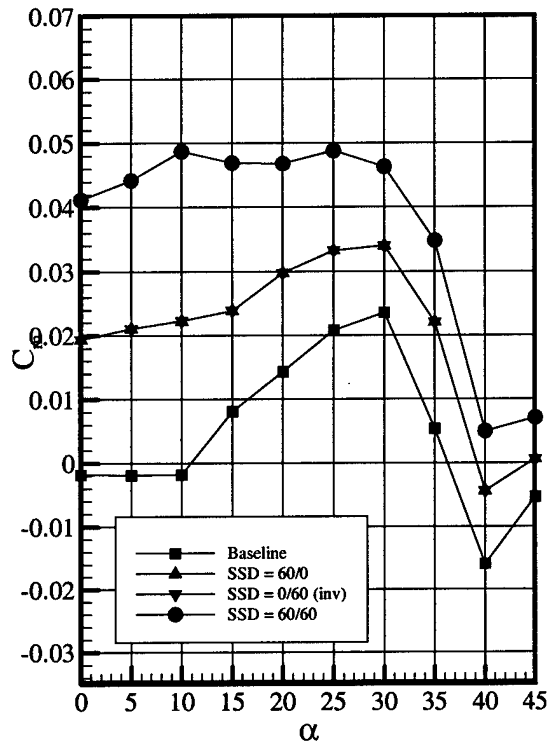

Figure K4b Pitching Moment Coefficient
as a Function of α, β = 0°

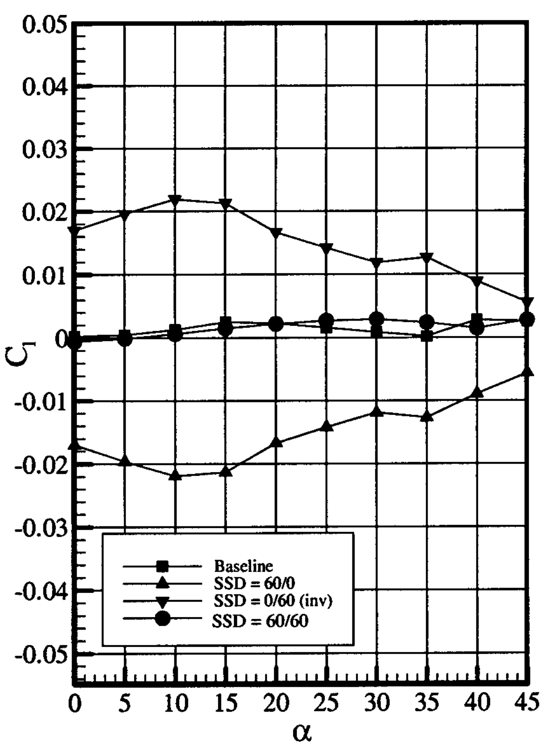

Figure K4c Rolling Moment Coefficient
as a Function of α, β = 0°

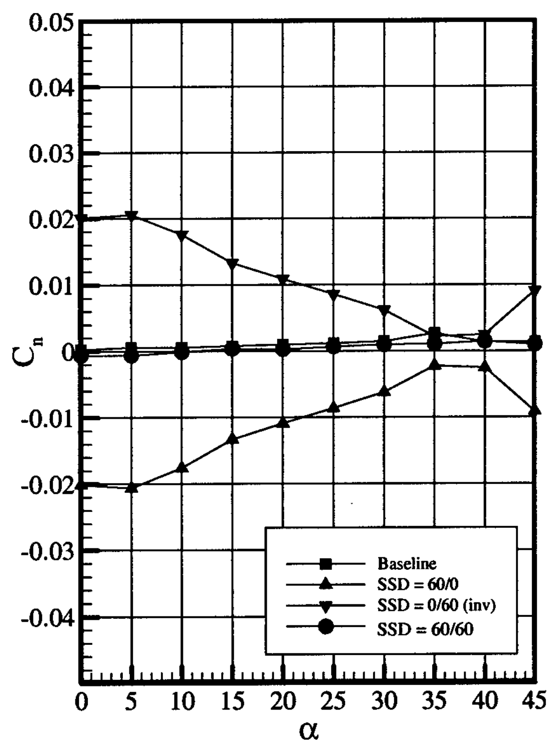

Figure K4d Yawing Moment Coefficient
as a Function of α, β = 0°

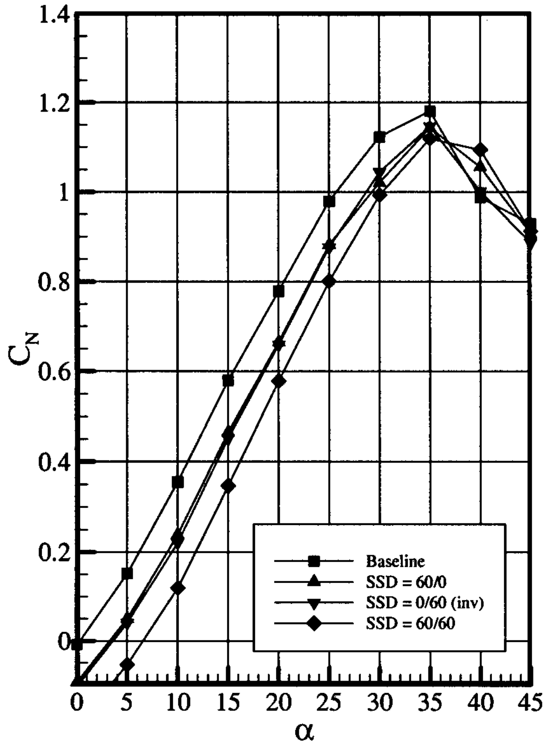

Figure K5a Normal Force Coefficient as a Function of α, $\beta = 2^{\circ}$

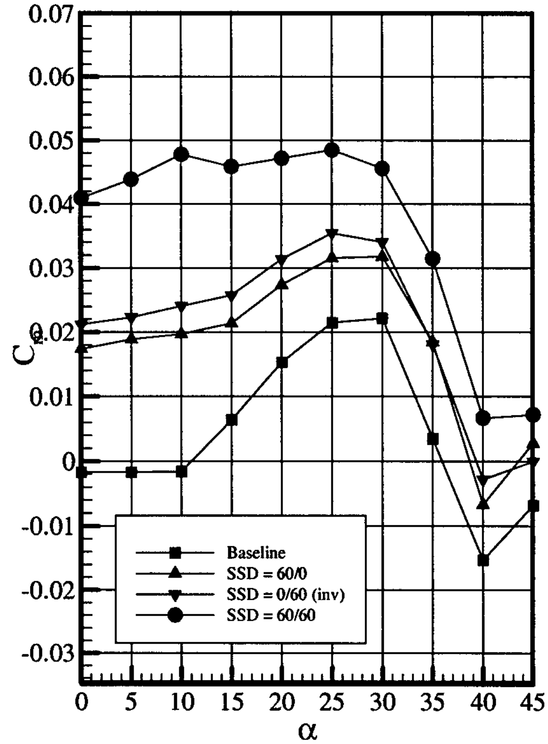

Figure K5b Pitching Moment Coefficient as a Function of α, $\beta = 2^{\circ}$

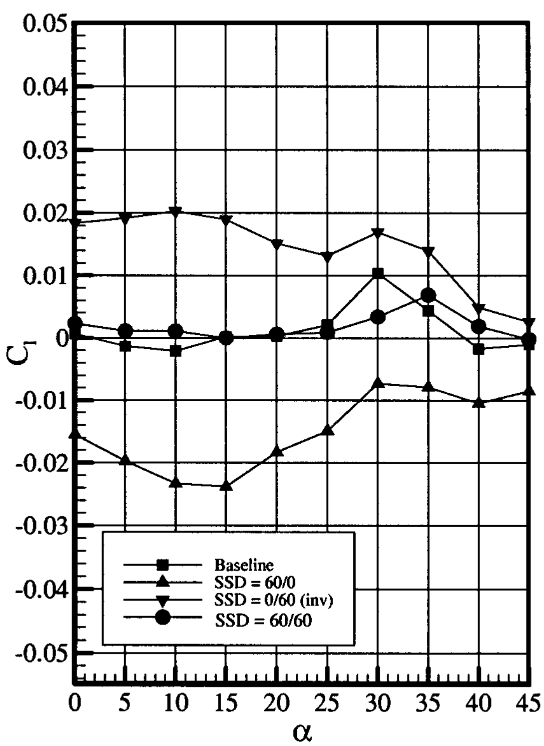

Figure K5c Rolling Moment Coefficient as a Function of α, $\beta = 2^{\circ}$

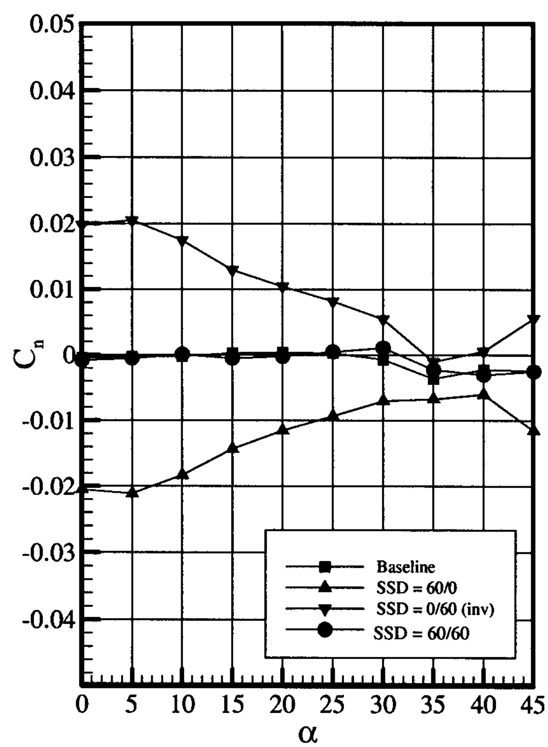

Figure K5d Yawing Moment Coefficient as a Function of α, $\beta = 2^{\circ}$

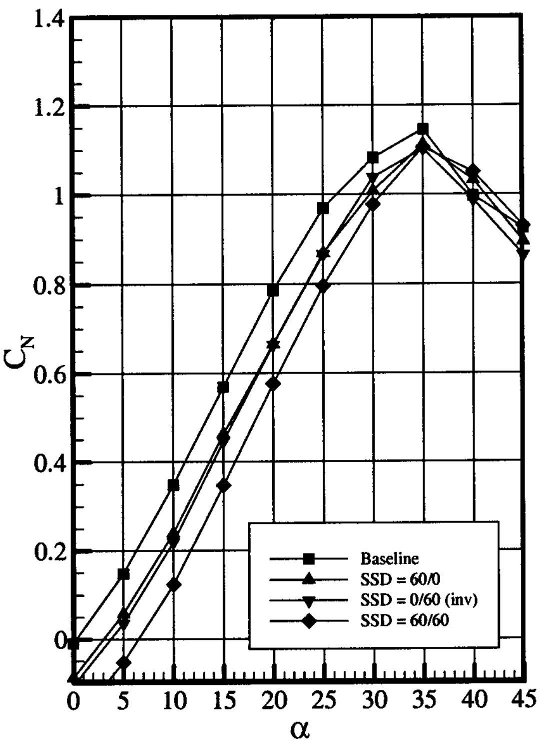

Figure K6a Normal Force Coefficient as a Function of α, $\beta = 4^{\circ}$

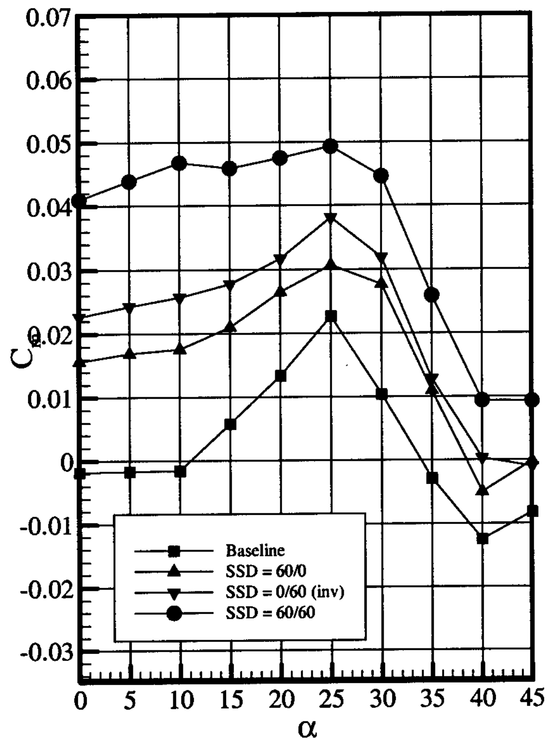

Figure K6b Pitching Moment Coefficient as a Function of α, $\beta = 4^{\circ}$

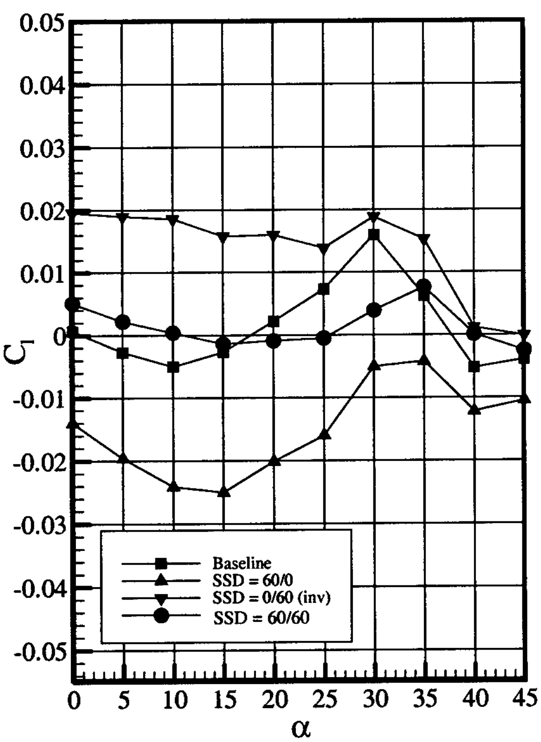

Figure K6c Rolling Moment Coefficient as a Function of α, $\beta = 4^{\circ}$

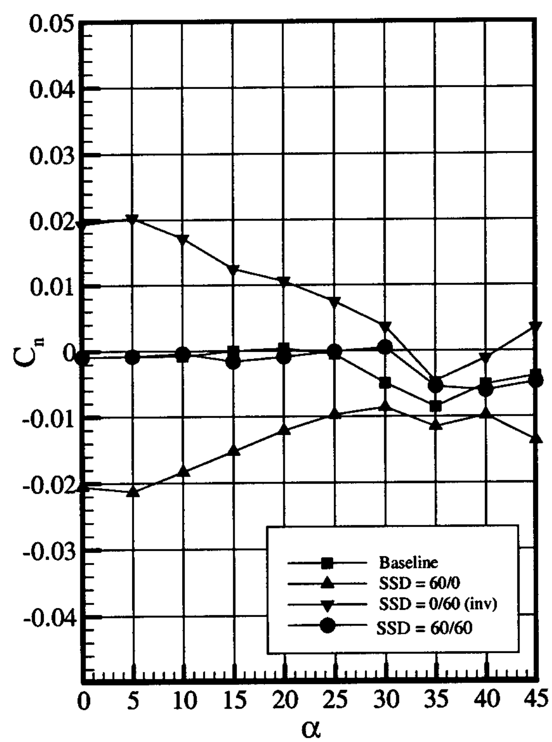

Figure K6d Yawing Moment Coefficient as a Function of α, $\beta = 4^{\circ}$

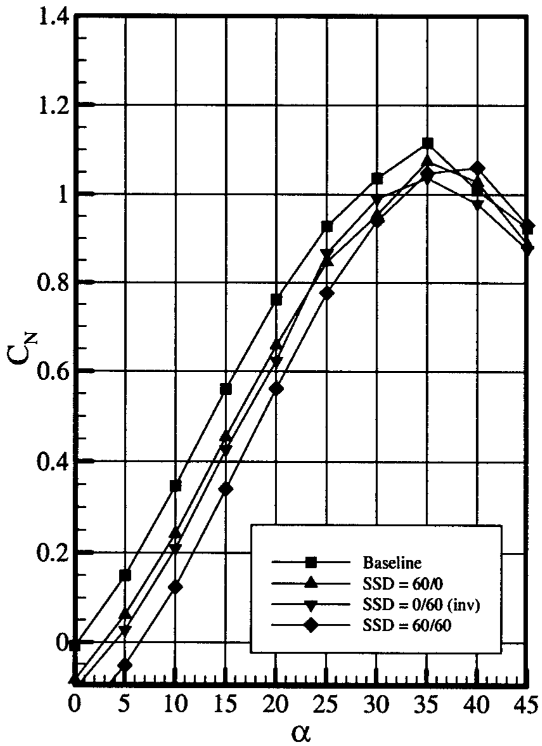

Figure K7a Normal Force Coefficient as a Function of α, $\beta = 6^{\circ}$

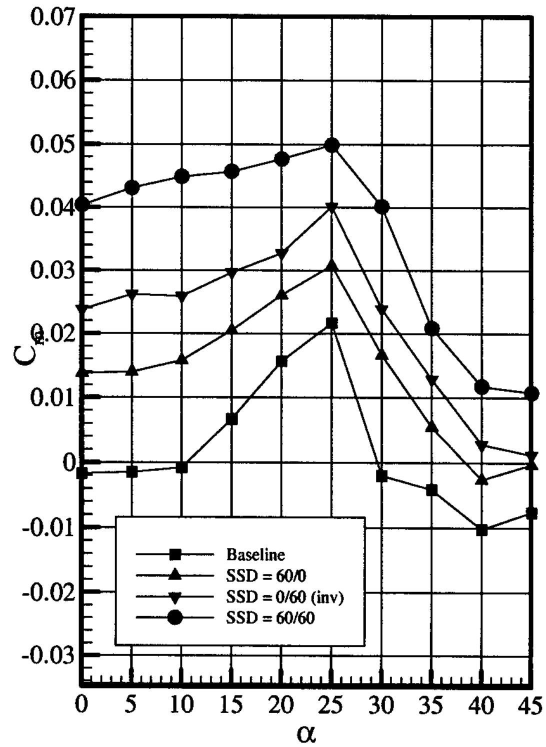

Figure K7b Pitching Moment Coefficient as a Function of α, $\beta = 6^{\circ}$

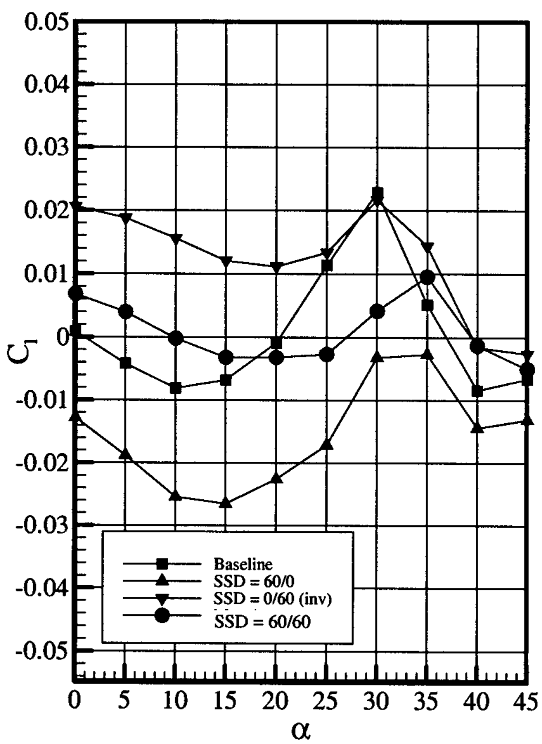

Figure K7c Rolling Moment Coefficient as a Function of α, $\beta = 6^{\circ}$

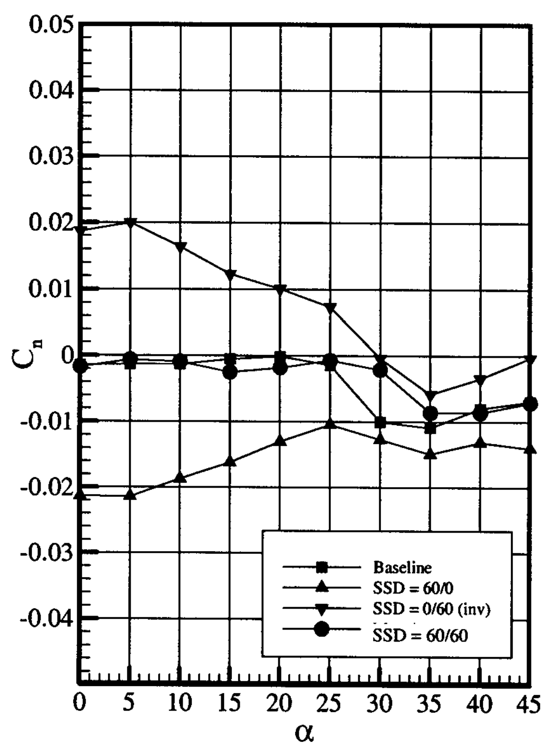

Figure K7d Yawing Moment Coefficient as a Function of α, $\beta = 6^{\circ}$

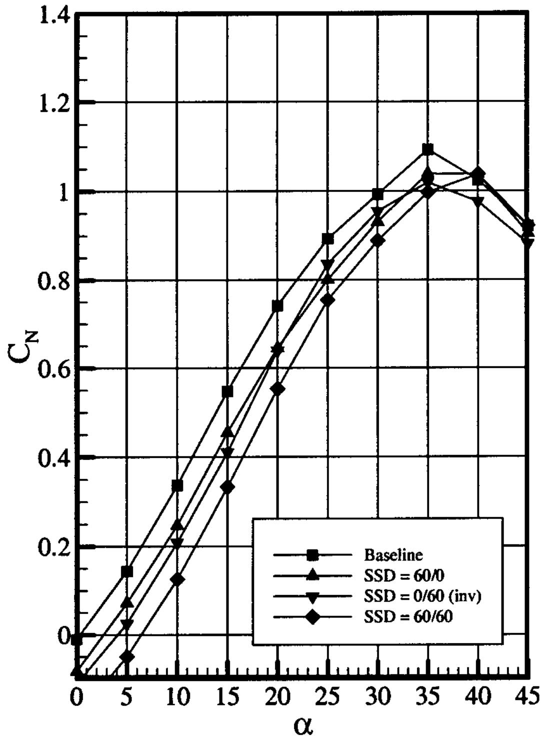

Figure K8a Normal Force Coefficient as a Function of α, β = 8°

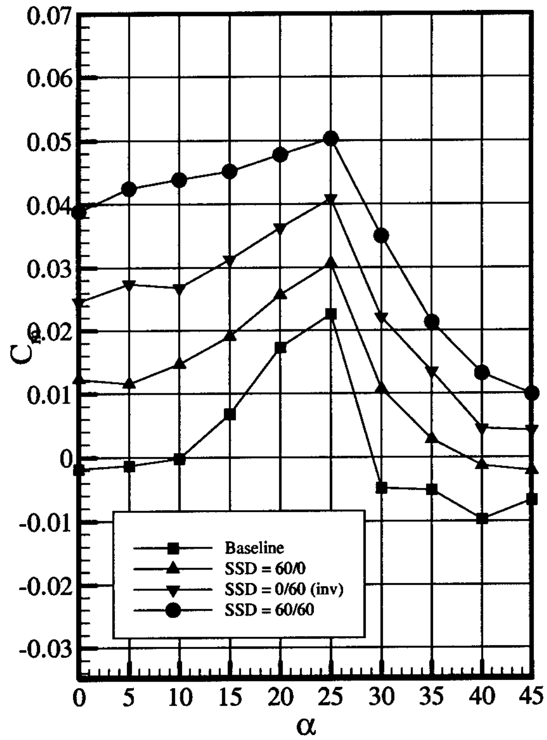

Figure K8b Pitching Moment Coefficient as a Function of α, β = 8°

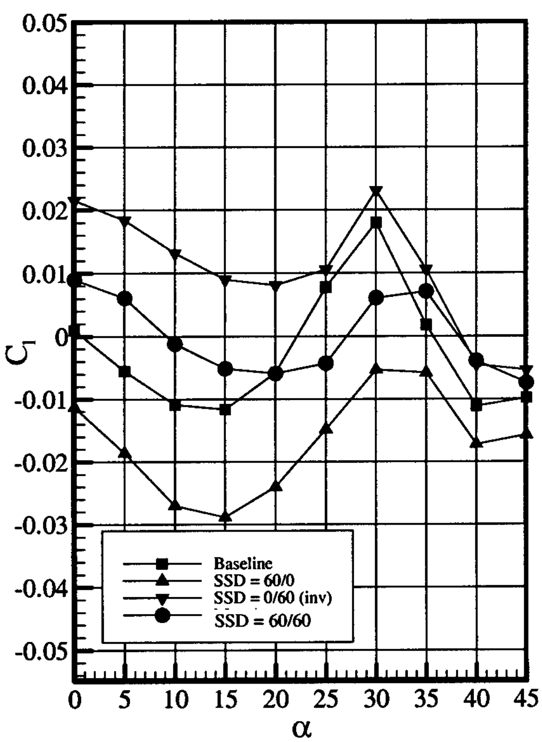

Figure K8c Rolling Moment Coefficient as a Function of α, β = 8°

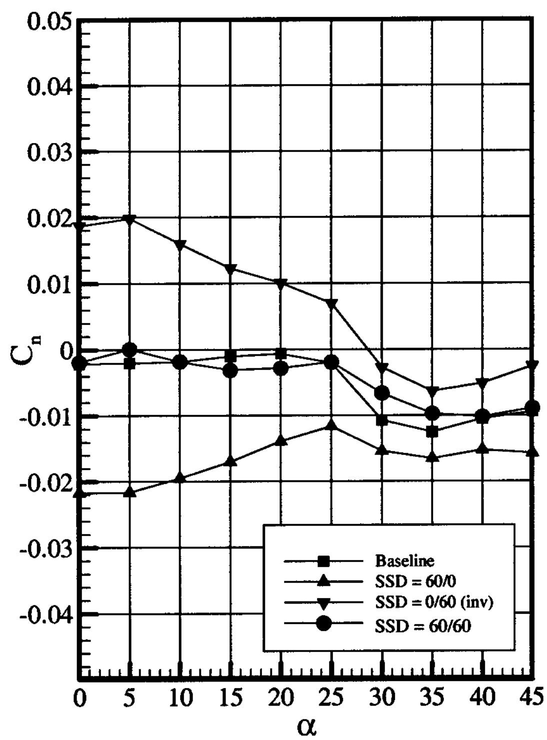

Figure K8d Yawing Moment Coefficient as a Function of α, β = 8°

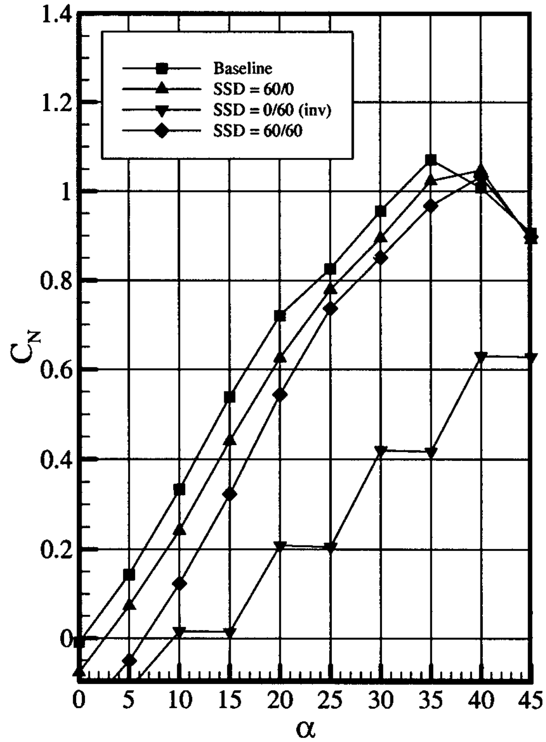

Figure K9a Normal Force Coefficient as a Function of α, β = 10°

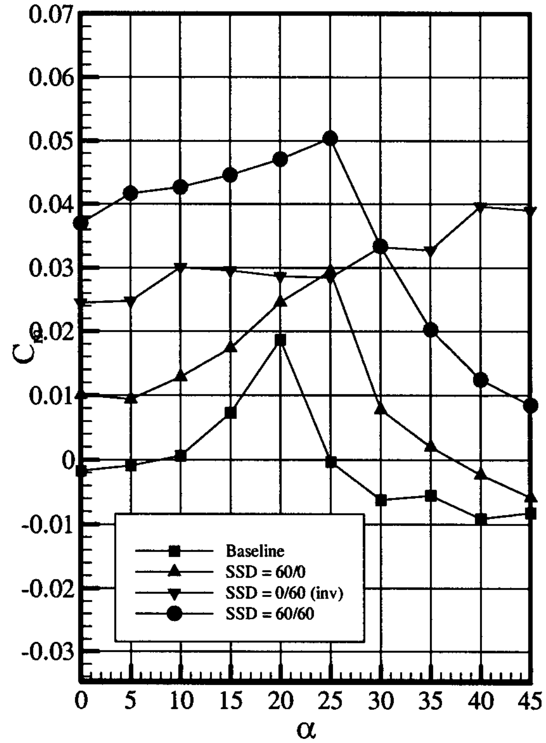

Figure K9b Pitching Moment Coefficient as a Function of α, β = 10°

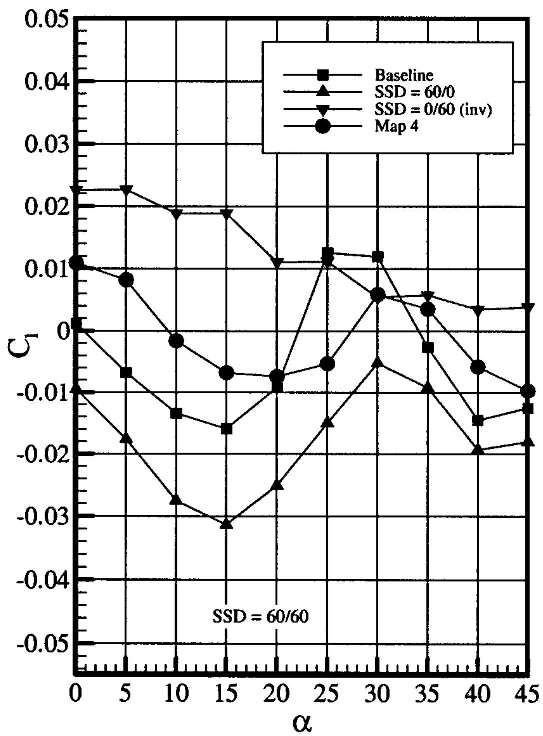

Figure K9c Rolling Moment Coefficient as a Function of α, β = 10°

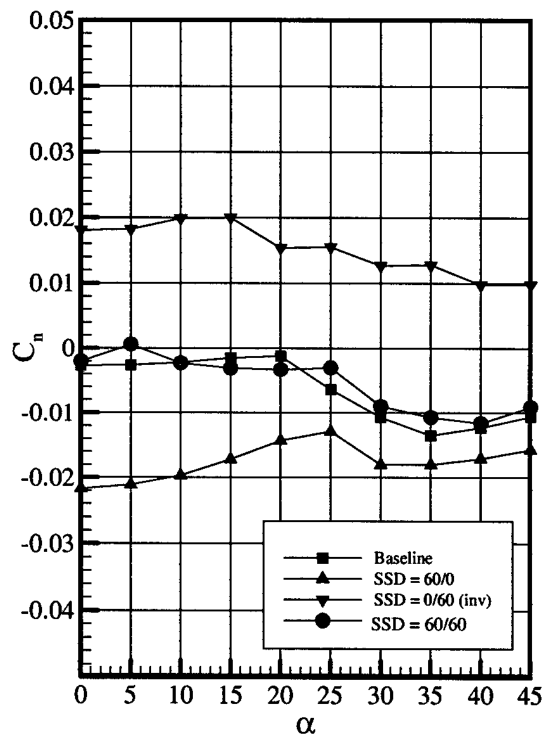

Figure K9d Yawing Moment Coefficient as a Function of α, β = 10°

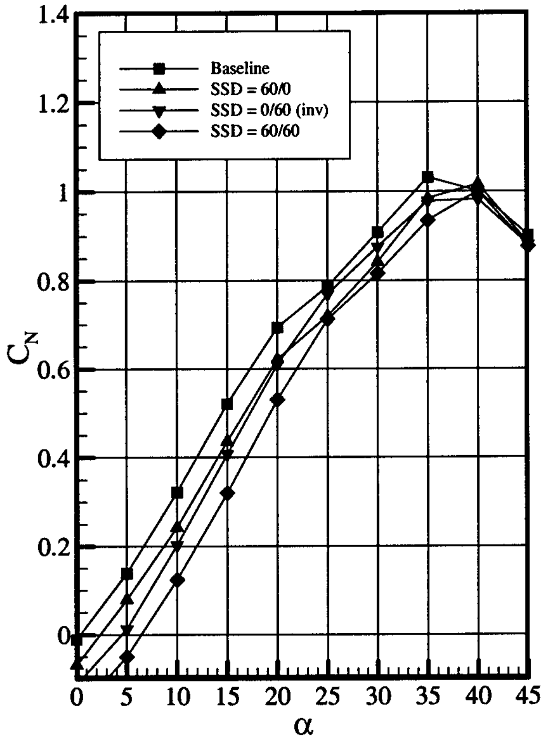

Figure K10a Normal Force Coefficient as a Function of α, β = 12°

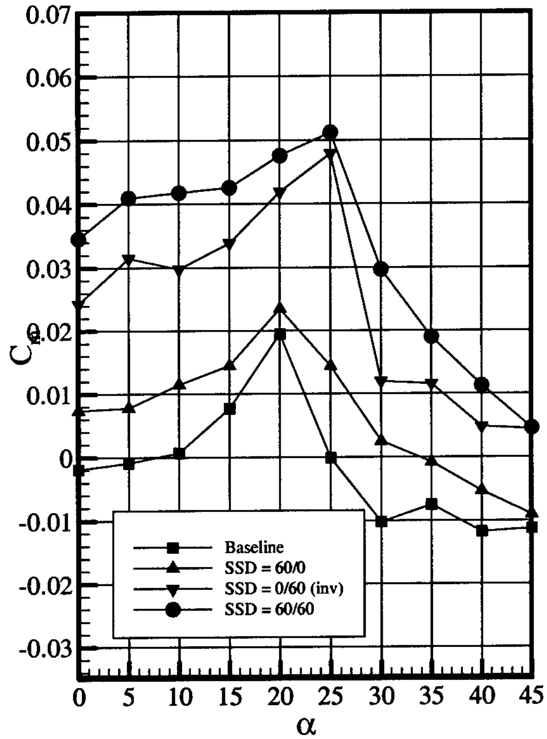

Figure K10b Pitching Moment Coefficient as a Function of α, β = 12°

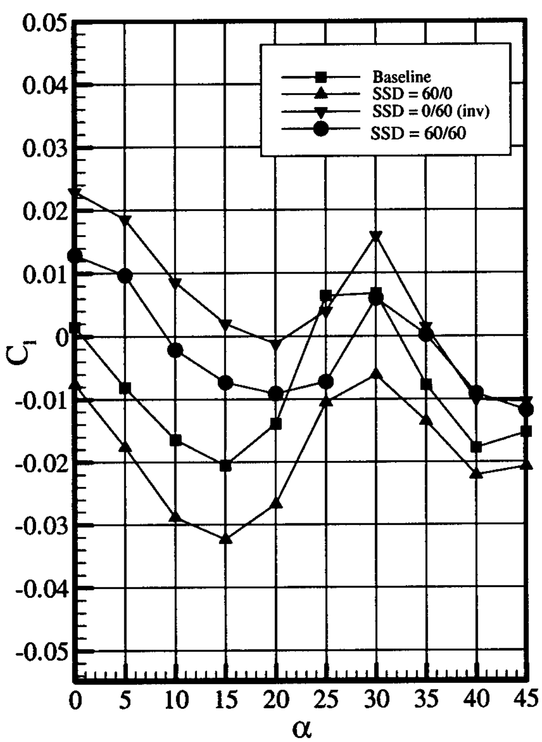

Figure K10c Rolling Moment Coefficient as a Function of α, β = 12°

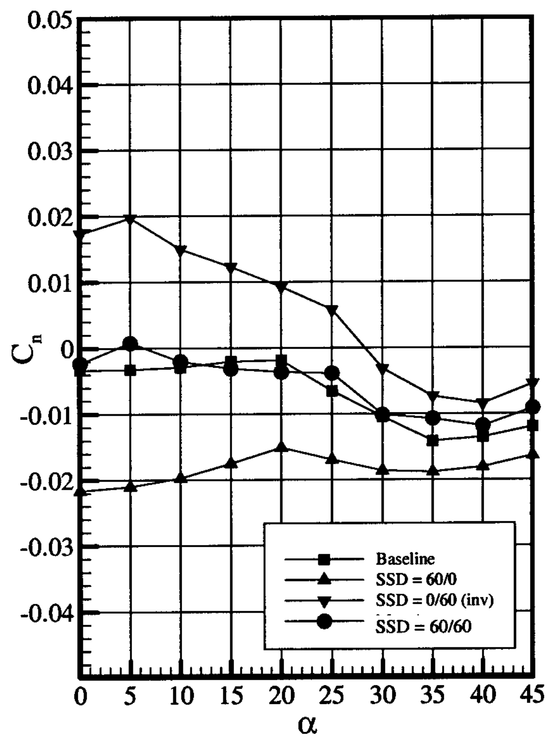

Figure K10d Yawing Moment Coefficient as a Function of α, β = 12°

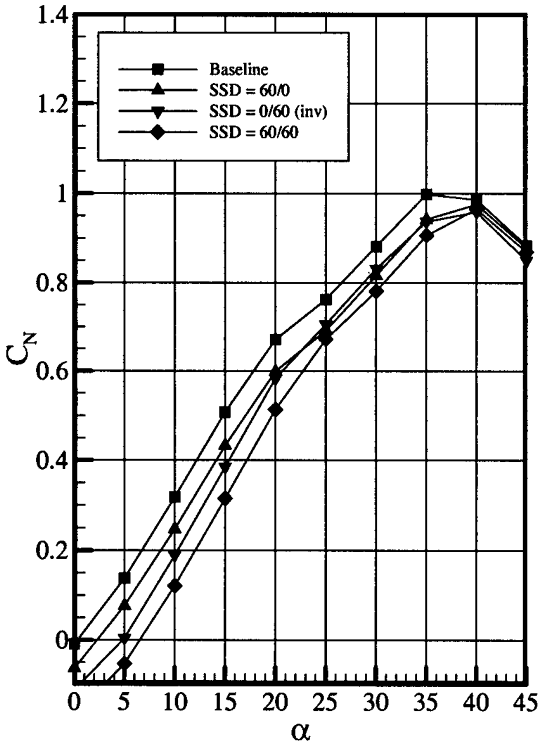

Figure K11a Normal Force Coefficient as a Function of α, β = 14°

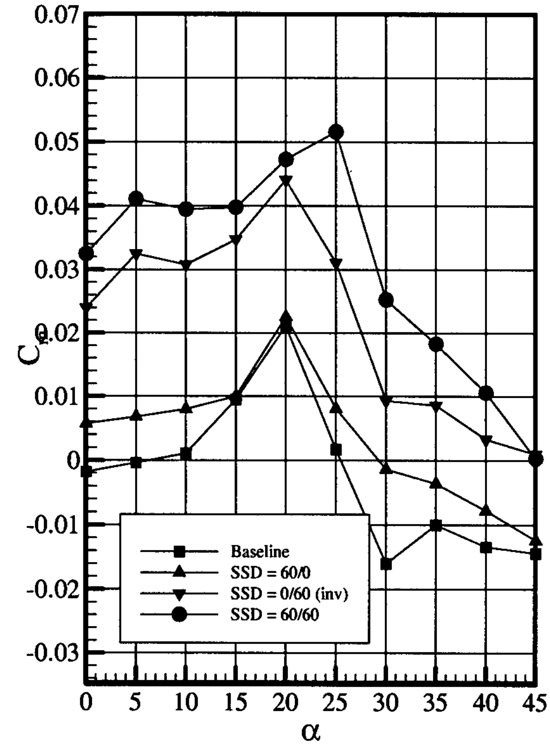

Figure K11b Pitching Moment Coefficient as a Function of α, β = 14°

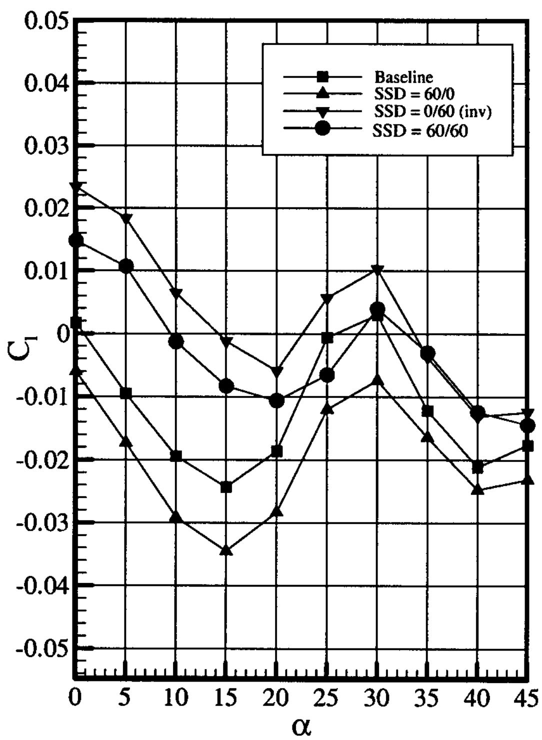

Figure K11c Rolling Moment Coefficient as a Function of α, β = 14°

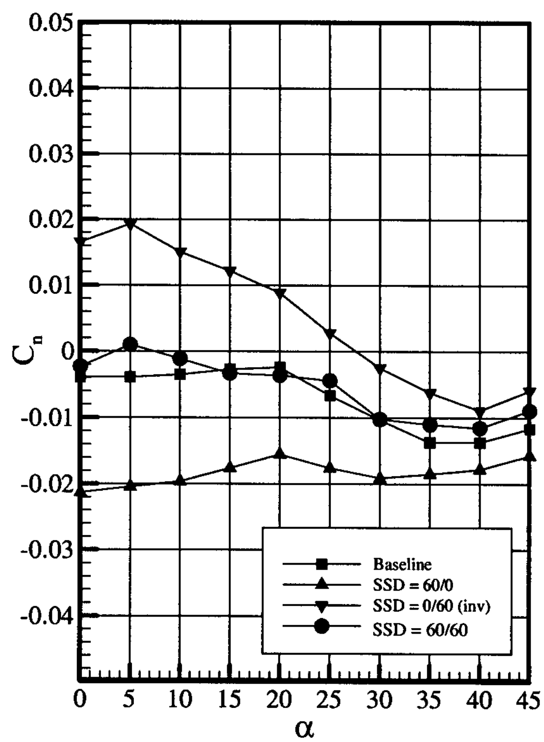

Figure K11d Yawing Moment Coefficient as a Function of α, β = 14°

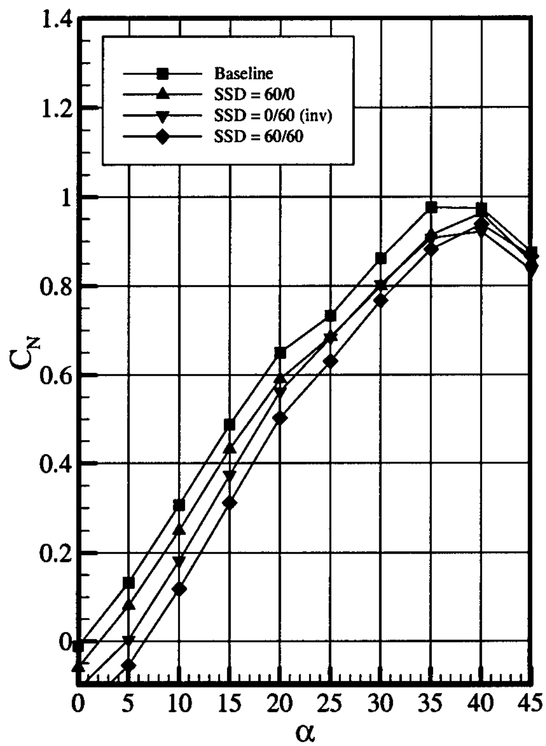

Figure K12a Normal Force Coefficient as a Function of α, $\beta = 16^{\circ}$

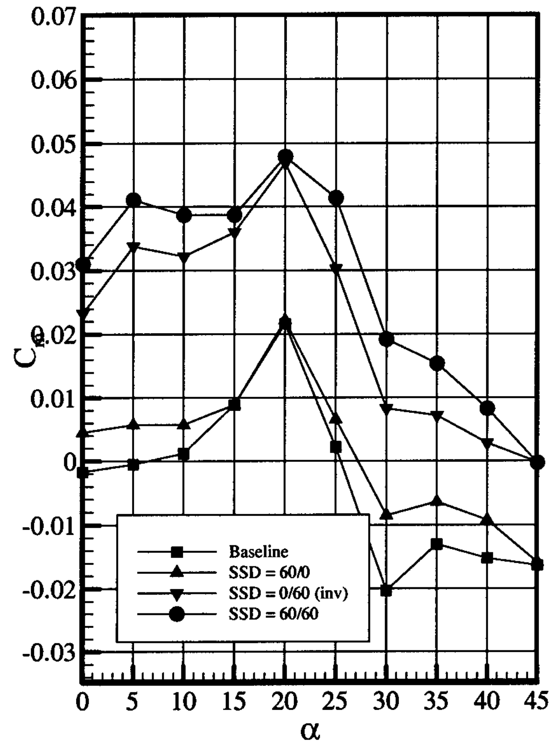

Figure K12b Pitching Moment Coefficient as a Function of α, $\beta = 16^{\circ}$

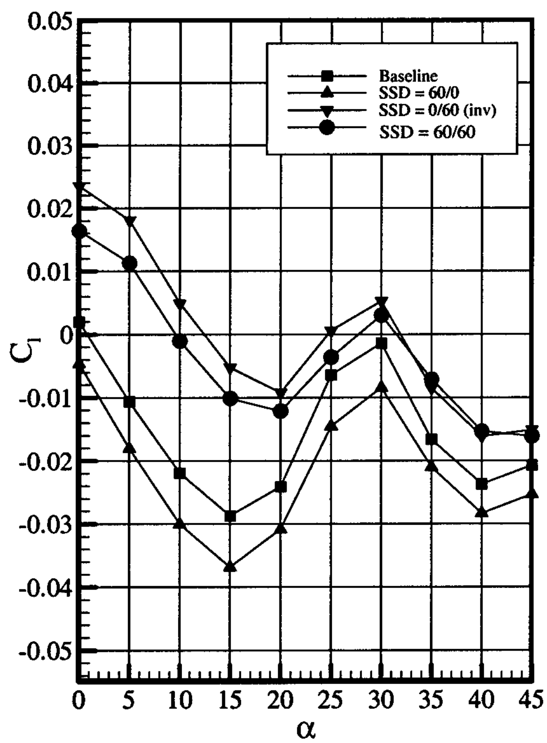

Figure K12c Rolling Moment Coefficient as a Function of α, $\beta = 16^{\circ}$

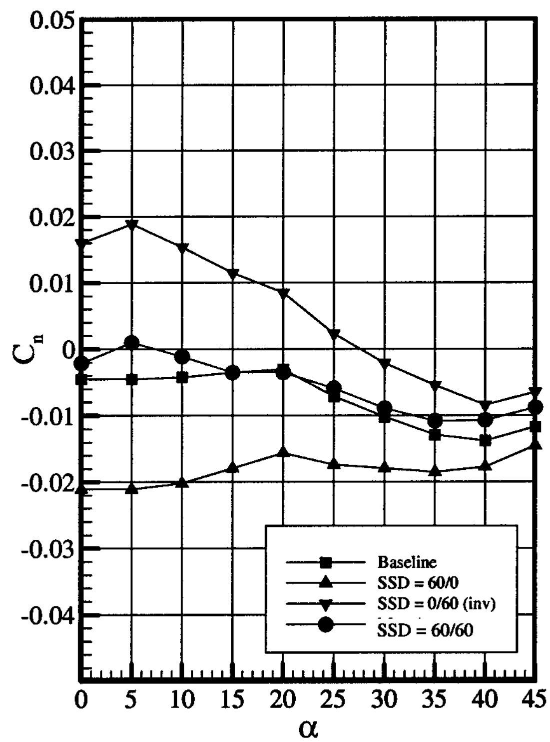

Figure K12d Yawing Moment Coefficient as a Function of α, $\beta = 16^{\circ}$

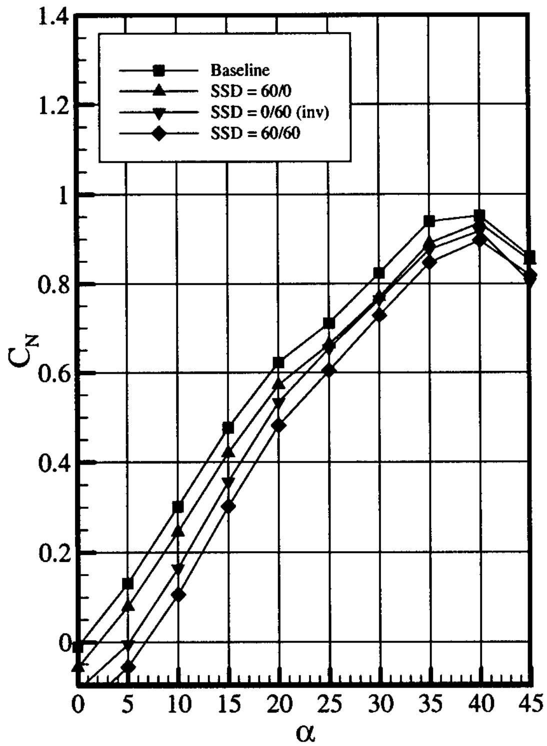

Figure K13a Normal Force Coefficient as a Function of α, β = 18°

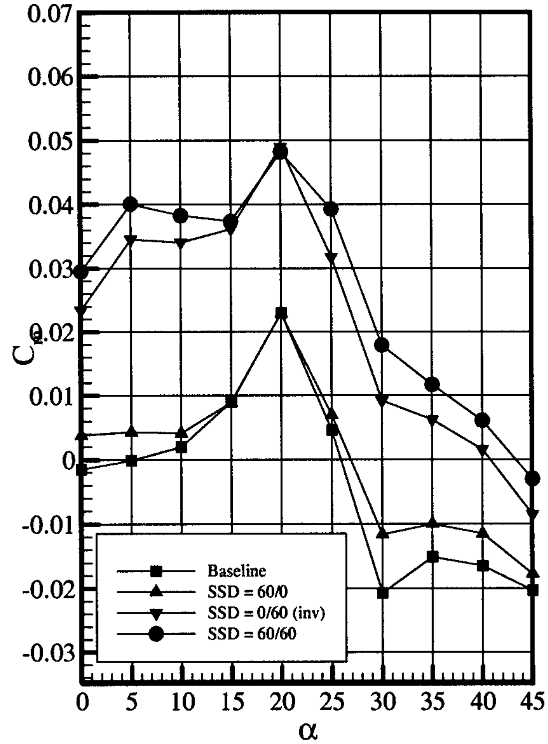

Figure K13b Pitching Moment Coefficient as a Function of α, β = 18°

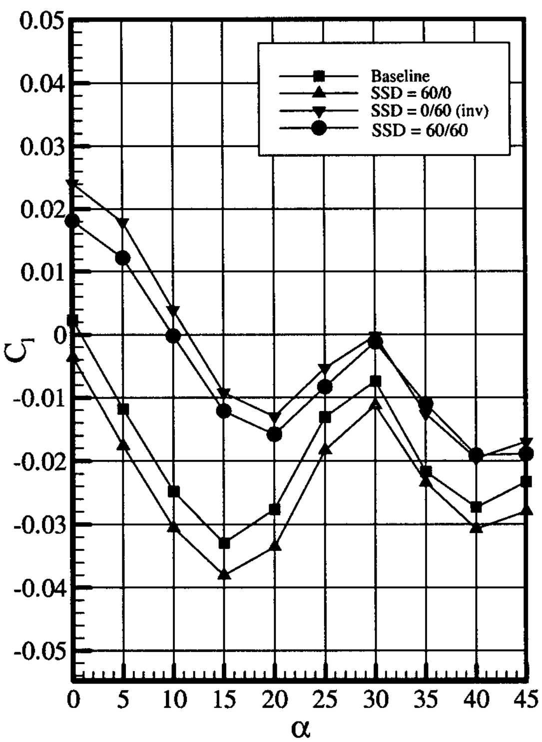

Figure K13c Rolling Moment Coefficient as a Function of α, β = 18°

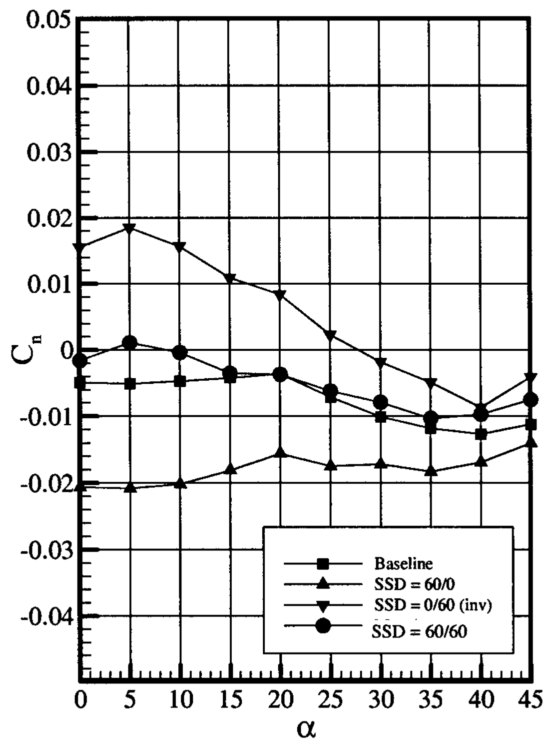

Figure K13d Yawing Moment Coefficient as a Function of α, β = 18°

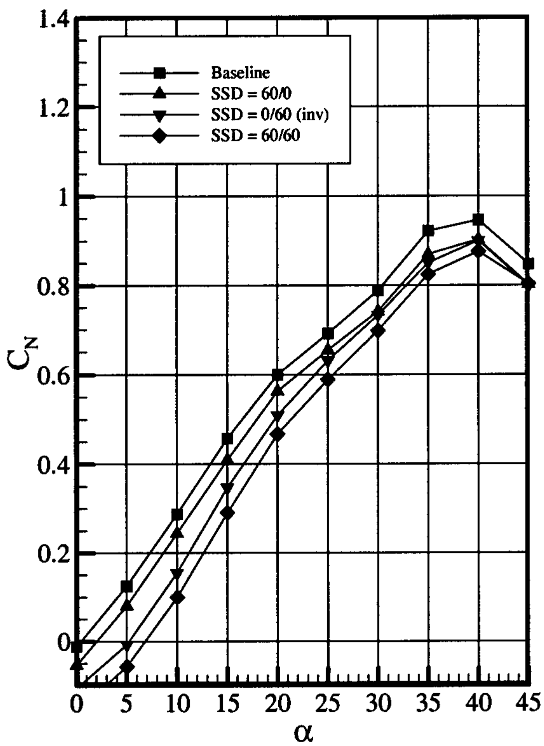

Figure K14a Normal Force Coefficient as a Function of α, β = 20°

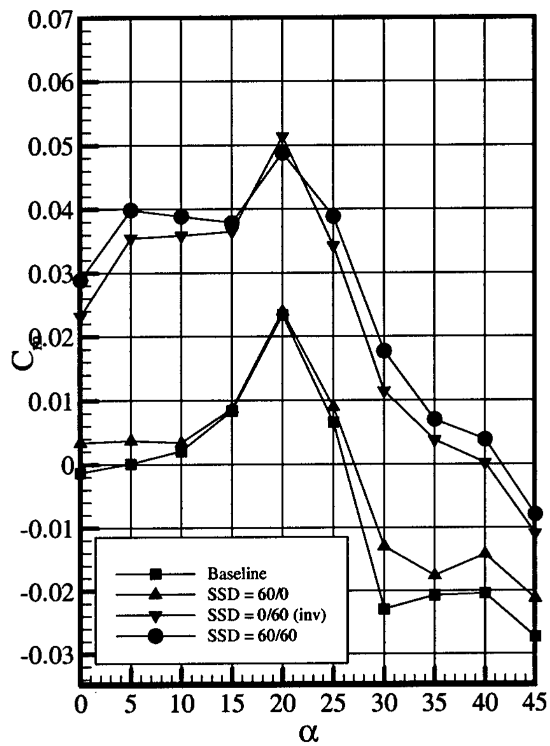

Figure K14b Pitching Moment Coefficient as a Function of α, β = 20°

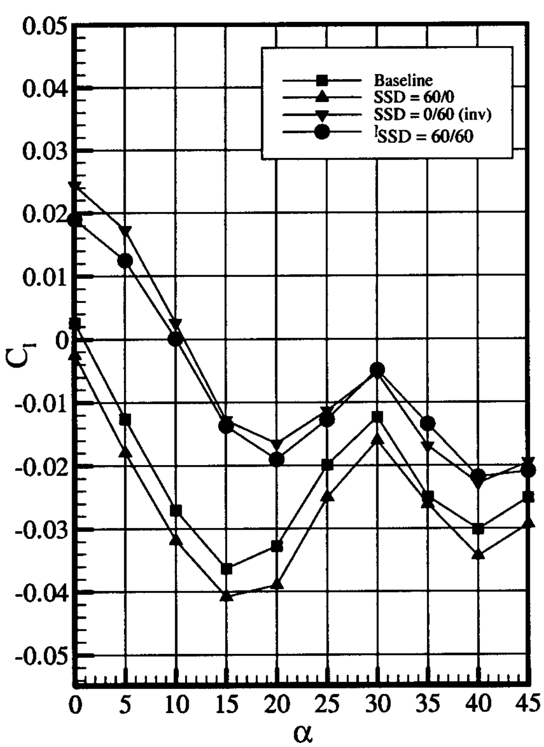

Figure K14c Rolling Moment Coefficient as a Function of α, β = 20°

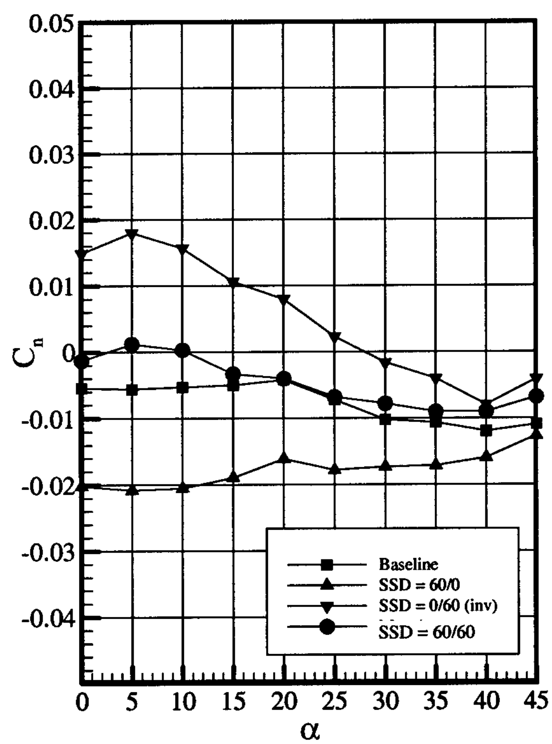

Figure K14d Yawing Moment Coefficient as a Function of α, β = 20°

Appendix L Spoiler-Slot-Deflector Deflection Data as a Function of Sideslip Angle

SSD = 60/60

SSD = 60/60

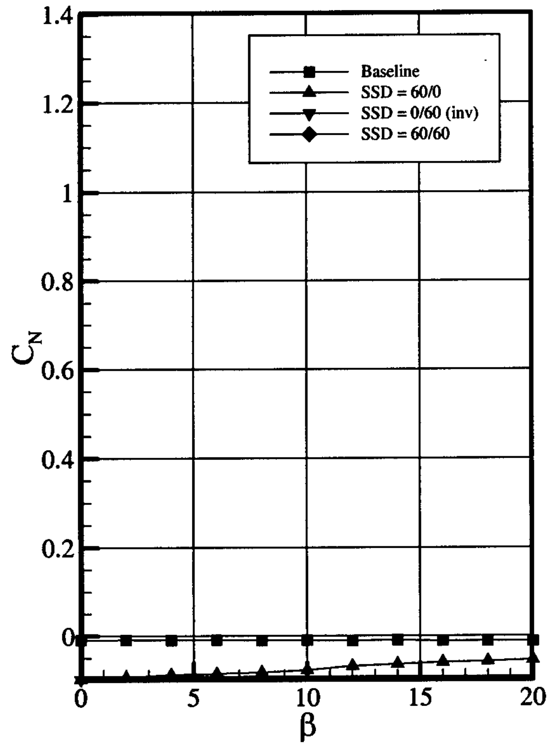

Figure L1a Normal Force Coefficient
as a Function of β, $\alpha = 0^{\circ}$

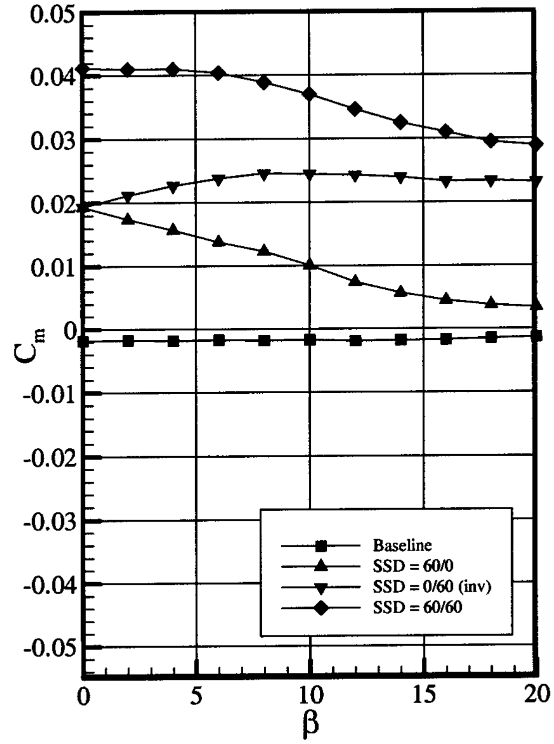

Figure L1b Pitching Moment Coefficient
as a Function of β, $\alpha = 0^{\circ}$

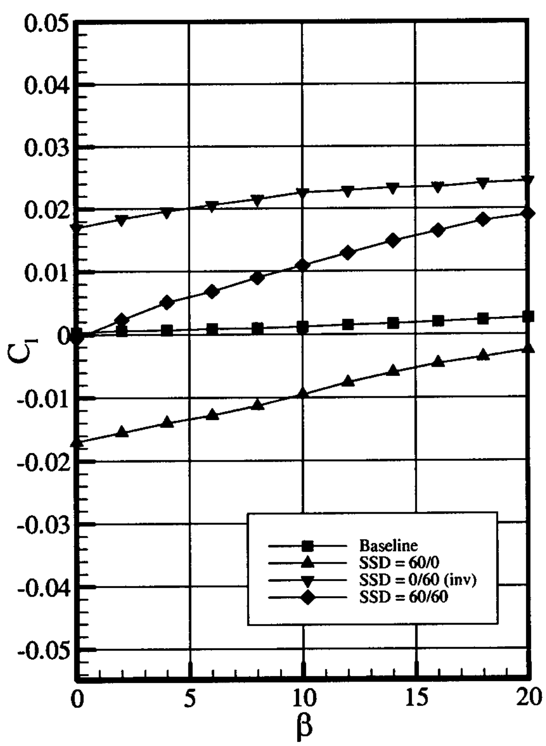

Figure L1c Rolling Moment Coefficient
as a Function of β, $\alpha = 0^{\circ}$

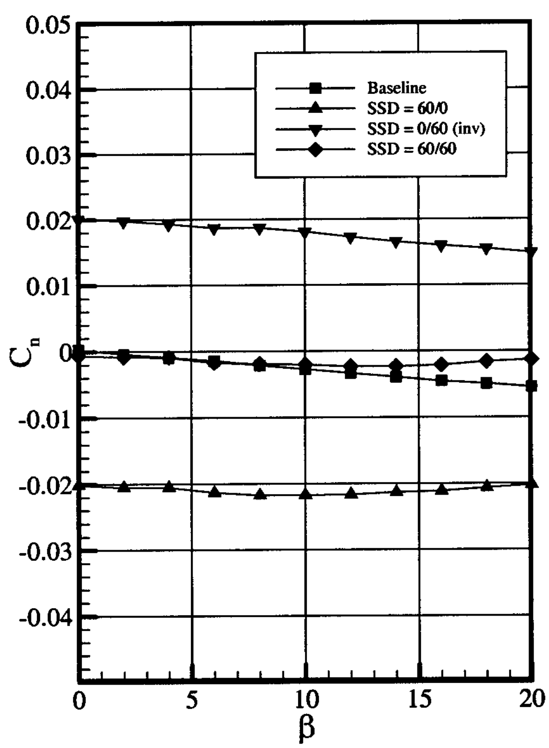

Figure L1d Yawing Moment Coefficient
as a Function of β, $\alpha = 0^{\circ}$

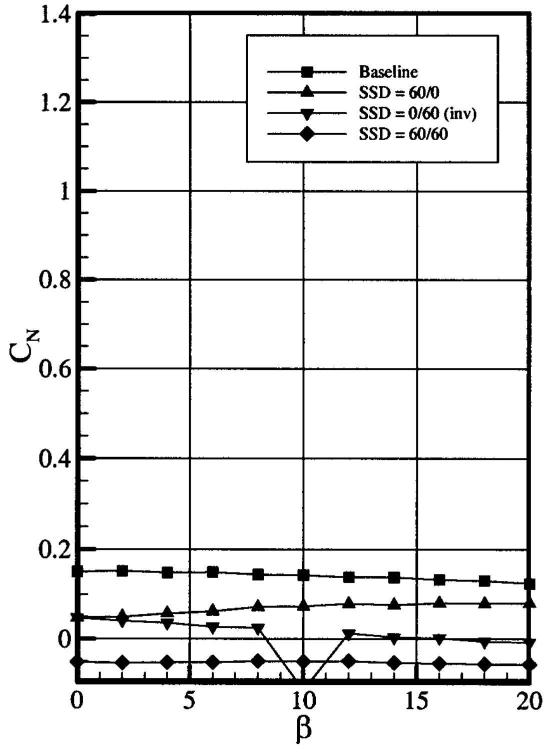

Figure L2a Normal Force Coefficient as a Function of β, $\alpha = 5^{\circ}$

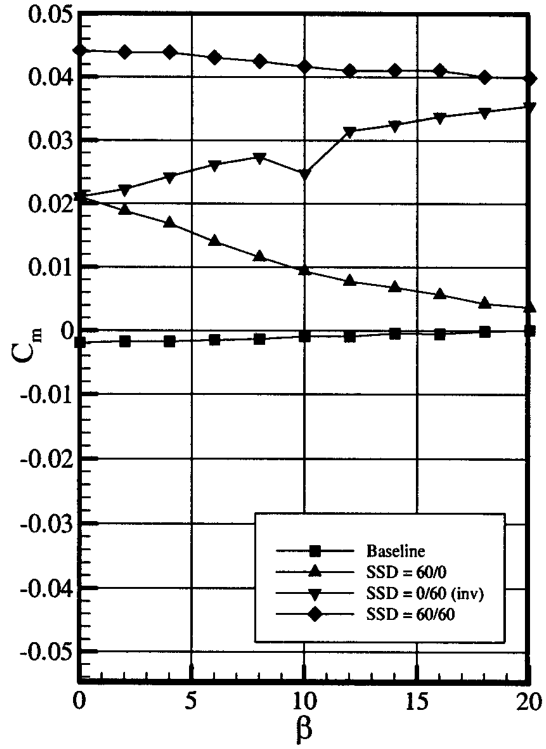

Figure L2b Pitching Moment Coefficient as a Function of β, $\alpha = 5^{\circ}$

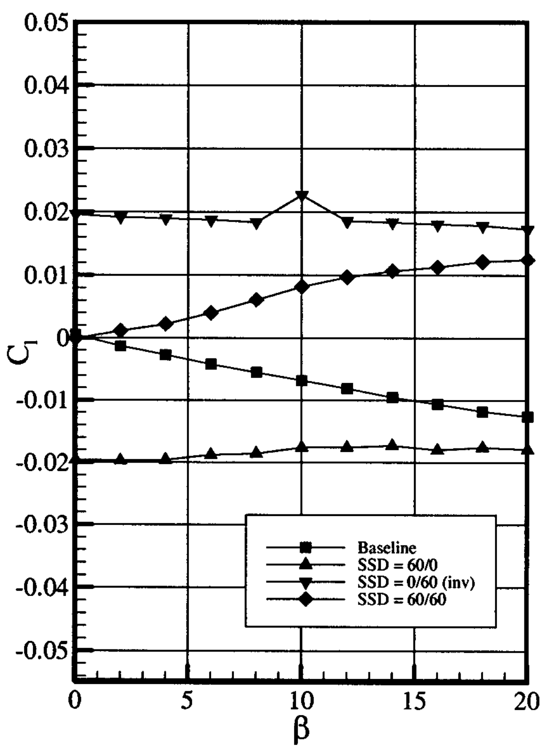

Figure L2c Rolling Moment Coefficient as a Function of β, $\alpha = 5^{\circ}$

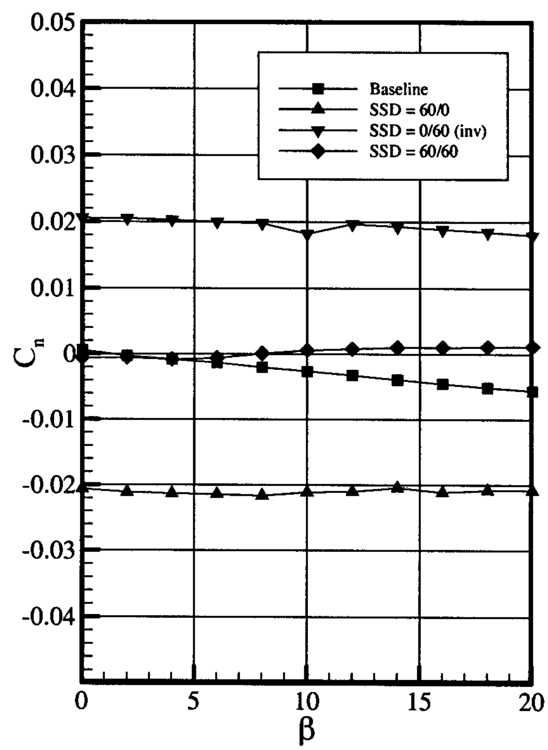

Figure L2d Yawing Moment Coefficient as a Function of β, $\alpha = 5^{\circ}$

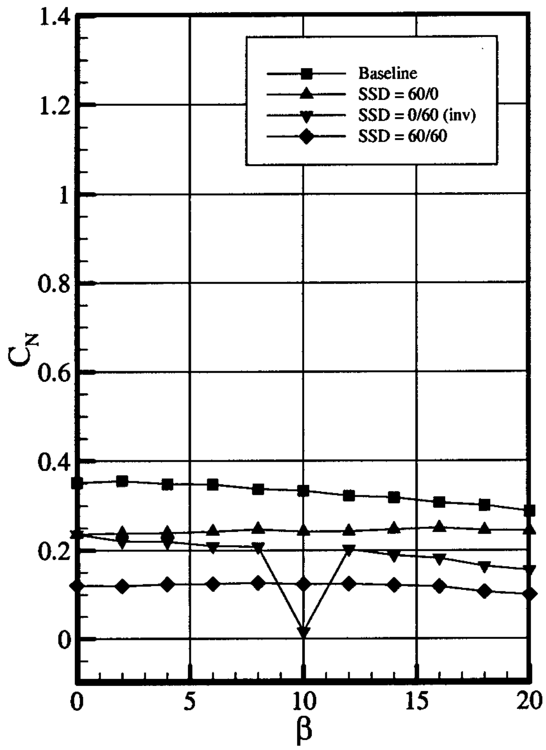

Figure L3a Normal Force Coefficient as a Function of β, α = 10°

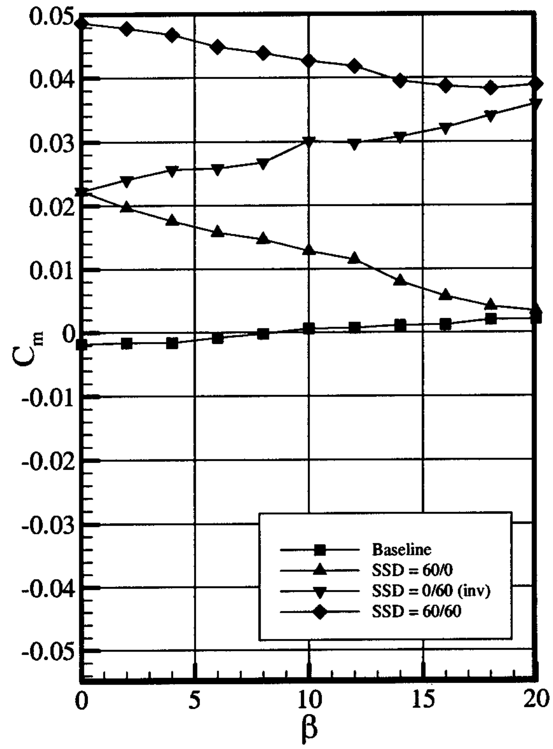

Figure L3b Pitching Moment Coefficient as a Function of β, α = 10°

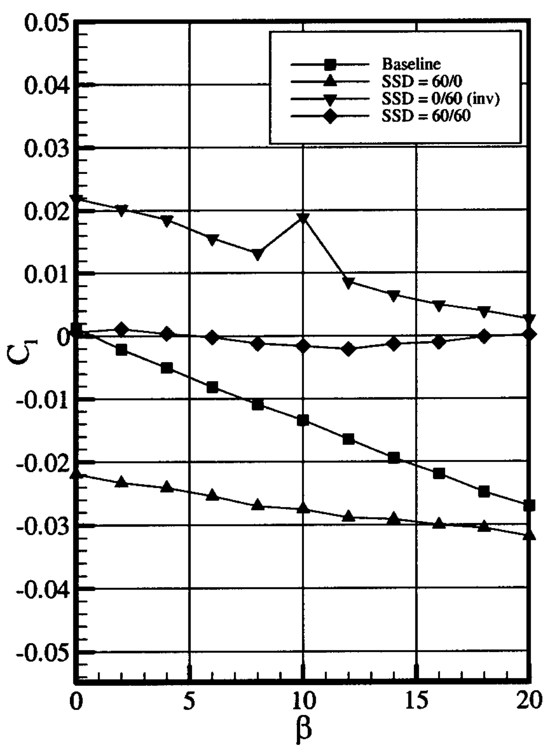

Figure L3c Rolling Moment Coefficient as a Function of β, α = 10°

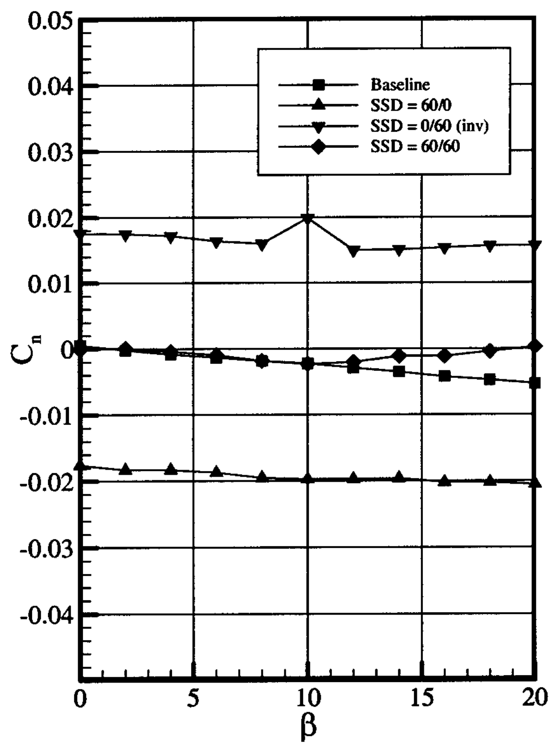

Figure L3d Yawing Moment Coefficient as a Function of β, α = 10°

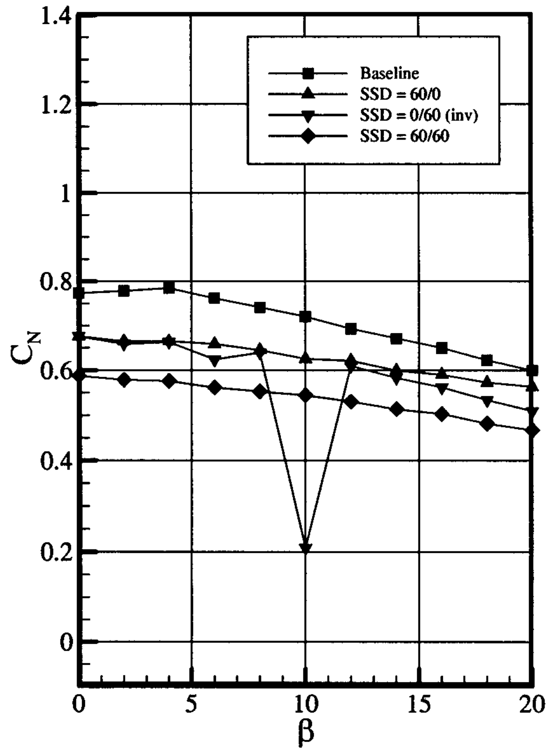

Figure L4a Normal Force Coefficient
as a Function of β, α = 15°

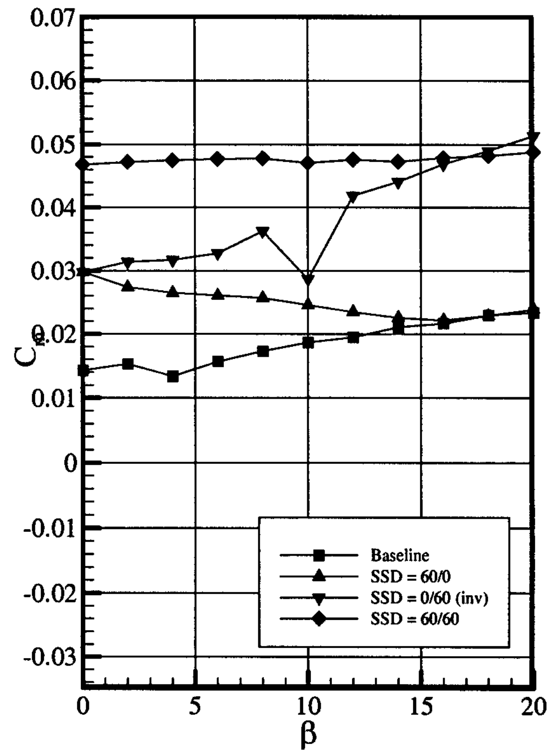

Figure L4b Pitching Moment Coefficient
as a Function of β, α = 15°

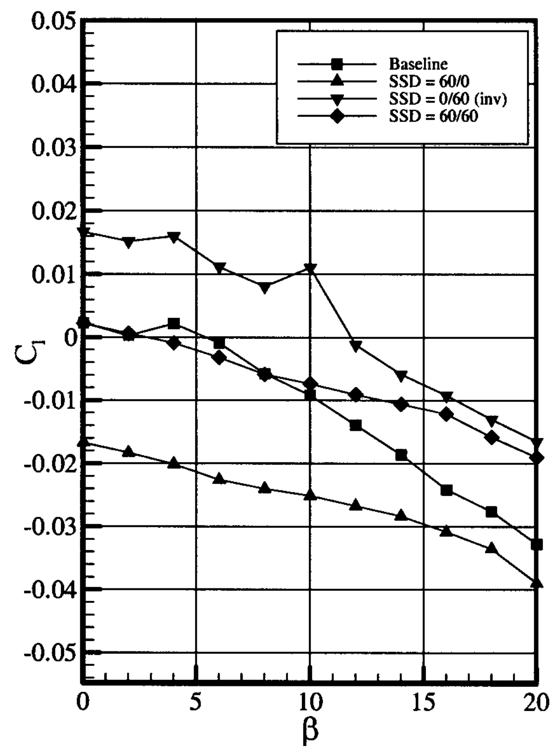

Figure L4c Rolling Moment Coefficient
as a Function of β, α = 15°

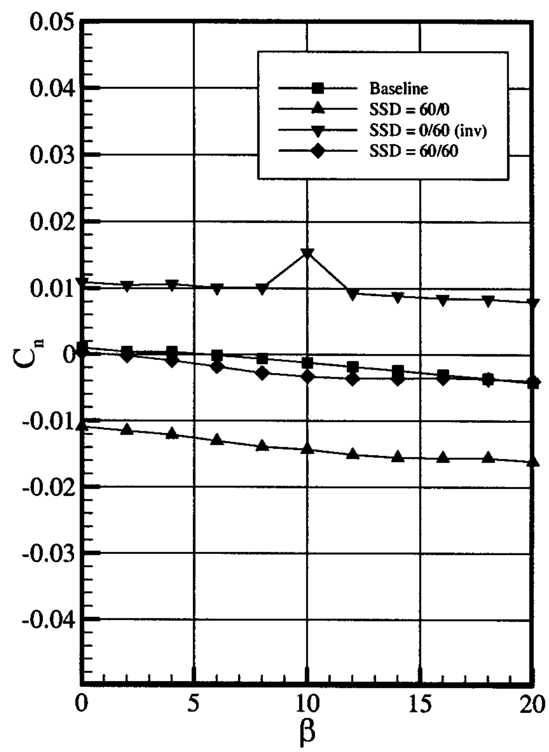

Figure L4d Yawing Moment Coefficient
as a Function of β, α = 15°

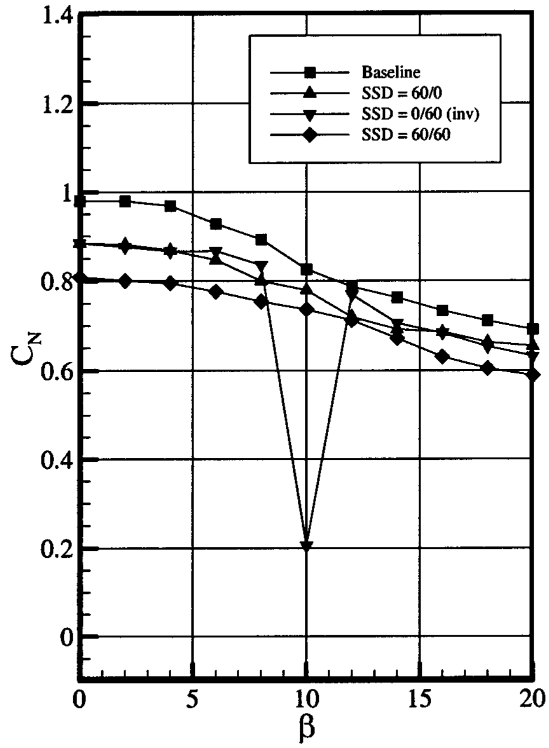

Figure L5a Normal Force Coefficient as a Function of β, α = 20°

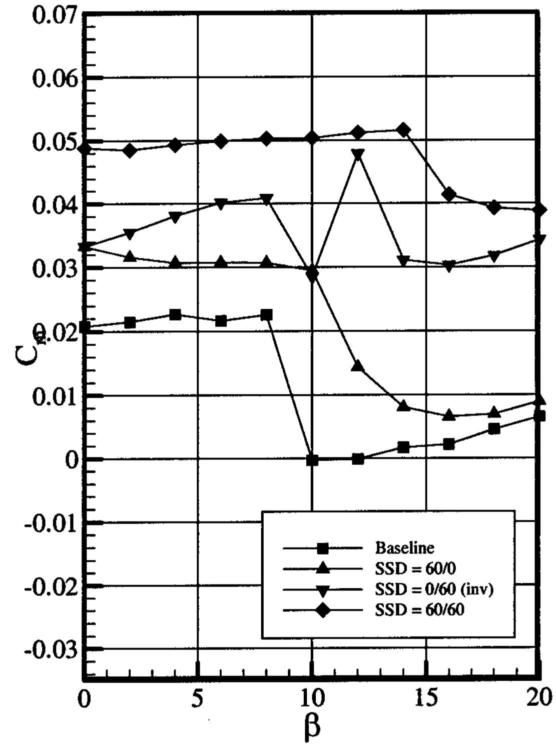

Figure L5b Pitching Moment Coefficient as a Function of β, α = 20°

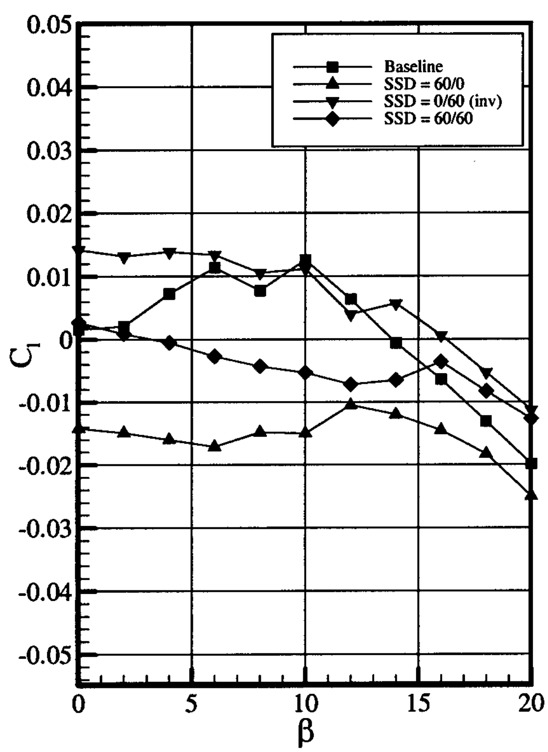

Figure L5c Rolling Moment Coefficient as a Function of β, α = 20°

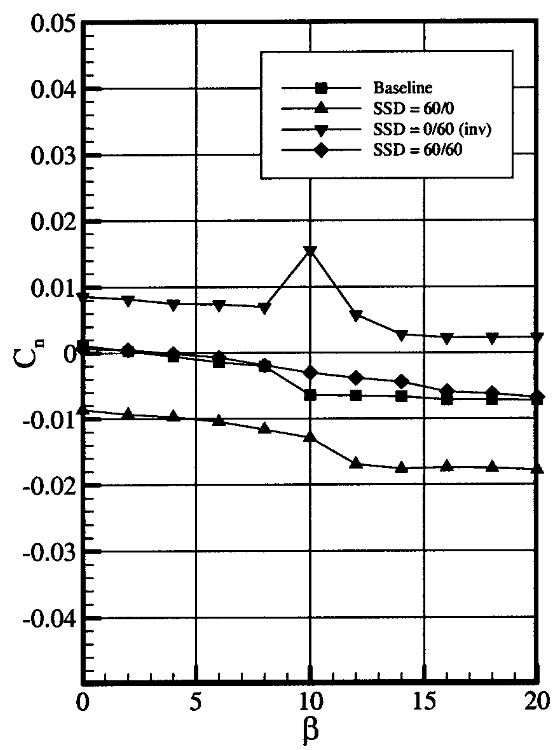

Figure L5d Yawing Moment Coefficient as a Function of β, α = 20°

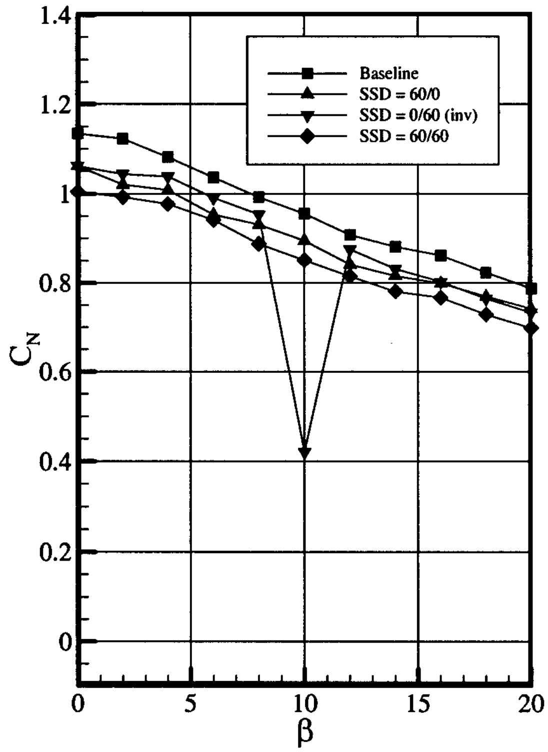

Figure L6a Normal Force Coefficient
as a Function of β, $\alpha = 25^\circ$

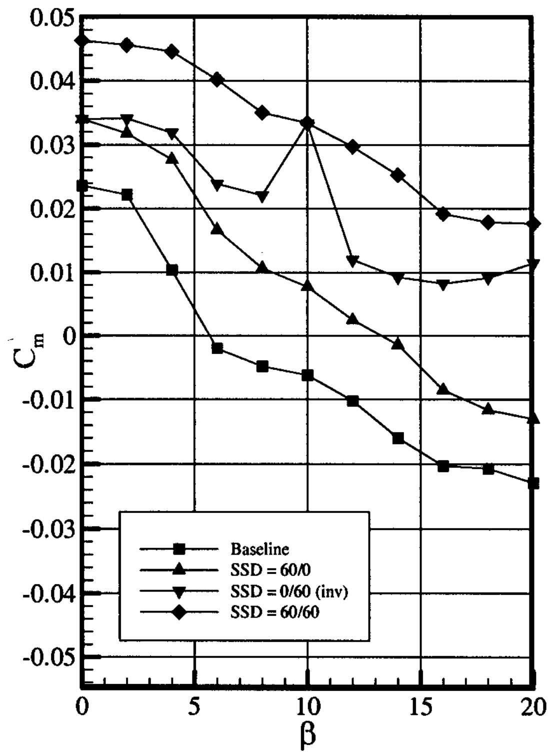

Figure L6b Pitching Moment Coefficient
as a Function of β, $\alpha = 25^\circ$

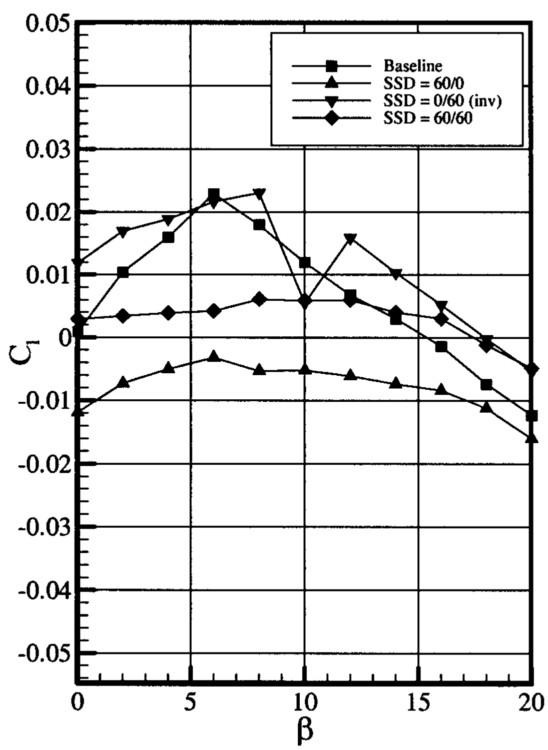

Figure L6c Rolling Moment Coefficient
as a Function of β, $\alpha = 25^\circ$

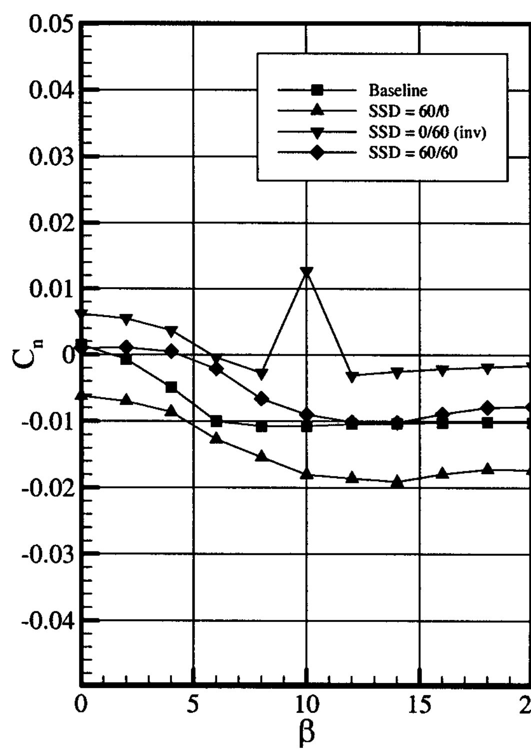

Figure L6d Yawing Moment Coefficient
as a Function of β, $\alpha = 25^\circ$

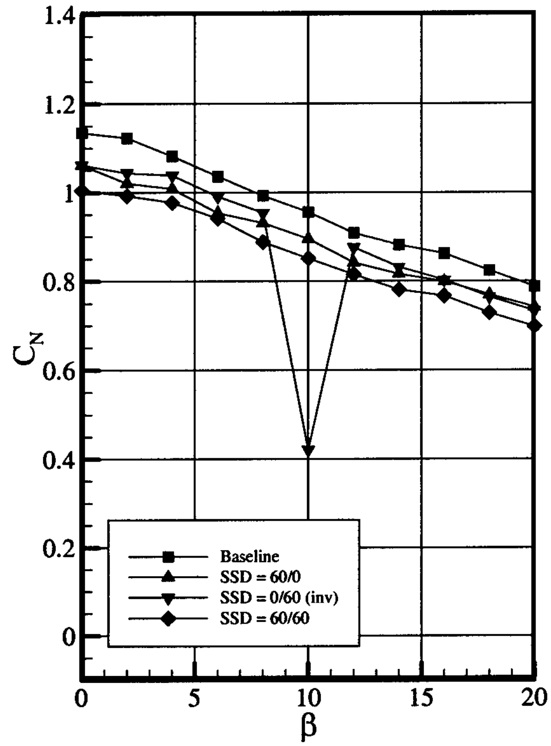

Figure L7a Normal Force Coefficient as a Function of β, α = 30°

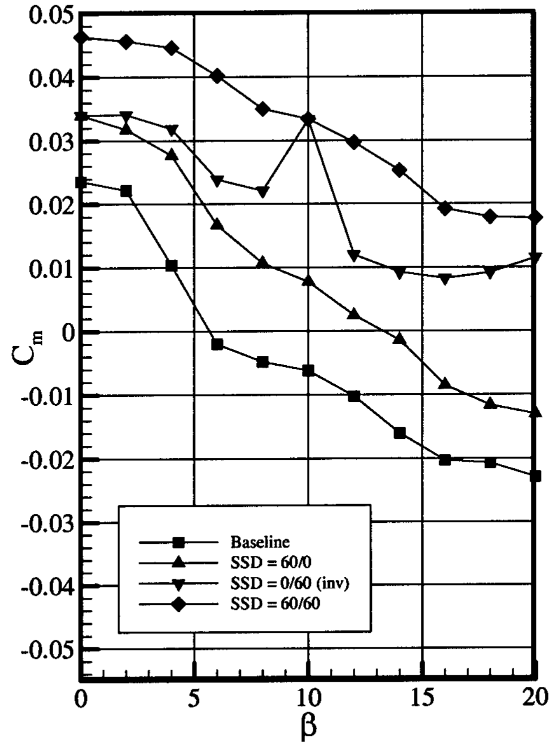

Figure L7b Pitching Moment Coefficient as a Function of β, α = 30°

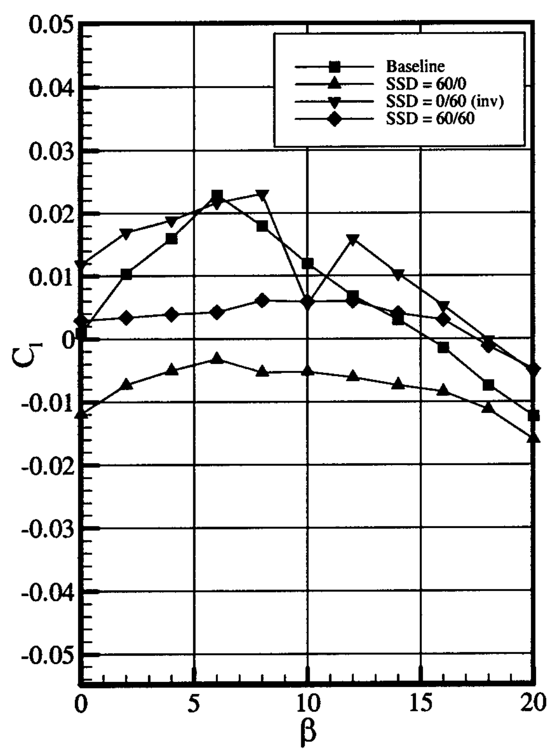

Figure L7c Rolling Moment Coefficient as a Function of β, α = 30°

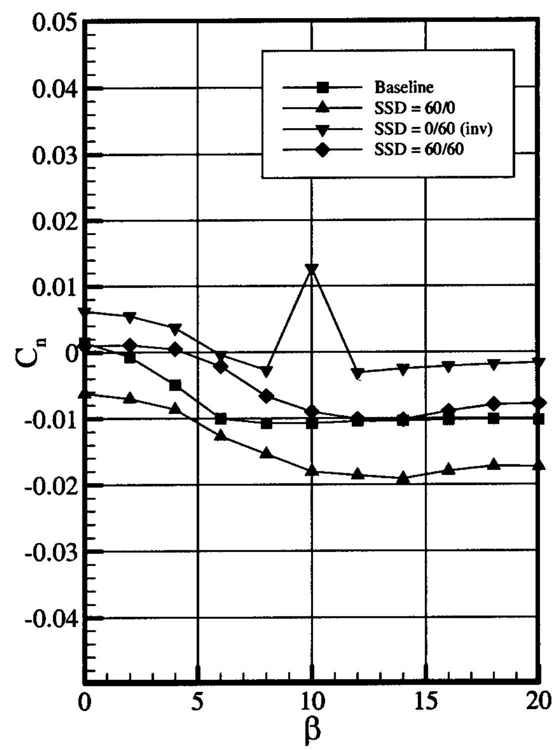

Figure L7d Yawing Moment Coefficient as a Function of β, α = 30°

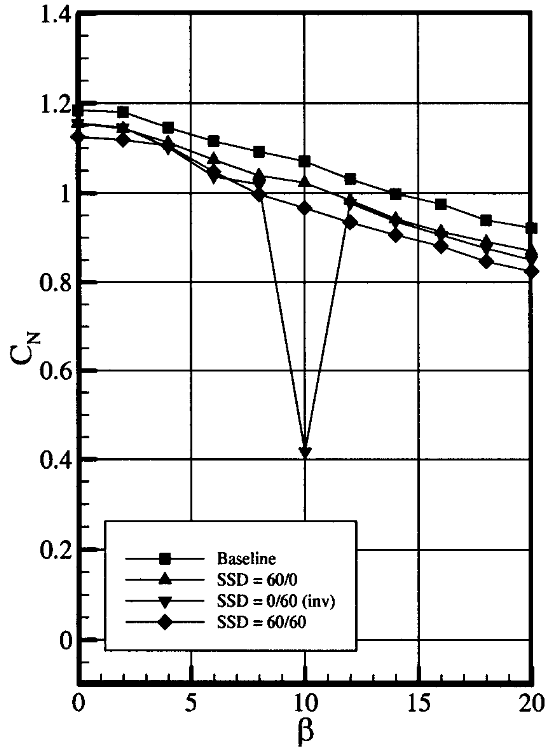

Figure L8a Normal Force Coefficient as a Function of β, α = 35°

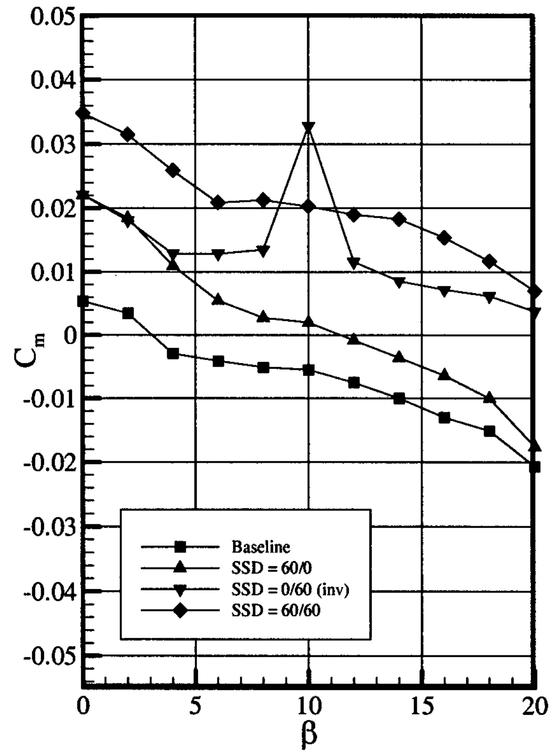

Figure L8b Pitching Moment Coefficient as a Function of β, α = 35°

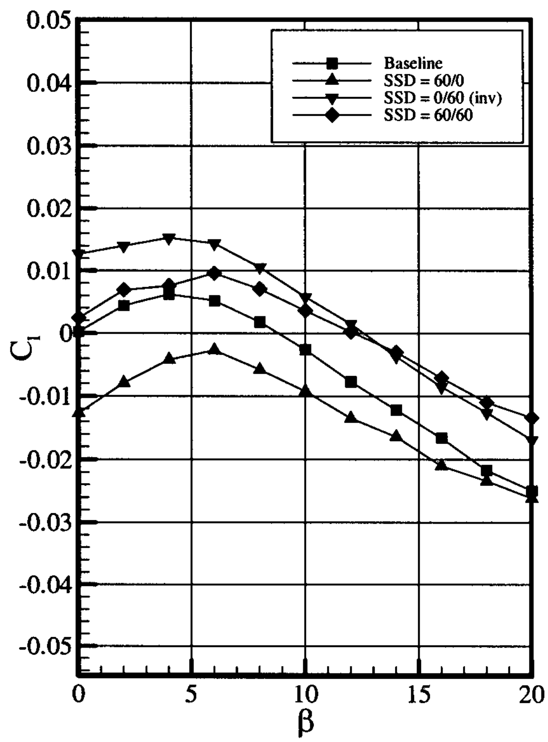

Figure L8c Rolling Moment Coefficient as a Function of β, α = 35°

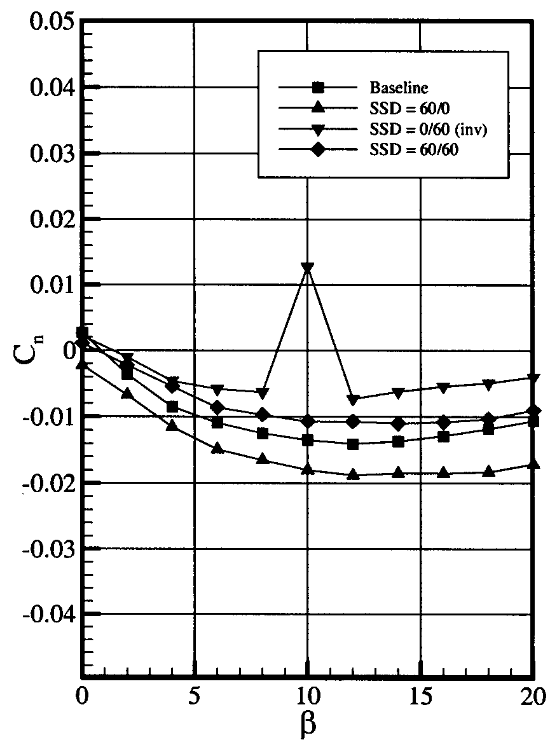

Figure L8d Yawing Moment Coefficient as a Function of β, α = 35°

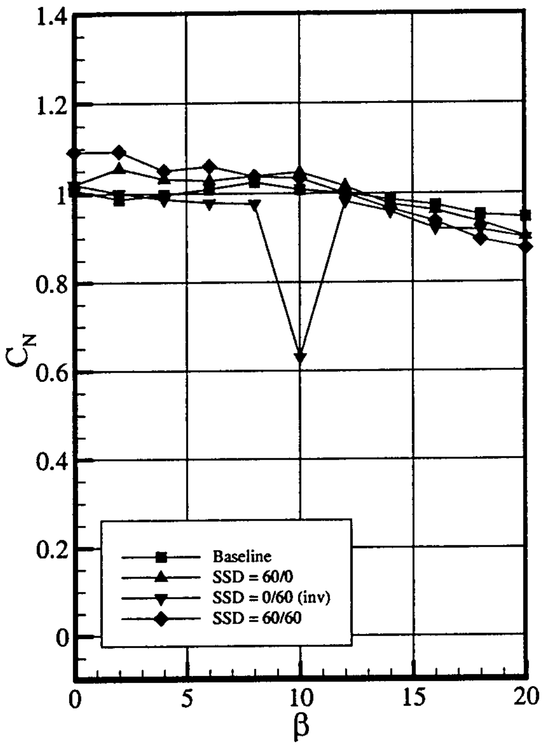

Figure L9a Normal Force Coefficient
as a Function of β, α = 40°

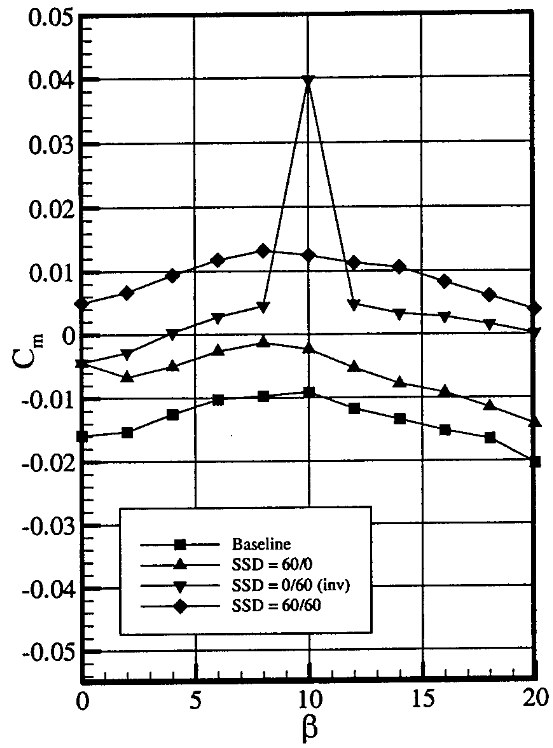

Figure L9b Pitching Moment Coefficient
as a Function of β, α = 40°

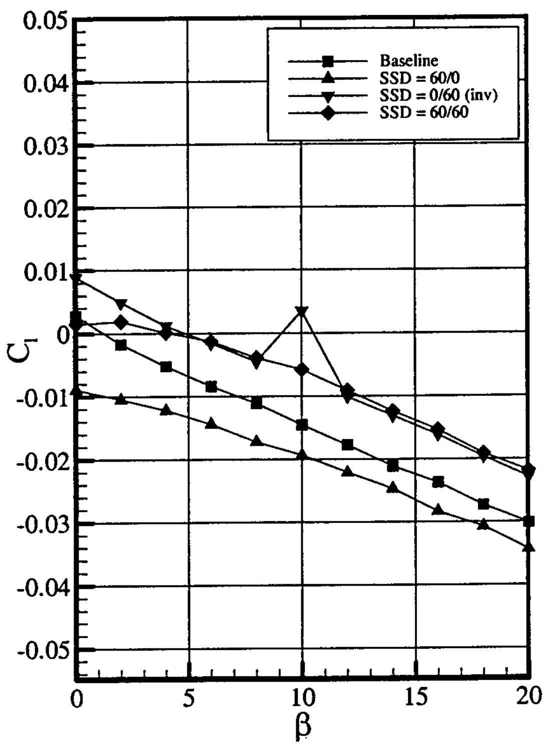

Figure L9c Rolling Moment Coefficient
as a Function of β, α = 40°

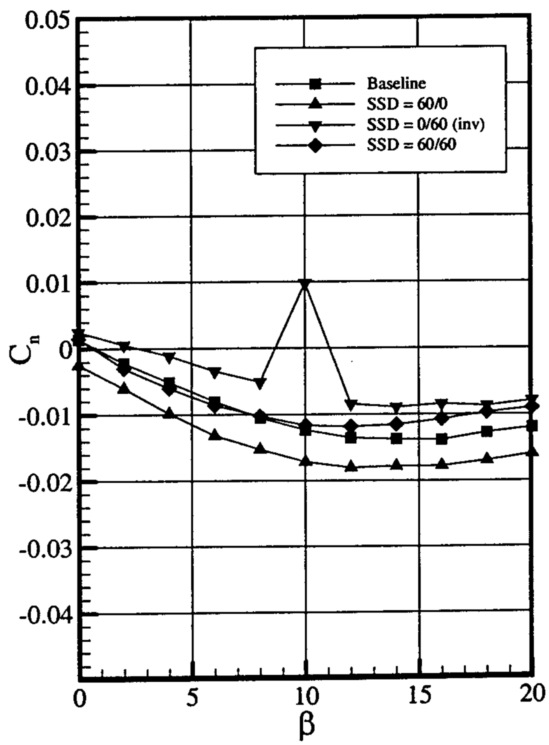

Figure L9d Yawing Moment Coefficient
as a Function of β, α = 40°